Schriftenreihe Umweltingenieurwesen

Fakultät für Agrar, Bau und Umwelt

Band 132

Dissertation

Ngoc Huan Tran

An Integrated Approach to Flood Risk Assessment Engaging Citizen Scientists for Bui River Basin, Vietnam

PROFESSUR

Hydrologie und Angewandte Meteorologie

Universität Rostock Traditio et Innovatio

ISBN 978-3-86009-571-3
DOI: https://doi.org/10.18453/rosdok_id00004833

Schriftenreihe Bd. 132 Umweltingenieurwesen ▪ Hydrologie und Angewandte Meteorologie

Schriftenreihe Umweltingenieurwesen

Band 132

Dissertation

Ngoc Huan Tran

An Integrated Approach to Flood Risk Assessment Engaging Citizen Scientists for Bui River Basin, Vietnam

Professur

Hydrologie und
Angewandte Meteorologie

Fakultät für Agrar, Bau und Umwelt

Universität Rostock Traditio et Innovatio

Dissertation

HERAUSGEBER

Prof. Dr. Konrad Miegel
Universität Rostock
Fakultät für Agrar, Bau und Umwelt
Professur Hydrologie und Angewandte Meteorologie
18051 Rostock

CIP-KURZTITELAUFNAHME

Ngoc Huan Tran
Universität Rostock
Fakultät für Agrar, Bau und Umwelt
Rostock, 2025

BEZUGSMÖGLICHKEITEN

Universität Rostock
Fakultät für Agrar, Bau und Umwelt
Professur Hydrologie und Angewandte Meteorologie
Satower Straße 48, 18059 Rostock
Tel.: 0381/498-3461, Fax: 0381/498-3462

ISBN 978-3-86009-571-3
DOI: https://doi.org/10.18453/rosdok_id00004833

Universität Rostock
Professur Hydrologie und Angewandte Meteorologie

Vorwort

Gegenstand der Dissertation von Herrn Ngoc Huan Tran ist die Hochwasserrisikoanalyse am Beispiel eines Einzugsgebietes in Vietnam, in dem die Hochwasservorsorge wie in Mitteleuropa, nicht nur unter dem Einfluss des Klimawandels, an Bedeutung gewinnt. Im Vergleich zu Mitteleuropa sind jedoch in vielen Ländern Asiens und Afrikas die Datengrundlagen spärlich, insbesondere in ländlichen Regionen. Dies stellte eine der größten Herausforderungen bei der Bearbeitung der vorgelegten Dissertation dar. Sie zu meistern, gehörte zu den Zielen dieser Arbeit, mit der ein integrierter Ansatz für die Hochwasserrisikobewertung in Gebieten mit spärlichen Datengrundlagen entwickelt worden ist. Die vorliegende Forschung stellt eine neue Methode zur Erhebung hochwasserbezogener Daten mithilfe von Citizen Science (Bürgerwissenschaft) vor. Dabei wird mit der Einbindung von Citizen Science, von der hier größere Effekte erwartet werden dürfen als in entwickelten Ländern, neueren Entwicklungen Rechnung getragen.

Methodisch ist die Arbeit durchaus anspruchsvoll. Die Studie nutzt Citizen Science, Fernerkundung, Feldarbeit und Literatur, um Überschwemmungskarten zu erstellen und landwirtschaftliche Schäden im Bui-Flusseinzugsgebiet zu bewerten. Die Felddaten wurden unter anderem genutzt, um Hochwasserschadensfunktionen für Reisanbau, Nicht-Reisanbau und Aquakultur zu entwickeln. Zu würdigen ist daneben, dass die Feldarbeiten und Befragungen vor Ort zum Teil unter Corona-Bedingungen durchgeführt worden sind und vieles von Deutschland aus organisiert werden musste, was erschwerend wirkte.

Prof. Dr. Konrad Miegel

Universität Rostock Traditio et Innovatio

From the Department of Hydrology and Applied Meteorology

of the Faculty of Agricultural and Environmental Sciences

An Integrated Approach to Flood Risk Assessment Engaging Citizen Scientists for Bui River Basin, Vietnam

Dissertation

to obtain the academic degree of Doctor of Engineering (DEng)

at the Faculty of Agricultural and Environmental Sciences

of the University of Rostock

submitted by M.Sc. Ngoc Huan Tran

Born in Nam Dinh, Vietnam

Rostock, 2025

Reviewers:

1. Prof. Dr. Konrad Miegel

   University of Rostock, Department of Hydrology and Applied Meteorology

2. Prof. Dr. Jan Seibert

   University of Zürich, Department of Geography

3. Prof. Dr. Robert Jüpner

   University of Kaiserslautern-Landau, Department of Civil Engineering, Hydraulic Engineering and Water Management

Year of submission: 2024

Year of defense: 2025

Summary

Flooding is the most prevalent natural hazard, significantly affecting humans, the economy, and society. Flood risk assessment plays a pivotal role in identifying potential risk areas, evaluating the efficacy of mitigation measures, and proposing suitable strategies. However, this assessment necessitates a substantial quantity of data and information, which is often inadequate in developing countries like Vietnam, particularly in rural areas. Recently, citizen science has emerged as a promising way to gather massive amounts of information. Combined with free and high-resolution remote sensing data, it has the potential to provide valuable data and information for all components of flood risk assessment. Therefore, the goal of this research is to propose an integrated approach for flood risk assessment in data-scarce areas, combining citizen science, remote sensing, field surveys, and literature data. This approach is being applied to a pilot area in the Bui River Basin, Vietnam.

Firstly, a citizen science program was developed to collect flood-related data including flooding situations in the residential area, land-use, flood damage to paddy fields, and rainfall in the Bui River Basin. Citizens in and around the flood-affected area proactively collected and shared flood-related data using data collection apps or paper forms as citizen scientists. 60 citizen scientists contributed 649 completed questionnaires and measurements for the study area over two years. 10% of the citizen scientists, who provided more than 50 data per person, contributed 55% of the data collection for two years, while 45% of the citizen scientists provided a single time. A comparison between citizen science data and other independent data was made, where the overall agreement or correlation coefficient was over 70%, indicating good data quality. The results of this research suggest that citizen involvement in rainfall monitoring fosters sustained participation in the collection of flood-related data, enabling updates on data timely.

Next, this research proposed a DTM-based approach to developing flood maps using flood levels and a digital terrain model (DTM). The flood levels on bare land were determined by intersecting flood boundaries retrieved from Sentinel-1 images with the DTM, while those in residential areas were determined based on the flooding depth from citizen science, field surveys, and terrain elevation at these flooded points. This method was used to develop inundation maps for three events that occurred in 2017, 2018, and

2022. The inundation maps of the two former events were compared with flood-affected areas retrieved from district authorities and a model-based approach. The results showed that this novel approach can reasonably estimate flood extent and depth. The accuracy of the inundation map depends on the number of flooding points in residential areas and the date of the flood image in comparison to the maximum flood level date. Flood probability analysis was conducted for the Bui River Basin, determining that the 2022, 2017, and 2018 flood events were equivalent to 10-, 13-, and 50-year flood events, respectively. This novel approach shows a promising way for developing flood maps in data-scarce areas.

Lastly, the flood risk to agricultural production was estimated by combining flood hazard maps, a land-use map, gross production values for three types of agricultural land, and stage damage functions. The stage damage functions for the paddy crop, nonpaddy crops, and aquaculture were developed based on damage rates and flooding depths gathered from field surveys, citizen science, and literature. The expected annual flood damage in the pilot area to agricultural production is approximately € 65,386, a crucial parameter used for estimating the effectiveness of flood mitigation measures in the future. The results of this research showed an integrated approach to flood risk assessment in data-scarce areas by integrating data from remote sensing, citizen science, field surveys, literature, and open-access sources.

Keywords: Bui River Basin, citizen science, data-scarce areas, flood mapping, flood risk, field surveys, land-use, rainfall monitoring, satellite images, stage damage functions, Vietnam.

Zusammenfassung

Ein integrierter Ansatz zur Hochwasserrisikobewertung unter Einbeziehung von Bürgerwissenschaftlern für das Bui-Flusseinzugsgebiet, Vietnam

Überschwemmungen sind die am verbreitetsten Naturgefahr und haben erhebliche Auswirkungen auf die Menschen, die Wirtschaft und die Gesellschaft. Die Hochwasserrisikobewertung spielt eine zentrale Rolle bei der Identifizierung potenzieller Risikogebiete, der Bewertung der Wirksamkeit von Abhilfemaßnahmen und der Entwicklung geeigneter Strategien. Für diese Bewertung ist jedoch eine große Menge an Daten und Informationen erforderlich, die in Entwicklungsländern wie Vietnam, insbesondere in ländlichen Gebieten, oft unzureichend sind.

In letzter Zeit hat sich die Bürgerwissenschaft als vielversprechender Weg erwiesen, um große Mengen an Informationen zu sammeln. Kombiniert mit kostenlosen und hochauflösenden Fernerkundungsdaten hat sie das Potenzial, wertvolle Daten und Informationen für alle Komponenten der Hochwasserrisikobewertung zu liefern. Ziel dieser Forschungsarbeit ist es daher, einen integrierten Ansatz für die Hochwasserrisikobewertung in datenarmen Gebieten vorzuschlagen, der Bürgerwissenschaft, Fernerkundung, Feldbesichtigung und Literaturdaten miteinander kombiniert. Dieser Ansatz wird in einem Pilotgebiet im Bui-Flusseinzugsgebiet in Vietnam angewendet.

Zunächst wurde ein Bürgerforschungsprogramm entwickelt, um überschwemmungsbezogene Daten zu sammeln, darunter zur Überschwemmungssituation in Wohngebieten, zur Landnutzung, zu Überschwemmungsschäden an Reisfeldern und zu Niederschlägen im Bui-Flusseinzugsgebiet. Bürger, die im von der Überschwemmung betroffene Gebiet oder in seiner Umgebung leben, sammelten proaktiv hochwasserbezogene Daten und teilten sie mit Hilfe von Datenerfassungs-Apps oder Papierformularen mit. 60 dieser Bürgerwissenschaftler trugen über zwei Jahre mit 649 ausgefüllten Fragebögen und Messungen für das Untersuchungsgebiet bei. 10 % der Bürgerwissenschaftler, die mehr als 50 Daten pro Person zur Verfügung stellten, waren zu 55 % an der Datenerhebung über zwei Jahre beteiligt, während 45 % der Bürgerwissenschaftler nur ein einziges Mal Daten lieferten.

Es wurde ein Vergleich zwischen den Daten der Bürgerwissenschaftler mit anderen unabhängigen Daten durchgeführt, wobei die Gesamtübereinstimmung bzw. der Korrelationskoeffizient über 70 % betrug, was auf eine gute Datenqualität hindeutet. Die Ergebnisse dieser Untersuchung legen nahe, dass die Beteiligung der Bürger an der Niederschlags- und Hochwasserüberwachung eine nachhaltige Beteiligung an der Erhebung hochwasserbezogener Daten fördert und eine zeitnahe Aktualisierung der Daten ermöglicht.

Als nächstes wurde ein DTM-basierter Ansatz zur Entwicklung von Überschwemmungskarten unter Verwendung von Hochwasserständen und einem digitalen Geländemodell (DTM) vorgeschlagen. Die Überschwemmungshöhen in unbebauten Gebieten wurden durch die Verschneidung von Überschwemmungsgrenzen aus Sentinel-1-Bildern mit dem DTM bestimmt, während die Überschwemmungshöhen in Wohngebieten auf der Grundlage von Bürgerbefragungen, Feldbesichtigungen und der Geländehöhe an diesen überschwemmten Punkten bestimmt wurden. Diese Methode wurde genutzt, um Überschwemmungskarten für drei Ereignisse in den Jahren 2017, 2018 und 2022 zu erstellen. Die Überschwemmungskarten der beiden vorangegangenen Ereignisse wurden schließlich mit den von den Bezirksbehörden ermittelten Überschwemmungsgebieten und einem modellbasierten Ansatz verglichen.

Die Ergebnisse zeigen, dass mit diesem neuartigen Ansatz das Ausmaß und die Tiefe von Überschwemmungen vernünftig abgeschätzt werden kann. Er ist damit ein vielversprechender Weg für die Erstellung von Überschwemmungskarten in datenarmen Gebieten. Ihre Genauigkeit hängt von der Anzahl der erfassten Überschwemmungspunkte in Wohngebieten und der zeitlichen Übereinstimmung des Hochwasserbildes mit dem Datum des maximalen Hochwasserstands ab. Die Analyse von Hochwasserwahrscheinlichkeiten im Bui-Flusseinzugsgebiet ergab, dass die Hochwasserereignisse von 2022, 2017 und 2018 einem 10-, 13- bzw. 50-jährlichen Hochwasser entsprechen.

Schließlich wurde das Hochwasserrisiko für die landwirtschaftliche Produktion durch die Kombination von Überschwemmungskarten, einer Landnutzungskarte, Bruttoproduktionswerten für drei Arten von landwirtschaftlichen Flächen und Schadenskurven geschätzt. Die Schadensfunktionen wurden für Reisanbau, Nicht-Reisanbau und Aquakultur auf der Grundlage von Schadensraten und

Überflutungstiefen entwickelt, die durch Feldbesichtigung, Bürgerforschung und Literatur gesammelt worden sind. Der erwartete jährliche Hochwasserschaden für die landwirtschaftliche Produktion im Pilotgebiet beträgt ca. € 65.386. Er ist ein entscheidender Ausgangswert für die Abschätzung der Wirksamkeit von Hochwasserschutzmaßnahmen in der Zukunft.

Schlüsselwörter: Bui-Flusseinzugsgebiet, Bürgerwissenschaft, datenarme Gebiete, Überschwemmungskarten, Hochwasserrisiko, Feldbesichtigung, Landesnutzung, Niederschlagsüberwachung, Satellitenbilder, Tiefenschadensfunktionen, Vietnam.

Acknowledgements

Pursuing a Ph.D. in Germany has been an unforgettable journey that I could not have done alone. Fortunately, I've had the constant support of my supervisor, organizations, colleagues, friends, and family throughout this journey.

Firstly, I would like to express my sincere gratitude to Prof. Dr. Konrad Miegel for giving me the opportunity to pursue a Ph.D. at Rostock University. This once-in-a-lifetime opportunity allowed me to explore the world, build personal development skills, and become an independent researcher. His guidance was instrumental in completing my research. His insightful ideas and suggestions have greatly enriched my dissertation, making it stronger and more compelling.

Secondly, I am grateful for the financial support of the Catholic Academic Exchange Service, the Friedrich and Irmgard Harms Foundation at the Rostock University, and the German Academic Exchange Service for my Ph.D. research. I would also like to thank Hanoi University of Natural Resources and Environment (Vietnam) and Technical University of Delft (Netherlands), for their additional financial support for my work and fieldwork in Vietnam. I also acknowledge the critical support I received from SmartPhones4Water, College of Land Management and Rural Development (Vietnam), and Institute of Ecological Research and Planning (Germany).

Next, I would like to thank my colleagues and friends, who support me not only in academic matters but also in daily matters. Although I cannot mention each of them by name, I want them to know that everyone I have met during this journey has left a lasting impression on me. Their support, understanding, and encouragement have made this journey not only possible but also enjoyable. I hope that, when they read this acknowledgment, they will recognize the special role they have played in my journey.

In addition, I would also like to thank the citizens who took the time and effort to participate in my Ph.D. research as citizen scientists. Their participation and input contributed to the success of this research.

Finally, I am deeply grateful to my parents, my brother, and my sisters for their unconditional love and support. To my wife, Thi Huong Vu, thank you for your constant encouragement, patience, and companionship. Living far from home has only deepened my appreciation of the saying, *"Family always comes first."*

List of Contents

List of Figures

List of Tables

List of Abbreviations

Abbreviations	Full descriptions
API	Application Programming Interface
dB	Decibel
DEM	Digital Elevation Model
DTM	Digital Terrain Model
CS	Citizen Science
ESA	European Space Agency
FAO	Food and Agriculture Organization
FRA	Flood Risk Assessment
GEE	Google Earth Engine
HEC	Hydraulic Engineering Center
GIS	Geographical Information System
ICT	Information and Communication Technology
LU	Land-use
MSI	Multispectral instrument
NASA	The National Aeronautics and Space Administration
NCHMF	National Center for Hydro-Meteorology Forecasting
NSE	Nash Sutcliffe Efficiency
OA	Overall Accuracy
ODK Collect	Open Data Kit (ODK) Collect app
QGIS	Quantum Geographical Information System
RMSE	Root Mean Square Error
RS	Remote Sensing
SRTM	Shuttle Radar Topography Mission
S-1	Sentinel 1
S-2	Sentinel 2
USACE	U.S. Army crops of Engineers
VH	Vertical transmission – horizontal receiver
VV	Vertical transmission – vertical receiver

1 Introduction

1.1 Background

Flooding significantly affects human society globally, causing 50% of all economic losses (Munich RE, 2013). In the past decades, flood consequences have increased because of rising flood frequency and magnitude, climate change, population growth, and economic development (B. B. Shrestha et al., 2016). For instance, Pakistan faced a historic flood that affected 20 million people and lost around € 40 billion in 2010 (UNISDR, 2017). One year later, a massive flood slammed southeast Asia, destroying numerous nations, including Cambodia, Laos, Myanmar, Thailand, and Vietnam (UNISDR, 2017). Recently, the 2021 exceptional flood event in western Germany and nearby regions damaged € 32 billion, being one of the five costliest natural disasters in the last fifty years in Europe (Mohr et al., 2022). With the immense losses and damage caused by floods, it is necessary to take action to manage floods effectively.

Flood risk assessment (FRA) is one of the first and most important stages in flood management, which determines the potential risk areas and proposes appropriate measures to reduce negative impacts in the future (Ferri et al., 2020). According to the Sendai Framework for Disaster Risk Reduction, flood risk is specified as a function of three main aspects: flood hazard (i.e. flooding depth, extent, and duration), exposure (i.e. the population, assets, and buildings), and vulnerability (i.e. the aspects that influence the susceptibility of the exposed objects to the hazard) (UNISDR, 2015a). Flood risk can be quantified in terms of monetary damage as annual flood damage used to estimate the effectiveness of structural and non-structural measures (Ferri et al., 2020). This approach has been indicated and assessed by Englhardt et al. (2019), Ferri et al. (2020) and Pham et al. (2018). FRA is a complex task consisting of many sub-components within each aspect (de Moel et al., 2015).

Flood hazard is the likelihood that a flood of a specific intensity will occur within a particular area and in a certain time period (Ferri et al., 2020). Flood hazard assessment and mapping are critical tasks in flood risk assessment and management to reduce flood impact (Sy et al., 2019). Flood hazard assessment anticipates flood magnitude and frequency by analyzing flood scenarios, while flood hazard mapping visualizes potential endangered areas following a given flood scenario (de Moel et al., 2015). Flood hazard

characteristics consist of many dimensions (flooding depth, duration, velocity, spatial and temporal dynamics) (de Moel et al., 2015), which are generally estimated through hydrological and hydraulic modeling (Trinh & Molkenthin, 2021).

The exposure reflects the economic values of objects affected by flood hazards (Ferri et al., 2020). Land-use maps (i.e., building, infrastructure, agricultural land) and population distribution maps are used to describe exposure regarding affected sectors or economic activities (Merz et al., 2010). Land-use maps are mainly obtained through remote sensing imageries with the support of ground truth data as validation datasets (Gerl et al., 2014; Phan et al., 2019). Exposed objects are conventionally determined by combining the land-use map with the flooding map using the spatial analysis tools in the Geographical Information System (GIS) (Merz et al., 2010). In addition, land-use can be used as input data for flood modeling, providing runoff or roughness coefficients (Trinh & Molkenthin, 2021).

Flood vulnerability, which is the extent to which different objects, such as paddy fields, crops, and aquaculture areas will suffer damage due to the flood hazard. Flood vulnerability is primarily indicated using stage damage curves, representing the relationship between the potential damage of the exposed elements for different hazard levels (commonly flooding depth) (Glas et al., 2020). The stage damage curves are often established from empirical data collected after flood events or synthetic data collected through what-if questions, experiments, and expert opinions. (Huizinga et al., 2017; Merz et al., 2010). The stage damage curves can be developed for specific land-use categories (e.g. plantains, maize, etc.) (Glas et al., 2020) or mixed land-use categories (e.g. agricultural and residential land) (Perera et al., 2015), depending on the purpose of the research and the data availability.

Nowadays, remote sensing plays a fundamental role in flood risk assessment by granting valuable information on and insights into flood hazard, exposure, and flood vulnerability (Dong et al., 2016; Peter et al., 2022; Rahman & Di, 2020). The remote sensing images allow to quickly determine flood extent from small to large areas in real-time, near-real time, and the past (Notti et al., 2018; Tazmul Islam & Meng, 2022). The utilization of a topographic map and flood extent data obtained from remote sensing images enables the identification of flooding depth (Cohen et al., 2018; Giordan et al., 2018). In addition, agricultural land and urban structure mappings were obtained from high-resolution

satellite images (Dong et al., 2016; Gerl et al., 2014), which were used to estimate flood-exposed objects.

For flood vulnerability assessment, remote sensing data have been widely applied to assess flood-affected crops by comparison of vegetation indices between pre- and post-flood conditions or with and without flood conditions (R. Shrestha et al., 2013; Silleos et al., 2002). Vegetation indices have been used to evaluate the vegetation growth phase during the flood, allowing the choosing of appropriate stage damage functions (Klaus et al., 2016). By integrating the validation dataset obtained from field surveying or reliable data sources, remote sensing aids in quantifying the potential impacts of floods. However, the validation datasets, which require time and finance to collect, are often inadequate.

Recently, citizen science has emerged as a promising approach to providing supplementary data to assess and manage flood risk for data-scarce areas (Scaini et al., 2021). Citizen science, which involves the general public in scientific research progress (Buytaert et al., 2014; Shirk et al., 2012) and is supported by the advances of Information and Communication Technology (ICT), facilitates the collection of massive amounts of information and data recently (Buytaert et al., 2014). Citizen science has been commonly utilized in collecting flood hazard information such as flooding extent (Sy et al., 2020), flooding depth (Fohringer et al., 2015), flow velocity (Le Coz et al., 2016), and flooding duration (Sy, 2019). Furthermore, citizen science has contributed to provide land-use information through field trips (Assumpcao et al., 2019) and web-based crowdsourcing platforms (Sparks et al., 2015). In terms of flood vulnerability, citizen science have provided information on flood damage and assessed local strategies for flood disaster reduction through field surveys implemented by researchers (Perera et al., 2015; Peters-Guarin, 2008). Additionally, citizen science programs might enhance locals' awareness of flood disaster prevention and strengthen community resilience, thereby acting as a nonstructural measure in flood risk management (Ferri et al., 2020; Pandeya et al., 2021).

Flooding is also a major threat in Vietnam, often resulting in casualties and substantial economic losses (Luu et al., 2019). The Bui River Basin, which is drained by the two main rivers, Tich and Bui, is a sub-catchment of the Nhue-Day River Basin in the northern Vietnam. Bui River Basin has been experiencing flooding challenges due to the

adverse effects of land-use change, climate change recently, and the complexity of terrain features. The frequency and intensity of flood events in the Bui River Basin have increased, with notable occurrences in 2017, 2018, and 2022 (N. H. Tran et al., 2022). Remarkably, the flood in July 2018, which lasted for over 20 days, significantly affected people, property, and agricultural production.

1.2 Problem statement

Flood risk assessment requires a large amount of data and information, such as meteo-hydrological and topographical data, land-use maps, and past flood damage data (Apel et al., 2009; Glas et al., 2016). Flood-related data collection, however, faces obstacles in developing countries, particularly in Asian and African regions, due to time constraints, limited funding, and inadequate tools (Glas et al., 2020; Huizinga et al., 2017; Sy et al., 2019). Many researchers used outdated land-use maps, which can reduce the accuracy of flood exposed objects and flood damage (Ferri et al., 2020; Glas et al., 2016). The absence of stage-damage curves in numerous areas presents a significant obstacle to the flood risk assessment (Huizinga et al., 2017). Some researchers employed stage damage curves developed from average continental or regional values, which might not accurately reflect the local characteristics of the study areas (Glas et al., 2020; N. Y. Nguyen et al., 2017).

Over the last two decades, many researchers have been applying citizen science programs engaging citizens in collecting flood risk-related data on flood hazard, land-use, and flood vulnerability (Assumpcao et al., 2019; Olteanu-Raimond et al., 2018; Peters-Guarin, 2008; Sy, 2019). However, current studies have rarely examined the potential of citizens in collecting data about three data types in one citizen science program. Additionally, some researchers have involved citizens for collecting data without validating data (Assumpcao et al., 2019; Le Coz et al., 2016), despite validation being essential to understand the reliability and limitations of this approach. Moreover, citizen science programs have collected data only once (Assumpcao et al., 2019; Perera et al., 2015) and have not involved citizens in ongoing updates to flooding situations, monitoring land-use change (Tsiakos et al., 2019), and updating flood damage (Merz et al., 2010).

Flood hazard assessment tools frequently rely on coupled hydrological and hydraulic

models to provide detailed information on flood hazards, such as flood extent, depth, duration, and velocity (Patel et al., 2017; Trinh & Molkenthin, 2021). However, such approaches require a large amount of data, such as topographic maps, cross-sections, and meteo-hydrological data, which can be challenging in ungauged catchments or data-scarce areas (de Moel et al., 2015; Glas et al., 2018). Remote sensing data, particularly Synthetic Aperture Radar (SAR) images, has been widely applied to document flood extent combined with photographic maps to estimate flooding depth.

While SAR image are effective in detecting the extent of flooding in large areas, theirs primary application has been in flood mapping of bare land and flat areas free of buildings (hereinafter referred to as "bare land") (Mason et al., 2021). These images are less effective in detecting the extent of flooding in built-up areas due to the complex backscattering mechanisms involved (Mason et al., 2021; Tsyganskaya et al., 2018a). In contrast, citizen scientists primarily contribute to flooding information in residential areas through images, videos, or their memories (Azizi et al., 2023; Fohringer et al., 2015). Therefore, combining the two approaches allows us to better determine the flooding situation for the entire area.

Although Bui River Basin experiences flooding regularly, there have been few studies on flood risk assessment here, particularly in rural areas. In fact, there is a lack of scientific attention in flood risk assessment in rural areas or for agricultural sectors (Klaus et al., 2016) due to the expected losses being much lower than in urban areas (Glas et al., 2016), or data unavailability (Chau, 2014). This lack of flood risk assessment can lead to poor decisions in identifying effective flood mitigation measures. It is, therefore, imperative to assess flood risk in rural areas in developing countries like Vietnam to better understand the impact of flooding on rural areas.

1.3 Research objectives and questions

The research aims at proposing an integrated approach to flood risk assessment in the context of data-scarce areas by utilizing citizen science, remote sensing, field surveys, and literature. The three research objectives are to

- Develop a citizen science approach to collecting flood risk-related data,
- Propose a novel approach to developing flooding maps, and

- Estimate the annual flood damage to agricultural production.

To achieve the research objectives, the following research questions are stated:

- Is engaging citizen scientists in the campaign of flood risk-related data collection an appropriate way to close the flood information gap?
- How can data from remote sensing, field surveys, and citizen science be combined to develop flood maps?
- How should stage-damage curves look? And
- What is the annual flood damage to agricultural land in the study area?

1.4 Research framework

The research framework comprises three main components: engagement of citizen scientists in flood data collection (N. H. Tran et al., 2024), a simple approach for flood hazard assessment (Mason et al., 2021), and annual estimation of flood damage for agricultural areas (B. B. Shrestha et al., 2016) (Figure 1.1).

Firstly, citizen scientists' engagement in flood risk-related data collection was implemented to gather key information for the study area (N. H. Tran et al., 2024). Citizen scientists residing in both the flood-affected areas and surrounding regions provide and update flood-related data, including flooding situations in residential areas, land-use information, flood damage to paddy crops, and rainfall. Secondly, flood hazard maps were generated using data on flooding information in residential areas collected by citizen scientists or during field surveys and flooding extent on bare land retrieved from remote sensing. Digital terrain model (DTM) was used for determining flood levels in residential and bare land, and estimating the flooding depth for the entire study area (Mason et al., 2021).

In addition, a particularly historical events-based flood hazard assessment was employed to estimate flood damage to agricultural land (Chau, 2014; Luu & von Meding, 2018; B. B. Shrestha et al., 2016). The land-use map, which includes agricultural land, was developed using remote sensing data. The validation dataset was achieved through citizen science and field surveys. The relative damage function approach was utilized to estimate flood damage to agricultural land, encompassing paddy fields, crops, and aquaculture. Since the majority of flood damage data gathered by citizen scientists or

provided by locals belongs to paddy fields, a stage damage curve specific to paddy fields was developed. Stage damage curves for other objects, which have been published in the literatures (N. Y. Nguyen et al., 2017; H. N. Pham et al., 2018) were adopted for the study area. Based on documented flood data at a gauging station, the flood frequency of the investigated flood events was estimated, enabling the development of a damage-probability curve. Subsequently, annual flood damage for the study area could be estimated.

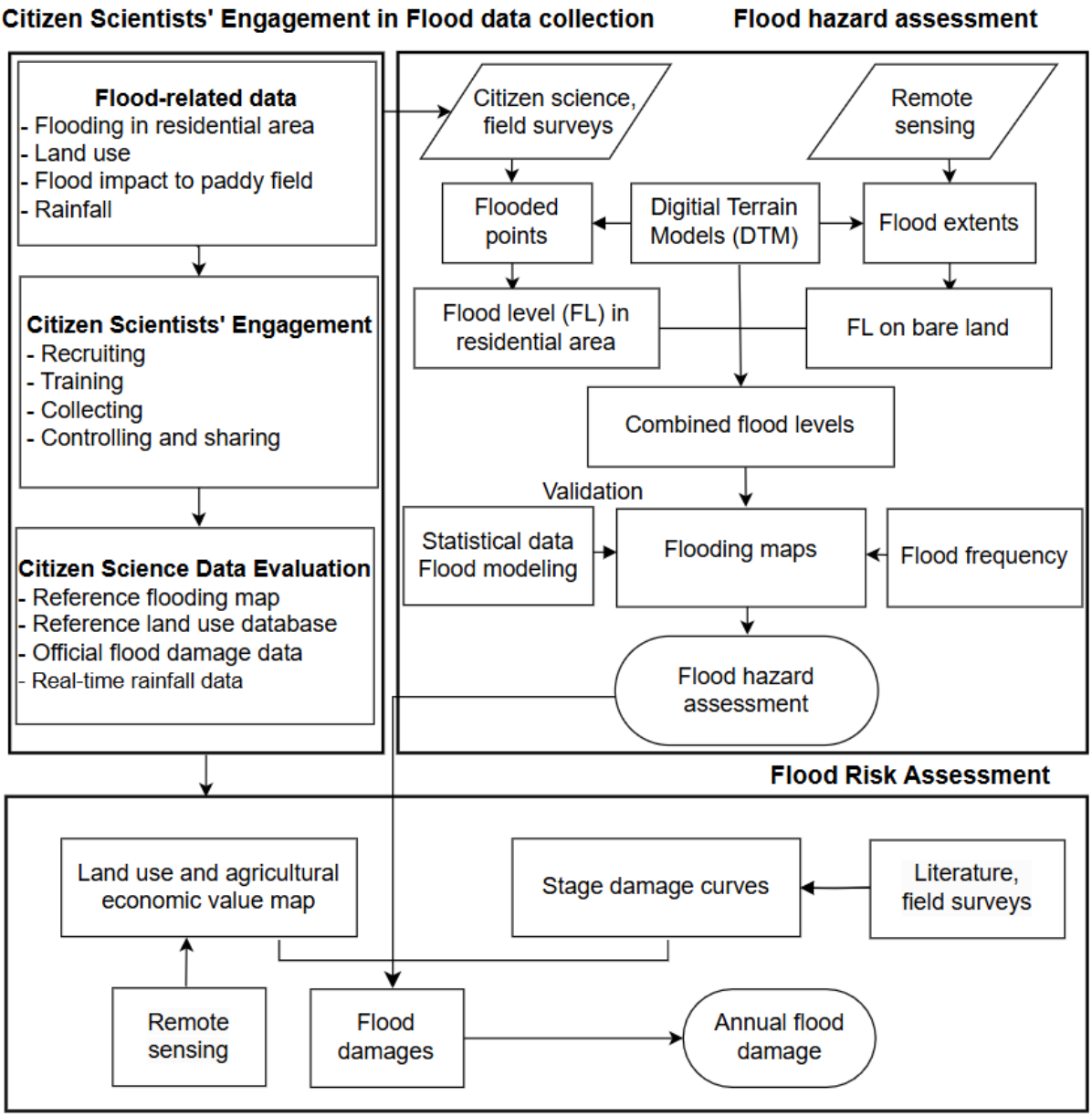

Figure 1.1. Conceptual framework of an integrated approach to flood risk assessment

1.5 The scope of work

This research focuses on flood risk assessment for the rural area in the Bui River Basin,

Vietnam, where flood-related data are limited. The flood hazards are confined to actual floods in 2017, 2018, and 2022. The flooding maps only consider the flooding depth aspect, which is the most important factor in assessing flood damage. When estimating the flood impact on the agricultural sector, the research is limited to the calculation of direct flood impact on agricultural production, including paddy rice, crops, and aquaculture areas, which contribute to more than 80% of agricultural production values in the study area. The land-use map of 2022 obtained from remote sensing was used to estimate flood-exposed agricultural land. The paddy field's stage damage curve is developed based on data from citizen science and field surveys, while previously published stage damage curves for crops and aquaculture areas were adjusted for the study area. This research did not consider the role of seasonal crop variability in flood damage as well as the impact of climate change on flood disasters in the study area.

1.6 Thesis structure

The thesis consists of six main chapters. Chapter 1 is about an introduction to the study, including background, problem statements, research objectives, and research scope. In Chapter 2, the theoretical and principal basics of flood risk assessment are presented. Also, the chapter provides an overview of applications of citizen science and remote sensing in flood-related data collection and flood risk assessment. In addition, the strengths and weaknesses of current approaches in flood risk component assessment are shortly discussed here. In chapter 3, the working basics and methodology presents the approach and methodology applied in this research. In addition, this chapter provides an overview of the study area and analyses data availability and the input data for the methods used. In chapter 4, the results of community-based flood data collection, flood hazard assessment, and estimated flood risk to agricultural land are denoted. Then, the findings of this research are discussed in chapter 5. Finally, chapter 6 highlights the conclusions, limitations and recommendations of this research.

All gathered, collected and calculated data relating to this research are presented in the Appendixes.

2 Theoretical and principal basics

This chapter presents essential definitions of terms associated with flood, flood risk, and its components. It also provides brief information on spatial scales and phases in flood risk assessment. A significant focus is placed on the role of remote sensing in estimating flood risk components, alongside an examination of citizen science as a contemporary approach to flood-related data collection. The text also addresses the limitations of these two approaches, anticipating challenges that may arise during their application. This chapter concludes by summarizing key features and identifying gaps associated with relevant issues, which is fundamental for proposing an integrated approach to flood risk assessment.

2.1 Flood and flood risk

2.1.1 Kinds of floods

A flood is defined as a temporary condition of surface water in a stream or other water bodies, where water levels or discharge exceed certain values, resulting in submergence of floodplain areas or usually dry regions (Luino, 2016). Floods are often triggered by heavy rains, storms, rapid snowmelt, dam bursts, or storm surges in coastal areas (David & Schmalz, 2020; Trinh, 2023). Based on their causes, floods are classified into four main types: coastal floods, flash floods, river floods, and urban floods (Kron, 2005). Each type has its own characteristics and affects different objects. River floods typically affects residential areas and agricultural production in rural areas (Forster et al., 2008; H. N. Pham et al., 2018).

2.1.2 Impact of flooding

Flooding happens when water levels rise, spilling over natural banks or dykes and submerging previously dry areas, or when rainwater accumulates on saturated ground (Luino, 2016). Flooding often occurs in rural areas, which have a weak adaptive capacity to floods (Forster et al., 2008; H. N. Pham et al., 2018). Rural areas often serve as flood retention zones to protect urban areas (Klaus et al., 2016). Consequently, some rural areas are not as well-protected as urban areas (Kuhlmann, 2010). Although rural areas regularly experience flooding, there is a lack of scientific attention in flood risk assessment or flood damage estimation (Klaus et al., 2016).

Generally, flood damage can be classified as direct or indirect damage, and tangible or intangible damage (Table 2.1) (Penning-Rowsell et al., 2003). It encompasses damages related to people and belongings, economic activities (industrial and agricultural productions), infrastructure, and environment, and cultural heritage sites (Yang, 2017). Direct damage encompasses losses incurred through directly physical contact with floods such as damage to buildings, their contents and infrastructure (Figure 2.1), while indirect damage is caused by direct impacts and happens – in space or time – outside the flood event (Merz et al., 2010). Tangible damage refers to damage to manufactured capital or resources flows that can be easily evaluated in monetary terms, while intangible damage comprises losses that cannot be easily calculated in terms of monetary values (Merz et al., 2010). It is imperative to define the types of flood damage before conducting flood risk analysis and damage assessment (Meyer et al., 2007). For instance, human loss or environmental loss symbolizes some intangible damage typically.

Table 2.1. Flood damage types

	Direct	Indirect
Tangible	Building Crops Infrastructures	House cleaning costs Traffic disruption Natural habitat
Intangible	Life loss Environmental pollution Land fertilizer reduction	Reduced trust in government Trauma Business opportunity

Source: (Penning-Rowsell et al., 2003)

Source: at https://www.channelstv.com/2021/07/15/updated-at-least-42-dead-in-germany-as-storms-ravage-europe/ – Ferdinand MERZBACH / NEWS5 / AFP

Figure 2.1. Houses, properties, and landscapes flooded after heavy rainfall and floods in western Germany in July 2021

Flooding affecting paddy fields in Bui River Basin, Vietnam, in May 2022

Flooding affecting a residential area and travel in the Bui River Basin, Vietnam, in September 2022 [1]

Figure 2.2. Flooding in the Bui River Basin, Vietnam in 2022

[1] https://infonet.vietnamnet.vn/ha-noi-nuoc-song-bui-len-cao-hang-tram-nha-ngap-bo-doi-xuyen-dem-giup-dan-chay-lu-419472.html

Many flood damage evaluations primarily focus on evaluating direct damages, aiming for simplicity (Messner & Meyer, 2005). Conventionally, indirect damages are typically evaluated by using a given percentage of the direct damage (Messner & Meyer, 2005). However, omitting other types of damage significantly underestimates the general flood damage, especially in rural areas. Pham et al. (2018) conducted a comprehensive assessment of direct and indirect damage estimation for agricultural production activities, demonstrating that indirect and intangible damages accounted for 60% of the total damage.

2.1.3 Flood risk components

Over the last few decades, there have been numerous definitions of flood risk, varying based on scientific fields and research purposes (de Moel et al., 2015; M. T. Nguyen et al., 2021). Blaikie et al. (1994) described risk as a consequence of both hazards and political and socio-economic conditions, making people and places vulnerable. For the engineering and natural sciences, 'flood risk' is defined as a combination of three main aspects: flood hazard, exposure, and vulnerability (de Moel et al., 2015; UNISDR, 2015a). This widely accepted concept was used in this research:

$$Flood\ Risk = Hazard \times Exposure \times Vulnerability \qquad (Eq\ 2.1)$$

Source: https://www.un-spider.org/risks-and- disasters/disaster -risk-management

Figure 2.3. The relationship between flood hazard, exposure, vulnerability, and flood risk

'Flood hazard' represents the probability of a flood of a specific intensity occurring within a particular area and during a certain time period (Ferri et al., 2020). The occurrence probability considers the likelihood of a flood due to events such as rainfall or storms and the probability of floodwaters reaching a specific location (Merz et al.,

2010). The intensity of flooding includes various aspects (e.g., depth, duration, velocity), making flood hazard assessment complex (de Moel et al., 2015). The flooding depth is most often utilized to assess flood hazard, which is estimated, or recorded conveniently, while other parameters are mostly not investigated (Luu et al., 2017; Ribeiro et al., 2020). The methodology for estimating flood hazard depends on the spatial scale, research purpose, and data availability (de Moel et al., 2015). However, the foundation of each flood hazard assessment is sufficient observational data (de Moel et al., 2015).

The term 'exposure' indicates the number of assets, people, land-use, etc., that may be affected by a flood (Yang, 2017). The population distribution or land-use maps were overlaid with inundation maps to determine the flood-exposed or non-flood-affected areas through operations within a geographic information system (Merz et al., 2010). Exposure assessments often involve physical assets and people (Ferri et al., 2020). Furthermore, other exposure objects can be considered, such as cultural, environmental values, and factors associated with indirect effects (disruption of public services or traffic outside the flooded area) (Ferri et al., 2020; Animesh K. Gain et al., 2015; Kittipongvises et al., 2020).

In addition to flood hazard and exposure, the flood risk also depends on flood vulnerability. ‘Flood vulnerability’ refers to the extent to which various objects, such as communities, structures, infrastructure, economic activities, etc., are susceptible to damage related to flood hazards (National Research Council, 2015). Blanco-Vogt & Schanze (2014) proposed a more comprehensive concept of vulnerability, defining it as a mathematical function of the susceptibility, and coping capacity of a system taking into account physical, ecological, institutional, social, and economic dimensions. Typically, economic flood vulnerability estimation often uses stage damage functions, relating flooding depth to a certain damage value (Blanco-Vogt & Schanze, 2014; Glas et al., 2020). There are two main approaches to developing stage damage functions: empirical data collected after flood events and synthetic data obtained through hypothetical scenarios, experiments, and expert opinions (Huizinga et al., 2017; Merz et al., 2010).

2.2 Flood risk assessment

2.2.1 Spatial scales in flood risk assessment

2.2.1.1 Risk assessment at different scales

Numerous techniques and approaches have been set up to assess flood risk, ranging from global to local scales for different uses (de Moel et al., 2015). This means that flood risk can be assessed for the entire globe, a continent, or just a specific area of a river, coast, or countryside (Yang, 2017). While there is generally little differentiation in the methodological frameworks across most studies, variations in assessments become apparent when considering different spatial scales (de Moel et al., 2015).

The assessment of flood risk can typically be categorized into supra-national, macro-, meso-, and micro-scales (de Moel et al., 2015). However, the distinction between these scales is inherently subjective (de Moel et al., 2015). The supra-national scale focuses on assessments of the entire globe or continent, covering numerous countries and transboundary river basins (de Moel et al., 2015). Meanwhile, the macro-scale focuses on evaluations of entire countries, for which nationally consistent data are typically existing, but it encompasses several watersheds (de Moel et al., 2015). Both scales consider administrative units in their entirety, as illustrated by examples such as the Global Assessment Report (GAR) on Disaster Risk Reduction (UNISDR, 2015b) and the public disaster relief funds program in Europe (Hochrainer et al., 2010).

The meso-scale predominantly operates at the sub-national level, focusing on assessments of specific provinces, watersheds, or large cities (de Moel et al., 2015). Conversely, the micro-scale is the smallest spatial scale considered, directing attention to a particular river stretch in urban or rural areas (de Moel et al., 2015). Different scales necessitate distinct methods and serve varied objectives in assessing flood risks. Despite not being entirely independent, these approaches often complement each other (Englhardt et al., 2019).

2.2.1.2 Rural-scale flood risk assessment

Flood risk assessment in rural areas is recognized as operating at a micro-scale. It empowers decision-makers to identify the most vulnerable zones, estimate crop damage for compensation payments, and assess the effectiveness of flood control measures

(Forster et al., 2008; Hess & Morris, 1988). At the micro scale, flood risk assessment demands detailed data, including terrain elevation, infrastructure, waterworks, and land-use types. Typically, the research at this scale aims to optimize investments by evaluating the cost-effectiveness of measures for flood risk reduction, as demonstrated in the previous study by Merz et al. (2010). Additionally, some studies focus on creating hazard and risk maps to support micro-scale flood management and land-use planning (Forster et al., 2008; Hess & Morris, 1988).

While numerous studies examine flood risk in urban areas, there are only a few that explore in rural areas. This scarcity is mainly due to limited data and low damage rates in the rural regions (Englhardt et al., 2019; H. N. Pham et al., 2018). Despite these challenges, few case studies have been conducted in rural settings, such as Southwestern England (Hess & Morris, 1988), the Elbe River in Germany (Forster et al., 2008), and central Vietnam (H. N. Pham et al., 2018).

2.2.2 Flood risk assessment phase

Typically, flood risk assessment provides information about flood risks in the past, present, and future, encompassing hazard, exposure, vulnerability, and risk identification (Maleska, 2021). Flood hazard, exposure, and flood vulnerability are three primary components inside a logical risk assessment, as suggested in numerous studies (Apel et al., 2009; de Moel et al., 2015; Merz et al., 2010). Flood risk can be assessed qualitatively and quantitatively. Qualitative assessment focuses on determining flood risk zones (i.e., low, medium, and high-risk areas), while quantitative assessment focuses on estimating monetary damage. This research is limited to quantitative flood risk assessment.

2.2.2.1 Hazard assessment

Flood hazard refers to the probability of a potentially damaging flood event characterized by factors such as flooding depth, duration, velocity, and spatial and temporal dynamics (Foudi & Oses-Eraso, 2014). The higher the flood hazard, the more substantial the negative impacts might be in the context of flood hazard assessment (Ferri et al., 2020). The conventional approach to flood hazard assessment relies on the occurrence probability of floods with specific characteristics and time, wherein the occurrence time is calculated based on two flood events with similar magnitudes (the

so-called return periods) (Foudi & Oses-Eraso, 2014). Generally, probabilistic and statistical analysis of historical hydrological data is used to determine the occurrence probability of an event with specific characteristics occurring (Foudi & Oses-Eraso, 2014). Subsequently, flood modeling is deployed to transform the design floods connected to different return periods into flooding duration, depth, and velocity (Ferri et al., 2020; Forster et al., 2008; Trinh, 2023). Many researchers have shown that flooding depth is the most important and popular factor in flood hazard assessment (Dang et al., 2011; Glas et al., 2016; H. N. Pham et al., 2018).

The conventional approach to flood hazard mapping involves the use of hydrologic and hydraulic models to estimate the extent and depth of flooding corresponding to different return periods (Ferri et al., 2020; Trinh & Molkenthin, 2021). Flood modeling is applied to simulate and predict detailed hydrologic and hydraulic processes in the past, present, and future (Anjaneyulu et al., 2023; Animesh K. Gain et al., 2015) and demonstrates a high level of accuracy. This method highly relies on input data, including hydro-meteorological data, topographic maps, cross-sectional data, and waterworks information (Sy et al., 2019). However, such data are often unavailable in many areas, particularly in data-scare developing countries (Glas et al., 2016).

In addition to modeling, GIS and remote sensing techniques are commonly utilized in mapping flood hazards. Remote sensing enables the rapid establishment of flood maps before, during and after flood events (Giordan et al., 2018). Satellite images efficiently identify flooded areas over large expanses, providing a cost-effective solution (Giordan et al., 2018). However, remote sensing data are typically less effective in documenting flooded areas in built-up areas (Giordan et al., 2018). Moreover, conventional remote sensing methods struggle to detect flood levels or water depth (Agnihotri et al., 2019). Flooding depth maps can be generated based on flood extent derived from satellite images, combining this information with Digital Elevation Models (DEMs) (Cohen et al., 2018). While this approach offers a potential solution for areas with limited data availability, it is constrained in simulating future flood scenarios. Additionally, flood marks, when combined with DEMs, can be utilized to determine flooding depth maps through spatial analysis techniques in GIS (Giordan et al., 2018; Ribeiro et al., 2020; Zeng et al., 2020). Nevertheless, gathering flood marks requires significant time and cost (Giordan et al., 2018).

2.2.2.2 Exposure analysis

Exposure to flooding relies on the spatial distribution of the flooded area (Foudi & Oses-Eraso, 2014). To estimate exposure to a flood event, it is required to identify the objects within the flooded areas. Distinctions are often made between urban and rural areas when assessing flood exposure (Herath & Dushmanta, 2020; H. N. Pham et al., 2018). Objects at risk primarily in urban areas include residential and non-residential properties, environmental and cultural-archaeological assets, and public infrastructure (Foudi & Oses-Eraso, 2014). The objects at risk in rural areas are mainly crops, paddy fields, and aquaculture areas (H. N. Pham et al., 2018). Additionally, people living in flooded areas also experience the consequences of flooding (Foudi & Oses-Eraso, 2014). Determining these objects can be achieved using remote sensing and GIS through land-use maps or population distribution maps (Ferri et al., 2020; Merz et al., 2010). Exposed objects are conventionally determined by combining land-use data with flooding maps using spatial analysis tools in the GIS (Merz et al., 2010).

2.2.2.3 Vulnerability analysis

Conducting a vulnerability analysis for each susceptible object enables the assessment of potential flood damages (direct and indirect, tangible and intangible damage, see Section 2.1.2) for various return periods (Foudi & Oses-Eraso, 2014). The prevalent approach for estimating direct flood damages involves applying stage damage curves, which show the relationship between flood level and damage degree either in monetary terms or as a damage ratio (Messner et al., 2007). The latter one is chosen in this research.

There are different approaches to develop stage damage curves, which can conventionally be classified into empirical and synthetic analyses. Empirical analyses are based on data collected after flood events, while synthetic analyses are based on data collected via what-if questions, experiments, and expert opinions (Huizinga et al., 2017; Merz et al., 2010). The stage damage curves display the increase in damage ratio under flood hazard characteristics, following exponential or logarithmic shapes (Parodi, 2019). The appropriate stage damage curves are often validated through actual flood damage (N. Y. Nguyen et al., 2017). For agricultural crops, the logarithmic shape (S shape) provided better results than the exponential shape (N. Y. Nguyen et al., 2017; Badri

Bhakta Shrestha et al., 2021). Depending on the purpose of the research and data availability, stage damage curves can be developed for specific land-use categories (e.g., plantains, maize, etc.) (Glas et al., 2020) or use one general or typical land-use category (Perera et al., 2015).

Stage damage curves are a major source of the epistemic uncertainty of damage estimates for riverine floods (De Moel et al., 2012; Merz & Thieken, 2009). Commonly, there is little grasp of the processes related to flood damage (Parodi, 2019). Stage damage curves have been developed based on data retrieved from historical records or insurance claims. Vulnerability analysis are particularly challenging in countries where such data about flood damage are unavailable (Parodi, 2019). Insufficient post-flood damage data will hinder the flood damage model validation (de Moel et al., 2015). The appropriate stage damage curves are currently accessible only for certain countries like Germany (Sairam et al., 2021) and Japan (Dutta et al., 2003), usually where flood risk assessments have been meticulously conducted (Olesen et al., 2016). In many cases, stage damage curves are unavailable for developing countries, particularly in rural areas (H. N. Pham et al., 2018). In addition, stage damage curves have been built using a set of different assumptions (Schultz et al., 2010). Therefore, it is difficult to use the stage damage curves for areas that are different from the areas where they were originally developed (Fuchs et al., 2019; Schröter et al., 2014).

2.2.2.4 Flood risk assessment

The final stage in flood risk assessment involves combining the flood hazard characteristics, the features of the exposed objects, and the function of stage damage curves. The relationship between the above components and flood risk can be summarized in a four-graph diagram (Figure 2.4) modified from Foudi and Oses-Eraso (2014). The risk of flood is quantitatively represented by risk curves, specifically, a damage-probability curve where risk is estimated by the integral under the curve (Maleska, 2021). The chart situated in the top-left corner (1) delineates features of flood hazard through an exponentially declining correlation between flood return periods and the probability of exceedance (Foudi & Oses-Eraso, 2014). The chart situated in the top-right corner (2) depicts exposure with a rising relationship between the flooded area (elements at risk) and flood return period: the higher the return period, the larger the flooded area becomes (Foudi & Oses-Eraso, 2014). The chart situated in the bottom-

right corner (3) demonstrates vulnerability as an increasing correlation between the flooded area (elements at risk) and the damage caused by flooding (Foudi & Oses-Eraso, 2014). The chart in the bottom-left corner (4) establishes a connection between the probability of exceedance and monetary damage in the final risk curve: rare flood events result in high damages following an exponential function (Foudi & Oses-Eraso, 2014). The connection in chart (4) is called the damage-probability curve.

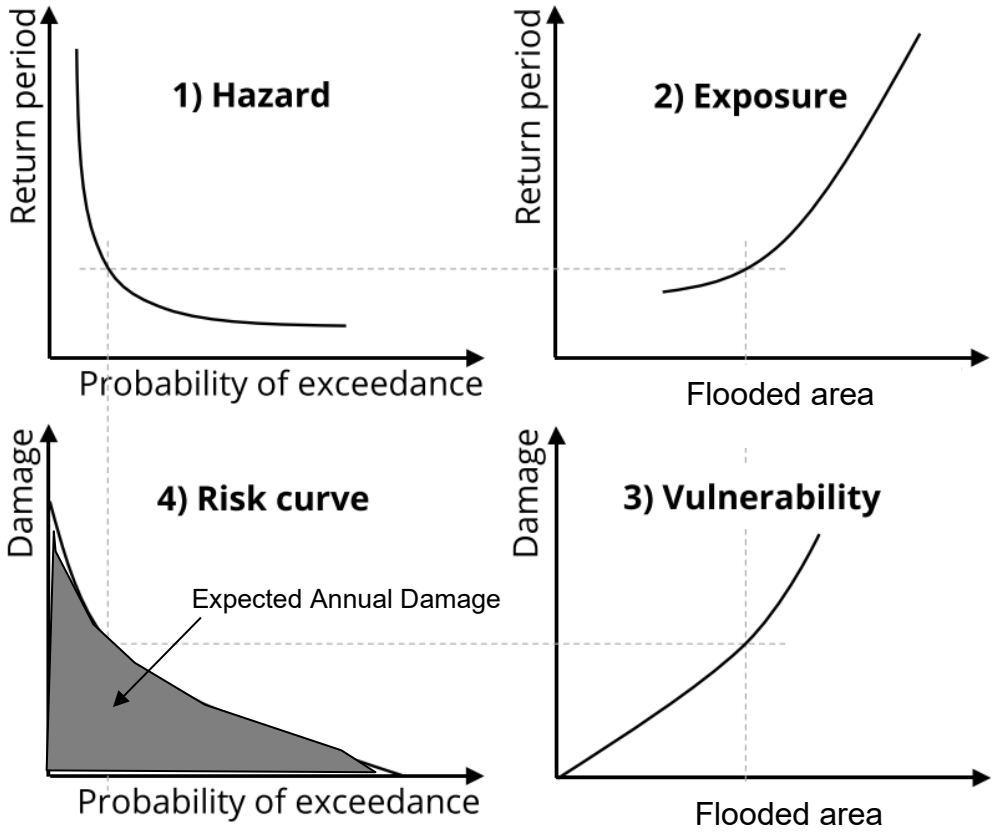

Source: (Foudi & Oses-Eraso, 2014)

Figure 2.4. Hazard, exposure, vulnerability, and risk curve

The damage - probability curve presents the relationship between flood damage and probability. To create precise the damage - probability curve, an adequate quantity of potential flood data should be informed (Foudi & Oses-Eraso, 2014). According to Messner et al. (2007), at least three and preferably six flood events with a range of severity magnitudes should be utilized to develop the risk curve. Most studies have used three flood events for developing risk curves (Ferri et al., 2020; Ţîncu et al., 2020). The risk curve is employed to estimate expected annual damage that is the most commonly utilized rate of flood risk (Foudi & Oses-Eraso, 2014).

Expected annual damage represents the mean of flood-related losses calculated across numerous years (Foudi & Oses-Eraso, 2014; Miegel, 2006). However, due to the limited availability of precise long-term data, the utilization of damage - probability curves becomes essential for estimation. The area below the damage - probability curve corresponds to the expected annual flood damage (Foudi & Oses-Eraso, 2014). Damage - probability curves and expected annual damage can be computed for the overall estimated flood damage or for specific categories such as buildings, agriculture, or health-related damages (Foudi & Oses-Eraso, 2014). These indicators are also used to estimate the benefits of flood mitigation measures (Foudi & Oses-Eraso, 2014; Miegel, 2006).

2.3 Remote sensing in flood risk assessment

2.3.1 Overview of remote sensing technologies

Remote sensing is a technology-driven method of data collection that involves gathering information about the Earth's surface from a distance (Mouazen et al., 2020). This is done by utilizing technology sensors installed at satellites, aircrafts, or unmanned aerial vehicles (UAVs) to record reflected or emitted energy from objects on the Earth's surface (Mouazen et al., 2020). Over the last decade, remote sensing data have been used for a wide range of applications, including environmental monitoring (Horning, 2008), agriculture (E. A. Beza, 2017), meteorology (Trinh & Molkenthin, 2021), urban planning (Bekele et al., 2022), and disaster management (Giordan et al., 2018). This research focuses on the application of remote sensing in flood disasters and its relevance.

Remote sensing equipment is normally classified into passive and active sensors (Horning, 2008). The passive sensor measures sun energy that is reflected from objects on the ground, while the active sensor creates its own signal which is emitted and measured after its reflection at the ground (Horning, 2008). A strength of the passive sensor is that it mainly depends on the sun's energy to sight the object and therefore does not need its own energy source. It means that they are suitable to measure objects during the daytime and cloud-free days (Horning, 2008). Some multispectral images (Landsat, and Sentinel 2), which are products of passive sensors, are used to estimate land-use (C. J. Davids et al., 2018), and permanent water bodies (DeVries et al., 2020a).

The active sensor, such as radar (RAdio Detection And Ranging) and lidar (LIght Detection And Ranging), release their own energy to irradiate objects, and are composed of a transmitter and receiver (Horning, 2008). Therefore, this sensor can operate in dark and all-weather conditions (Horning, 2008). The radar sensor can provide synthetic aperture radar (SAR) images (Sentinel 1, COSMO-SkyMed) to estimate flood extent in day and night time (Giordan et al., 2018). The lidar sensor provides the digital terrain models (DTM) such as Shuttle Radar Topography Mission (SRTM) and Advanced Spaceborne Thermal Emission and Reflection Radiometer (ASTER), which can be used to estimate flooding depth (Cohen et al., 2018; Giordan et al., 2018).

In the last two decades, advances in remote sensing and technology have presented the opportunity of developing flooding maps and estimating flood damage quickly (Cohen et al., 2019; DeVries et al., 2020b; Giordan et al., 2018). Satellite remote sensing data can be used to map the largely flood-effected area at different spatial and temporal resolutions (Notti et al., 2018). Furthermore, the increasing availability of free satellite data with global coverage (e.g., Sentinel-1 and -2, Landsat, and MODIS) allows for low-cost analysis of flooded areas (Notti et al., 2018). Typically, the massive amount of satellite data are inconvenient to process, manage, and store on local applications or hardware in personal computers (DeVries et al., 2020a). To support a variety of management decisions, especially timely response to an emergency, data must be rapidly identified, collected, integrated, processed, distributed, and visualized on the Internet (Liu et al., 2018). The emergence of a cloud computing flatform like the Google Earth Engine (GEE) opens an impressive chance for assessing, analyzing, and probably displaying flooding maps in near real time (DeVries et al., 2020a).

Nowadays, GEE has absolutely become the most powerful cloud processing tool, that significantly supports geographical big data analysis (Tamiminia et al., 2020). First, GEE contains an impressive number of datasets, both raw and pre-processed, and products accessible from local to global scale (Pérez-Cutillas et al., 2023). Second, GEE offers climatic, and geophysical datasets that are used as input for numerous models or applications, updated daily, and instantly available for assessment (Pérez-Cutillas et al., 2023). Finally, GEE provides the ability to use both information available on the platform and the user's own data, and to combine the GEE platform and GIS applications, a traditional approach in spatial analysis (DeVries et al., 2020a). Water

resources, natural disasters and agriculture-related topics are the three most widely applied areas on the GEE (Pérez-Cutillas et al., 2023; Tiwari et al., 2020).

2.3.2 Application of remote sensing in flood risk assessment

2.3.2.1 Flood hazard

a) Flood extent

Flood extent information is crucial for gaining a general understanding of flood phenomena, facilitating aid and mitigation efforts before, during, and after floods (Agnihotri et al., 2019; Munasinghe et al., 2018). In the early stages, flood extent detection often relies on remote sensing data, as it allows for the rapid capture of information during or right after the flood event (Giordan et al., 2018; Munasinghe et al., 2018; Shen et al., 2019). Remote sensing data are particularly useful for mapping and monitoring flood events in near real time, thanks to their ability to capture information in short revisit time and continuity (Agnihotri et al., 2019; Giordan et al., 2018; Singha et al., 2020; Tsyganskaya et al., 2018b). Furthermore, a series of satellite images can be employed to estimate flood dynamics throughout the year or to compare flooding situations between different years (Tiwari et al., 2020). This information is valuable for assessing the impact of floods on agricultural land on the GEE (Phan et al., 2019), and on river morphology (Agnihotri et al., 2019) in post flood studies.

Optical images, including MODIS, Landsat (7, 8), and Sentinel 2, have been used to determine the extent of floods (Giordan et al., 2018; Munasinghe et al., 2018; Vu et al., 2022). Decadal satellite surveillances (e.g., Landsat and MODIS) offer prospects for analyzing the flood extent changes over long time periods, supporting a holistic analysis of the relationship between flooding situations and other relevant factors (Vu et al., 2022). Recently, Sentinel 2 has been widely applied to determine flooded areas in Piedmont, northwestern Italy, particularly during the 2016 flood (Giordan et al., 2018). With the characteristics of multispectral data, optical images can be composed into true color images to identify objects such as flooded areas, roads, or flat areas (Giordan et al., 2018). However, the passive optical sensor relies on the solar energy and is unable to detect the Earh's surface during days filled with clouds (Singha et al., 2020). Additionally, medium-high-resolution multispectral satellites such as Sentinel-2 or Landsat 8, have a long revisit time, posing a challenge to capture flood images on the peak flow days (Giordan et al., 2018).

Radar images are primarily used for flood mapping (Shen et al., 2019). The Sentinel-1 series, which provides free data with high spatial and temporal resolution, serves as a leading example of this type of dataset (Agnihotri et al., 2019). Agnihotri et al. (2019) utilized Sentinel-1 to monitor the flood extent situation in near real-time in the Ramganga River in the Ganges basin, India. Furthermore, Phan et al. (2019) rapidly investigated the paddy field-affected flood area using Sentinel-1A images in the Red River Delta, Vietnam. Their results revealed that paddy fields were significantly affected by flooding, particularly in floodplain areas, where the fields were flooded more than four times during the flood season. Recently, Tiwari et al. (2020) employed Sentinel-1A SAR to detect the extent of the 2018 flood after using optical images to validate image classification methods. Additionally, these authors utilized satellite rainfall data to analyze rainfall patterns and comprehend the investigated flood event in Kerala state, located in southwestern India.

Several digital image processing techniques are available to detect flooded areas from SAR images, including thresholding (Phan et al., 2019), complex prediction models (DeVries et al., 2020a), and machine learning approaches (Shen et al., 2019). The thresholding approach such as Otsu thresholding algorithm is mostly applied for flood detection, because this approach is simple and more accurate compared to other methods (Liang & Liu, 2020). Otsu is one of the most useful approaches in automatic binary thresholding techniques (Wunnava et al., 2020), defining the best grey value for splitting interest objects (flooded areas) from the background in an image (Moharrami et al., 2021). Sentinel-1 SAR images supply VV and VH polarizations, in which VV backscatter has a stronger signal than VH backscatter. Therefore, researchers mainly have used VV polarization to detect flood extent (Liang & Liu, 2020; Phan et al., 2019).

Nevertheless, several disadvantages remain when utilizing SAR for flood extent detection (Notti et al., 2018). First, the shadows of mountains or smooth surfaces (i.e. roads, parking) on the SAR image appear dark, which can be misclassified as a flooded area (Phan et al., 2019; Tazmul Islam & Meng, 2022). Second, the double-bounce backscatter signal and radar shadows produced by the high density of built-up areas make it difficult to properly identify flooded areas (Giordan et al., 2018; Moharrami et al., 2021), as well as flooded vegetation areas (Tsyganskaya et al., 2018a). As a consequence, the flood extent obtained from Sentinel 1 is often smaller than the actual

flood (Moharrami et al., 2021). In addition, SAR images are affected by speckle, introducing the noise known as "salt and pepper" into the images, posing a challenge in image classification (Moharrami et al., 2021). Finally, remote sensing-based flood extent does not determine flooding depths, which are important for emergency services during disaster events and for post-event impact assessment (Giordan et al., 2018; Peter et al., 2022).

b) Flooding depth

Flooding depth maps have been developed using flood extents retrieved from RS and the Digital Terrain Model (DTM) (Tazmul Islam & Meng, 2022). Peter et al. (2022) developed a tool to determine flooding depth on the GEE based on a DEM and flood extents derived from a flooding map with a 100-year return period. Additionally, flooding depth can be determined by integrating water levels or flooding depth from various sources with a Digital Elevation Model (DEM), including field surveys, citizen science, and monitoring stations (Fohringer et al., 2015; Giordan et al., 2018). Giordan et al. (2018) used flood images on the internet, which left marks on walls to determine flooding depth. The DEM-based flooding depth map is compared to results from modeling, showing good agreement, with an average flooding depth difference ranging from 0.18 to 0.31 m (Peter et al., 2022). Chau et al. (2013) discussed the similarities of flooding depth maps between DEM-based depth models and flood modeling.

While this approach can determine flooding depth maps easily and simply, there are several limitations. This approach is suitable for relatively flat areas where the slope is less than 5% (Munasinghe et al., 2018; Peter et al., 2022), and floodplain elevation variability ranges about 50 m (Munasinghe et al., 2018). Detailed elevation data are the most sensitive input for flooding depth maps (Cohen et al., 2019; Wolff, 2020), which is unavailable in many areas. Additionally, DEM-based flooding depth cannot reflect hydraulic relationships between river, dykes, and flood-protected areas (Fohringer et al., 2015; Giordan et al., 2018).

2.3.2.2 Flood exposure

A land-use map normally presents fundamental spatial information for assessing flood exposure (Englhardt et al., 2019; Ferri et al., 2020). A land-use map is also a parameter for hydrological and hydraulic modeling (Steinhausen et al., 2018; Trinh & Molkenthin,

2021). The land-use map is often classified into several categories, depending on detailed input data and research purposes. Some studies focus solely on urban areas (Englhardt et al., 2019), rural areas, or even specific features such as paddy fields (Phan et al., 2019), while many researches consider comprehensive land-use maps, including buildings, roads, and crops classes (Glas et al., 2020). Land-use maps are primarily obtained from remote sensing, which can develop maps over extended periods, even capturing crop growth stages throughout the year. Both SAR and optical remote sensing data have been exploited for land-use mapping (C. J. Davids et al., 2018; Phan et al., 2019).

Optical remote sensing data are mainly applied in land-use mapping (C. J. Davids et al., 2018; Dibaba et al., 2020; Dong et al., 2012). C. J. Davids et al. (2018) utilized Landsat 8 images to develop a land-use map for the Kathmandu Valley in 2015, employing a pixel-based supervised classification method. Dibaba et al. (2020) applied a series of Landsat images from 1987 to 2017 to build land-use maps for the Finchaa catchment in Ethiopia, quantifying changes over time. H. T. D. Vu et al. (2022) analyzed land-use maps in the Vietnamese Mekong River Delta from 2000 to 2021 using MODIS time-series images, focusing on assessing changes in agricultural land, such as paddy fields and aquaculture areas as well as changes in flood situations over 21 years. Recently, the deployment of Sentinel-2 images has gained significant attention for land-use mapping due to their fine spatial and temporal resolution (H. T. T. Nguyen et al., 2020; Steinhausen et al., 2018).

There are two classification methods for developing land-use maps based on satellite images: supervised and unsupervised classifications (Pérez-Cutillas et al., 2023). The former employs an ensemble of classifier algorithms, such as Classification and Regression Tree (CART) (Shelestov et al., 2017), random forest (RF) (Shelestov et al., 2017), support vector machine (SVM) (Man et al. 2018), and other supervised classification methods (C. J. Davids et al., 2018). For instance, Shelestov et al. (2017) utilized Random Forest, SVM, and CART methods to classify multitemporal satellite images for 2013 crop mapping in Kyiv, northern Ukraine. Although the CART method provided the best performance with 75% overall accuracy in this study (Shelestov et al., 2017), Random Forest is the most frequently utilized algorithm for mapping land-use (Pérez-Cutillas et al., 2023). The robust algorithm and low sensitivity to training data

quality are the main reasons explaining this high frequency (Shamshiri et al., 2022). The latter comprises the normalized difference vegetation index (NDVI), enhanced vegetation index (EVI), and leaf area index (LAI) to determine the properties of land-use classes (Rahman & Di, 2020). These indices are used to determine the existence of vegetation zones in general (Giordan et al., 2018).

There are numerous challenges in flood exposure assessment using remote sensing. Optical satellite images are a useful source for land-use mapping; however, these images are mainly affected by clouds during rainy season, particularly in Asian tropical regions (Steinhausen et al., 2018). The accuracy of image classification relies on validation datasets for training and validating of classification methods. Gathering in-situ data, such as developing paddy fields over large areas in the Vietnamese Mekong River Delta, requires significant effort (Clauss et al., 2018).

2.3.2.3 Flood vulnerability

Remote sensing can be employed to estimate flood damage to crops through the vegetable growth condition index (Rahman & Di, 2020). Various indices were used, including the comparison between pre- and post-flood situations and regression analysis between vegetation indices (VIs) and crop yield (Rahman & Di, 2020). A traditional approach involves the documentation of NDVI changes in flooded cultivation areas, assuming that NDVI generally weakens in flood-affected cropland (Rahman & Di, 2020). To assess flood impact on crops, R. Shrestha et al. (2013) compared the NDVI time series with the past average NDVI from 2000 to 2014. Comparing the NDVI of the flood-affected area with standard NDVI requires documented data on NDVI (Rahman & Di, 2020). Regression analysis between vegetation indices (VIs) and crop yield was mainly used for flood damage assessment to crops, where VIs serves as independent variables to anticipate crop yield or crop loss (Rahman & Di, 2020). For example, Silleos et al. (2002) developed a linear regression model between the Normalized Difference Vegetation Index (NDVI) and wheat loss percentage collected from field surveys in Greece.

There are some restrictions on the application of remote sensing in flood vulnerability assessment, particularly in crops. The NDVI approach is widely applied and can indicate crop damage, but it is impossible to quantify the damage level (Rahman & Di, 2020).

Regression analysis often requires documented data on yield and independent variables to develop regression functions (Rahman & Di, 2020). Consequently, this approach cannot be used in areas where documented data are inadequate or even missed (Rahman & Di, 2020).

2.4 Citizen science in flood risk-related data collection

2.4.1 Definition and application of CS in environmental science

Citizen science refers to the voluntary participation of amateur scientists in collecting, and analyzing data, and disseminating knowledge for scientific research (Cohn, 2008; Silvertown, 2009). In broader terms, public participation in scientific research is also known as citizen science (Irwin, 1995; Kruger & Shannon, 2000). This philosophy is also related to concepts like community-based monitoring (Whitelaw et al., 2003), community-based management (Keough & Blahna, 2006), and community-based data collection (Le Coz et al., 2016; Starkey et al., 2017). The sphere of 'active participation' is what distinguishes citizen science from less collaborative forms of public participation in scientific research, as highlighted by Wiggins & Crowston (2011). Their participation can benefit themselves directly (e.g., improved scientific knowledge) or indirectly (e.g., improved social capital) (Buytaert et al., 2014).

Citizen science has become increasingly popular in natural science recently (Silvertown, 2009). For instance, E. Beza et al. (2018) carried out research to investigate the aims of farmers in accepting Short Message Service for developing digital citizen science in agriculture in Ethiopia. Pernat et al. (2021) launched a national citizen science program to monitor mosquitoes in Germany in 2012. The research utilized professional data obtained from a research group for comparison with citizen science data related to habitat coverage, species composition, and the detection of invasive mosquitoes. Citizen scientists detected invasive species better than researchers due to their largely spatial residence. Recently, von Gönner et al. (2023) developed a citizen science program based on the Water Framework Directive, allowing citizen scientists to provide data related to ecological conditions across 28 central German stream sites. The results showed that data gathered by citizen scientists, when trained and supported properly, is highly correlated with professional data.

Citizen science is a novel approach aimed at comprehensively understanding the water resource system (J. C. Davids, 2019). In 2019, Davids utilized citizen science to monitor rainfall, water levels, groundwater quality, and land-use, thereby providing a comprehensive understanding of water resources in the Kathmandu River basin in Nepal, where data availability is often low (J. C. Davids, 2019). Furthermore, in-depth investigations highlight the effectiveness of this approach to discharge monitoring (Fehri, Bogaert, et al., 2020) and in the qualitative and quantitative observation of floods in small rivers (Starkey et al., 2017). Citizen engagement, as demonstrated by (Azizi et al. (2023) and Etter et al. (2020), contributes to enhancing the accuracy of flood models.

The application of citizen science in data collection and monitoring offers numerous advantages. Firstly, it serves as a complementary approach to traditional methods such as ground observation, field surveys, and remote sensing, while still adhering to accuracy and objectivity in citizen science data (C. J. Davids et al., 2019; de Bruijn et al., 2019). Secondly, public participation in scientific research fosters an improved understanding of local issues among participants (Overdevest et al., 2004). Beyond this educational aspect, communities can actively engage in the decision-making process, serving as representatives at the local level in a bottom-up approach (Buytaert et al., 2014; Cheung & Feldman, 2019; Minkman et al., 2017).

2.4.2 Low-cost monitoring equipment and ICT facilities

The provision of low-cost monitoring equipment, in conjunction with information and communication technology (ICT), creates favorable conditions for developing community-based hydrological monitoring networks (Buytaert et al., 2014; C. J. Davids et al., 2019). The utilization of low-cost monitoring equipment has proven highly effective in capturing the attention of local communities engaged in water resources monitoring. A cost-effective S4W rain gauge, constructed from soda bottles, concrete, and rulers with a total cost of less than 1 USD, led to the participation of over 150 citizen scientists in the 2018 monsoon rainfall monitoring in various regions of Nepal (C. J. Davids et al., 2019). Similarly, in Tunisia, Fehri, Khlifi, et al. (2020) employed cost-effective rain gauges to measure daily rainfall with the involvement of citizen scientists, aiming to enhance the existing water monitoring system. This ongoing approach engaged participants from diverse generations and educational backgrounds.

Regarding water level monitoring, Weeser et al. (2018) installed water level gauges at public structures (e.g., bridge pillars, sluice gates) and engaged passers-by through signboards explaining the monitoring procedures. This initiative resulted in 124 citizen scientists reporting thousands of valid measurements for remote regions in Kenya. Furthermore, Pandeya et al. (2021) used low-cost sensors for water level measuring, allowing citizen scientists to operate from installation to data control and reading. The real-time monitoring data can be displayed. They are suitable to support a flood early warning system. In an innovative approach, Seibert et al. (2019) have utilized the virtual-staff gauges approach on smartphones, encouraging citizen scientists to measure water levels at any location. This approach has the potential to reduce the cost of physical gauge installation and maintenance expenses.

Advances in ICT assist in the data and knowledge flow, both for uploading data to services and for querying databases using powerful interfaces (Buytaert et al., 2014). Lowry et al. (2019) and Weeser et al. (2018) used Short Message Services to receive stream water level information (e.g., station ID and water level value) obtained from citizen scientists via cell phones. This approach seems simple and has stable applicability for remote areas or low-tech participants, but it incurs message services fees, which might be a barrier to participants (Weeser et al., 2018). Recently, many researchers have used smartphones, which can access broadband internet as well as offer GPS receivers and camera functions to collect and transmit information to centralized databases (J. C. Davids, 2019; Fehri, Khlifi, et al., 2020; Ribeiro et al., 2020). The photos and videos gathered by smartphones reflect the objectivity of data and provide extra information for users (C. J. Davids et al., 2019; Seibert et al., 2019). Alternatively, Fehri, Khlifi, et al. (2020) asked participants to utilize the web application platform to gather rainfall data. Additionally, communication technologies can help scientists engage with participants easily through social networks, encouraging their involvement, maintaining their participation as well as displaying citizen science data (Sy et al., 2019; N. H. Tran et al., 2021).

2.4.3 The role of citizen science in flood risk-related data collection

2.4.3.1 Flood hazard data collection

Citizen science has been extensively employed to gather the flooding extent (Sy et al.,

2020), flooding depth (Fohringer et al., 2015), flow velocity (Le Coz et al., 2016), and flooding duration (Sy, 2019) information for understanding and assessing flood hazard.

The identification of processes and chains of flood events typically relies on on-site surveys in the field. However, these surveys are usually conducted by experts from outside the flood-affected area, and limitations, both techniques and in terms of temporal and spatial information of the area, can occur, affecting the comprehension of the flood situations (Sy et al., 2019). The utilization of flood information obtained from locals residing in the flood-affected area can be crucial for evaluating potential floods or understanding past events (P. Tran et al., 2009). First, locals possess a deeper understanding of their environment and existing issues, such as sewage system failures and jams, which could exacerbate the flood phenomenon (Gebremedhin et al., 2020; Sy et al., 2020). Besides, locals serve as observers during events; therefore, valuable information on chains of flood events can be gathered through explicit memory recall via interviews (Sy et al., 2020), focus groups (Peters-Guarin, 2008), or P-mapping (Sy et al., 2020). The facts have shown that many flood events not registered in Munich Re's NatCatSERVICE (natcatservice.munichre.com), a global flood events database, have been reported by locals via social media data (de Bruijn et al., 2019).

Citizen science has been commonly applied in flood extension determination. First, Canevari-Luzardo et al. (2017) used PGIS to record local spatial knowledge about potential flooding areas. Participants, who are members of the Community Disaster Response Team, drew potential flooding areas map based on historical observational records (Canevari-Luzardo et al., 2017). The map is useful to develop risk reduction measures. Second, Sy et al. (2020) also used the PGIS technique to determine the flood extent of past flood series in Yeumbeul North (YN), Senegal, where authoritative flood records was missing. Researchers asked two groups of citizens, including commune chiefs and locals, to determine the flooded areas in their neighborhoods (Sy et al., 2020). The results showed that the flooded maps obtained from the two groups overlapped relatively well (Sy et al., 2020). Furthermore, Rosser et al. (2017) demonstrated the efficacy of integrating social media, remote sensing and topographic data for developing flood extent. The flood information on social media data, including messages, and photos in conjunction with geolocated information, plays an important role in

developing flood maps, particularly in rapidly estimating flood inundation extent (Rosser et al., 2017).

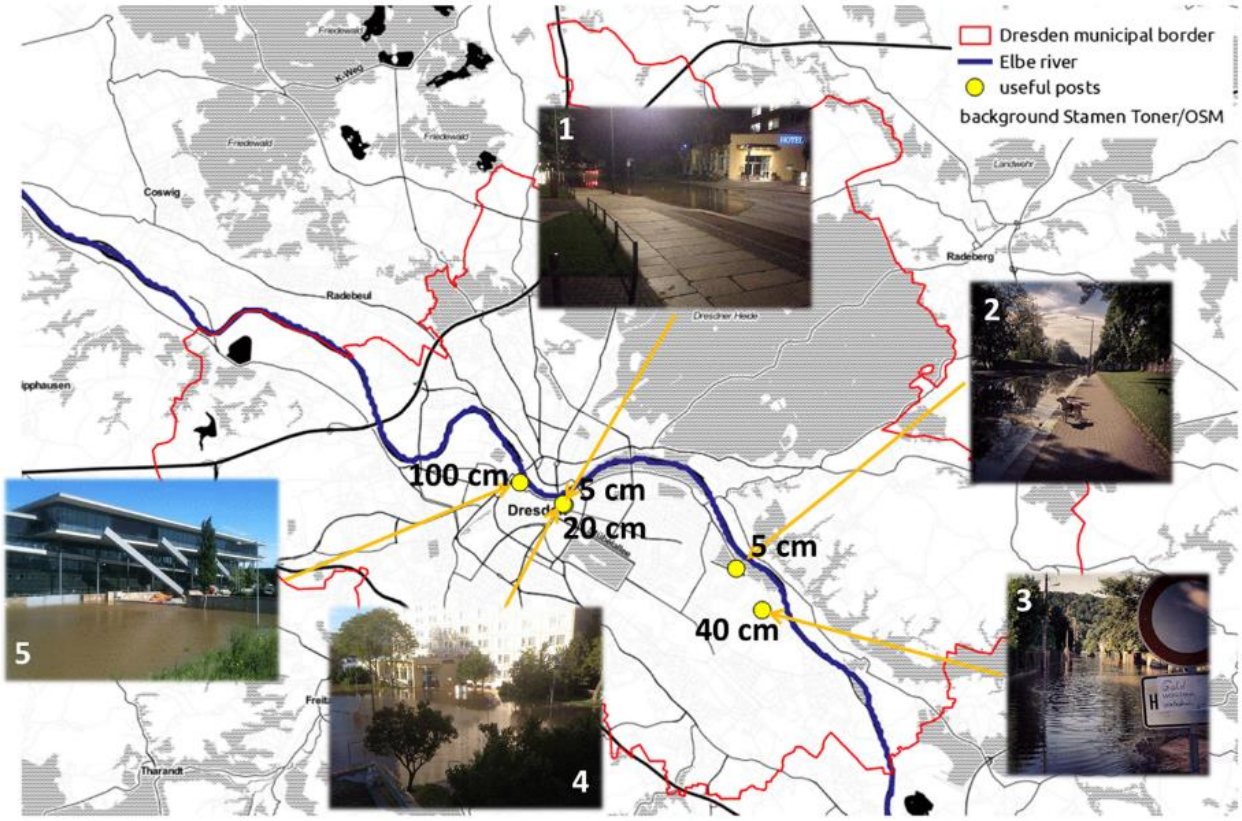

Source: (Fohringer et al., 2015)

Figure 2.5. Flooding photos of 2013 flood in Dresden, Germany taken by locals

Flooding depth is a critical parameter in assessing flood hazard, but it is complicated to survey and monitor (Sy et al., 2020). Consequently, there have been attempts to involve citizens in retrieving data from past events. Glas et al. (2018) utilized a questionnaire survey to obtain historical flooding depth data from locals through field surveys in data-scarce areas, which is also considered as a citizen science approach. Additionally, Sy et al. (2020) have explored the use of P-mapping to gather information on flooding depth of historical flood events. Citizens indicated flooding depth level using different colors (yellow, green, and red corresponding to low, medium, and high flooding depths) on the map qualitatively. Subsequently, the flooding depth was measured in the field to create a flooding depth map, which was then compared with the qualitative flood depth map provided by citizen science, particularly in high flooding areas (Sy et al., 2020). In the context of real-time flood occurrences, the advent of web 2.0 technologies facilitates diverse approaches to data collection, particularly in social media. Fohringer et al.

(2015) extracted relevant data from text messages or photos posted on Twitter and Flickr to estimate a flooding depth map for the major flood in Dresden, Germany, in 2013 (Figure 2.5).

Flood extension and flood depth are easier parameters to gather, while measuring flood velocity or discharge proves challenging during events (Sy et al., 2019). Le Coz et al. (2016) analyzed flood flow videos posted on social media after events, demonstrating a compelling method to obtain on-site measurements in situations where official instruments either failed or were absent. Recently, citizens monitored river discharge in Tunisia using a smartphone application (Fehri, Bogaert, et al., 2020). The results showed good agreement with reference data, proving that citizen science-based discharge data collection is cost-effective and can be applied at larger scales (Fehri, Bogaert, et al., 2020). Apart from velocity and discharge parameters, citizens can provide information about flood duration, which was collected via household surveys (Peters-Guarin, 2008; Sy et al., 2016).

2.4.3.2 Exposure data collection

Many researchers have employed images captured by citizens to authenticate land-use maps from local to global scales. At the local scale, P-GIS has been employed to complement and update land-use maps derived from satellite images for a suburban area in Dakar, Senegal, as demonstrated by Sy et al. (2016). Olteanu-Raimond et al. (2018) developed an experimental framework using citizen science to update and correct the land-use database for the French national mapping agency. Furthermore, Dong et al. (2012) utilized geo-referenced field photos gathered by researchers and citizens to validate existing land-use data derived from high-resolution satellite imagery in mainland southeast Asia. Their research has shown that citizen science proves valuable for tracking territorial change, especially in cities (Dong et al., 2012). At a global scale, Iwao et al. (2006) have launched an initiative where citizen scientists collect land-use information in their surroundings by uploading photos and comments to enhance the world's land-use map.

2.4.3.3 Flood vulnerability data collection

Many researchers used information provided by locals to estimate the flood vulnerability of locals or develop stage damage curves. Sy et al. (2016) also revealed that information

of locals is a crucial source to gather socio-economic and house property information (i.e., material, land prices) to improve the understanding of flood vulnerability. Besides, Peters-Guarin (2008) and Glas et al. (2018) utilized interviews with affected households and focus group discussions with community officials and leaders to estimate the flood damage to livelihoods, homes, and facilities in monetary terms, depending on the depth and duration of flooding.

Data collection methods for flood damage have changed in the last two decades. In the 2010s, citizens shared information about flood damage and their perspectives on disaster management mainly during field surveys implemented by researchers (Peters-Guarin, 2008; P. Tran et al., 2009). In the last decade, crowdsourced geolocated videos or photos of floods posted on social media platforms such as YouTube or Twitter were utilized to estimate flood damage to streets after a flood event in New York City (Schnebele et al., 2014). Recently, Fuchs et al. (2019) highlighted the potential of citizen science using mobile applications to more effectively document flood damage in real-time.

2.4.4 The challenges of CS in flood risk-related data collection

The potential of citizen science in flood risk-related data collection is becoming increasingly evident, with applications ranging from gathering information about past events to updating real-time data during events. However, certain problems and challenges need to be taken into account.

First, one of the primary concerns revolves around the quality and dependability of citizen science data, whether obtained directly or through crowdsourcing, as highlighted by various authors (Sy et al., 2020; Weeser et al., 2018). The accuracy of flooding information provided by citizens depends on their random behavior, memory, recognition, and social class (Peters-Guarin, 2008). For instance, the flood extension given by local leaders showed better agreement with remotely sensed images than those given by locals (Sy et al., 2020). Detailed information of flooded photos, such as location and timing extracted from social media, is limited (Fohringer et al., 2015), leading to uncertainties of such flooding information. Recently, von Gönner et al. (2023) investigated the quality of data gathered by citizen scientists by comparing them with data collected by a research team (referred to as professional data). Their research revealed that citizen science data aligns well with professional data and emphasized that

citizen scientists can produce reliable data if they are properly trained and supported (von Gönner et al., 2023). Some researchers used clear and simple data collection procedures with sustainable data collection tools to reduce errors during measurement (Lowry et al., 2019; Weeser et al., 2018). In a study by David et al, citizen scientists were required to take photos during measurements, which were used to cross-check with citizen science data (C. J. Davids et al., 2019).

Secondly, the spatial distribution of citizen science data is uneven. Citizen scientists often gather data in residential areas, particularly in urban areas (Fohringer et al., 2015; Pernat et al., 2021; Sy, 2019) or nature centers, where they often walk or hike (Lowry et al., 2019). As an example, flooding information is often provided in residential areas (Fohringer et al., 2015; Sy, 2019). Therefore, flood information in crop land or flat areas is often missing, posing a challenge to develop flooding maps for the entire study area (Sy, 2019). Some researchers combine citizen science data with authoritative data, such as satellite images, to create flooding maps (Schnebele et al., 2014; Schnebele & Cervone, 2013).

Another significant challenge involves securing long-term citizen science programs (Prajapati et al., 2021). Firstly, the majority of citizen scientists participate in citizen science projects only once (C. J. Davids et al., 2019; Lowry et al., 2019), affecting the continuous monitoring of data and the distribution of the monitoring station. Therefore, understanding motivational drivers and factors like regular feedback, recognition of volunteers, and local meetings can help establish partnerships and foster long-term involvement (Weeser et al., 2018). Secondly, citizen science programs often last a short period due to a lack of funds. Some research uses modern expensive monitoring equipment, restricting the number of participants who can access and use this equipment (Pandeya et al., 2021). Additionally, many citizen science programs took place one time or for a short period, which cannot motivate citizen science update or monitor data for a long time (Seibert & van Meerveld, 2022).

2.5 Chapter summary

Flood risk assessment requires a numerous amount of data to evaluate flood effect on social, economic, and environmental spheres. de Moel et al. (2015) listed many data types, including topographic, meteoro-hydrological, socio-economic, historical flood

damage data, and validation datasets, as the input data for flood modeling and remote sensing analysis. However, these data are often missing or insufficient in developing countries (Glas et al., 2016). With the blooming of participatory research and advances in ICT (e.g., mobile technology), researchers and other stakeholders can exploit a massive amount of data about flood hazard, flood exposure, and flood damage with low cost and large coverage. These data can serve as ground-truth data to complement or validate traditional approaches like modeling or remote sensing, even ground observation, field surveys. Although citizen science has been widely applied for three flood risk assessment components separately—flood hazard, flood exposure, and flood damages - it has not been applied for all three components collectively. Additionally, further assessments are required regarding the reliability of citizen science data and improvements in updating data from the citizens.

Another prominent theme in the literature is the use of a rapid and simple approach to constructing flood hazard maps in the context of data-scarce areas. Nowadays, thanks to easy access to free radar data, flood monitoring and observation have become more convenient. Many studies have utilized remote sensing data to determine flood extent maps. Additionally, the flood extent is combined with the DTM to generate a flooding depth map - an important parameter in estimating flood damage. However, most satellite data is only suitable for bare land, making it difficult to determine the flooding situation in residential areas. This limitation can be supplemented using citizen science data, primarily collected in residential areas.

The literature review also highlights the important role of flood risk assessment in rural or agricultural land areas. However, few studies assess flood risk for rural areas, which are highly vulnerable and where data are often missing. This issue reduces the effectiveness of flood management measures. To overcome the lack of information, it is necessary to use a combination of citizen science, remote sensing, field surveys, and literature data to assess the components of flood risk and flood damage for agricultural areas. This research seeks to address these gaps by proposing an integrated approach for flood risk assessment in the context of data-scarce areas. The detailed approach is presented in the following chapter.

3 Working basics and methodology

3.1 Study area

3.1.1 Physical characteristics

The Bui River Basin, a sub-catchment of the Nhue-Day River Basin, is situated in northern Vietnam (Figure 3.1). It is primarily drained by two rivers, the Bui and Tich Rivers, which pass through Hoa Binh and Hanoi provinces (N. H. Tran et al., 2024). The Bui River, which originates from Luong Son district, Hoa Binh province, receives water from the Tich River at the Tien Truong confluence before joining the Day River at Ba Tha, My Duc district, Hanoi (T. T. Nguyen & Le, 2019). Covering an area of 1365 km², the Bui River Basin contributes 92% of the Day River Basin's area, as measured at the Ba Tha station (N. H. Tran et al., 2022).

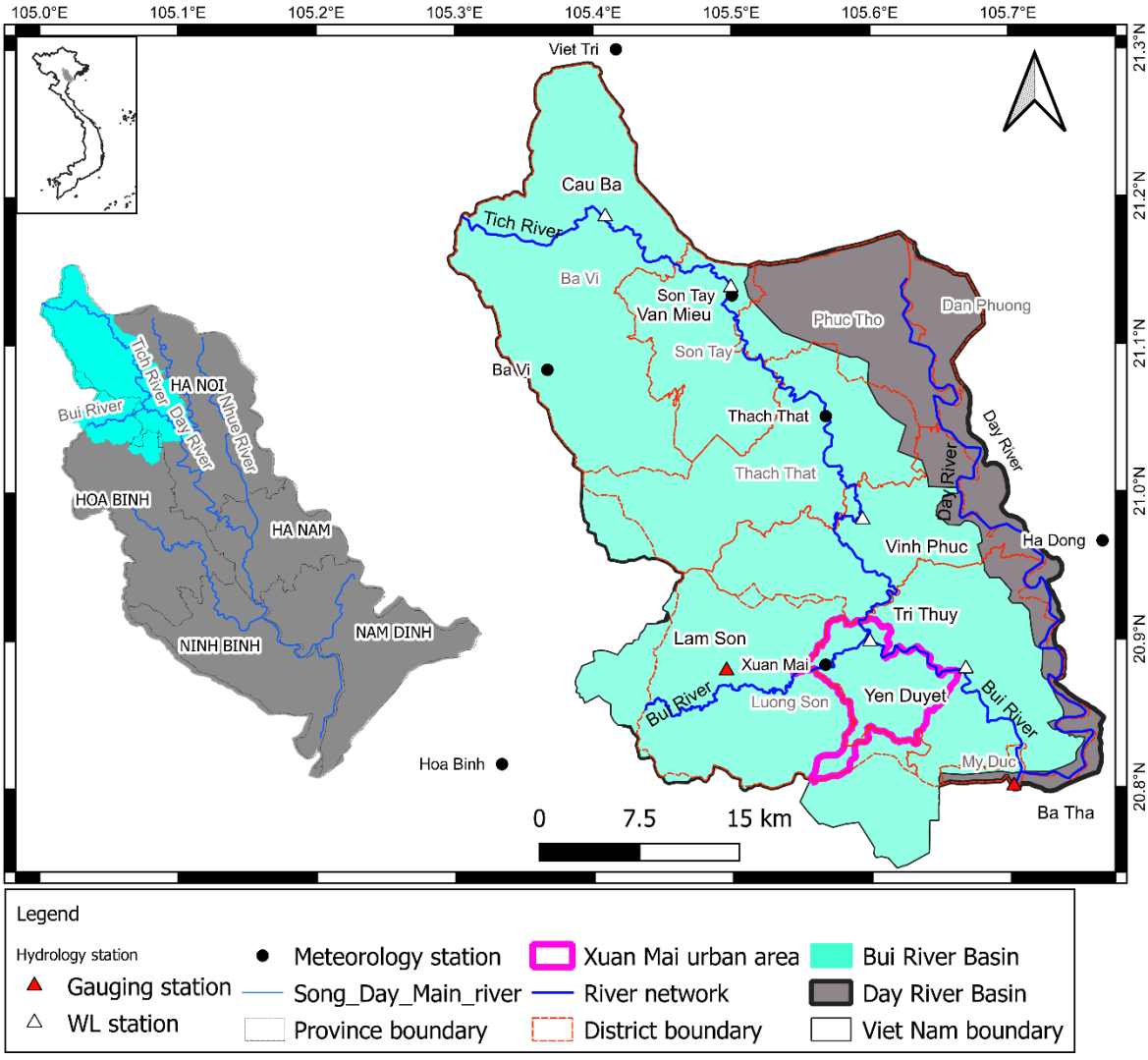

Figure 3.1. Maps of the Bui River Basin, the pilot area, river networks, and hydrometeorological stations

The characteristics of topography, land-use, and soil in the Bui River Basin are relatively diverse. The area's topography, derived from the SRTM (United States Geological Survey, n.d.), gradually declines from west to east, and from north to south, encompassing a range of terrain types, including mountainous, semi-mountainous, hilly, and flat regions (Figure 3.2A). Elevations range from 1231 m in the Ba Vi mountains or Lam Son area in the west to -1 m in the flat southeastern region. The land-use map was developed from Sentinel 2 satellite images in 2022 between January and May (Figure 3.2B). The approach applied to develop the land-use map in this research is described in section 3.5.1. The primary land-use classes in the Bui River Basin include built-up areas, agricultural land (i.e., paddy and nonpaddy crops), and forests. For soil characteristics, soil types in the Bui River Basin mainly consist of acrisol and gleysol, distributed in mountainous and flat regions, respectively (Figure 3.2C). These soils are mainly used for agricultural development, particularly in paddy fields (Chuc et al., 2006).

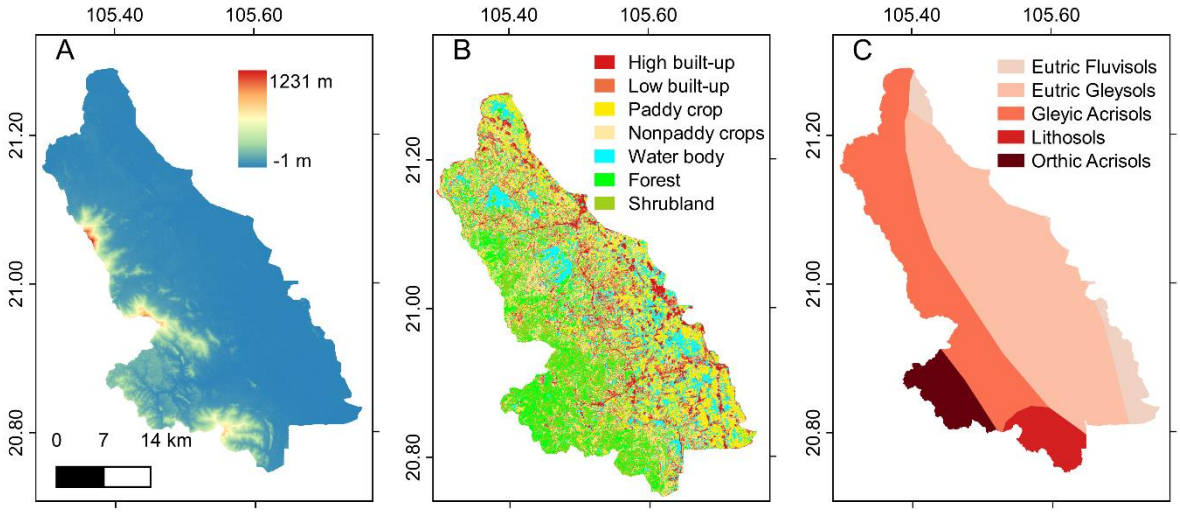

Figure 3.2. Maps of topography (A), land-use in 2022 (B) and main soils in 2016 (C) within the Bui River Basin

The density of hydrometeorological stations in the Bui River Basin and surrounding area is high, but the proportion of station types is uneven. The national hydrometeorological station network comprises seven meteorological stations: Viet Tri, Ba Vi, Son Tay, Hoa Binh, Lam Son, Xuan Mai, and Ha Dong. The density of the meteorological stations in the region is approximately one station per 10 km², which is the highest rate in Vietnam (NAWAPI, 2009). However, only one gauging station, Lam Son, situated on the upstream Bui River, has been measuring discharge and water level since 1960. The

station's catchment area encompasses 33.7 km², representing one-fortieth of the total area of the Bui River Basin. Furthermore, there is no hourly rainfall monitoring stations in the upstream of Bui River Basin. Therefore, estimating the flood characteristics in the Bui River Basin is challenging. Another gauging station, Ba Tha, is located downstream of the confluence of the Bui and Day Rivers. However, this station ceased measuring discharges in 1981.

Alongside the national hydrometeorological station network, there is a rain gauge and water level monitoring station network used to operate irrigation activities in the Bui River Basin. Some of the water level stations are named Van Mieu, Tri Thuy, and Yen Duyet. In 2019, Hanoi's People Committee installed new stations and upgraded some existing ones (Vinh Phuc and Yen Duyet) to monitor water levels and rainfall in real time. These data are available on the following websites (https://vrain.vn/home/43/overview and https://bit.ly/3JrX1N7).

Table 3.1. Annual rainfall at rain gauge stations in and surrounding Bui River Basin between 1975 to 2022

ID	Station	Period	Annual Rainfall (mm)
1.	Viet Tri	1975-2006	1551
2.	Ba Vi	1975-2010	1836 (1867*[2])
3.	Son Tay	1975-2010	1683 (1703*)
4.	Hoa Binh	1975-2006	1854
5.	Lam Son	2008, 2013, 2017, 2018, 2020-2022	2204
6.	Xuan Mai(**[3])	1975-2017	1726 (1744*)
7.	Ha Dong	1975-2018, 2020-2022	1645 (1607*)

The study area belongs to the subtropical climate. Annual average temperature is about 23 °C, and annual average rainfall ranges from 1500 to 2200 mm (T. C. Nguyen, 2018). The climate of the Bui River Basin is characterized by two distinct seasonal weather patterns: rainy and dry seasons. The rainy season occurs from May to October, contributing about 80% to the total annual rainfall (C. T. Nguyen et al., 2018). Table 3.1

[2] Annual Rainfall between 1975 and 2006.
[3] Xuan Mai stopped measuring rainfall in 2018.

displays the annual average rainfall observed between 1975 and 2020 at some gauge stations in and around the Bui River Basin. Annual rainfall varies spatially, with higher precipitation in the upstream areas of the Tich-Bui River, such as Ba Vi or Lam Son, compared to downstream areas.

Table 3.2. Annual flow characteristics of the Bui River Basin and surrounding areas

No	Station	F (km^2)	Period	Annual discharge (m^3/s)	Volume (Mil. m^3)	Flood flow volume (%)	Drought flow volume (%)
1	Lam Son	33.1	1970-2015	1.17	36.8	74	26
2	Ba Tha	1365	1961-1980	48	1510	77	23

The annual discharge in the Bui River Basin at Lam Son station is approximately 1.17 m^3/s. As expected, the hydrological regime of the Bui River Basin is highly influenced by the rainfall pattern (Doan & Bui, 2016). The flood season in the Bui River Basin typically spans from June to October, during which flood volumes constitute 74% to 77% of the total annual flow volume (Table 3.2). The maximum flood level recorded at Tri Thuy station from 1972 to 2022 mainly occurs in June, August, and September, with monthly relative frequencies of occurrence of 25%, 25%, and 22%, respectively (Table 3.3). Additionally, some flood events also occur in June, marking the onset of the flood season, or in November, after the rainy season.

Table 3.3. Statistics of occurrence frequency of maximum flood level at Tri Thuy station between months from 1972 to 2022

Month	**VI**	**VII**	**VIII**	**IX**	**X**	**XI**	**Total**
Occurrence number	3	13	13	11	7	3	51
Frequency (%)	6	25	25	22	14	6	100

3.1.2 Social economic characteristics

The Bui River Basin spans across Ba Vi, Son Tay, Phuc Tho, Dan Phuong, Thach That, Quoc Oai, My Duc, and Chuong My districts in Hanoi, as well as Luong Son district and Hoa Binh town in Hoa Binh province. According to the Hanoi and Hoa Binh Statistical Yearbook 2017, this region is home to approximately 1.71 million people

(Hanoi, 2018; Hoabinh, 2018). Politically, this region plays an important role in expanding Hanoi toward the west, in which Xuan Mai remote urban area is one of the key areas (Chuong My district, 2015). The Xuan Mai urban area encompasses five communes: Xuan Mai, Thuy Xuan Tien, Tan Tien, Nam Phuong Tien, and Hoang Van Thu in Chuong My district, situated at the confluence of the Tich and Bui rivers (Figure 3.3). This area is 30 km away from downtown Hanoi.

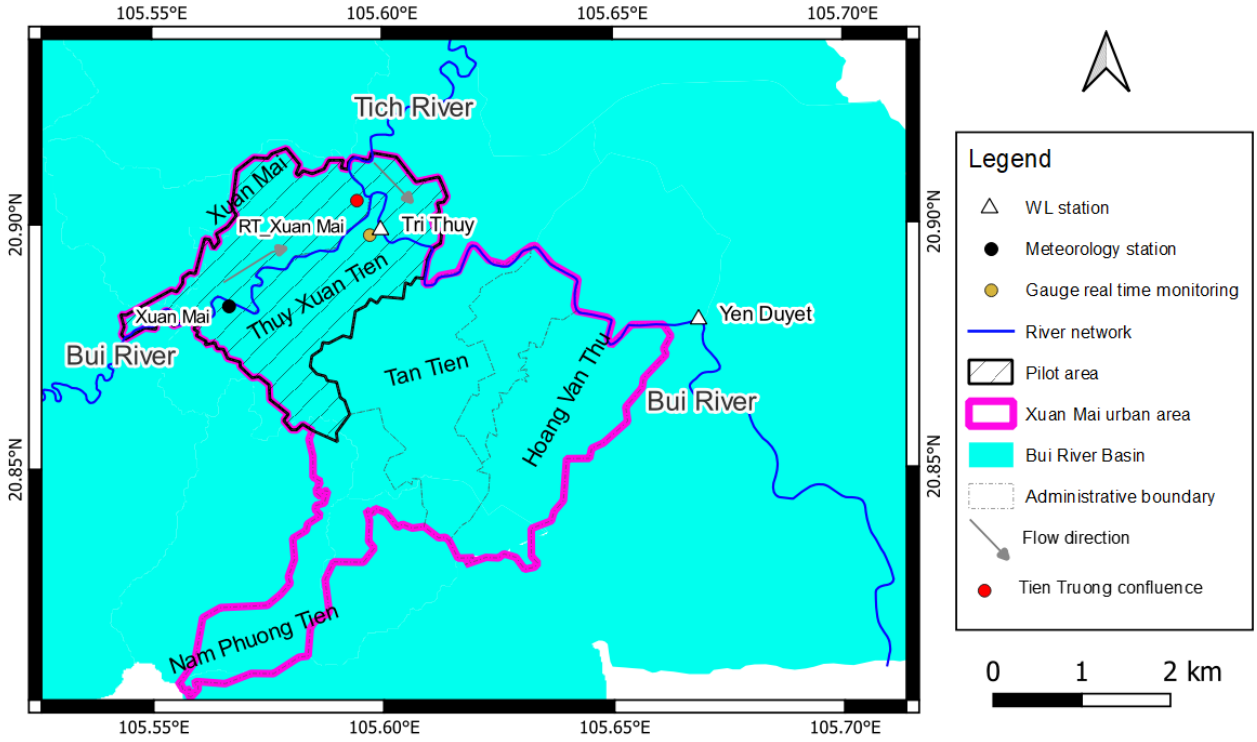

Figure 3.3. Maps of the pilot area, river networks, and hydrometeorological stations

The economy of the Bui River Basin highly relies on the industrial and construction sectors, contributing to over 50% of the total regional production value (T. K. O. Pham et al., 2019). The service sector accounts for more than 35%, while agriculture, forestry, and aquaculture collectively contribute over 10% (T. K. O. Pham et al., 2019). Although the contribution of the agricultural sector is comparatively lower than other sectors, it remains the primary source of livelihood for a majority of the population in the Bui River Basin (Chuong My district People's Committee, 2020). Moreover, nearly 50% of the land is dedicated to agricultural production (T. K. O. Pham et al., 2019), with prevalent activities including paddy fields, crops, and aquaculture areas.

3.1.3 Flooding situation in Bui River Basin

The Bui River Basin is subject to regular flooding, although this does not occur annually.

Terrain characteristics in this area pose challenges for draining flood. The upstream section of the Bui River is characterized by steep terrain, which results in the rapid accumulation of floodwater. In contrast, the downstream section displays meandering river channels, which diminish the river's capacity to effectively drain floods. For instance, during the 2018 flood (Figure 3.4), the rising limb periods, counted from the warning threshold level 1, lasted 2-3 days, while the falling limb endured 1-2 weeks. Certain areas along the Tich-Bui Rivers, particularly on the right bank, display semi-mountainous and semi-plain topography, resulting in floodwaters flowing directly into low-lying regions causing flooding (Le et al., 2022). Additionally, the right bank areas of the Tich-Bui Rivers serve as flood retention basins to mitigate flood damage in the downtown Hanoi (Hanoi, 2009). The elevation of the dyke crest on the left riverbank is typically higher than that on the right riverbank. Consequently, once bankfull discharge occurs, floodwaters initially overflow onto the right river bank.

The frequency and intensity of floods in the Bui River Basin have been increasing in recent years, with notable floods occurring in 2008, 2017, and 2018 (N. H. Tran et al., 2022). Among these, the 2018 flood was the biggest flood ever recorded at the Tri Thuy station (N. H. Tran et al., 2022). This event lasted for over 20 days and the maximum flood level at the Tri Thuy station exceeded the warning threshold level 3 (Figure 3.4). The flood resulted in the bursting of numerous dykes, and flooding in districts, including Chuong My, Quoc Oai, and Thach That, situated along the Tich and Bui Rivers. The 2018 flood had a significantly negative impact on the locals, infrastructure, and agricultural production. The total estimated damage to the Chuong My district was 10.8 million euros (equivalent to 278 billion Vietnamese dong) (C. M. D. P. Committee, 2018). In 2022, another alarming flood occurred at Yen Duyet station, where water levels surged rapidly from the warning threshold of level 1 to level 3 within just six hours (Figure 3.5). This sudden rise caused significant damage to paddy fields, crops, and aquaculture areas in this district (C. M. D. P. Committee, 2023).

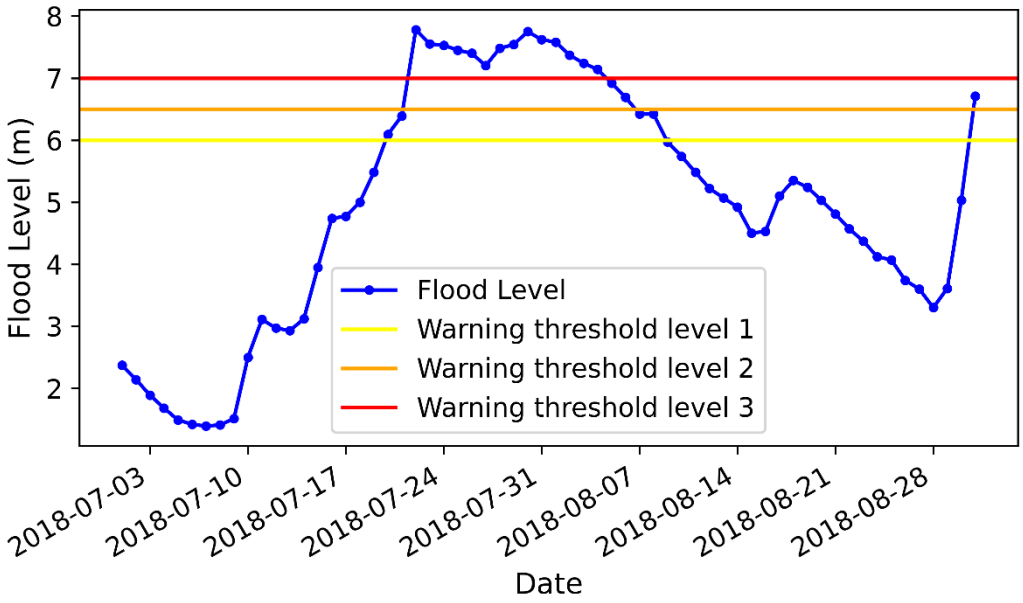

Figure 3.4. Water level on the Bui River at Tri Thuy in 2018 flood

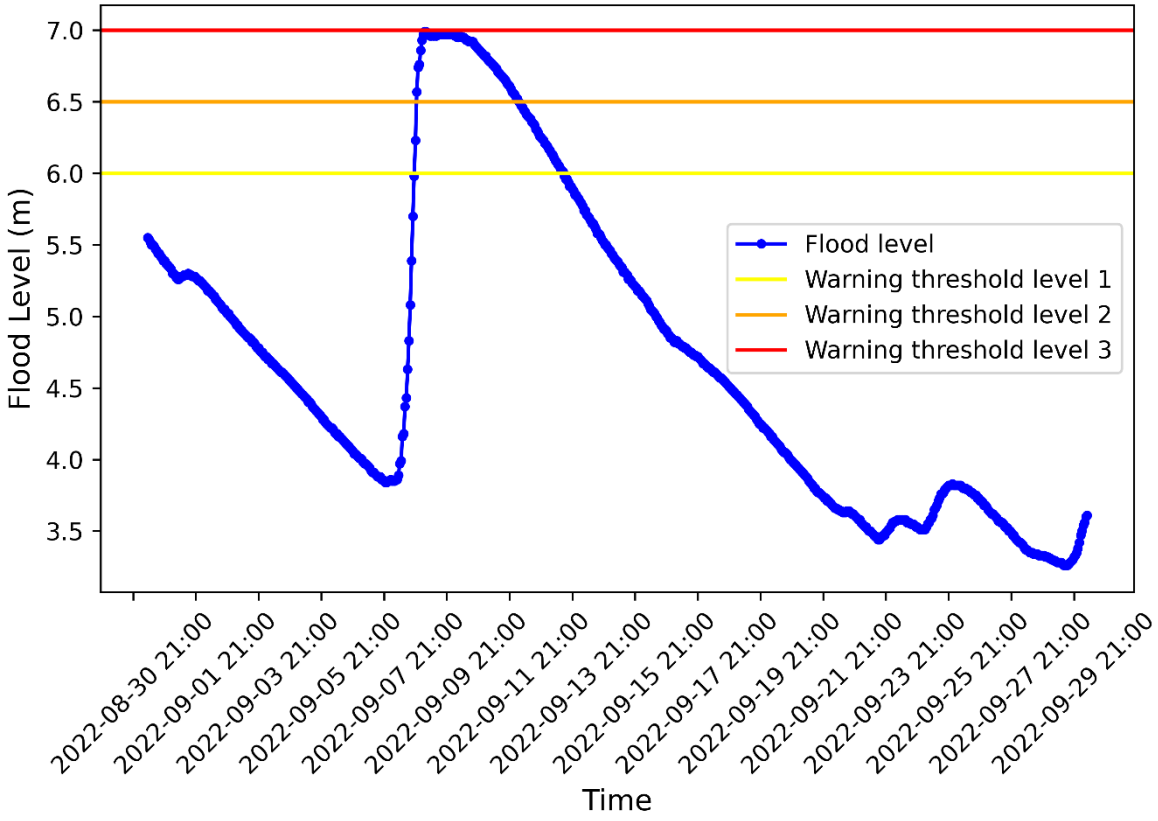

Figure 3.5. Water level on the Bui River at Yen Duyet in September 2022 flood

There are two primary reasons contributing to the worsening flooding in the Bui River Basin in recent years. Firstly, there has been an increase in rainfall intensity and a prolongation of the rainfall duration, which is considered a phenomenon of climate

change. The annual rainfall in Lam Son in the last fifteen years is much higher than that at other stations before 2010 (Table 3.1). Notably, the abnormal storm in May 2022, with 195 mm of rainfall within two days in Chuong My district, marked a new record for monthly rainfall in May in the study area since measurements began. Secondly, there has been a recent decrease in forested areas and an increase in built-up areas (Doan & Bui, 2016; T. K. O. Pham et al., 2019). This phenomenon exacerbates flood flows in the Bui River Basin despite stable annual rainfall, as an increase in impervious surfaces results in increased surface flow and as a result in increased flood flows.

Although flooding in the Bui River Basin is a complex problem, there have been few studies assessing the flood impact on people, economy, and environment. This research focuses on assessing the flood impact on agricultural production, one of the main economic activities in the Bui River Basin. The pilot area encompasses Xuan Mai town and Thuy Xuan Tien commune in Chuong My district, situated at the confluence of the Tich and Bui Rivers (Figure 3.3). This pilot area was chosen, because it has several monitoring stations (i.e., Xuan Mai and Tri Thuy) that have provided historical data for a long time. Furthermore, an automated real-time rainfall monitoring station, designated RT_Xuan Mai in this study, was installed at the People's Committee of Thuy Xuan Tien commune in 2019 with the objective of enhancing flood control services. The rainfall data from this station was used to compare with rainfall data obtained from citizen scientists. Additionally, the area is home to several schools and a university, offering an ideal environment for implementing citizen science programs.

3.2 Data basics

3.2.1 Hydrometeorology data

Hydrometeorological data were collected from various organizations, such as the National Center for Hydro-Meteorology Forecasting (NCHMF), Day River Irrigation Company, Tich Rivers Irrigation Company, and Chuong My District People's Committee. The data collection consists of several data types, including discharge, water levels, and rainfall data in the Bui River Basin and the surrounding areas. Table 3.4 presents a brief overview of the gathered hydrometeorological data. Most of the data are measured at a 24-hour interval. Some meteorological stations have measured rainfall hourly, such as Viet Tri, Ba Vi, and Hoa Binh. Recently, some water level stations along

the Bui River have been automatically monitoring water levels at hourly intervals, such as Yen Duyet and Tri Thuy. There is only one station, Lam Son, which measures discharge in the Bui River Basin. Statistical characteristics of hydrometeorological stations which were used to describe rainfall and flood flow characteristics can be found in section 3.1.1.

Table 3.4. List of hydrometeorological data gathered in the thesis

No	Station	Station type	River	Period	Measurement interval	Data type
1	Viet Tri	Meteorology		1975-2006	Daily, hourly	Rainfall
2	Ba Vi	Meteorology		1975-2010	Daily, hourly	Rainfall
3	Son Tay	Meteorology		1975-2010	Daily, hourly	Rainfall
4	Hoa Binh	Meteorology		1975-2006	Daily, hourly	Rainfall
5	Lam Son	Discharge	Bui	1970- 2022	Daily, 6 hourly	Rainfall, Discharge
6	Xuan Mai	Meteorology		1975-2017	Daily, hourly	Rainfall
7	Ha Dong	Meteorology		1975-2018, 2020-2022	Daily, hourly	Rainfall
8	Cau Ba	Water level	Tich	2010-2022	Daily	Water level
9	Van Mieu	Water level	Tich	2010-2022	Daily	Water level
10	Yen Duyet	Water level	Bui	2014-2022	Daily, hourly	Water level
11	Tri Thuy	Water level	Bui	1972-2022	Daily, hourly	Water level
12	Ba Tha	Discharge	Day	1961-1980	Daily	Discharge

3.2.2 Sentinel data

3.2.2.1 Sentinel 1 images

The publicly accessible radar dataset, Sentinel 1 (S-1) images, offers high-resolution data that is suitable for extensive geographic analysis. The S-1 satellites, launched in 2014 (S-1A) and in 2016 (S-1B), are operated by the European Space Agency (ESA) (Trinh, 2023). The S-1 satellites provide free, continuous imageries with a 6-day revisit time over Europe and 12-day revisit time over the remainder of the Earth's surface, utilizing both ascending and descending orbits (DeVries et al., 2020a). The S-1 dataset comprises a variety of image modes, including interferometric wide swath (IW), strip map (SM), extra-wide swath (EW), and wave mode (WM). In particular, the IW S-1 dataset, which has a wide swath of 250 km and a resampled spatial resolution of 10 by

10 meters, is suitable for land observation and flood monitoring (Bekele et al., 2022). This dataset offers different combinations of co-polarization (VV) and cross-polarization (VH) channels based on the direction of transmitted microwave radiation and the reception of the signal backscatter intensity. S-1 images with the VV channel are often used to detect floods, because they have stronger backscatter compared to images with the VH band (Agnihotri et al., 2019; Moharrami et al., 2021; Phan et al., 2019).

Based on the peak flow periods of the three investigated floods and the satellite overpass dates, three flood images taken during or right after peak flow periods were chosen for this research (Figure 3.6). These images can provide the maximum flooding extent (Giordan et al., 2018). Additionally, reference images from the three driest months (January to March) (P. C. Duong et al., 2016) were utilized to determine permanent water bodies, as proposed by Singha et al. (2020). The S-1 images were retrieved from Google Earth Engine (GEE), and detailed information on the selected images is shown in Table 3.5.

Table 3.5. Information on Sentinel-1 images used to determine flood extent on bare land

No	Flood year	Peak flow time (date/month)	Flood image acquisition time (date/month)	Reference image acquisition time (month)	Resolution	Orbit type	Polarization
1	2017	12/10	22/10	Jan - March	10 m	Ascending	VV
2	2018	22/07	22/07	Jan - March	10 m	Descending	VV
3	2022	09/09	11/09	Jan - March	10 m	Descending	VV

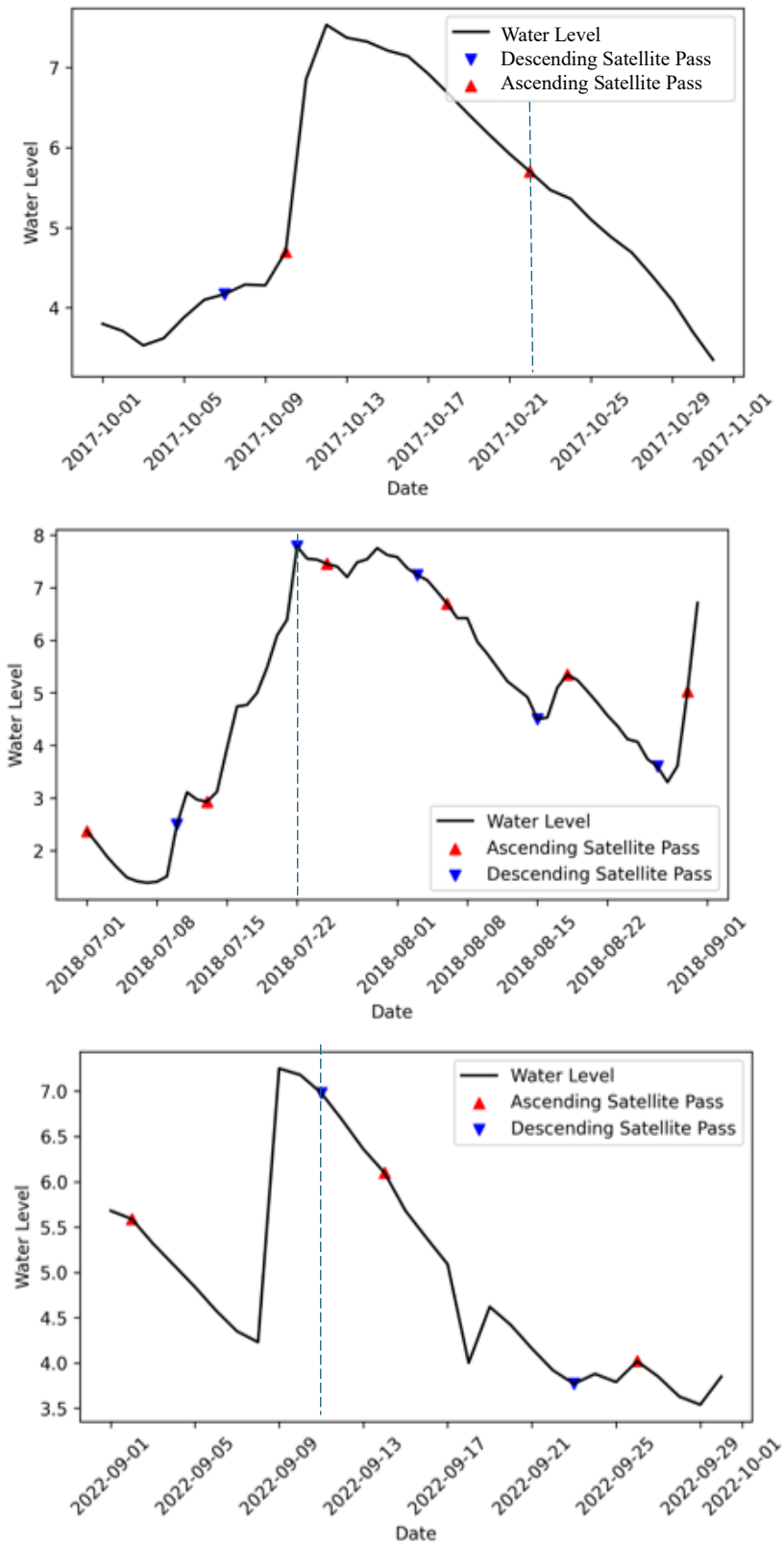

Figure 3.6. Tri Thuy flood level hydrographs for flood in 2017 (A), 2018 (B), and 2022 (C) versus the satellite overpass dates (vertical dashed lines present chosen images)

3.2.2.2 Sentinel 2 images

The land-use map was developed by using data from Sentinel-2 (S-2) multispectral instrument (MSI) images. These images, provided by ESA, comprise 13 spectral bands with resolutions ranging from 10 m to 60 m (Singha et al., 2020). S-2 provides free continuous imagery with a revisit time of 2 to 3 days at mid-latitudes and 5 days at the equator (ESA, n.d.). In this research, the red (band 4), green (band 3), and blue (band 2) spectral bands were employed, with a 10 m pixel size Level-2A product. The images were captured during the dry season of 2022, coinciding with the period of collecting land-use samples from January to May. These images were retrieved from the Google Earth Engine platform.

3.2.3 Other data

3.2.3.1 Statistics data

Data on annual flood damage in Chuong My district and two pilot communities were collected for the period from 2013 to 2022. These data included detailed statistics on flood-affected agricultural land and the number of households impacted by flooding. Additionally, statistical yearbooks from Hanoi city, Hoa Binh province, and Chuong My district covering the years 2017 to 2022 were obtained. The yearbooks provided information on the economic value of crops and aquaculture areas. Moreover, a comprehensive list of farmers cultivating paddy fields damaged by floods in 2018, along with corresponding damage rates, was gathered.

3.2.3.2 Soil map

Soil data, classified according to the Food and Agriculture Organization (FAO), was collected from Open Development Mekong (Opendevelopmendevelopment, n.d.). The soil data map, established from a reference database in 2016 in geospatial polygon format, is shown in Figure 3.2C.

3.2.3.3 Stage damage curves

Stage damage curves illustrate the relationship between flooding depth and damage rate typically derived from surveys on historical flood damage, or from laboratory experiments (Dutta et al., 2003). This work demands considerable time or investment, resulting in limited research on developing stage damage curves in Vietnam. N. Y. Nguyen et al. (2017) and H. N. Pham et al. (2018) developed stage damage curves for

crop and aquacultural land for two river basins in Vietnam, respectively. Their work was used in this research to reduce the need for extensive field surveys.

3.2.3.4 River geometry data

A total of 52 river cross-sections, surveyed in the field and spanning approximately 100 km of the Tich and Bui Rivers, were compiled. The distance between the two sequencing cross sections varies from 0.5 to 3.5 km. These data were gathered in 2021 as part of a project supported by Hanoi University of Natural Resources and Environment, Vietnam. Additionally, several typical cross-sections of tributaries of Bui River were obtained from the Day River Irrigation Company.

3.2.3.5 Terrain elevation data

This research collected available topographic maps in the Bui River Basin. A topographic map (1:2000 scale) of low-lying areas in Xuan Mai urban region, surveyed between 2014 and 2016 by the Mapping and Surveying Center was acquired for the thesis. Another topographic map (1:2000 scale) along the Tich-Bui River, surveyed in 2009 as part of the Tich-Bui River upgrading project by Hanoi's People Committee, was also obtained. The elevation data points from these topographic maps have a vertical accuracy ranging from 0.5 to 0.7 mm and a horizontal accuracy ranging from 0.13 to 1.7 m (MONRE, 2019).

The research necessities to collect a Digital Elevation Model (DEM) for the entire Bui River Basin to define the basin and sub-basins boundaries as well as basin characteristics. Currently, three global DEMs, which are freely accessible and widely used in developing countries, are 12.5 m Alos PALSAR, 30 m Shuttle Radar Topography Mission (SRTM), and 30 m ASTER (Al-Areeq et al., 2023) . According to Al-Areeq et al. (2023), 30 m STRM is the most suitable digital elevation model for flood hazard assessment. Therefore, the research used this data for further analysis. A list of Sentinel 2 images and other data collected in this research is shown in Appendix 8.1.

3.3 Citizen science in flood risk-related data collection

A citizen science program was deployed from September 2021 to August 2023 to collect flood risk-related data. This program includes three primary components: determination of collected flood risk-related data, involvement of citizen scientists, and comparison of citizen science data, followed the approach outlined by Bonney et al. (2009) (Figure 3.7).

These three components are explained in the following subsections. In addition, a community-based rainfall monitoring network was established to encourage citizen scientists to regularly participate and update flood risk-related data. The reliability of rainfall data collected by citizen scientists was evaluated by comparing them with automated rainfall measurements at an official station in the pilot area.

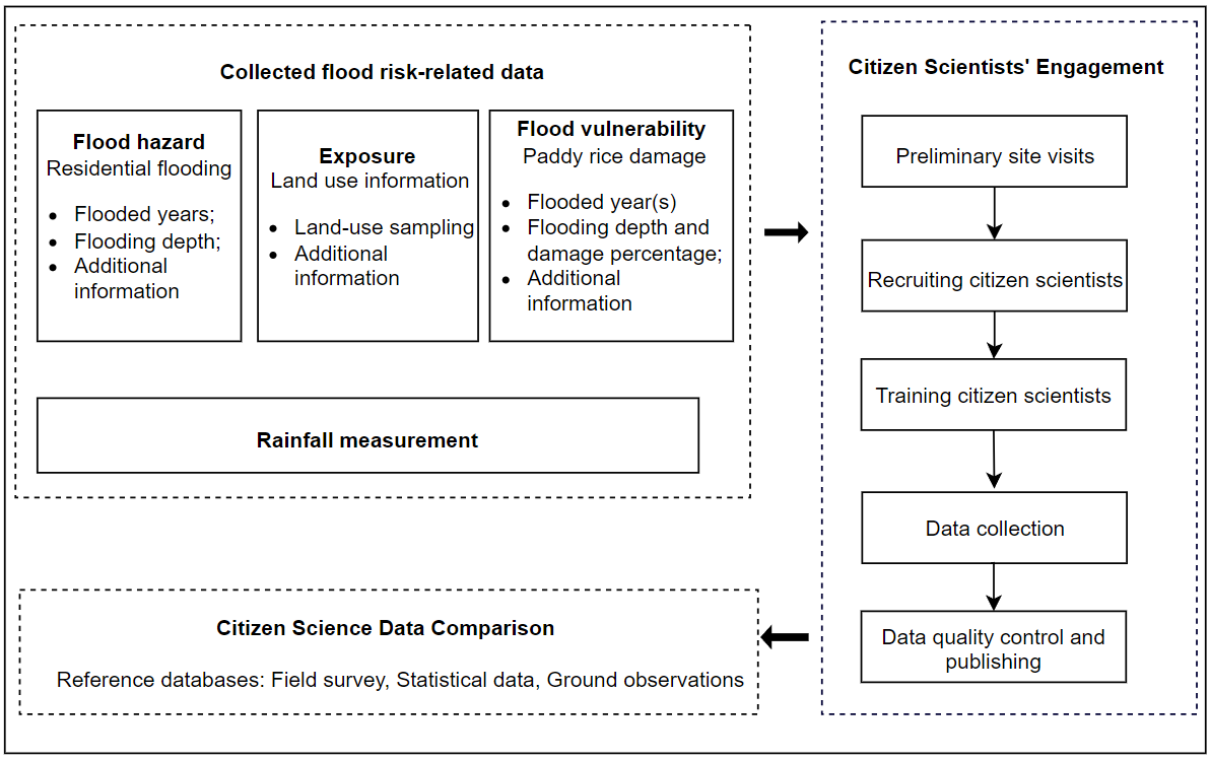

Figure 3.7. Research approach in flood risk-related data collection based on citizen scientists' engagement

3.3.1 Determining flood risk–related data

A flood risk assessment must be based on data on flood hazards, exposure, and flood vulnerability (Apel et al., 2009). Flood hazards refer to flood probability and intensity, including flood extent, flooding depth, and velocity data (Trinh & Molkenthin, 2021). Exposure data mainly refer to land-use, building datasets, and population distribution maps (de Moel et al., 2015). Flood vulnerability is mainly considered through stage damage curves showing the relationship between flood depth and damage rate of objects such as buildings, crops, and people (Merz et al., 2010).

In this study, data on flooding depth in residential areas and the flood damage to paddy fields (including flood depth and rice yield decline) of flood events within the past decade, and current land-use data in a pilot area were gathered. Land-use types were

categorized into seven classes, including high built-up area, low built-up area, paddy crop, nonpaddy crops, water body, forest, and shrubland (more detailed in section 3.5.1). Additionally, rainfall was measured in the pilot area and surrounding areas using low-cost rain gauges, as proposed by C. J. Davids et al. (2019).

A questionnaire, which was developed to gather essential data, consisted of two portions: respondents' biodata and flood risk-related data. The questions about flood hazards and flood vulnerability data followed the approach illustrated by Glas et al. (2018). The depth of flooding in residential areas was assessed using reference heights based on human body's and house's parts. This approach was chosen to create questions that are easy for citizen scientists to understand, as demonstrated by Peters-Guarin (2008) and Sy et al. (2020). The questions about exposure and rainfall data were derived from the research works of C. J. Davids et al. (2018, 2019), which required taking photographs of the surveyed objects. The questionnaire was built on the Open Data Kit (ODK) Collect app (Hartung et al., 2010) and the Kobo Toolbox web form (Klonner et al., 2021) for Android and non-Android mobile devices, respectively. Paper forms were used and delivered to citizen scientists to collect hazard data and vulnerability information. The list of questions used to collect data in this research, available via the Kobo Toolbox web form, can be accessed through the following link (https://bit.ly/3yPZ2R6).

3.3.2 Engaging citizen scientists

3.3.2.1 Site-preliminary visits

Site-preliminary visits were used for gaining a comprehensive understanding of the flood situation in the Bui River Basin, selecting the pilot area, and establishing reference datasets for comparison with citizen science data. ODK Collect app was deployed to gather flood marks in residential areas and current land-use data in the pilot area. Flooding depths of the 2018 flood, the biggest event in the past decade, were measured at flooded points using a steel tape measure (Figure 8.1 in Appendix 8.2). It is important to note that these recorded flooding depths may not accurately represent the maximum water level of an actual event. Although the accuracy of the recorded flood depths depends on the clarity of the flood marks on buildings and other objects, they still provide valuable information for reconstructing flood events.

The field sites where a typical land-use class from seven classes within a 20-meter radius can be determined were chosen to conduct a field experiment on land-use classification (Visser, 2015). The land-use type of these sites was classified by the author, and then was verified by a land management expert to ensure the consistency of the reference database (N. H. Tran et al., 2024).

3.3.2.2 Recruiting and training citizen scientists

The target group for this research was citizens living in or around the pilot area who were over 12 years old, regardless of their educational background. Personal relationships, social media, outreach at educational institutes, and field visits were used to recruit citizen scientists (C. J. Davids et al., 2019). The outreach programs were organized for secondary-school, high-school, and university students, and their content was amended to match the participants' backgrounds. The recruitment campaign period took place during the COVID-19 pandemic. Thus, the format of outreach events was adopted flexibly, with three being held on site, one virtually, and three through hybrid meetings. Participants who expressed interest in rainfall monitoring were provided with low-cost rain gauges (Appendix 8.3) that were set up in their residences (H. N. Tran et al., 2024).

Citizen scientists were trained to collect data through surveys or self-surveys using their preferred questionnaire forms. The training was offered through in-class, virtual, or on-site meetings. To further aid the training process, tutorial videos have been made available on the YouTube channel (https://bit.ly/44lfjHL; Vietnamese language only) to guide participants through data collection application installation and surveying procedures. Furthermore, picture-added explanations have been provided on digital forms.

3.3.2.3 Collecting data

The citizen scientists were classified into two groups. The first group was composed of individuals who either self-reported or interviewed their relatives on flood risk-related data or measured rainfall. These individuals were referred to as 'self-investigators'. They were requested to provide flood risk-related data at their convenient time within two weeks after the training session. The self-investigators were contacted to acknowledge their contributions, collect the completed paper forms or to request that they provide the

data again after two weeks. Furthermore, they were requested to measure rainfall at their residences frequently on days filled with rain and less frequently in periods with less rain.

The second group consisted of individuals who participated in field surveys to collect flood risk-related data from locals. These individuals were referred to as 'investigators'. The surveys were conducted by the investigators using digital forms (ODK Collect, Kobo Toolbox web form) after joining training sessions. Each investigator was assigned to specific areas to gather information on flooding in residential areas and flood damage to paddy fields. Land-use data in the field were sampled by both investigators and self-investigators during their daily activities or field surveys. To compare the results of land-use classification between citizen scientists and the author, a group of eight investigators performed a field experiment for one day in April 2022. This group visited the fourteen sites mentioned in the site-preliminary visits section to sample and classify land-use.

3.3.2.4 Controlling and publishing citizen science data

To control the quality of citizen science data, completed questionnaires of flood risk-related and rainfall data were reviewed every two or four weeks manually. During this process, popular errors such as wrong rainfall units, unclear pictures, and inconsistent data between answers and pictures were identified. Feedback was promptly provided to citizen scientists to reduce implausible data later on. Incorrect coordinates due to GPS signal errors and non-GPS-generated paper forms were processed based on the survey areas' address, Google Maps, and survey pictures (E. Beza et al., 2018; Ribeiro et al., 2020). All above discrepancies have been fixed, and edits have been recorded for future assessment. The data collected using ODK Collect is available on website (https://data.smartphones4water.org/, retrieved on October 19, 2024) apart from land-use data category, which is currently under development.

3.3.3 Evaluating citizen science data

In order to assess the dependability of citizen science data, a comparison between citizen scientists' data and reference datasets generated by the author or obtained from district authorities was made. The data of flooded and nonflooded points, and the flood damage rate to the paddy field in 2018, and land-use samples collected during the field survey in April 2022 obtained from citizen scientists were compared, which depends on the

reference datasets achieved from site-preliminary visits. The error matrices were used to estimate the overall agreement (OA) and individual agreement levels (Congalton, 1991) (see in section 3.5.1). In addition, the community-based rainfall data were compared with data measured at RT_Xuan Mai. The Pearson Correlation Coefficient (R) was applied to evaluate the significance of the agreement between the monthly CS data at one station with the longest measurement period and monthly rainfall at the RT_Xuan Mai (hereinafter called reference station) (Figure 3.3) (Fehri, Khlifi, et al., 2020). The equation of R is expressed below:

$$R = \frac{N \sum_{i=1}^{n} R_{CS}.R_R - (\sum_{i=1}^{n} R_{CS}) \times (\sum_{i=1}^{n} R_R)}{\sqrt{(N \sum_{i=1}^{n} R_{CS}^2 - (\sum_{i=1}^{n} R_{CS})^2) \times (N \sum_{i=1}^{n} {R_R}^2 - (\sum_{i=1}^{n} R_R)^2)}} \qquad (Eq\ 3.1)$$

with R_{CS} = citizen science data; R_R = reference data; N = number of data pairs.

To analyze flood hazard data, a comparison between flooded and nonflooded points gathered by citizen scientists with the flooding map for the 2018 flood was made. Additionally, differences in flood depth estimation at flooded points between citizen scientists' data and the flooding map were investigated. A flooding map was generated using the Digital Terrain Model (DTM) and the flood depth points, which is based on Ribeiro et al.'s approach (2020). The DTM, which reflects the earth's surface elevation excluded elevation of building and trees (Guth et al., 2021), was built using the Multilevel B-Spline method to interpolate elevation points of 1:2000 topographic maps. A 3-metre resolution DTM was developed to reflect the terrain changes of infrastructure along the river, such as roads and embankments, in the pilot area (hereinafter called the 3m DTM).

The flood level of flooded points was determined by summing the flooding depth and elevation values at these points (Giordan et al., 2018). A local combination method was used to define a typical flood level for each subdomain of 1 km x 1 km area for the pilot area (Mason et al., 2021) *(more detailed explanation is given in* section 3.4.2). Regions where elevation values were lower than the flood level surface were identified as inundated. The flood map was validated using statistics data on flood-affected areas gathered from district authorities. However, the lack of spatial distribution details in the statistics data meant that the total estimated flooded area was compared with statistics numerically.

To analyze flood vulnerability data, the flood damage to paddy fields collected by citizen scientists was compared with official flood damage data provided by the local authority for the 2018 flood event. The local authority's investigation primarily focused on damage information from households with affected areas ranging from 30% to 70% and equal to or more than 70%, as these damage rates were essential for compensation claims. In contrast, our research examined a more detailed classification of paddy field damage rates, categorized into 20% intervals (e.g., 20%- 40%, 40%- 60%). Therefore, the paddy field damage rates derived from citizen scientists were taken as the median values of their intervals (e.g., 30%, 50%) to compare with official data. These damage rates were then regrouped into three categories: less than 30%, from 30% to less than 70%, and equal to or more than 70%, corresponding to low, medium, and high levels of damage, respectively.

3.4 Flood hazard assessment

In this section, remote sensing, citizen science, and field survey data were explored to develop flood hazard maps for three floods in the pilot area in 2017, 2018, and 2022. Floods could potentially affect bare land and built-up areas, including residential areas. The S-1 satellite image taken during or right after the maximum water level period was utilized to detect flood extent on bare land. This image was analyzed utilizing the Otsu automatic threshold on the Google Earth Engine (GEE). The flood extent of each flood event was determined by subtracting the permanent water body area. Additionally, morphological transformation and refinement techniques were applied to eliminate misclassified flooding pixels. The research workflow employed to determine flood extent on bare land area is shown in (Figure 3.8A). Through engagement with citizen scientists and author-conducted field surveys, the flooding situation in residential areas was defined.

The flood extent boundary was intersected with the 3m DTM to estimate flood levels on bare land. Simultaneously, the flood level in residential areas was determined by summing the flooding depth and elevation values at flooded points. These two flood level types were combined to create a spatially varying flood level surface. Then, the flood level surface is overlaid on the 3m DTM. Pixels with elevation values lower than the flood level are considered flooded. The flooded area was compared with other independent data sources to evaluate the effectiveness of this approach. Based on the

flood frequencies of actual floods, the probabilities of flooding maps were determined to assess flood hazards. The research workflow employed to develop inundation maps is illustrated in Figure 3.8B.

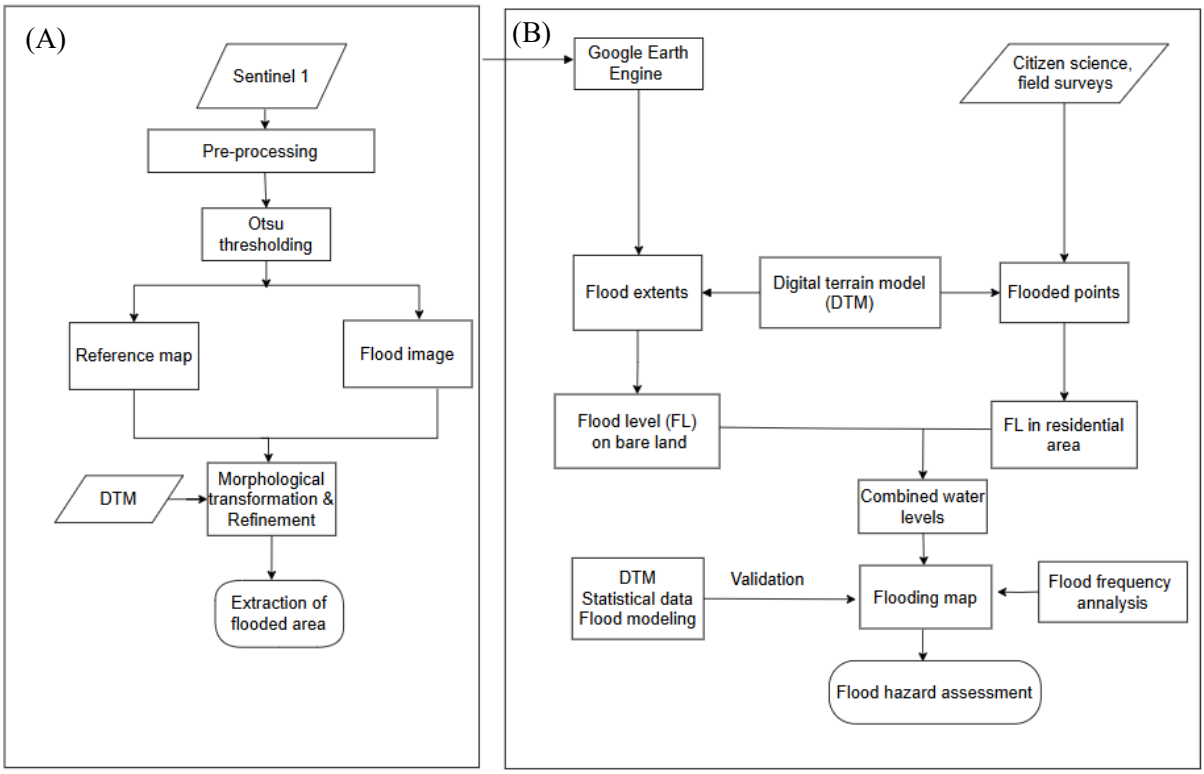

Figure 3.8. Workflow of flood hazard assessment in Bui River Basin

3.4.1 Flood extent on bare land

3.4.1.1 Pre-processing

Utilizing the Sentinel-1 toolbox, the S-1 images were preprocessed (Moharrami et al., 2021). Typically, the Sentinel-1 Level 1 image on the GEE has already been undergone validation for satellite orbital correction and thermal noise removal (Moharrami et al., 2021). However, in this research, the required pre-processing consisted of three steps: identifying the study area, filtering the images from the Sentinel-1 data collection with VV polarization for the chosen date range encompassing the study area, and applying speckle filtering.

In the first step, the boundary of the pilot area in the Bui River Basin was uploaded as an asset to localize S-1 coverage over the study area. In the second step, the Sentinel-1 image collection was filtered by instrument mode (Interferometric Wide (IW) swath mode), polarization (VV), orbiting pass (ascending and descending options), and image

resolution (10-meter resolution). Two filtered image collections were created: one containing a flood image taken during or right after peak flow date, and another containing pre-flood images taken during the three driest months in the study area in the same year as each flood event (Table 3.5). These images were mosaicked and clipped for subsequent analysis. In the final step, a speckle filter was applied to suppress noise pixels in S-1 radar images, addressing the inherent graininess property known as "salt and pepper appearance." The filtering method employed was a basic smoothing average filter with a circular radius of 50 meters (Moharrami et al., 2021; Tazmul Islam & Meng, 2022).

3.4.1.2 Image classification

The Otsu automatic threshold was employed to distinguish between water and non-water classes in the images based on backscatter values. Backscatter values in water areas are typically low due to their smooth surface, whereas other terrestrial objects exhibit higher backscatter intensity. Consequently, pixels falling below the identified threshold are considered to represent water areas. The optimal scenario for establishing a threshold occurs when the histogram displays a bimodal distribution with two peaks separated by a valley (Figure 3.9A) (Tazmul Islam & Meng, 2022). One mode corresponds to pixels in water areas, characterized by low backscatter values due to specular reflection on the water surface, while the other mode represents pixels with higher backscatter in non-water areas (Tazmul Islam & Meng, 2022).

The Otsu automatic algorithm is an iterative method that identifies the optimum threshold where the between-class variance of the two segments is maximized and the within-class variance is minimized (Otsu, 1979) (Figure 3.9B). The optimal threshold was determined for each image. Subsequently, the average optimal threshold was used to detect water and non-water classes in the flood and pre-flood images.

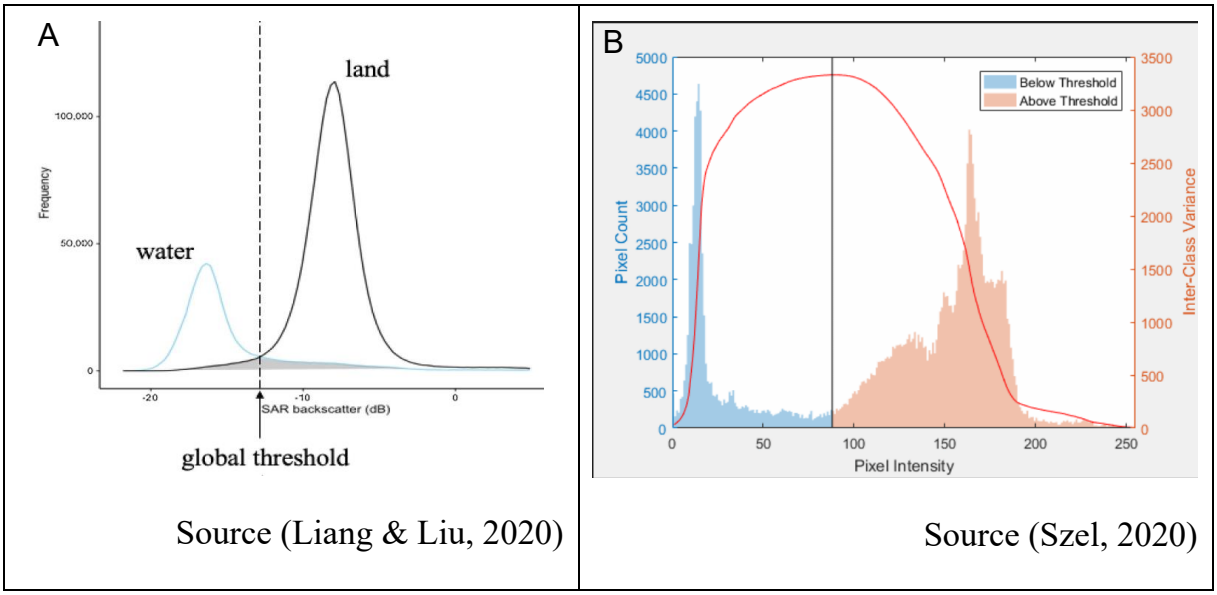

Source (Liang & Liu, 2020)

Source (Szel, 2020)

Figure 3.9. Example histogram of SAR backscatter intensity (A) and Otsu method visualization (B)

3.4.1.3 Defining flooded areas

To define the flooded area, the permanent water was subtracted from water class in the flood image corresponding to the flood year. Following the delineation of potential flooding areas, two refinement steps were applied, namely the removal of high-slope pixels and the elimination of areas with fewer than 8 connected pixels, to mitigate any misclassified regions. The first step involved eliminating pixels with high slopes, as areas with slopes exceeding 5% typically do not retain water and tend to drain to lower elevation regions (Tazmul Islam & Meng, 2022). For this refinement, the 3m DTM was utilized to estimate the slope in the GEE, uploaded as an asset. The second step involved removing any flooded areas with fewer than eight connected pixels (Tazmul Islam & Meng, 2022). These areas are typically very small and would not significantly contribute to the delineation of flooded regions in this study.

3.4.2 Flooding map

3.4.2.1 Flood levels on bare land

The estimation of flood levels in the bare land was conducted by intersecting the flood extent with the DTM, utilizing the elevation data at the flood boundaries (Mason et al., 2021). To address potential flood level outliers resulting from inaccuracies in the DTM interpolation method, specific satellite image properties, and the applicability of image classification methods, the flooding threshold within the study area was adjusted

(Huang, 2020; Mason et al., 2021). Specifically, areas characterized by elevated terrain, featuring large smooth surfaces or being shadowed in satellite images, which might be misclassified as flood points, were removed using the maximum flood level threshold (Tazmul Islam & Meng, 2022). Moreover, flooded points associated with water bodies such as active river channels, lakes, or ponds situated in low-lying areas were excluded by applying the minimum flood level threshold. The selected flood levels, ranging from 4 to 12 meters, was determined based on the flooding report specific to the study area (Hanoi, 2019).

Table 3.6. Flood level threshold in Bui River Basin

Elevation (m)		
Water body	Flooded areas	Nonflooded areas
< 4	[4-12]	> 12

Source (Hanoi, 2019)

3.4.2.2 Flood levels in residential area

Identifying flooding situations in built-up areas presents challenges when using S-1 images due to the high backscatter intensity caused by the double bounce mechanism (Giordan et al., 2018; Moharrami et al., 2021). This issue extends to flooded vegetation areas as well (Tsyganskaya et al., 2018a). To overcome the limitations of S-1 images, information about flooding in residential areas was gathered through the citizen science program and additional field surveys, as discussed in the Section 3.3. Furthermore, flooded points in crop areas were also documented during field surveys. Flood levels in residential areas were calculated based on the flooding depth and terrain elevation at these flooded points.

3.4.2.3 Flood level combination

In the subsequent step, the flood levels from the bare land were integrated with the flood levels in residential areas to generate a comprehensive flood level surface for the entire pilot area.

To account for the variation in flood levels along the reach and across different parts of the pilot area, a local combination method was employed (Mason et al., 2021). The pilot area was divided into non-overlapping rectangular m x n-pixel subdomains with 1-km

side (Figure 3.10). The combined flood level for each subdomain was computed by averaging the flood levels from the bare land and the residential area (Mason et al., 2021). This combined flood level was a weighted mean of the two averages, with the weighting determined by the number of flood levels of each type within the domain (Mason et al., 2021).

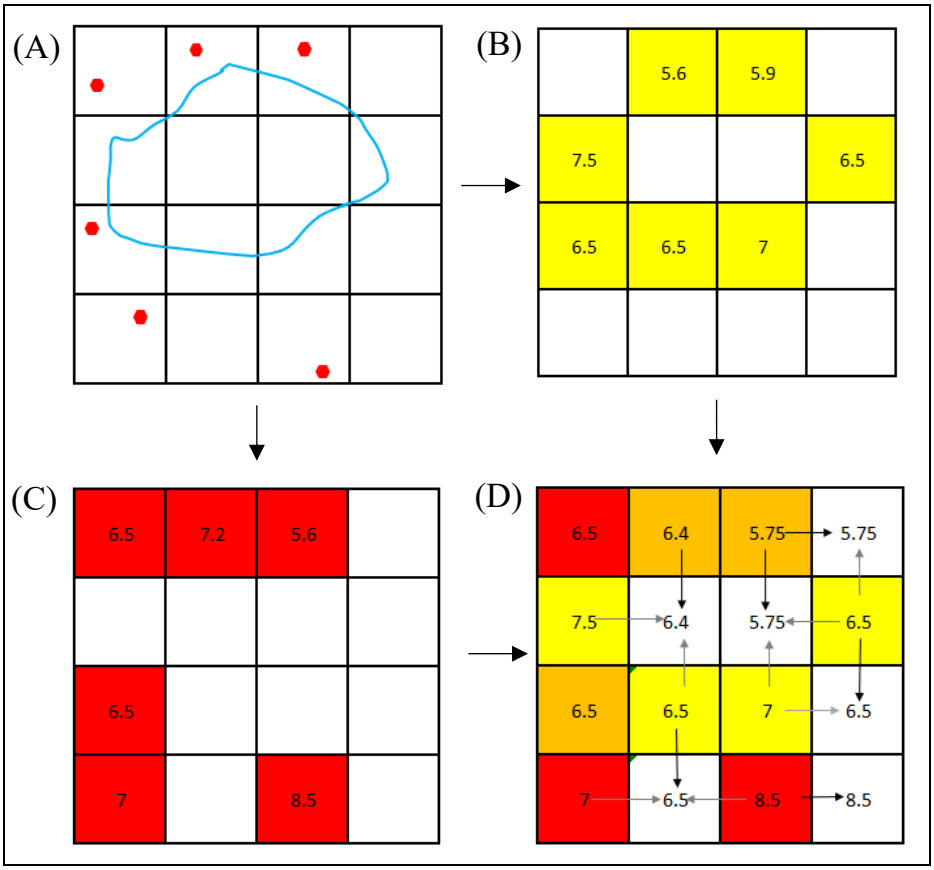

Figure 3.10. Illustration of the m x n subdomains map and the calculation of the combined flood level from bare land and residential area at subdomains: The illustration of flood boundary on bare land (blue line) and flooded points in residential area (red points) (A); average flood levels at flood boundary at each subdomain (B) average flood levels at flooded points (C); combined flood level at each subdomain (D)

In cases where only one type of flood level was available in a subdomain, the average flood level for that type was accepted as the subdomain's combined flood level (Mason et al., 2021). If a subdomain lacks any flood level, combined flood level was set to that of the nearest subdomain with the lowest flood level (Cohen et al., 2018). A flood level surface for a subdomain is created by creating a plane perpendicular to the vertical axis at the elevation corresponding to the combined elevation level. A flood level surface for

the entire domain was then gained by assembling the flood level surface of the individual subdomains (Mason et al., 2021).

3.4.2.4 Inundation maps

The inundation maps were generated by comparing the digital terrain model with the flood level surface (Mason et al., 2021) (hereinafter called DTM-based approach). Pixels where the flood level exceeded that of the digital terrain were identified as flooded, while those where the flood level was lower or equal remained unflooded (Mason et al., 2021). Flooding depth was calculated by estimating the difference between the flood level and the DTMs at each flooded pixel. This depth was obtained by subtracting the digital terrain model value from the flood level value. The inundation map was corrected by removing areas identified as floodplains but located in protected areas, such as by embankments, on the left riverbank of the Bui River Basin (Giordan et al., 2018).

3.4.3 Inundation map evaluation

The inundation maps using the DTM-based approach were cross-checked with various data sources to assess their reliability. Firstly, the estimated flooding area was compared with the flooded area calculated from the annual flood reports and the statistics of flooded agricultural land and the number of flooded households from Chuong My District (Chuong My District People's Committee, 2018). The percentage of flood area error was computed to measure the difference between the estimated flooding area and statistics data. Secondly, a model-based approach was utilized to evaluate the suitability of the flooding map (Peter et al., 2022). The HEC-RAS hydrodynamic model, briefly described and presented in Appendix D: Flood modeling in Bui River Basin, was employed for this purpose. The root mean square difference (RMSD) and the mean absolute difference (MAD) of all cells between the two flooding depth maps, widely applied for validating different approaches (Apel et al., 2009; Fohringer et al., 2015), were utilized in this research.

3.4.4 Flood frequency analysis

Flood hazard maps are traditionally estimated to correspond to specific flood frequencies. Previous research mostly utilized historical rainfall and discharge data to determine the characteristics of flood events with different return periods (A. K. Gain &

Hoque, 2013; Trinh, 2023). These data were then used as input for hydrologic and hydraulic modeling to simulate flood hazard maps (A. K. Gain & Hoque, 2013; Trinh, 2023). Due to the unavailability of flood discharge data in the pilot area, the maximum flood level at the Tri Thuy station from 1960 to 2022 was utilized to assess flood frequencies and their corresponding values. Based on these flood values, the probability of the three investigated floods was determined (Chau, 2014; V. H. T. Duong, 2018). Several probabilistic distributions, such as Pearson type III, log Pearson type III, and the Gumbel distribution, are used for analyzing extreme values in hydrology (A. K. Gain & Hoque, 2013). This research employed Pearson type III, successfully used for assessing flood characteristics in Vietnam and other Asian countries (A. K. Gain & Hoque, 2013; H. L. Nguyen et al., 2017).

3.5 Exposure and Vulnerability modeling

3.5.1 Exposure

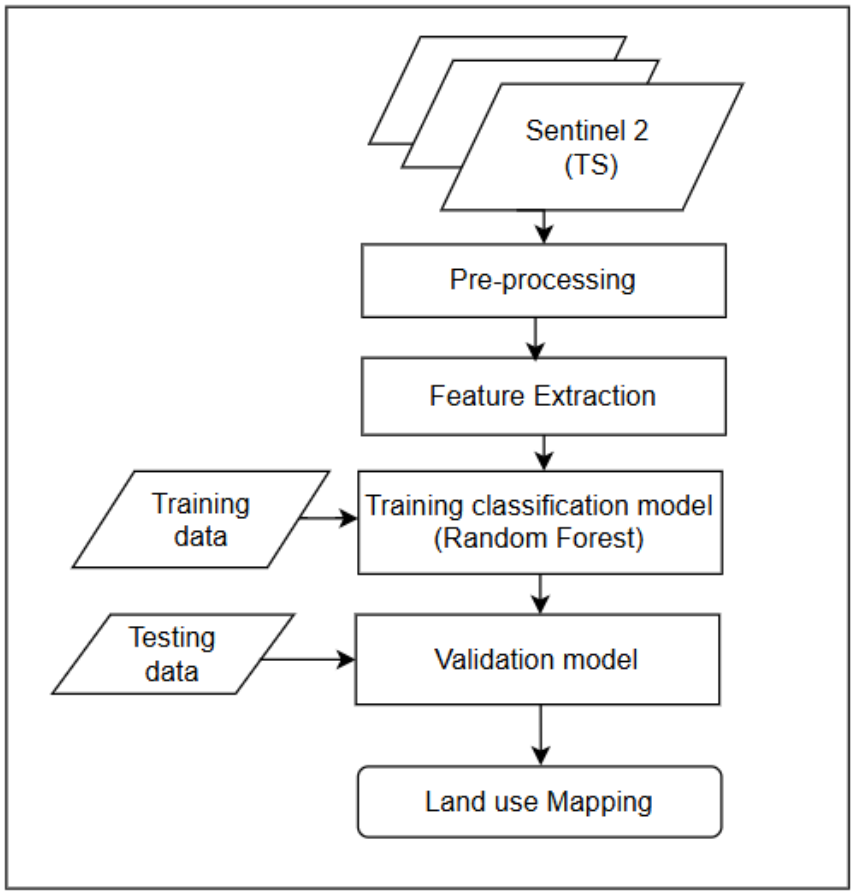

Figure 3.11. Workflow for land-use map development using Sentinel 2 on Google Earth Engine (adapted from Phan et al. 2019)

The research workflow for mapping land-use obtained from S-2 images on the GEE is shown in Figure 3.11, comprising preprocessing, classifying, and evaluating steps. The land-use map was divided into seven classes: high built-up area, low built-up area, paddy crop, nonpaddy crops, water body, forest, and shrubland. The definitions of these land-use classes were outlined in the research's C. J. Davids et al. (2018). The land-use map in this research serves not only to identify potential agricultural land exposed to flooding but also to determine model parameters for hydrological and hydraulic modeling (Trinh, 2023).

3.5.1.1 Image pre-processing

S-2 remotely sensed data in the dry season of 2022 from January to May, were collected to develop the land-use map on the GEE. The boundary of the Bui River Basin in shapefile format was uploaded to the GEE as an asset to delineate the calculation boundary. In addition to identifying agricultural land for the pilot area to estimate flood-exposed objects, it was imperative to determine the land-use map for the entire Bui River Basin. This allowed for the estimation of basin characteristics related to land-use for further analysis. Images with cloud cover exceeding 30% of the image area were excluded by the selection process. All collected images were then combined into a single image by using the median function on the GEE (H. T. T. Nguyen et al., 2020).

3.5.1.2 Training and testing data

Ground truth samples are crucial for the image classification model, serving as training data for training model or testing data for validating model. The sample size needs to be at least 50 for each class (Dibaba et al., 2020), with the sample locations well distributed within the study area. These requirements pose challenges in acquiring sufficient training and testing data (H. T. T. Nguyen et al., 2020), necessitating significant effort and financial resources. In this research, the author integrated different data sources through field surveys, citizen science, and very high-resolution images from Google Earth.

A total of 388 ground truth samples were collected. The data set was augmented by 206 geo-tagged photos from field sites, which were captured by citizen scientists and the author. These images provided insight into the current land-use situation in the study area. Additionally, 25 geo-tagged photos shared by the community on Google Maps

from 2017 to 2021 were utilized. These images were captured close to the investigated year. Figure 3.12 illustrates a photograph provided by the community on Google Maps. This approach is also considered as citizen science approach, as employed in the research of Dong et al. (2016). The remaining 157 samples were randomly collected using Google Earth, primarily in remote areas for the forest and shrubland classes. The map displaying the locations of the sample sites is presented in Appendix 8.6. 70% of the ground truth samples were allocated for training, while the remaining samples were reserved for validating image classification methods.

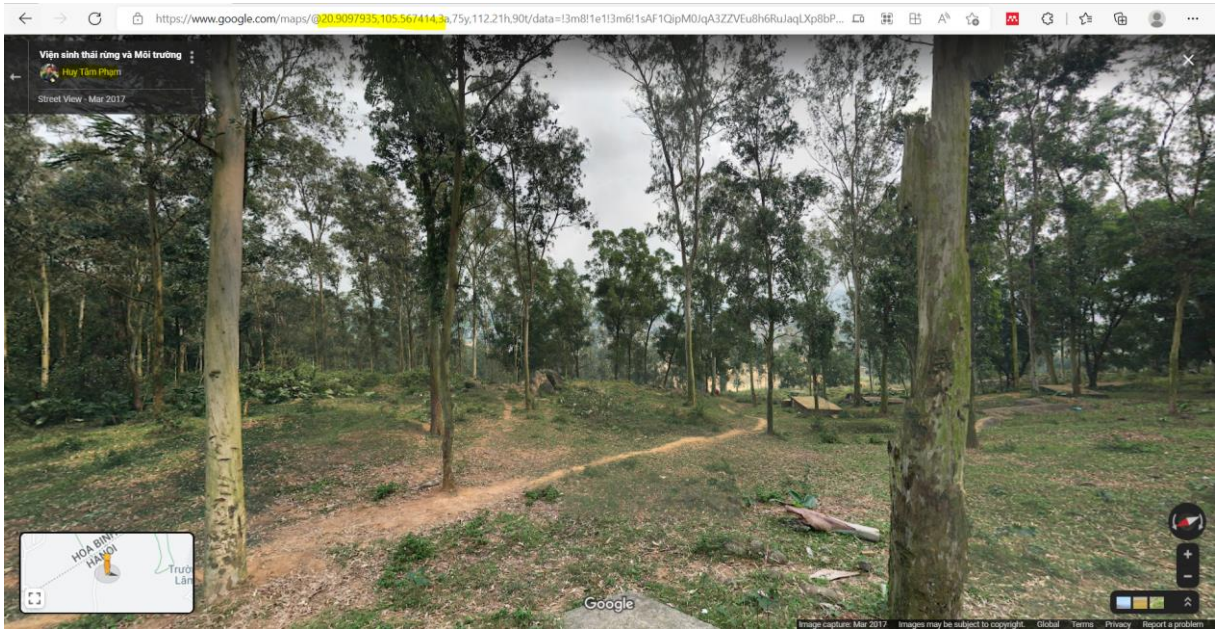

Figure 3.12. A forest land sample in Xuan Mai town, Chuong My, shared by the community on Google Maps

3.5.1.3 Image classification

Random Forest (RF), developed by Breiman (2001), is a supervised classification algorithm that combines decision trees, bootstrapping, and bagging techniques. Bootstrapping, introduced by Efron (1979), is a well-known statistical method. A decision tree is a growing diagram with a branching tree structure extending from the root (root node) to the leaves (leaf nodes) (T. T. H. Nguyen & Doan, 2018) (Figure 3.13). The connections between nodes are referred to as branches. At each node, the decision tree checks the value of the classification classes from the sample. Each training sample generates a specific tree structure from the root (i.e., the input data) to the leaves (i.e., the output prediction classification results), representing the prediction of their

subclassification value. The training sample, which is a bootstrap, was randomly selected from a sample set. N bootstraps were created by resampling n times with replacement of components from the original sample. N bootstraps generate N trees. The bagging is considered a synthesized method, aggregating results from decision trees to enhance accuracy (T. T. H. Nguyen & Doan, 2018).

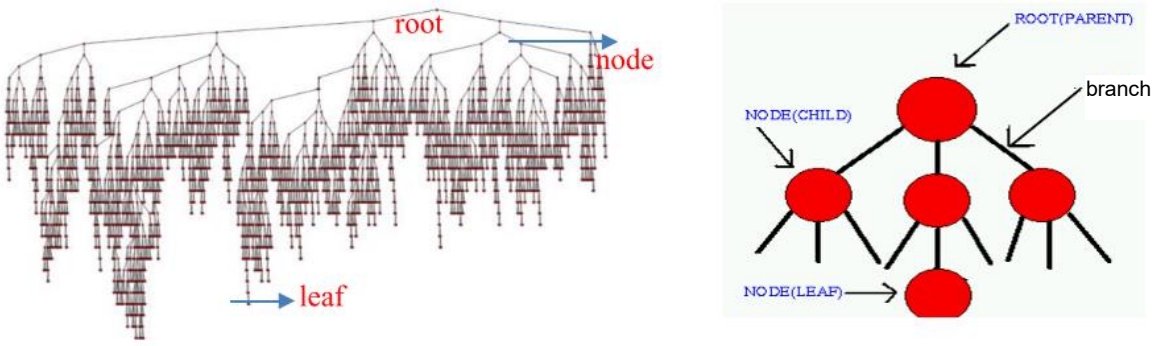

(Basten, 2016)

Figure 3.13. Diagram of the decision tree

The RF classifier requires the choice of two parameters: ntree (the number of trees to grow) and mtry (the number of variables to split each node) (H. T. T. Nguyen et al., 2020; Steinhausen et al., 2018). The number of trees depends on the shortest calculation period, during which the error rate is lowest. The author used the optimal value, 300 trees, which was invested in classifying the land-use map in one case study in Vietnam by (H. T. T. Nguyen et al., 2020). According to Steinhausen et al. (2018), the mtry can be estimated by calculating the square root of the total input features or the number of land-use classes (7 land-use classes were considered in this research). In the implementation of the RF classifier on the GEE, the mtry parameter is randomly selected and hidden for efficient use on cloud-based computing platforms.

3.5.1.4 Accuracy assessment

An error matrix commonly used to assess the accuracy of image classification results (Steinhausen et al., 2018). The error matrix tabulates the counts of samples classified concerning both classification results and reference data, organized in rows and columns (Figure 3.14) (Steinhausen et al., 2018). The rows represent the classification results assigned in the remote sensing data, while the columns indicate the reference data (Congalton, 1991). The diagonal of the error matrix represents the data categorized

correctly. Data that are misclassified do not feature on the diagonal and give an indication of the confusion between the different land-cover classes in the class assignment (Rwanga & Ndambuki, 2017).

		Reference data				
	Classes	A	B	C	D	Σ
Classified data	A	n_{AA}	n_{AB}	n_{AC}	n_{AD}	n_{A+}
	B	n_{BA}	n_{BB}	n_{BC}	n_{BD}	n_{B+}
	C	n_{CA}	n_{CB}	n_{CC}	n_{CD}	n_{C+}
	D	n_{DA}	n_{DB}	n_{DC}	n_{DD}	n_{D+}
	Σ	n_{+A}	n_{+B}	n_{+C}	n_{+D}	N

Source: https://gofcgold.umd.edu/sites/default/files/docs/ReportSeries/GOLD_25.pdf

Figure 3.14. A structure of an error matrix

The error matrix is useful for evaluating overall accuracy, Kappa coefficient, user's accuracy, and producer's accuracy (Foody, 2002). Firstly, the overall accuracy is calculated by dividing the total correct data (i.e., the sum of the diagonal elements) by the total number of samples (Congalton, 1991). Additionally, this research estimates individual category accuracies, namely user's accuracy and producer's accuracy, which indicate the probability that the data classified on the map actually represents that category on the ground and the probability of the reference data being correctly classified (Congalton, 1991). These accuracies are computed by dividing the number of correct data in that category by the total number of data in the corresponding row and column, respectively. Finally, Kappa coefficient, a discrete multivariate technique, is conventionally used to estimate the accuracy of image classification (H. T. T. Nguyen et al., 2020; Steinhausen et al., 2018). The formulation of these four factors is expressed as follows and is described in Congalton (1991):

$$\text{Overall Accuracy (OA)} = \frac{\sum_{k=1}^{q} n_{kk}}{N} \text{ x } 100\%$$

$$\text{User's Accuracy (UA)} = \frac{n_{ii}}{n_{i+}} \text{ x } 100\%$$

$$\text{Producer's Accuracy (PU)} = \frac{n_{ii}}{n_{+i}} \text{ x } 100\%$$

$$\text{Kappa Coefficient} = \frac{N \sum_{k=1}^{q} n_{kk} - \sum_{k=1}^{q} n_{+k}\, n_{k+}}{N^2 - \sum_{k=1}^{q} n_{+k}\, n_{k+}}$$

where;

N = total number of reference data (pixels), q = number of row and column in the error matrix;

n_{kk} = observation in row i, and column i;

n_{+k}, n_{k+} are the marginal total of column i, and the marginal total of row i, respectively.

3.5.1.5 Production value of agricultural land

The agricultural land map, encompassing paddy fields, nonpaddy crops, and aquaculture, was derived from the land-use map. The gross production values for agricultural land-use type, which represent the cost to replace these elements if they are completely damaged, have been estimated based on the economic value expressed in euros per m^2. The gross production value of each agricultural land type was derived from the statistical yearbook of Chuong My district in 2018 (Chuong My, 2019) (Table 3.7). The gross production values of paddy crops and aquaculture land were derived from statistics on the economic value of summer-autumn rice cultivated land and the annual cultivated aquaculture area in 2018, respectively. The gross production value of other crops was calculated based on the mean annual economic value of annual crops and perennial crops.

Table 3.7. Gross production values for different agricultural land-use types

No	Agricultural land	Gross production value (Euro /m^2)	Notes
1	Paddy crop	0.12	Paddy crops are harvested twice per year. The winter-spring season is from January to May, while the summer-autumn season is from June to October.
2	Nonpaddy crops	0.51	Crops are harvested once to twice per year.
3	Aquaculture	0.69	Aquacultural areas are harvested once per year.

3.5.2 Flood vulnerability

The flood vulnerability is primarily assessed through stage damage curves, also known as vulnerability curves (Englhardt et al., 2019). In this study, stage damage curves for agricultural land were constructed using data obtained from the field survey, citizen science, and literature. The field survey on flood damage to paddy fields of the 2018 flood was conducted in Thuy Xuan Tien commune. Based on the number of households with flood-affected paddy fields (n =422) and a desired confidence interval of 1.96 (95% confidence level), the target sample size was determined (n=164) (Adam, 2020). Additionally, flood vulnerability data on paddy fields collected by citizen scientists, as mentioned in Section 3.3 were utilized.

The relationship between the ratio of paddy field damage and flooding depth levels was plotted to select an appropriate curve. According to (N. Y. Nguyen et al., 2017; Win et al., 2018), the S-shaped curve yields results closer to actual damages. The study adopted the stage damage curves for nonpaddy crops and aquaculture proposed and developed by (N. Y. Nguyen et al. (2017) and H. N. Pham et al. (2018), respectively. After compiling the stage damage curves, flood damage for three actual events was estimated by overlaying flood hazards, an agricultural production value map, and these curves.

3.6 Flood risk assessment

The flood risk assessment was formulated through the utilization of the risk curve, also known as the damage-probability curve (Ţîncu et al., 2020). The risk curve was constructed by plotting the total damage values for three floods against their corresponding probabilities. Therefore, each scenario represents a point whose position depends on the probability of occurrence and the total consequences (Ţîncu et al., 2020). The entirety of the annual flood risk is depicted as the area under the risk curve. The calculation of the total annual flood risk was carried out using Eq 3.2, as introduced in Ţîncu et al's research (2020).

$$Risk = \frac{1}{T_1} \times \frac{S_1}{2} + \left(\frac{1}{T_1} - \frac{1}{T_2}\right) \times \frac{(S_1 + S_2)}{2} + \left(\frac{1}{T_2} - \frac{1}{T_3}\right) \times \frac{(S_2 + S_3)}{2} \qquad Eq\ 3.2$$

where: T represents the return period (T1 < T2 < T3), and S represents the sum of damages calculated for each return period.

3.7 Used applications

3.7.1 Google Earth Engine

GEE is a cloud-based computing platform for processing remotely sensed data and other geospatial and observation data (Portengen, 2017). It offers an extensive library of satellite images, including Sentinel 1 and 2, as well as Landsat and MODIS long-existing data (Portengen, 2017). Its functionality is accessible through an Application Programming Interface (API) provided in both JavaScript and Python. For the JavaScript API, there's a web-based integrated development environment (IDE) known as the Earth Engine code editor, accessible at https://code.earthengine.google.com/.

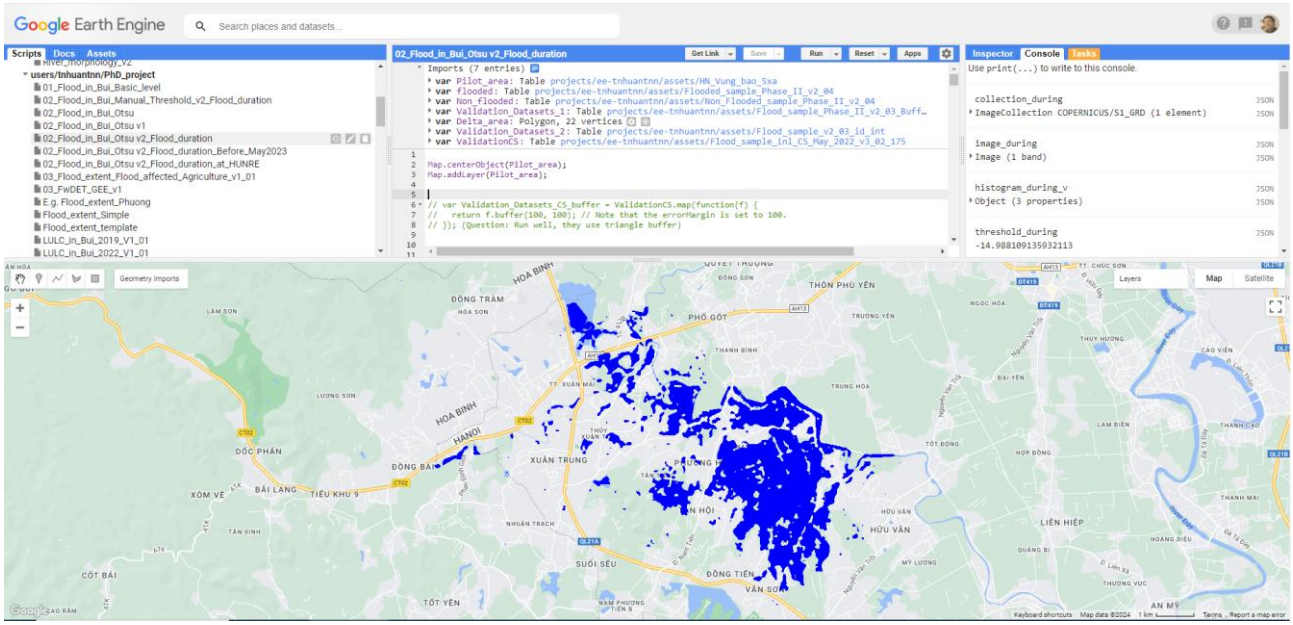

Figure 3.15. Main interface of the Google Earth Engine JavaScript API

An illustration of this code editor, utilized in this study, is shown in Figure 3.15. The left panel of the code editor includes a script manager ("scripts"), comprehensive documentation of the JavaScript API algorithms ("docs"), and an asset manager ("assets"). Within the script manager, various example scripts are accessible to demonstrate different operations. The middle section hosts the JavaScript API, where users can create their scripts. There's a click tool that gives values from the maps below ("inspector"), the "console" where the print commands are shown, and a task manager ("task") on the right panel of the code editor. A "Get Started Guide" is provided at https://developers.google.com/earth-engine/getstarted, offering guidance on

fundamental operations such as data importing, filtering, sorting, masking, and visualizing image collections (Portengen, 2017).

3.7.2 HEC software suite

The Hydraulic Engineering Center (HEC) software suite, which includes HEC-HMS and HEC-RAS models, was used to simulate the floods. This research simulates hydrological processes by applying the HEC-HMS model developed by the U.S. Army Corps of Engineers (USACE). Detailed documentation of all model components and their mathematical descriptions can be found in the technical reference manual (HEC, 2000). Additionally, 2D overland flow is assessed using the hydrodynamic model HEC-RAS, also developed by the USACE. The theoretical foundation for 2D unsteady flow hydrodynamics is extensively documented in the technical reference manual (HEC, 2016).

3.7.3 QGIS

Quantum Geographical Information System (QGIS) is an open-source and free desktop application that facilitates the viewing, editing, and analyzing of geospatial data (Maleska, 2021). This research used QGIS 3.22. For instance, QGIS was utilized to create a digital terrain model from elevation points based on the interpolation method. Additionally, river basin or sub-basin characteristics were analyzed and determined using QGIS based on SRTM data, leveraging toolboxes and plugins (Mancusi et al., 2015). Furthermore, outputs from GEE were processed and calculated within QGIS to streamline script complexity and reduce calculation time. Following the determination of flood hazards, exposure, and stage damage functions, QGIS was employed to estimate flood damage.

3.7.4 Computer programming language

Python, an interpreted, high-level, general-purpose programming language, was used to preprocess raw data and plot charts in this research. This application is an open-source software provided by a non-profit organization, the Python Software Foundation (PSF) (Maleska, 2021). In addition, this research used JavaScript to analyze the satellite images on GEE as mentioned in Section 3.7.1.

3.7.5 Data collection application

This research utilized the smartphones4Water (S4W) data collection platform developed by the S4W organization to collect, store, manage, and disseminate flood-related data measured and collected through citizen science program and field trips (J. C. Davids, 2019). An Android smartphone application called ODK Collect, a part of S4W data collection platform, was used for gathering data in the field, including measurement location and photos of investigated objects (J. C. Davids, 2019; Hartung et al., 2010). Additionally, the Kobo Toolbox web form was employed for non-Android-based mobile devices to reach a larger number of participants.

3.8 Chapter summary

This chapter presents a comprehensive methodology for assessing flood risk, leveraging the synergistic potential of citizen science, remote sensing, field surveys, and literature. It encompasses three key components: engagement of citizen scientists in flood data collection, a simplified approach for flood hazard assessment, and an annual estimation of the flood damage for agricultural land. This methodology was applied to the Bui River Basin, Vietnam.

The Bui River Basin, located in northern Vietnam, is known for its complex hydrological dynamics and has experienced frequent and intense flooding over the last fifteen years, notably in 2017, 2018, and 2022. Factors contributing to flooding include intense rainfall, complex topography with semi-mountainous and semi-plain landforms, and rapid land-use changes. This research focuses on specific areas within the basin, such as Thuy Xuan Tien commune and Xuan Mai town in the Xuan Mai urban area, which is well-known as the “flooded village” of Hanoi, the Vietnam’s capital. By narrowing the scope to these critical areas, the methodology aims to provide targeted insights into the applicability of citizen science for collecting flood risk-related data, developing flood hazard mapping, and conducting annual flood damage assessments on agricultural land tailored to local conditions.

Various types of data to assess flood risk in the study area were gathered for this research, including meteorological and hydrological data, S-1 and S-2 images, a soil map, topography maps, and statistics on flood-affected areas and gross production value of agricultural land. These data were collected from various institutes, such as

government agencies, district authorities, and research institutions. Additionally, data from published literature was used to contribute to data availability. The data are generally reliable with good spatial and temporal resolutions, making them suitable for this research's purposes. However, the lack of some crucial data or inconsistent data caused by measurement or collection could affect the accuracy of results, which is discussed in the results and discussion sections.

Citizen scientists played a vital role in complementing flood-related data collection. The research focused on gathering three types of flood data: flooding in residential areas, land-use, and flood damage to paddy fields. Leveraging their local knowledge and community connections, participants from various educational backgrounds contributed actively their own information or conducted surveys to provide flood-related data. Through tailored training sessions and the utilization of user-friendly data collection tools, citizen scientists were empowered to contribute historical data, real-time observations, photographs, and geographical data. The citizen science data were compared with different sources created by the author or gathered by the local authority to evaluate their reliability. By establishing the community-based rainfall monitoring network, this research encouraged citizen scientists to measure rainfall regularly and update flood data. The rainfall data collected by citizen scientists were also compared with rainfall data collected from the official station.

The integration of remote sensing, citizen science, and field survey data served as a simplified approach for mapping and analyzing flood hazards within the study area. Remotely sensed S-1 images were used to detect flood extent on bare lands where backscattering is not affected by double bounces like in the residential area, utilizing GEE. The boundary of the flood extent was combined with DTM to determine the flood level at these boundaries. In addition, citizen science, and field survey data provided flooding depths at flooded points in residential areas, which were combined with ground elevation values on DTM to identify the flood level. These two types of flood levels were combined to estimate the flood level surface for the whole area. Then, the flood level surface was subtracted from the DTM to determine the flooding depth. Subsequent validation of flood mapping outputs was conducted, comparing them with statistical and modeling-based information.

To assess flood damage to the agricultural land in the study area, apart from the flood hazard mapping development, the agricultural land was required to be established based on S-2 images. Besides, the stage damage curves of paddy fields, nonpaddy crops, and aquaculture were developed. Based on documented flood data at a gauging station, the flood frequency of the investigated flood event was estimated, enabling the development of a damage-probability curve. Subsequently, annual flood damage for the study area, often called flood risk, was estimated.

By integrating citizen science, remote sensing, field surveys, and literature, this methodology offers a comprehensive approach to flood risk assessment, providing valuable insights into flood dynamics, hazard mapping, and damage estimation for data-scarce areas like the Bui River Basin, Vietnam. The results and applicability of each methodology will be presented in the next chapter.

4 Results

4.1 The citizen scientists' engagement in flood-related data collection

4.1.1 General information about data collected by citizen scientists

4.1.1.1 Demographics of citizen scientists

Table 4.1 shows the demographics of citizen scientists in this research. General information about each citizen scientist can be found in Appendix 8.7. 60 citizen scientists participated in the citizen science program, with nearly half (49%) aged between 18 and 33. 56% of participants had a college degree or lower, whereas 36% held a bachelor's degree. 47% of participants were recruited for the citizen science program through personal relationships, while only 2% were recruited through social media. The number of self-investigators was approximately three and a half times greater than the number of investigators.

Table 4.1. Demographic characteristics of citizen scientists

Characteristics	Categories	Number	Percent (%)
Gender	Female	31	52%
	Male	29	48%
Age ([4])	12-17	22	39%
	18-33	28	49%
	34-60	7	12%
	> 60	0	0%
Educational background ([5])	< Bachelor	33	56%
	Bachelor	21	36%
	> Bachelor	5	8%
Recruitment method	Outreach	13	22%
	Personal relationships	28	47%
	Social media	1	2%
	Random visit	18	30%

[4] Some citizen scientists did not provide this information. Therefore, not all categories total exactly 60 samples.
[5] <Bachelor's, Bachelor's, and >Bachelor's imply the top education degree acquired or currently matriculated by the citizen scientists.

Characteristics	Categories	Number	Percent (%)
Type of survey	Self-investigators	46	77%
	Investigators	14	23%

4.1.1.2 Received data

60 citizen scientists provided 649 flood-related data for two years (Figure 4.1). The distribution of the data number per citizen scientist decreased with increased data per citizen scientist. 27 citizen scientists (45%) provided data a single time. Six citizen scientists (10%) provided more than 50 data per person, which are considered "active participants." This active group contributed 55% of the data for two years, expanding the total data number from 289 to 649.

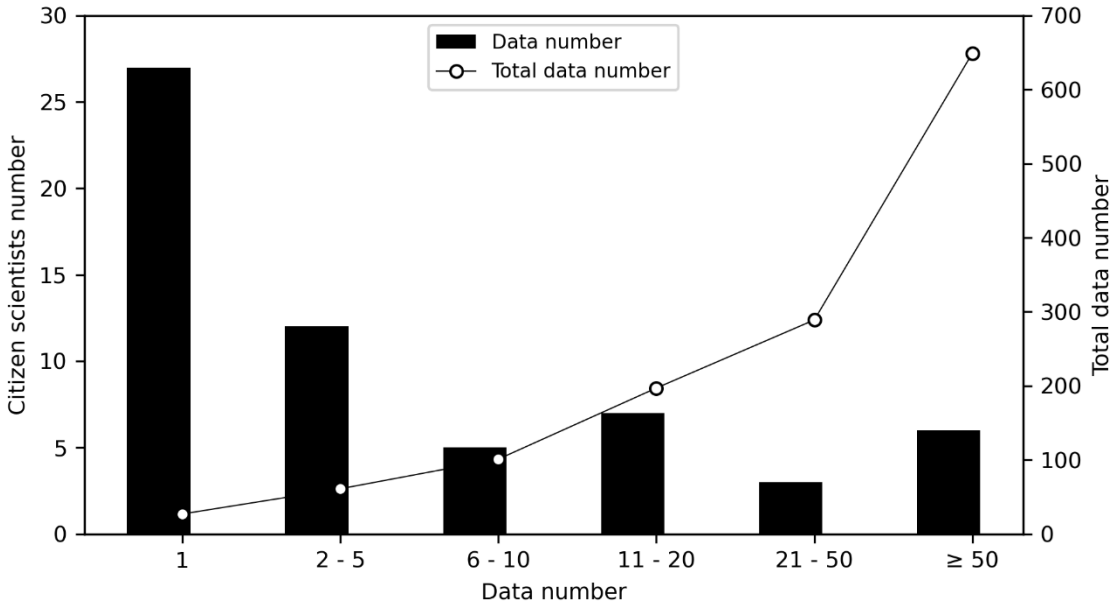

Figure 4.1. Data number collected per citizen scientist

Table 4.2. Flood-related data number collected by citizen scientists for two years

Data types	Hazard	Exposure	Vulnerability	Rainfall	Total data
Number	70	138	46	395	649
Percent (%)	11	21	7	61	100

Table 4.2 illustrates the distribution of the 649 data points across four categories: flood hazard, exposure, flood vulnerability, and rainfall. Notably, exposure and rainfall data constitute the majority of the total, representing 21% and 61%, respectively. In contrast,

data on flood vulnerability and flood hazard are considerably lower, comprising only 7% and 11%, respectively.

4.1.2 Data quality evaluation

4.1.2.1 Flood hazard

Citizen scientists collected 70 flood hazard data points, of which 64 were located within the pilot area (Figure 4.2, and Appendix 8.8). Among these 64 points, 25 have never experienced flooding, while 39 had experienced flooding in the past. Flood events of 2013, 2017, 2018, 2019, and 2021 were frequently mentioned. Additionally, a flood event in 2022 was documented by citizen scientists at 8 flooded points. The citizen science-based survey sites (IDs 7, 9, 10, 17, 39 in Figure 4.2) provided valuable information, such as videos, photos, and additional information, which significantly enhanced the interpretation of the citizen science data. The 2018 flood, which was the largest in the last decade, was mentioned at 20 locations. Of these, twelve points included detailed information on the depth and duration of the flood. In this research, these twelve flooded points and twenty-five non-flooded points collected by citizen scientists were used for comparing to a flooding map for 2018, as explained in the following paragraph.

The 2018 flooding map was constructed using 89 flooding depth points collected by the author during preliminary site visits and a topographic map (Figure 4.2). The flooded area on the flooding map was 447 hectares, which is 2% greater than the flood-affected area provided by the local authority, making the flooding map suitable for comparison with citizen science data. The comparison revealed a substantial overall agreement (OA) of 86% between flood survey points collected by citizen scientists and the flooding map for 2018 (Table 4.3). Notably, nonflooded points reported by citizen scientists demonstrated higher reliability compared to flooded points, with agreement rates of 96% and 67%, respectively. With regard to flood intensity (i.e., flooding depth), the average flooding depth of the eight flooded points documented by citizen scientists was found to be 0.34 meters higher than the depth extracted from the flooding map (Appendix 8.8).

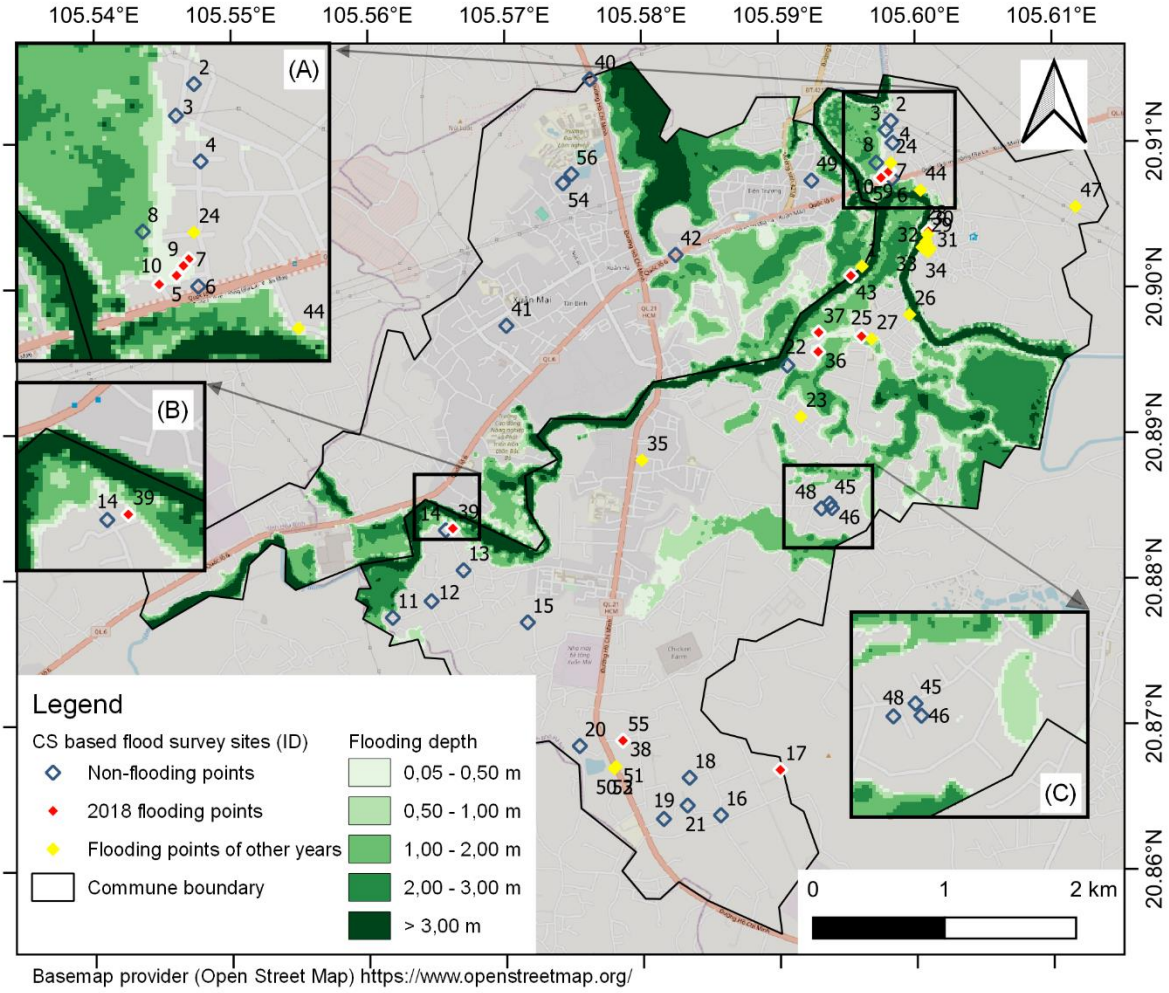

Figure 4.2. Flooding map for 2018 in study area and flood hazard surveying points from citizen scientists

Table 4.3. Error matrix of flood hazard data for 2018 collected by citizen scientists

Flooding map / Citizen scientists	Flooded points	Nonflooded points	Total reference points	Participants' agreement
Flooded points	8	4	12	67%
Nonflooded points	1	24	25	96%
			Total: 37	**OA =86%**

4.1.2.2 Exposure data

The degree of agreement in land-use classification between citizen scientists and the author was evaluated using an error matrix (Table 4.4). During the field experiment

conducted in April 2022, eight citizen scientists collected 100 land-use samples, which accounted for approximately 90% of the expected total samples (112 samples: 8 citizen scientists visited 14 sites to take land-use samples), through data collection applications. The map displaying the locations of land-use sample sites is provided in Appendix E. The overall agreement reached a value of 82%, indicating significant concordance in land-use classification between citizen scientists and the author. Citizen scientists demonstrated accurate classification of high-built-up, paddy crop, and water body areas with no instances of confusion. Additionally, they exhibited nearly perfect agreement in the classification of forest and low-built-up lands, achieving 81% and 85% agreement, respectively. However, the nonpaddy crops and shrubland classes proved to be the most challenging for participants, with only 47% and 64% accuracy in classifying nonpaddy crops and shrubland, respectively.

Table 4.4. Error matrix of land-use classification performed by citizen scientists

Authors / Citizen scientists	High built-up	Low build-up	Paddy crop	Nonpaddy crops	Water body	Forest	Shrubland	Total reference points	Participants' agreement
High built-up	16	0	0	0	0	0	0	16	100%
Low built-up	2	11	0	0	0	0	0	13	85%
Paddy crop	0	0	18	0	0	0	0	18	100%
Nonpaddy crops	0	3	6	7	0	0	0	15	47%
Water body	0	0	0	0	8	0	0	8	100%
Forest	0	0	0	0	0	13	3	16	81%
Shrubland	0	0	0	5	0	0	9	14	64%
								Total: 100	**OA =82%**

4.1.2.3 Flood vulnerability

Citizen scientists collected paddy crop damage data for the last 10 years from 46 households. Of these, 30 belonged to the list of households affected by flooding on their paddy crop, as documented by the local authority during the 2018 flood (Appendix 8.9). Subsequently, the paddy crop damage data of these 30 households was compared with

data provided by the local authority (Figure 4.3 and Table 4.5). The overall agreement was calculated to be 73%, indicating the potential of citizen scientists to investigate or self-investigate data on paddy crop flood damage. Notably, the paddy crop damage rate reported by citizen scientists was generally lower than that documented by district authorities. For instance, despite all compared households having a paddy field damage rate of at least 30% according to data provided by district authorities, four households collected by citizen scientists exhibited damage rates below 30% or were completely undamaged (Household IDs: 2, 13, 24, and 28; Figure 4.3).

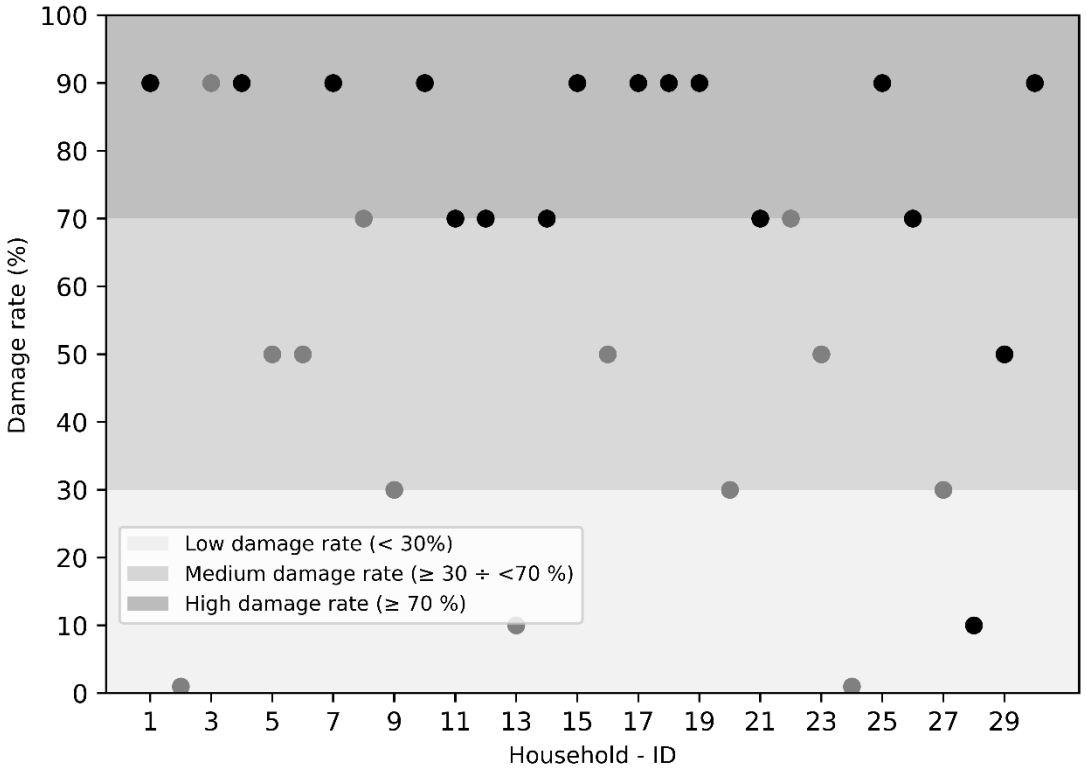

Figure 4.3. Paddy crop damage rates recorded by citizen scientists for 30 households for 2018 flood. (Dots denote flood damage rates reported by citizen scientists; black dots indicate households with damage levels ranging from 30-70%, while gray dots indecate households with damage levels exceeding 70%, as determined by the local authority)

Table 4.5. Error matrix of paddy crop damage rate data gathered by citizen scientists

Local authority / Citizen scientists	Low damage	Medium damage	High damage	Total reference points	Participants' agreement
Low damage	0	0	0	0	-
Medium damage	3	7	3	13	54%
High damage	1	1	15	17	88%
				Total: 30	**OA =73%**

4.1.2.4 Rainfall monitoring

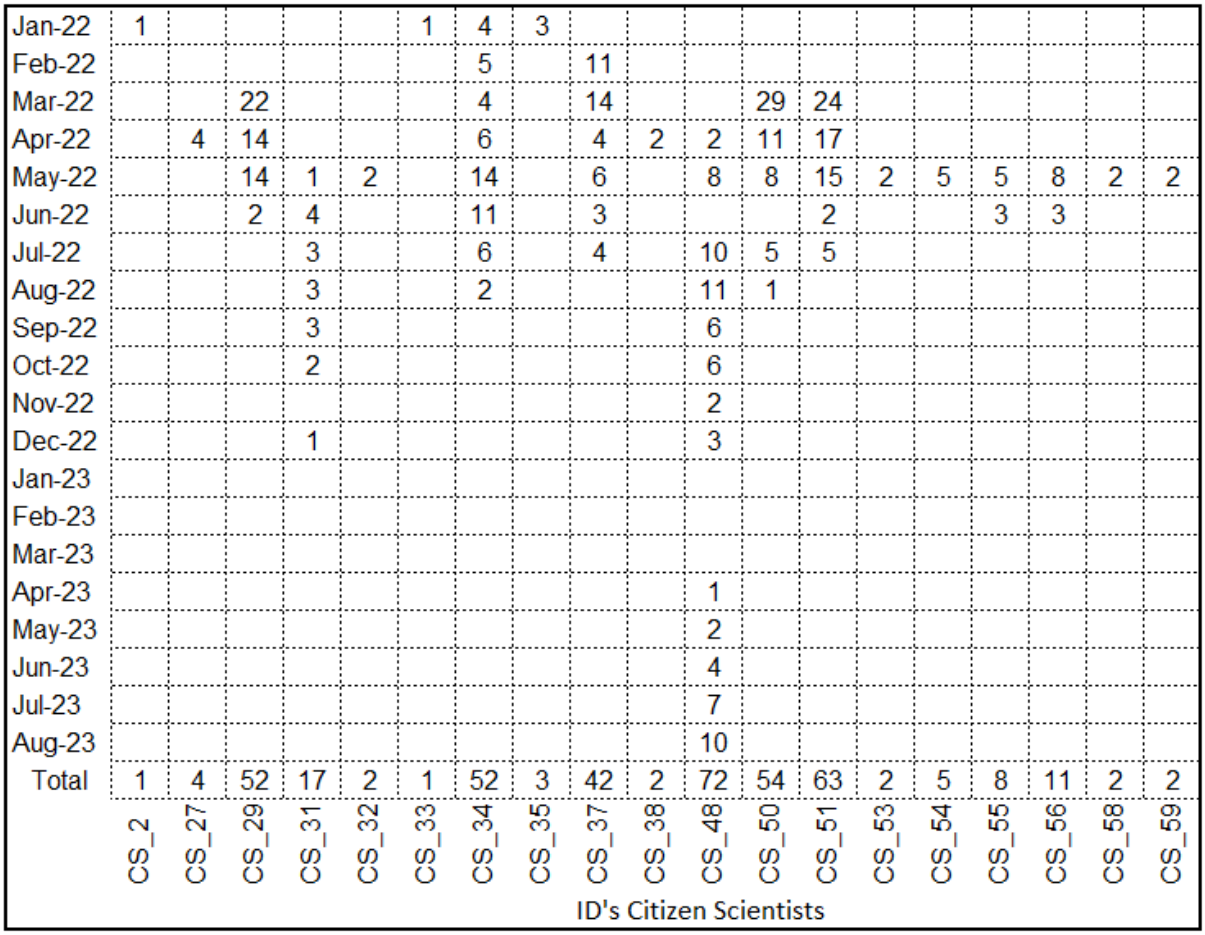

Figure 4.4. Monthly rainfall data number for each citizen scientist in the Bui River basin from Jan 2022 to August 2023

Figure 4.4 shows the monthly rainfall data number of 19 citizen scientists. Between January 2022 and August 2023, 19 citizen scientists measured 395 rainfall data at their

houses. Among them, 10 (53%) recorded rainfall only in their first month, with observation frequencies being from one to five times. Four citizen scientists measured rainfall for more than six months, notably CS_48, who recorded 72 rainfall data from April 2022 to August 2023. Although some citizen scientists, such as CS_29, CS_50, and CS_51, measured rainfall almost daily in their first month, their frequency gradually decreased in subsequent months, with participation lasting only three to five months.

The comparison of monthly rainfall between CS_48 and RT_Xuan Mai reference station illustrates similar trends (Figure 4.5). The monthly rainfall correlation coefficient of 0.9 between the two stations indicates good agreement. Monthly rainfall measured by the citizen scientist tended to be lower than that recorded by the reference station. Irregular rainfall measurements by the citizen scientist may have resulted in water loss due to evaporation from the rain gauge. Conversely, during the rainy months with monitoring every 3 days (e.g., August 2022 and August 2023), the rainfall observed by the citizen scientist exceeded that measured at the reference station. This difference is as the result of using low-cost rain gauges made of curved plastic bottles (Figure 8.2), causing reported rainfall values to be higher than actual ones.

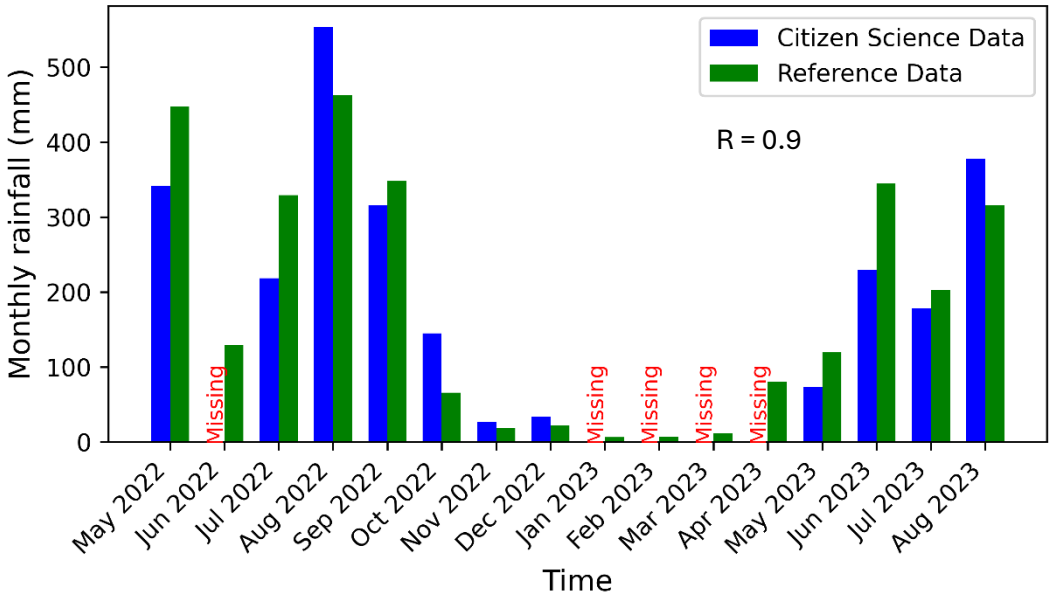

Figure 4.5. Monthly rainfall data recorded by CS_48 and at RT_Xuan Mai from May 2022 to August 2023

4.1.3 Monthly citizen science data collection

The number of flood-related data collected monthly by citizen scientists from September 2021 to August 2023 is shown in Figure 4.6. The citizen science program was affected by the COVID-19 pandemic during the first four months, resulting in limited data collection. When the community-based rainfall monitoring was administered in January 2022, there was a notable increase in the number of flood-related data, particularly in the first four months of 2022. April marked the peak of data collection, with 181 records coinciding with a field experiment on land-use classification. However, data collection gradually decreased in the remaining months.

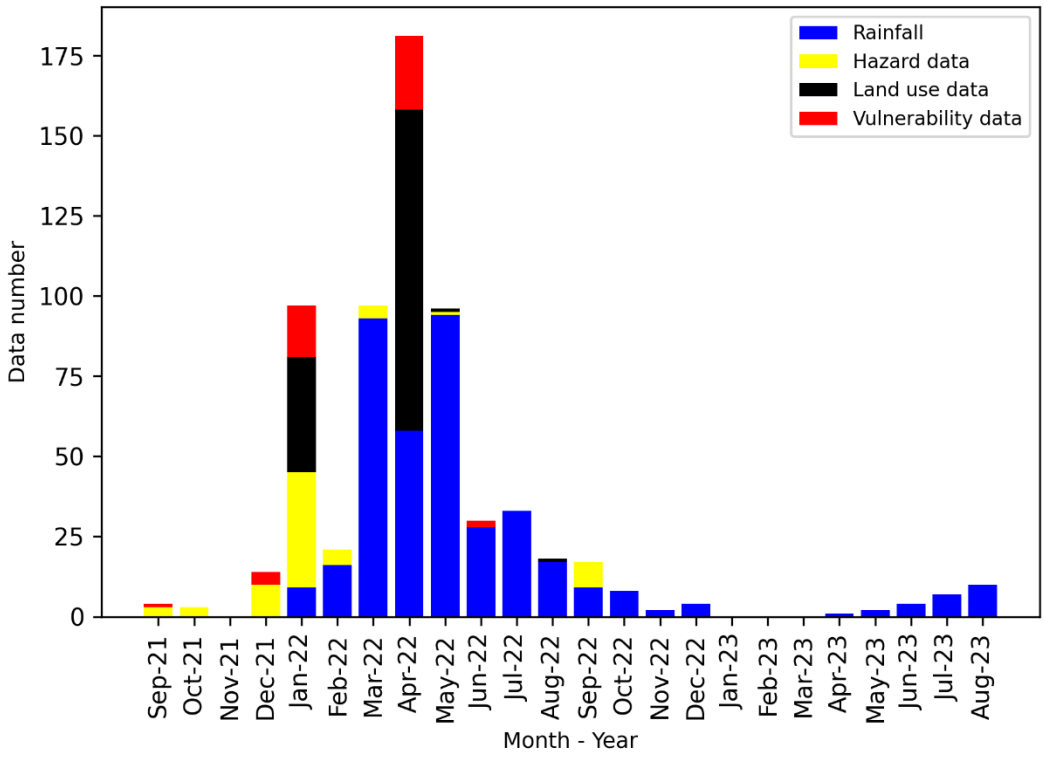

Figure 4.6. Monthly data contributed by citizen scientists for two years

It is noteworthy that during the data collection period, floods occurred in October 2021 and September 2022, accompanied by an unusually severe storm in May 2022, which resulted in inundation of residential areas and damage to paddy fields in the Bui River Basin. Citizen scientists residing in or near flood-prone areas conducted surveys on the flooding situation in the residential areas during the floods of 2021 and 2022 (Figure 4.7A and Figure 4.7B) and reported paddy crop damage due to flooding one month since the 2022 storm occurred (Figure 4.7C). Furthermore, a citizen scientist conducted land-use surveys in a specific area in April and August 2022. The surveys clearly documented

the abandonment of paddy-cultivated areas in flood-prone areas during flood season (Figure 4.7D and Figure 4.7E).

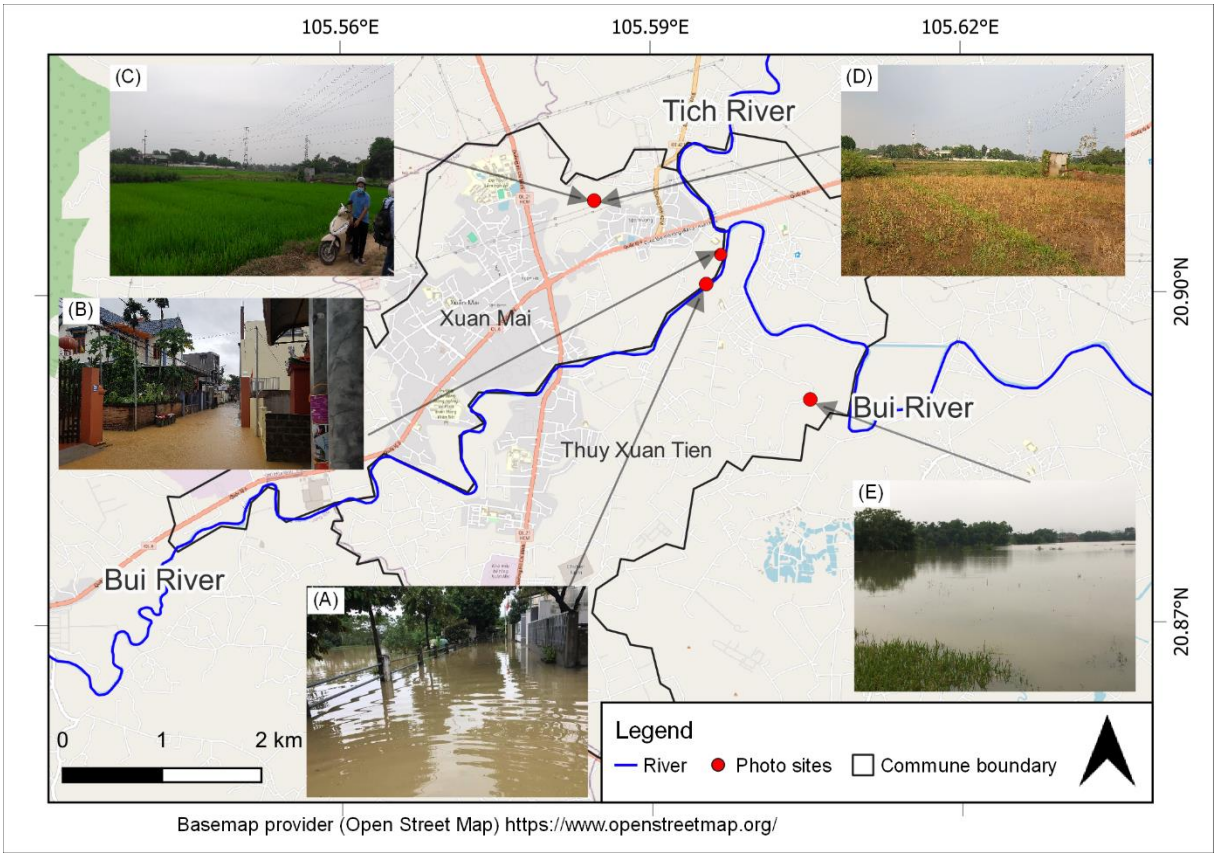

Figure 4.7. Positions of citizen scientists documenting residential flooding in October 2021 (A), in September 2022 (B), rice growing area in April 2022 (C), abandoned rice growing area in August 2022 (D), and flood damage to rice field in May 2022 (E)

4.2 Analyzing flood hazard

4.2.1 Flood extent on bare land

The Otsu algorithm was applied individually to the flood images to determine the optimal threshold for classifying water and nonwater areas. The threshold values for the flood events of 2017, 2018, and 2022 were -14.93 dB, -14.99 dB, and -14.95 dB, respectively. That means that the defined thresholds showed only minor variations among the three flood events, with the largest difference being just 0.06 dB. An average value of -14.97 dB was consequently selected as the standard threshold. As a result, pixels with backscattering values below -14.97 dB were designated as water areas, and those above as nonwater areas. This value also applied to the pre-flood image collected during the three driest months to detect water and non-water areas.

The permanent water class in the three driest months of 2018 was relatively small, measuring only 19.7 hectares (Figure 4.8A). In contrast, the water class during the flood on July 22nd, 2018, coinciding with the maximum water level period, expanded significantly to 264.1 hectares (Figure 4.8B). The flooded area was estimated to be approximately 221 hectares (Figure 4.8C), which is 9 percent less than the flooded area (244.4 hectares) calculated by subtracting the permanent water class from the water class of the flood image. This difference can be attributed to the effects of two flood image refinement methods.

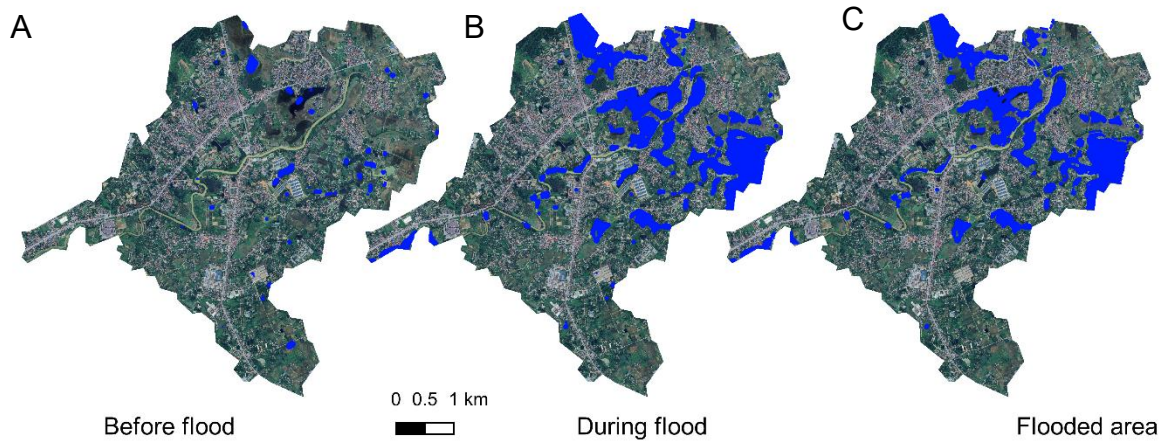

Figure 4.8. Water class before (A), during (B) 2018 flood, and flooded area (C) of 2018 flood obtained from GEE

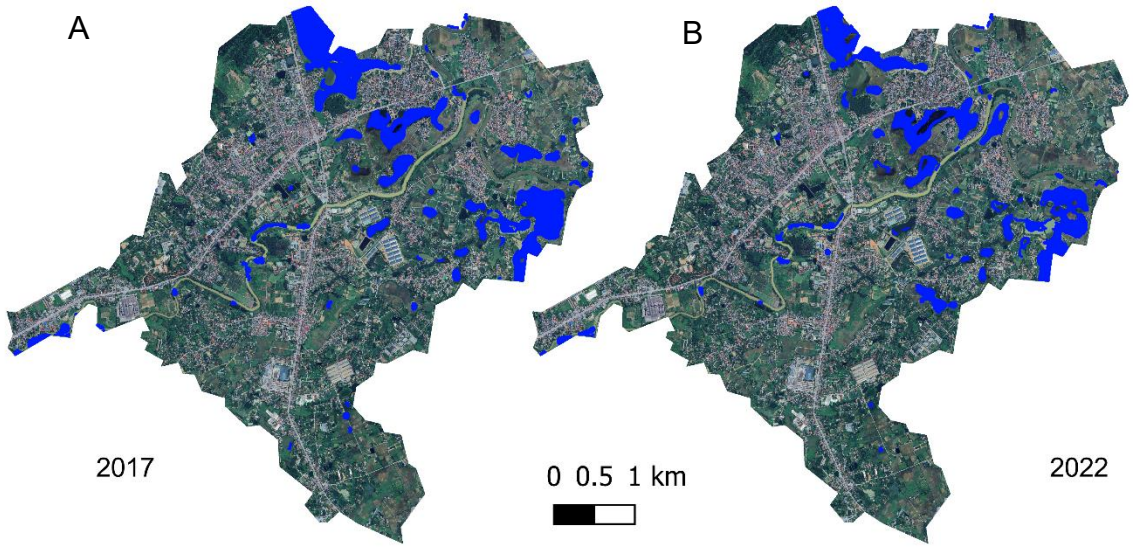

Figure 4.9. Flooded area on bare land of 2017 (A) and 2022 (B) floods obtained from GEE

The flooded areas in 2017 (Figure 4.9A) and 2022 (Figure 4.9B) were 140 and 114 hectares, respectively. Although the water level corresponding to the flood image of 2017 was approximately 1 m lower than that of 2022 (Figure 3.6 in Chapter 3), the flood extent of the former was 26 hectares larger than that of the latter. The maximum flood level in 2017 was 7.53 m, while the maximum flood level in 2022 was 7.25 m. The maximum flood level could affect the extent and duration of flooding. Some low-lying areas, which are located in the northern and eastern parts of the pilot area remained flooded for 10 days after the maximum flood level occurred in 2017 (Figure 4.9A).

The local authority's reports (C. M. D. P. Committee, 2018) indicated that the magnitude and impacts of the floods in 2017 and 2018 were similar. However, the flood extent in 2017, based on remote sensing data, was 81 hectares smaller than in 2018 and equivalent to 63% of the flooded area during the latter event. The flood image of 2017 was collected 10 days after the maximum water level period, while the flood image of 2018 was collected on the date of maximum water level. This result demonstrates that the date of flood image acquisition significantly affects the detectability of flood extent.

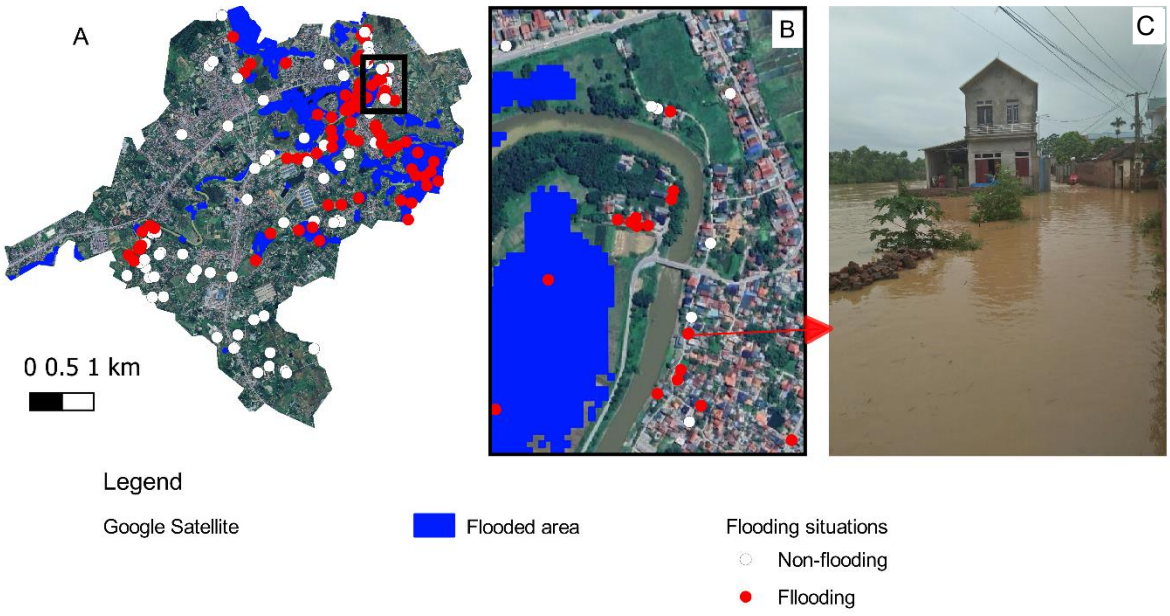

Figure 4.10. Flood extent map with flooding surveying points (A); Zoom-in on flooded points in residential area (B), and a flooding photo of 2018 captured by a local (C)

A comparison of the flood extent map with information from other data sources is crucial for evaluating the accuracy of the flood extent and the applicability of the methods

employed. A comparison was conducted between the produced flood extent of 2018 and the flooding surveying points, including both flooded and non-flooded points, gathered by the author and citizen scientists (Figure 4.10A). The data are mentioned in sections 3.3.2 and 4.1.2.1. All nonflooded points were located outside the flooded area, while some flooded points were either inside or in close proximity to the flooded area (Figure 4.10A and Figure 4.10B). For instance, a flooded point in a residential area where a local captured an image of the flooding, which was a reliable source of information, but was situated outside the flood extent (Figure 4.10B and Figure 4.10C). This result confirms the limitations of S-1 images in detecting floods in built-up areas due to its backscattered properties.

4.2.2 Flooding mapping for pilot area

4.2.2.1 Flood level surface

The pilot area was divided into non-overlapping rectangular subdomains, each with a side length of 1 km (Figure 4.11). Some subdomains (e.g., A1, A2, B1) were not considered in the estimation of flood level surface or flooding depths due to their location outside the pilot area or within flood-protected areas (A7, A8, and B8). The flood extent on bare land of the three investigated floods (i.e., the 2017, 2018, and 2022 floods) were converted into flood boundaries overlaid with DTM to estimate the flood level at each subdomain. This research collected 106 flooding depth points of 2017, 2018, and 2022 in residential areas within the pilot area. This information was gathered through field trips and the citizen science program. Further details on these flooding points, which were used to estimate flood levels in residential areas, can be found in Appendix 8.10. The flood levels of points in residential areas were determined by adding the flooding depth to the ground elevation, based on the DTM.

Table 4.6 and Table 4.7 show the mean flood levels of the 2018 flood within subdomains of the pilot area in the bare land and residential areas, respectively. Flood levels on bare land were estimated at 18 subdomains, with a range of 4.75 to 7.07 meters, while ten subdomains remained nonflooded. Flood levels in residential areas typically range from 7.01 to 9.12 meters. In some residential areas where the ground elevation is high, the flood levels reached more than 10 meters. For example, flood levels in F4 and F5 subdomains reached 10.77 meters and 12.00 meters, respectively. The flood levels in the

bare land were approximately 0.95 to 3.92 meters lower than those in residential areas within the same subdomain. This difference can be explained by the ground elevation difference between the bare land and the residential area. In addition, flood levels in the bare land are highly dependent on the flood extent obtained from satellite images, which is often smaller than the actual flood extent due to SAR slant, image resolution, and the image acquisition time.

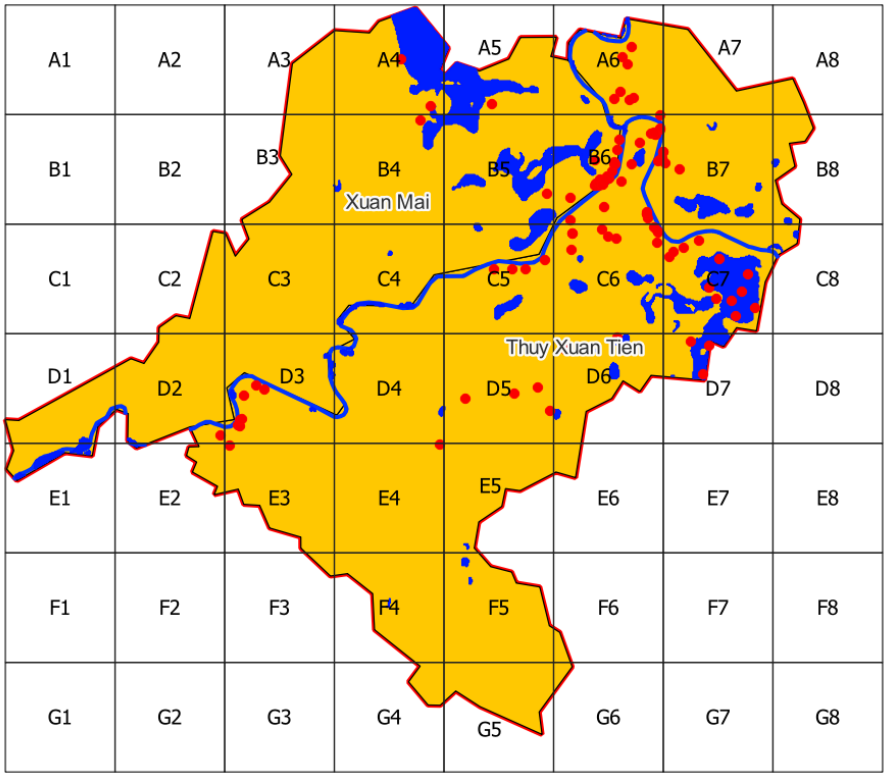

Figure 4.11. Map of subdomains, flooding point (red points), and flood extent on bare land (blue area) of 2018 flood in the pilot area

Table 4.6. Flood level at subdomains based on flood boundary on bare land in 2018

	1	**2**	**3**	**4**	**5**	**6**	**7**	**8**
A	NA	NA	-	5.29	5.28	5.95	PA	PA
B	NA	NA	-	4.75	6.63	6.39	-	PA
C	NA	NA	-	5.17	7.00	5.88	5.81	5.68
D	6.42	5.08	6.77	7.26	6.29	5.81	5.36	NA
E	5.69	-	-	-	7.07	-	NA	NA
F	NA	NA	-	-	-	-	NA	NA
G	NA	NA	NA	NA	NA	NA	NA	NA

Note: NA, -, and PA represent non-accounting, non-value, and flood-protected areas, respectively.

Table 4.7. Flood level at subdomains based on flood boundary in residential areas in 2018

	1	**2**	**3**	**4**	**5**	**6**	**7**	**8**
A	NA	NA	-	7.79	7.92	8.25	PA	PA
B	NA	NA	-	7.95	8.79	7.90	8.20	PA
C	NA	NA	-	-	8.52	7.80	7.39	-
D	-	9.00	9.03	-	7.24	7.39	7.01	NA
E	-	-	9.12	8.05	-	-	NA	NA
F	NA	NA	-	10.77	12.00	-	NA	NA
G	NA	NA	NA	NA	NA	NA	NA	NA

Note: NA, -, and PA represent non-accounting, non-value, and flood-protected areas, respectively.

Table 4.8. Combined flood level in subdomains of pilot area in 2018 flood

	1	2	3	4	5	6	7	8
A	NA	NA	**6.35**	6.54	6.60	7.10	PA	PA
B	NA	NA	**5.17**	6.35	7.71	7.14	**8.20**	PA
C	NA	NA	**5.17**	5.17	7.76	6.84	6.60	5.68
D	6.42	7.04	7.90	7.26	6.76	6.60	6.18	NA
E	5.69	**5.69**	**9.12**	**8.05**	7.07	**6.18**	NA	NA
F	NA	NA	**8.05**	**10.77**	**12.00**	**7.07**	NA	NA
G	NA	NA	NA	NA	NA	NA	NA	NA

Note: The flood level values shown in underlined, bold, and underlined and bold numbers, were extracted from the values of the bare land, residential area, and lowest and nearest neighborhood, respectively.

Table 4.8 presents the flood level combined between flood level on bare land and in residential area (in Section 3.4.2.3) in each subdomain within the pilot area of 2018 flood. The flood levels ranged from 5.17 meters to 12.00 meters. The variation in flood levels between subdomains (e.g., A4, A5, and A6) that exhibit two types of flood level remains relatively stable, ranging from 6.35 to 7.90 meters. In contrast, subdomains with only one type of flood level show significant differences compared to adjacent subdomains. The flood level in the subdomain which is estimated based on the flood level on bare land or in residential area is lower or higher than that of the neighboring

subdomain. The flood levels in some subdomains, such as A3, B3, or C3, were assigned based on the lowest values from the nearest neighboring. Based on the combined flood level in each subdomain, the flood level surface for each subdomain and whole domain can be calculated.

Similarly, the flood level surface in subdomains in the pilot area for 2017 and 2022 were determined. The details of combined flood levels in subdomains in the pilot area are presented in Table 4.9 and Table 4.10 below. It can be observed that the flood level surface in the two flood events is quite similar. In particular, the flood level surface in 2017 ranged from 4.16 meters to 10.27 meters, while those in 2022 ranged from 4.59 meters to 10.66 meters. In general, the flood level surface in 2017 was higher than that in 2022. The majority of flood level surfaces in the subdomains were derived from flood levels observed on the bare land, due to the lack of information about flooding in the residential areas for the investigated flood events. The flood levels from the bare land and residential areas for both cases are presented in Appendix 8.4.

Table 4.9. Combined flood level in subdomains of pilot area in 2017 flood

	1	**2**	**3**	**4**	**5**	**6**	**7**	**8**
A	NA	NA	**5.18**	5.32	5.34	6.71	PA	PA
B	NA	NA	**4.94**	5.18	6.18	6.87	4.58	PA
C	NA	NA	**4.94**	4.94	6.71	6.68	6.30	4.58
D	6.55	4.16	7.40	7.01	5.86	5.87	4.90	NA
E	5.68	5.96	**4.16**	**5.86**	9.48	**4.90**	NA	NA
F	NA	NA	**5.96**	**9.48**	10.27	**9.48**	NA	NA
G	NA	NA	NA	NA	NA	NA	NA	NA

Note: The flood level values shown in underlined, bold, and underlined and bold numbers, were extracted from the values of the bare land, residential area, and lowest and nearest neighborhood, respectively.

Table 4.10. Combined flood level in subdomains of pilot area in 2022 flood

	1	2	3	4	5	6	7	8
A	NA	NA	**4.73**	5.18	5.51	5.70	PA	PA
B	NA	NA	**4.73**	4.73	6.21	6.53	**4.59**	PA
C	NA	NA	**4.73**	4.94	6.80	5.47	5.64	4.59

	1	2	3	4	5	6	7	8
D	4.59	**4.59**	8.97	6.79	6.10	5.74	5.13	NA
E	5.59	**4.59**	**6.79**	**6.10**	9.21	**5.13**	NA	NA
F	NA	NA	**4.59**	**9.21**	10.66	**9.21**	NA	NA
G	NA	NA	NA	NA	NA	NA	NA	NA

Note: The flood level values shown in underlined, bold, and underlined and bold numbers, were extracted from the values of the bare land, residential area, and lowest and nearest neighborhood, respectively.

4.2.2.2 Flood mapping accuracy analysis

The flooding areas derived from DTM-based approach for 2017 and 2018 correspond reasonably with the flooded area reported by the district authority (Table 4.11). The flooding areas derived from DTM-based approach were 279.5 ha and 439.8 ha for 2017 and 2018, respectively. The flooding area difference between the DTM-based approach and the district authority is -6% and 1% for 2017 and 2018, respectively. These results demonstrate the accuracy of the estimated flooding areas in aligning with the flood-affected area reported by the local authority. It is noteworthy that the local authority only investigated flood-affected cropland, aquacultural, and residential areas without geospatial data. Consequently, this research compared the estimated flooding area with statistics on flood affected areas numerically.

Table 4.11. Accuracy evaluation of estimated flooding areas

Flood events	DTM-based approach (ha)	Local authority-based flooded area (ha)	Difference (%)
2017	279.5	297.2	-6%
2018	439.8	437.6	1%

The results of the comparative analysis of the flooding areas between DTM-based approach and the model-based approach are shown in Figure 4.12, Figure 4.13, and Table 4.12. The results of the calibration and validation of flood models are presented in Appendix 8.5. The performance of the flood models is acceptable, which is suitable to simulate actual flood events in the Bui River Basin.

The difference between the flooded area obtained from DTM-based approach and modeling is 29% for 2017, and 9% for 2018. This comparison focuses on flooding areas

of each method numerically. The flooded area obtained from DTM-based approach overlapped with186 hectares out of 396.2 hectares (47%) of the modeling-based results for 2017 and 294 hectares out of 404 hectares (73%) for 2018. Although the difference of the flooded areas between two methods is moderate, the degree of overlap of flooding areas between two methods is still low, particularly in the 2017 flood.

Some flooded areas in the northern and southern parts of the pilot area were overestimated by the DTM-based approach. These areas are located in low-lying zones linked to small streams and controlled by sluices. These areas were not considered in the flood modeling process due to the complexity of the system. In contrast, some floodplain areas near the Tich and Bui Rivers were identified as flooded in the modeling process, but these areas were not detected by the DTM-based approach. This discrepancy is attributed to limitations of the SAR images, such as image resolution, reduced sensitivity to flooding beneath vegetation, and the timing of image acquisition.

Table 4.12. Comparison of flooding extent and depth between DTM- and model-based approach

Flood event	DTM-based approach (a)		Model-based approach (b)		Comparison					
					Flood extent				Flooding depth	
	Flooded area (ha)	Average flooding depth (m)	Flooded area (ha)	Average flooding depth (m)	Diff.t (%)	Over-lapped area (ha) (%)	Over-estimated by DTM-based approach (ha)	Under-estimated by DTM-based approach (ha)	Mean absolute difference (MAD) (a-b) (m)	RMSE (m)
2017	279.5	0.87	396.2	1.48	29%	186 (47%)	93.5	210	1.02	1.30
2018	439.8	1.18	404	1.53	-9%	294 (73%)	151	110	0.97	1.80

The DTM-based approach consistently underestimated flood depth compared to the model-based approach, with average depths of 0.78 m in 2017 and 1.18 m in 2018. These values were 0.61 m and 0.35 m lower, respectively, than those estimated by the model for the same years. The mean absolute difference (MAD) in flood depth across all cells was approximately 1 m for both flood events. The root mean square errors (RMSE) were estimated at 1.30 m for 2017 and 1.80 m for 2018, indicating a substantial discrepancy in the DTM-based results. This level of error is consistent with the findings of Apel et al. (2009), who reported RMSE values exceeding 1 m, likely influenced by the coarse

resolution of the underlying topographic data. Furthermore, the limited spatial overlap between flooded areas identified by the two methods contributes to the elevated MAD and RMSE values.

The 2018 flooding map, derived from the DTM-based approach, was suitable with the flood affected area investigated by local authorities and model-based approach. Two reasons explain this outcome. Firstly, the extent of flooding in areas of bare land during the 2018 flood event was determined based on satellite imagery captured during the maximum flood level period. Secondly, the majority of flooding points in residential areas used in this research, gathered by the author and citizen scientists, were associated with the 2018 flood event.

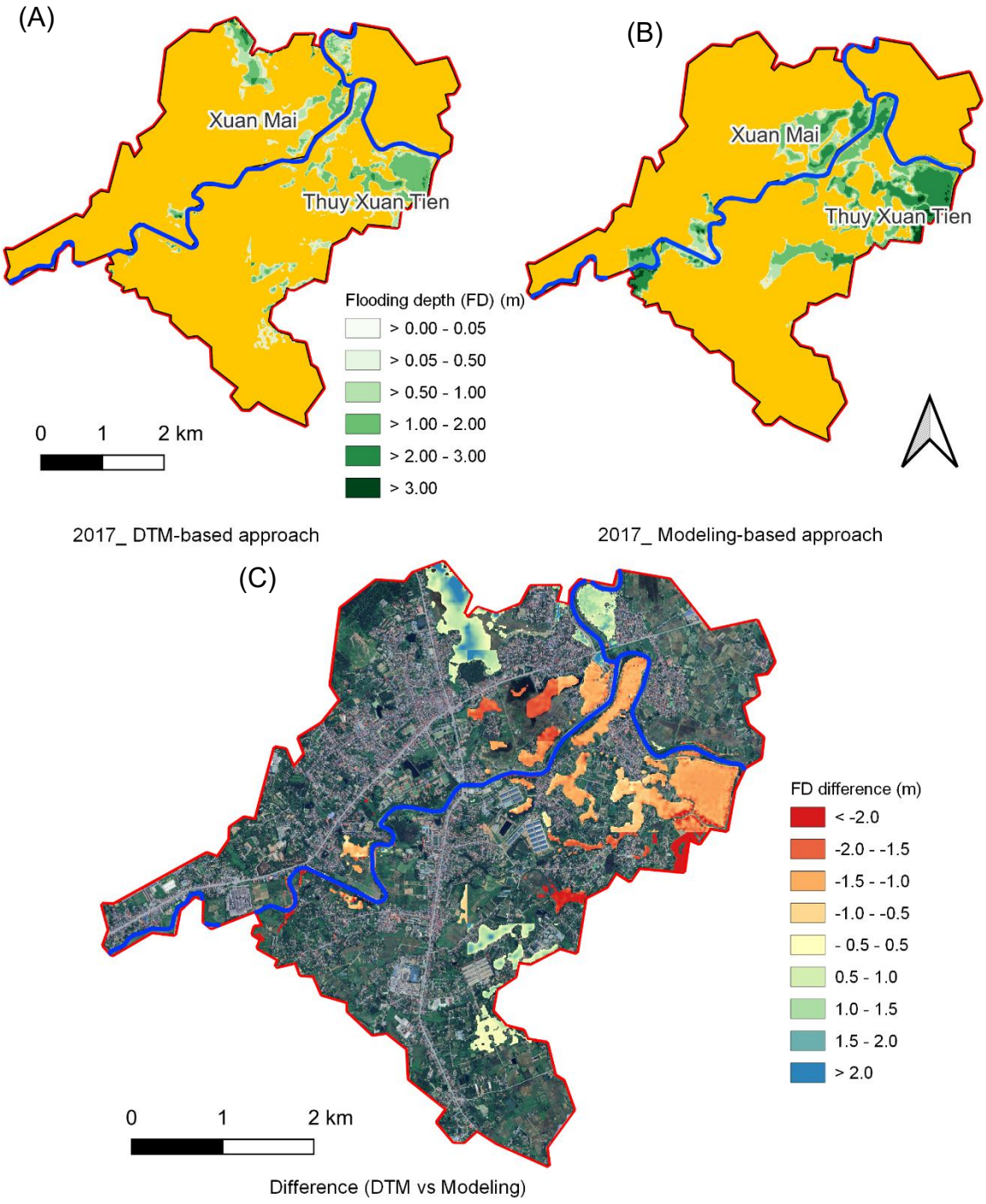

Figure 4.12. Inundation map in the pilot area in 2017 by DTM-based approach (A), Model-based approach (B); Flooding depth difference map between (A-B) (C)

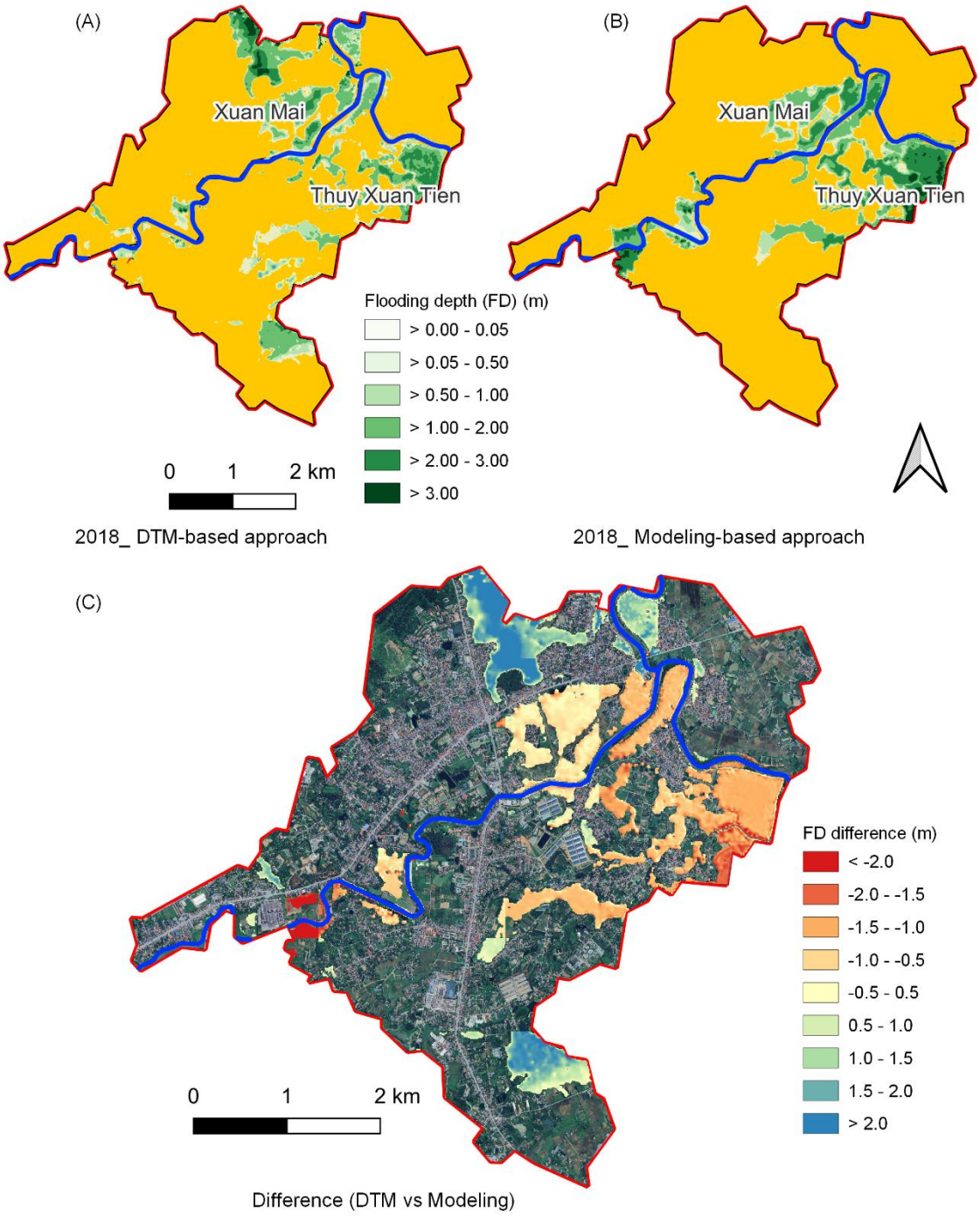

Figure 4.13. Inundation map in the pilot area in 2018 by DTM-based approach (A), Model-based approach (B); Flooding depth difference map between (A-B) (C)

4.2.2.3 Flooding maps

Figure 4.14 shows the DTM-based flooding maps for the three investigated flood events, while Table 4.13 provides a detailed summary of the statistical values associated with these flooding maps. The 2018 floods exhibited the largest flood extent, covering 439.8

ha, followed by the 2017 and 2022 events, which affected 279.5 ha and 265.4 ha, respectively. In line with the reduction in flood extent, the average flooding depth also decreased across the three flood events. However, the maximum flooding depths between (the flooding depth grid cell with the highest value) did not follow this trend. Notwithstanding the 2022 flood had the smallest extent, it exhibited the highest maximum flooding depth among the three investigated floods. The maximum flooding value, which reflects a local ground elevation value, depends on the elevation point interpolation method or the location of flooding information. The flooding depth during the 2018 flood with the largest flooded area was mainly between 1.0 m and 2.0 m, with an average depth of approximately 1.18 meters. The maximum flooding depth recorded during the 2018 flood was 5.59 meters.

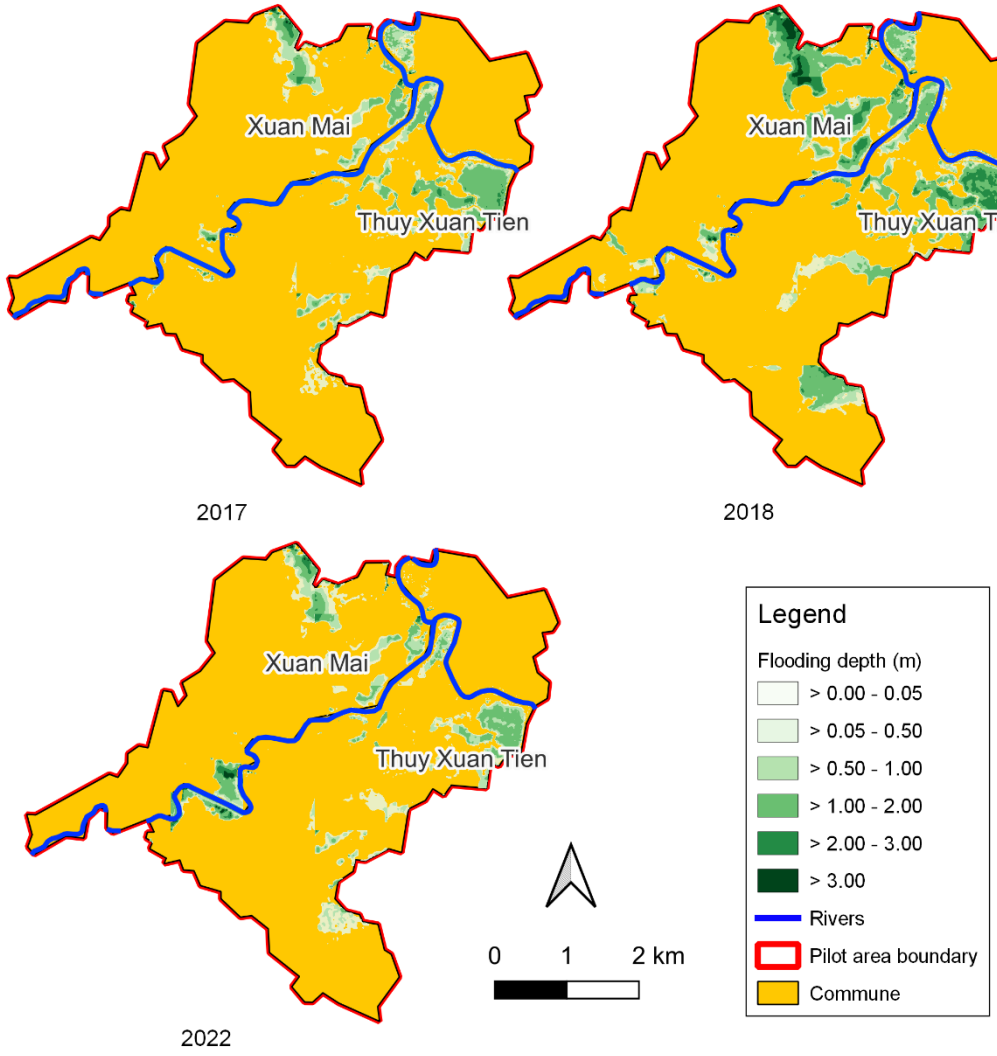

Figure 4.14. Inundation maps of the study area in 2017, 2018, and 2022

Table 4.13. Inundation characteristics of 2017, 2018, and 2022 flooding maps

No	Flood event	Flooded area (ha)	Average flooding depth (m)	Maximum flooding depth (m)
1	2017	279.5	0.87	4.71
2	2018	439.8	1.18	5.69
3	2022	265.4	0.78	6.21

4.2.3 Flood hazard assessment

The probability of flooding in the Bui River Basin is analyzed using the Pearson Type III distribution model, which is based on the maximum water levels recorded at the Tri Thuy station from 1972 to 2022 (Table 4.14 and Figure 4.15). These floods that occurred in 2022, 2017, and 2018 can be considered equivalent to 10-, 13-, and 50-year flood events, respectively. Based on this, the flooding maps developed in the previous step were used for analyzing flood hazard.

Table 4.14. Flood probability in the Bui River Basin at the Tri Thuy station

No	Probability P(%)	Return period (year)	Water level (m)	Study year
1	0.01	10000	9.41	
2	0.10	1000	9.00	
3	0.20	500	8.85	
4	0.50	200	8.63	
5	1.00	100	8.44	
6	**2.00**	**50.0**	**8.22**	**~ Flood 2018**
7	5.00	20.0	7.87	
8	**7.5**	**13.3**	**7.69**	**~ Flood 2017**
9	**10.00**	**10.0**	**7.55**	**~ Flood 2022**
10	20.00	5.0	7.15	
11	25.00	4.0	6.99	
12	50.00	2.0	6.34	
13	70.00	1.4	5.79	
14	85.00	1.2	5.39	
15	97.00	1.0	4.32	
16	99.99	1.0	1.54	

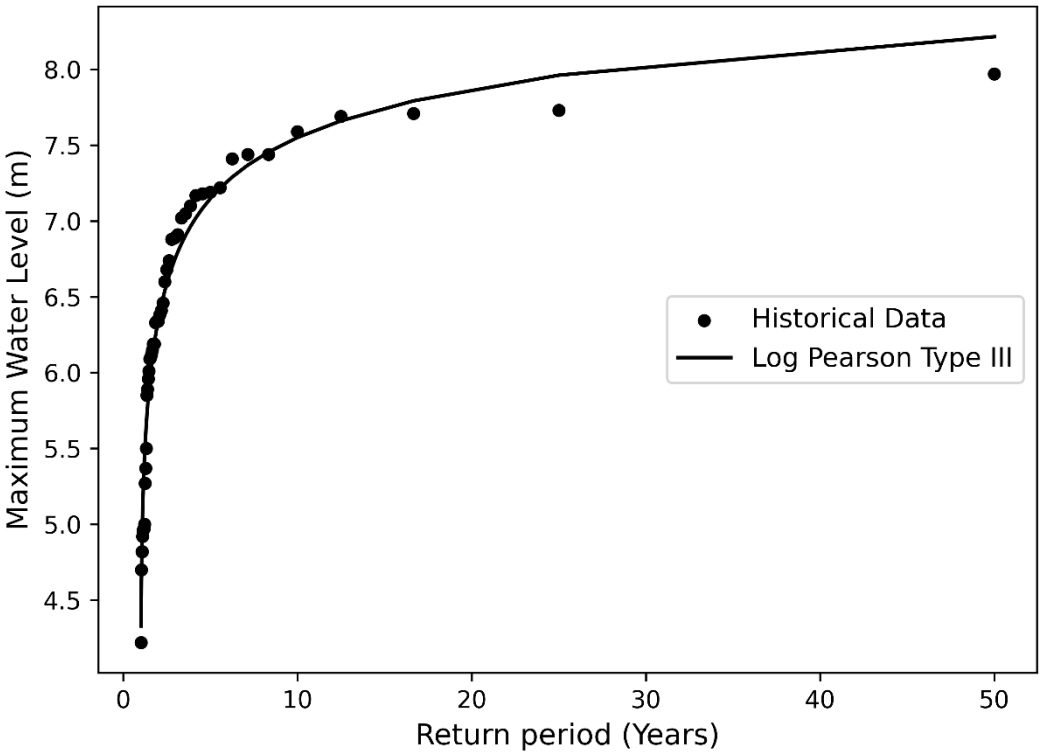

Figure 4.15. Flood probability curve in the Bui River Basin at Tri Thuy station

The level of flood hazard was classified into five ranges, as follows: <0.5 m, 0.5 m - 1 m, 1 m - 2 m, 2 m – 3 m, and greater than 3 m. The inundation area with classified hazard depths according to 10-, 13-, and 50-year flood events is shown in Table 4.15. In the case of the 10-year flood event, the flooding depth is primarily less than 0.5 m, accounting for 40% of the total flooded area. The area flooded at a depth of 0.5 m to 2 m represents over 50% of the total flooded area. The area flooded over 2 m represents a small portion of the total flooded area, occupying only 4%.

The flooded area of the 13-year flood event is comparable to that of the 10-year flood event. The area flooded between 0.5 m and 1 m in the 10-year flood event case was more deeply flooded in the 13-year flood event. The proportion of the area flooded between 1 and 2 meters increased from 27% in the former case to 36% in the latter.

The flooded area of the 50-year flood event is approximately 440 ha, representing an increase in flooded area of 66% compared to the 10-year flood event. About three-fifths of this area experienced flood depths between 1.0 and 2.0 meters. The area flooded to a depth of less than 0.5 meters and between 0.5 and 1.0 meters are relatively equal, together accounting for more than 20% of the total flooded area. It is noteworthy that

15% of the total flooded area is flooded to a depth of over 2 meters, with some being more than 3 meters deep.

Table 4.15. Flood inundation area with different flooding depths corresponding to various return periods

Flooding depth (m)	10-year flood event		13-year flood event		50-year flood event	
	Area (ha)	%	Area (ha)	%	Area (ha)	%
$D \leq 0.5$	105.8	40%	100.3	36%	97.1	22%
$0.5 < D \leq 1.0$	77.2	29%	73.0	26%	93.3	21%
$1.0 < D \leq 2.0$	70.6	27%	97.0	35%	185.0	42%
$2.0 < D \leq 3.0$	9.1	3%	8.2	3%	55.1	13%
$D > 3.0$	2.7	1%	1.0	0%	9.3	2%
Total	**265.4**	100%	**279.5**	100%	**439.8**	100%

4.3 Estimating flood damage

4.3.1 Land-use and agricultural production value maps

4.3.1.1 Analysis of land-use map accuracy

The accuracy of the land-use (LU) map of the Bui River Basin was calculated by comparing the classified results against the validation datasets. The error matrix provides a detailed calculation of the classification results, indicating the number of validation sample points that were correctly classified for each land-use class (Table 4.16). The overall accuracy and the Kappa coefficient were 0.67 and 0.61, respectively. In general, the Random Forest algorithm applied to Sentinel 2 imagery for land-use classification performed well. There may be areas for improvement to enhance classification performance further, which will be discussed in the subsequent chapter.

The user's accuracy (in Section 3.5.1) ranged from 45% to 90%, while the producer's accuracy (in Section 3.5.1) ranged from 45% to 100%. The high-built-up area class exhibited the highest accuracy in both the user's accuracy and producer's accuracy, because the spectrum of these objects is clear and rarely changed on Sentinel 2 images. The user's accuracy and the producer's accuracy of the paddy crop were 73% and 61%, respectively. The user's accuracy and producer's accuracy of shrubland exhibited the lowest performance, with same values of 45% for both. This was due to the spectrum of shrubland being nearly similar to nonpaddy crops or forests.

Table 4.16. Error matrix between classified land-use maps and validation datasets

Land-use	High-built up	Low-built up	Paddy crop	Nonpaddy crops	Water body	Forest	Shrubland	Total classified pixels	User's Accuracy (UA) (%)
High-built up	**13**	2	0	0	0	0	0	15	0.87
Low-built up	1	**9**	0	0	0	0	0	10	0.90
Paddy crop	0	0	**11**	3	0	1	0	15	0.73
Nonpaddy crops	1	3	2	**10**	0	1	3	20	0.50
Water body	0	3	5	0	**14**	0	0	22	0.64
Forest	0	0	0	2	0	**10**	3	15	0.67
Shrubland	0	1	0	2	0	3	**5**	11	0.45
Total ground truth pixels	15	18	18	17	14	15	11	108	***OA = 0.67***
Producer's accuracy (PA) (%)	0.87	0.50	0.61	0.59	1.00	0.67	0.45		Kappa = 0.61

4.3.1.2 Current land-use map

The land-use map of 2022 in the Bui River Basin is presented in Figure 3.2B in Section 3.1.1, and the statistics of land-use area divided by class are shown in Table 4.17. The proportions of the paddy crop and nonpaddy crops are the largest, with 18.2% and 21.9% of the total land area, respectively. The proportions of low-built up area and water bodies are approximately 15% for each class. The forest and shrubland lands occupy one-fifth of land area, with 13.3% forest and 12.2% shrubland. The proportion of high-built-up land is the lowest, accounting for only 5.0%.

Table 4.17. Land-use area by class in the Bui River Basin in 2022

Unit: km^2

Land	High-built up	Low-built up	Paddy crop	Nonpaddy crops	Water body	Forest	Shrub-land	Total
Total	50.2	153.9	184.1	222.4	144.6	134.6	123.6	1013.4
Proportion (%)	5.0%	15.2%	18.2%	21.9%	14.3%	13.3%	12.2%	100.0%

Figure 4.16 shows the land-use map of the pilot area. The two red stripes in the map extending from the north to the south and from the southwest to the northeast represent Ho Chi Minh Road and QL6 Roads, respectively. The high and low

built-up areas are mainly located near the roads. The water body encompasses the Tich and Bui River network and aquaculture areas. The paddy crop is primarily cultivated alongside the river's two sides located in the northeastern area of the pilot area.

Table 4.18 shows statistics of the land-use area classified by types in the pilot area. The pilot area covers 22.70 km^2, which is significantly covered by agricultural land, including paddy crops, non-paddy crops, and water bodies, which collectively account for over 50% of the land area. The built-up area occupies one-third of the total land area. The forest and shrubland areas account for 7% and 3% of the total land area, respectively.

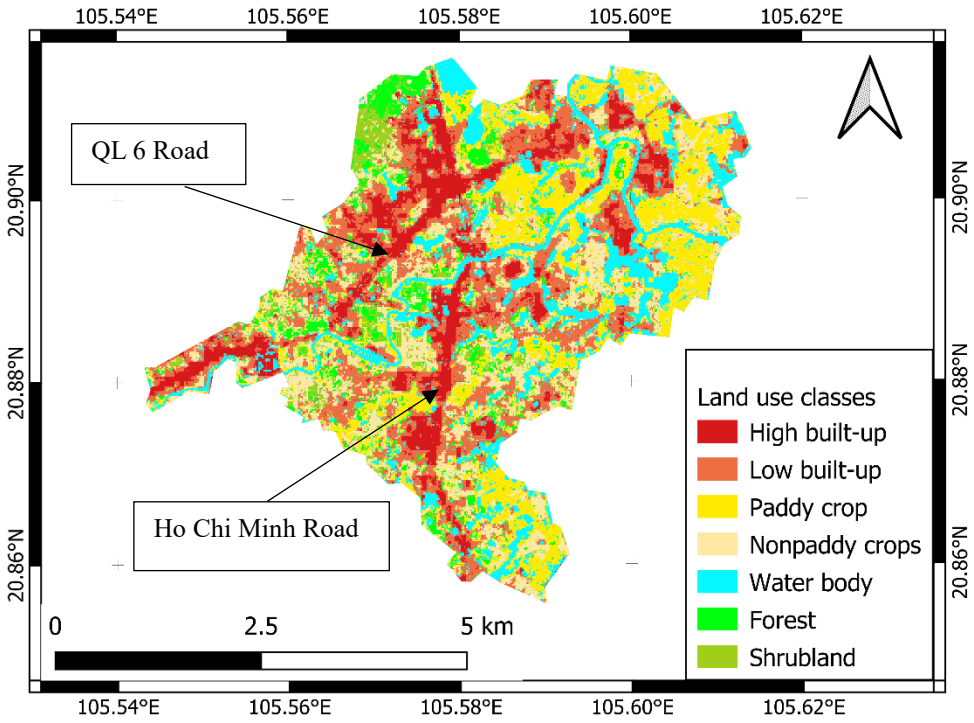

Figure 4.16. Land-use map of 2022 in the pilot area

Table 4.18. Land-use area statistics by land-use class of the pilot area

Land	High-built up	Low- built up	Paddy crop	Nonpaddy crops	Water body	Forest	Shrubland	Total
Area (km^2)	2.84	5.18	5.00	3.84	3.47	1.63	0.74	22.70
Percent (%)	13%	23%	22%	17%	15%	7%	3%	100%

4.3.1.3 Agricultural production value map

An agricultural production value map (Figure 4.17) was developed by combining the agricultural land map with the gross production values for each agricultural land-use category (Table 3.7). When agricultural land is fully destroyed, this map shows the maximum damage cost. Although the paddy crop area is the largest in the pilot area, the total production value for the paddy crop is equivalent to approximately three-fifths of the production value for nonpaddy crops due to their different gross production values (Table 4.19). The aquaculture area has the highest production value, which is approximately € 1.00 million. The total production value for agricultural land in the pilot area is nearly € 1.83 million.

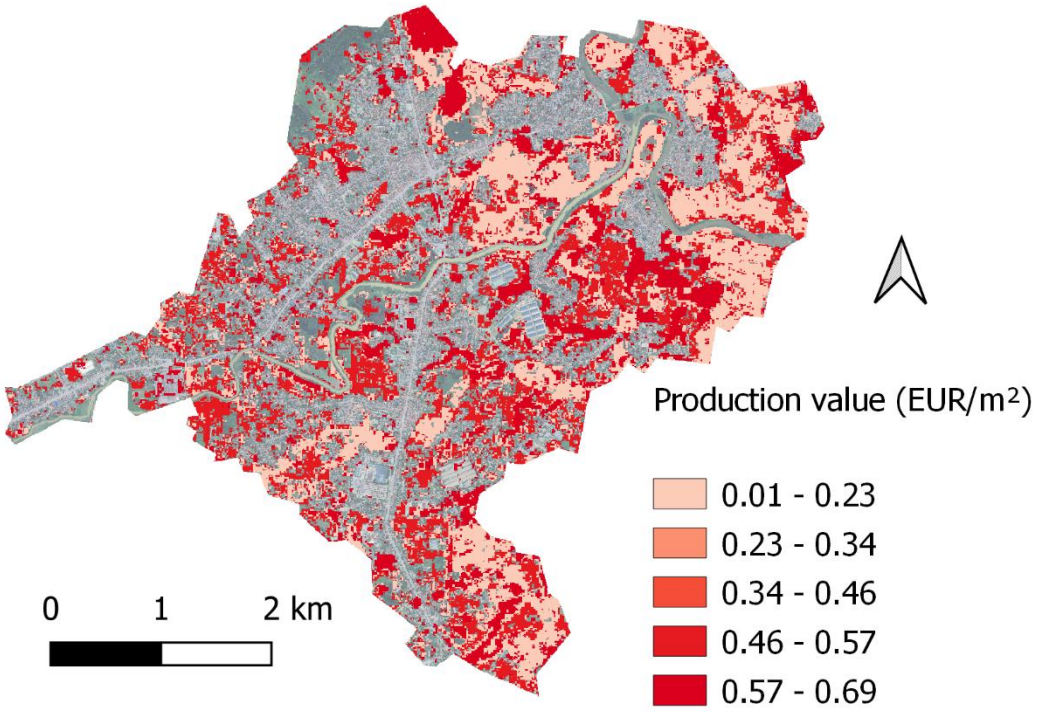

Figure 4.17. Production value map for agricultural land in the pilot area

Table 4.19. Overview of the production values for agricultural land in pilot area

Land-use	Total production values (EUR)
Paddy crop	326,859
Nonpaddy crops	505,730
Aquaculture	992,583
Total	1,825,172

4.3.2 Stage damage curves

The stage damage curve for the paddy crop was developed based on flood damage rate and flooding depth data collected through field surveys and the citizen science program (Figure 4.18). The research yielded 203 data about flood damage to the paddy crop corresponding to the flooding depth of recent floods, particularly the 2018 flood, in which 30 data points were collected by citizen scientists, as mentioned in Section 4.1.2.3. The result of the curve demonstrated a high correlation coefficient between mean damage rate for paddy crops and flooding depth, with R = 0.93. The paddy crop is susceptible to damage when the flooding depth reaches 0.25 m. A reduction in paddy yield of 50% to 60% is observed when the flooding depth is between 0.5 and 0.8 m. The paddy crop may be completely damaged when the flooding depth is between 1.5 and 3.0 m.

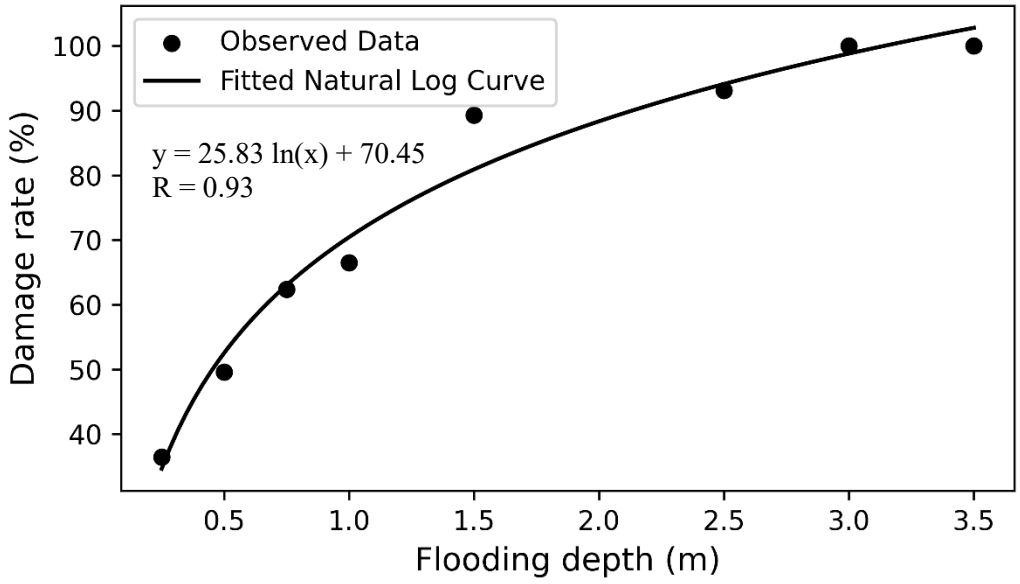

Figure 4.18. Stage damage curve for paddy crops

Figure 4.19 shows the stage damage curves for nonpaddy crops and the aquacultural area. The flood damage rates corresponding to different flooding depths for nonpaddy crops and the aquacultural area were derived from stage damage curves developed by N. Y. Nguyen et al. (2017) and H. N. Pham et al. (2018). Two of these curves were also applied to case studies in Vietnam, which share similar geographic, climatic, and demographic conditions with the pilot area (N. Y. Nguyen et al., 2017; H. N. Pham et al., 2018). My research employed logarithmic curves instead of linear curves, which is consistent with the flood damage curve for the paddy crop mentioned above and facilitates the

calculation of flood damage conveniently. The shape of the two curves is similar. When the flooding depth is less than 2.5 meters, the crop damage rate is higher than that of aquaculture. However, this trend is reversed when the flooding depth is greater than 2.5 meters.

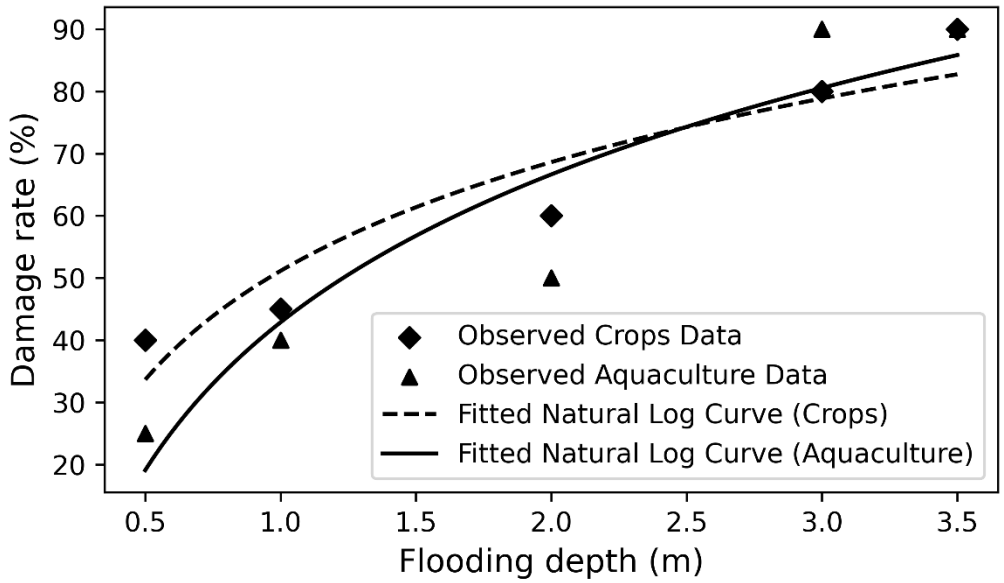

Figure 4.19. Stage damage curves for nonpaddy crops and aquaculture area

Table 4.20. Stage damage functions for the paddy crop, nonpaddy crops and aquaculture area

No	Objects	Damage functions (D) (%)	Range of flooding depth (h) (m)
1	Paddy crop	D = 25.83 x ln(h) + 70.45	(0.07) 0.25– 3.14
2	Nonpaddy crops	D = 25.22 x ln(h) + 51.14	0.13 – 3.14 (6.94)
3	Aquacultural area	D = 34.29 x ln(h) + 42.88	0.29 – 3.14 (5.29)

Note: The values in brackets are maximum damageable flooding depths determined by using stage damage functions.

In Table 4.20 the stage damage functions for agricultural objects are summarized. Based on the stage damage functions and damage ratio ranging from 0 (no damage) to 1 (complete damage), the relevant range of flooding depth for each object was determined. For the paddy crops, the onset of damage is determined as a flooding depth of 0.07 m. However, a 0.25 m flooding depth was utilized in the research as the minimum damageable flooding threshold, in accordance with the findings in a case study in Vietnam (JICA, 2014). For nonpaddy crops and aquaculture land, the maximum damage

is calculated at a flooding depth of 6.94 m and 5.29 m, respectively. However, during the field trips, the author observed that the maximum height of crops or embankment of cultivated aquaculture land ranges from 2 to 3 m. Therefore, this research assumed that the maximum damageable flooding thresholds are the same as those for the paddy crop.

4.3.3 Flood risk analysis

Figure 4.20A, Figure 4.20B, and Figure 4.20C show the flood damage maps corresponding to annual exceedance probability (AEP) of 10%, 7.5%, and 2%, respectively. These maps were generated by integrating the agricultural production value map with the flooding depth maps corresponding to three different flood scenarios, and the stage damage functions for each agricultural land-use type. It is evident that the distribution of flood damage levels between AEPs differs significantly. Although the change of the flooding area between flood scenarios was moderate, the change of flood damage value between flood scenarios was significant. The total damage cost for the 2% AEP flood was nearly 2.5 times higher than that for the 10% AEP flood (Table 4.21). It can be observed that the damage costs for aquaculture areas consistently account for more than 50% of the total damage in all flood scenarios.

Table 4.21. Flood damage of each land-use category corresponding to different flood scenarios

Unit: Euros

Land-use category	**Flood scenarios**			**Annual damage**
	10%	**7.50%**	**2%**	
Paddy crop	72,300	83,679	171,680	17,303
Nonpaddy crops	51,182	45,683	100,318	10,349
Aquaculture	159,164	220,538	399,439	37,735
Total	**282,646**	**349,900**	**671,437**	**65,386**

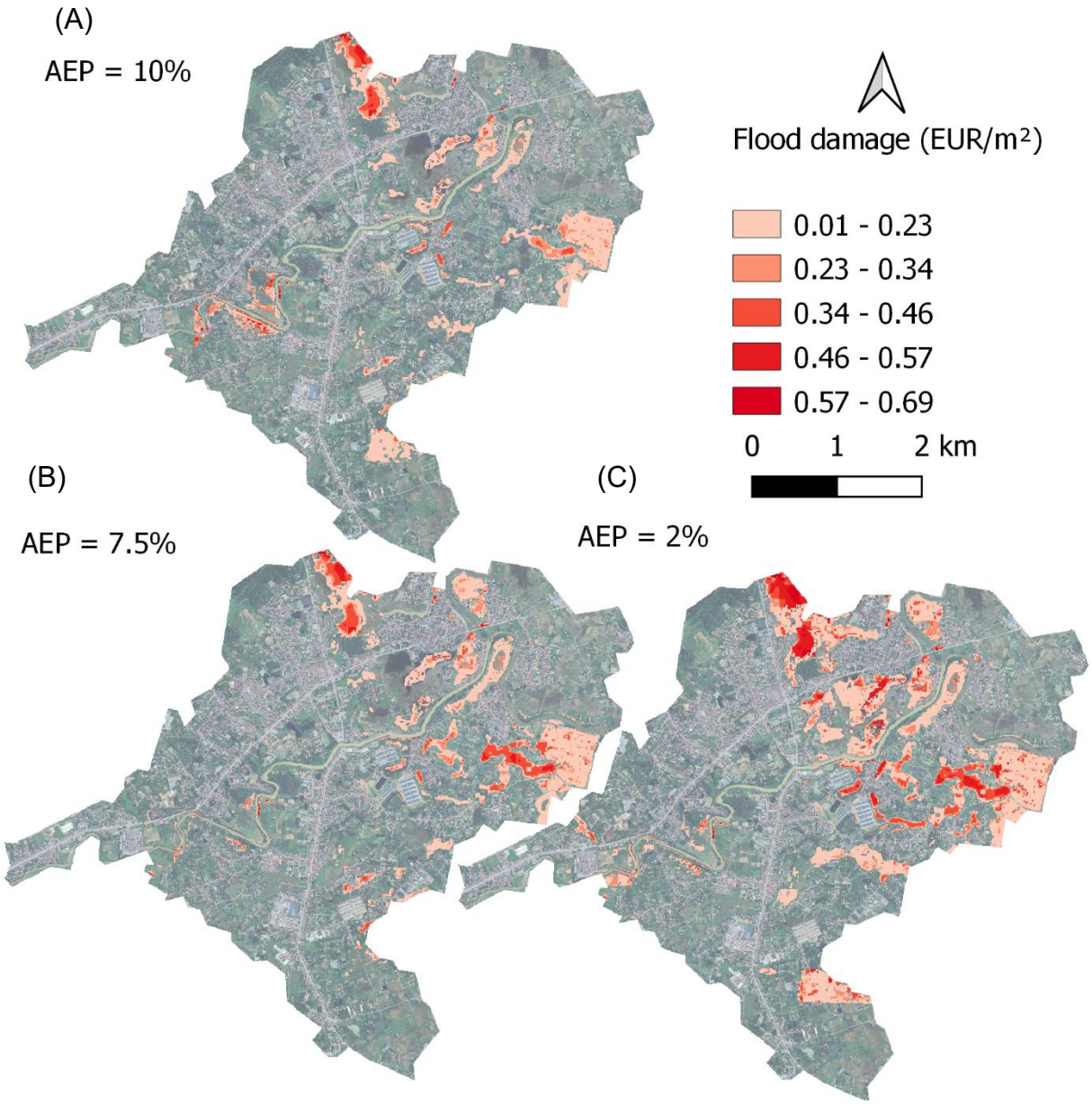

Figure 4.20. Flood damage maps for floods with an AEP of 10% (A), an AEP of 7.5% (B), and an AEP of 2% of the pilot area (C)

The final stages of the economic flood risk analysis involved the merging of the three flood damage maps into a single economic risk map that indicates the risk in EUR/m²/year (Figure 4.21). This stage also included the development of the flood risk curve, and the calculation of the annual flood damage using Eq 3.2. Figure 4.22 shows the risk curve by plotting the estimated flood damage values against the different return periods. The estimated annual flood damage is approximately € 65,386, which represents approximately 4% of the total agricultural production value and 6% of the fiscal revenues of the pilot area in 2021 (Thuy Xuan Tien's People Committee, 2021; Xuan Mai's People Committee, 2021). The annual flood damage for paddy crops, other

crops, and aquacultural areas is estimated at € 17,300, 10,348, and 37,734, respectively (Table 4.21).

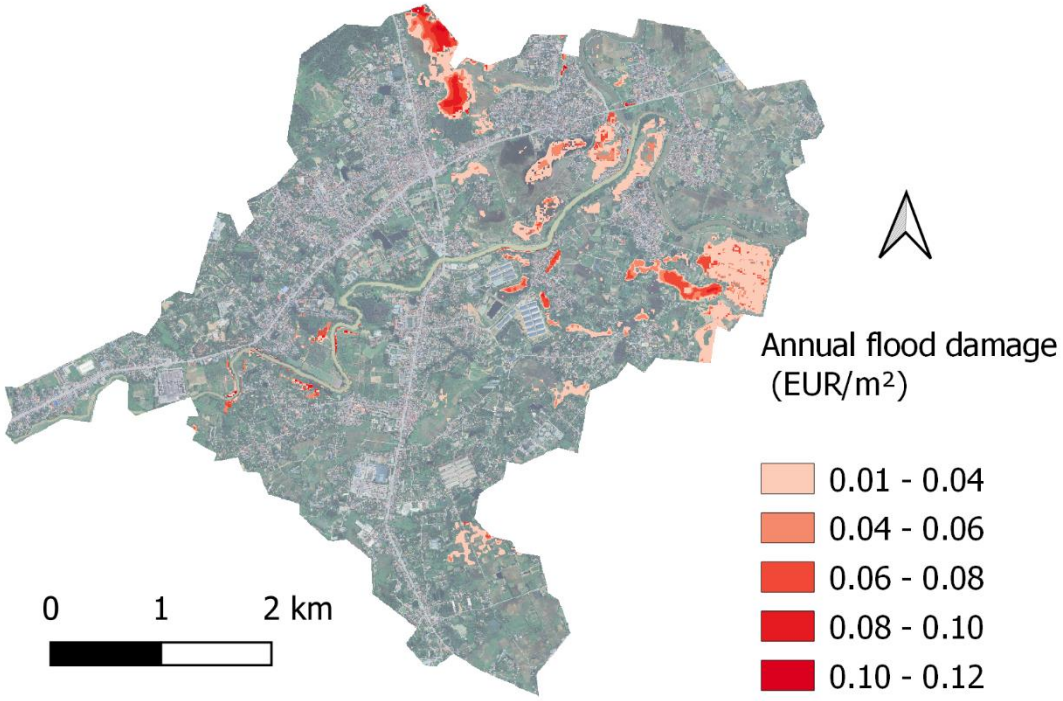

Figure 4.21. Flood risk map for the agricultural land in the pilot area

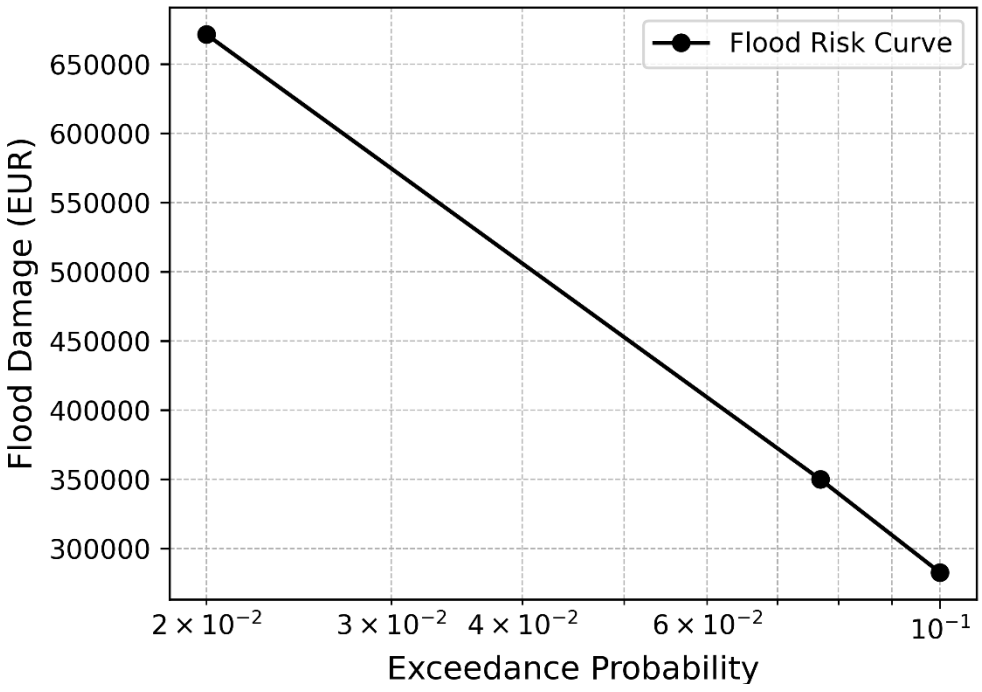

Figure 4.22. Flood risk curve for the agricultural land in the pilot area

4.4 Chapter summary

This chapter presents the results of flood risk assessment, which employed a combination of citizen science, remote sensing, field surveys, and existing literature. This integrated approach enabled a comprehensive and robust analysis for data-scarce areas. Here, the author summarizes the key findings.

The involvement of the general public in scientific research, known as "citizen science," proved to be a valuable addition to our flood data collection efforts at the local level. The participation of local residents included self-investigation or investigation of flooding in residential areas, land-use, flood impact on paddy crops, and rainfall using data collection applications. The majority of participants were young individuals, and they were recruited through personal relationships.

This research has demonstrated that only one-sixth of the participants actively engaged in the citizen science program, while the remaining participants were involved in the first investigations or for a few months. The citizen science data were found to be consistent with the data gathered by the author and district authorities as well as the automatic monitoring station, with an overall accuracy or correlation coefficient exceeding 70%. The involvement of citizen scientists in rainfall monitoring proved conducive to the generation of updated flood-related data during the citizen science program.

The study introduced an innovative methodology for developing flood hazard maps for the years 2017, 2018, and 2022. These maps were generated based on flood levels in both bare land and residential areas, utilizing remote sensing, field surveys, and citizen science. Additionally, topographic maps were incorporated. This approach did not require specific input data such as meteorological data and river cross-sections. The findings indicated that remote sensing is highly effective for detecting the extent of flooding on bare lands, while citizen science and field surveys are more suited for determining flood information in residential regions. This new methodology's flood maps were validated against statistics provided by district authorities or derived from model-based approaches, showing high agreement. A statistical analysis of maximum flood levels revealed that the 2022, 2017, and 2018 floods corresponded to 10-year, 13-year, and 50-year flood events, respectively.

The 2022 land-use map of the Bui River Basin was developed using S-2 satellite images and a random forest algorithm on Google Earth Engine. The map primarily consists of agricultural land, including paddy crops, nonpaddy crops, and aquacultural areas within the Bui River Basin and pilot area. Furthermore, stage damage curves for agricultural objects were developed using historical data from the pilot area for the paddy crop or adopted from previous literature for nonpaddy crops and aquacultural areas. All stage damage curves were displayed as logarithmic curves to estimate flood damage, with damage to paddy crops beginning when the flooding depth exceeds 0.25 meters.

To estimate flood damage to agricultural land under three flood scenarios, the flood hazard mapping, a land-use map, gross production values, and stage damage curves were combined. From this, the annual flood damage was calculated to be approximately € 65,386, equivalent to 4% of the maximum flood damage in the pilot area. Damage to the aquacultural areas accounted for over 50% of the total damage.

These findings demonstrated the value of integrating data from diverse sources and employing a simplified methodology to estimate flood risk components and flood damage in data-scarce regions.

5 Discussion

Flood risk assessment typically requires extensive datasets, the collection and analysis of which demand significant financial resources, time, and specialized tools. Consequently, comprehensive assessments are often limited to developed countries or urban areas, where data availability and collection infrastructure are more favorable. These requirements present substantial challenges for conducting flood risk assessments in developing countries, particularly in rural and data-scarce regions.

In this study, an innovative approach was developed to obtain flood-related data through the involvement of citizen scientists residing in or near flood-affected areas over a two-year period, from September 2021 to August 2023. A novel methodology was proposed that integrates remote sensing, citizen science, and field survey data with topographic maps to create detailed flooding maps. Furthermore, annual flood damage was assessed to agricultural land in the pilot area by combining flood hazard maps, exposure maps, and stage-damage curves to facilitate cost-benefit analysis of flood mitigation measures in the future.

5.1 Discussion of citizen science in flood data collection

5.1.1 Citizen scientists' engagement

The results of this research indicate that the personal relationship network plays a significant role in recruiting citizen scientists. Approximately 50% of citizen scientists were recruited through introductions from their relatives and friends, while only 1% were recruited through social media. This finding is consistent with the results reported by Davids *et al.*, (2019) for a case study on community-based rainfall monitoring in Nepal. In Vietnamese culture, which leans towards collectivist norms (Ho et al., 2022), the participation of citizen scientists or introductions from personal connections can significantly influence others' decisions to join. In contrast, citizen science programs in developed countries such as Germany and Italy often engage participants through unions, agencies, mass media (Pernat et al., 2021; Scaini et al., 2021; Schmitz et al., 2020), or direct email invitations (Phillips et al., 2019). Experience during field trips shows that participants in Vietnam may feel safer and more confident about joining citizen science programs when informed by trusted personal connections.

Student participation is a common feature of citizen science initiatives (J. C. Davids, 2019; Prajapati et al., 2021). Nevertheless, in predominantly rural areas with a low density of students, recruiting student citizen scientists proved challenging. A total of 44% of citizen scientists were students or postgraduates (Table 4.1 and Appendix 8.7). These individuals were mainly recruited as investigators for flood surveying. Additionally, efforts were made to engage students from flood-affected areas to self-survey or measure rainfall during weekends or social distancing periods due to the COVID-19 pandemic. Despite these efforts, their participation was limited as they did not permanently reside in the study area.

Secondary-school and high-school students as well as locals were recruited to participate in the citizen science program. The data collected by these citizen scientists demonstrated that they generally performed straightforward tasks, such as rainfall monitoring and land-use sampling (Table 4.2 and Appendix 8.7). In contrast, data collection on flood hazards and vulnerabilities required recalling past flood events or applying specialized skills to gather information from locals, especially regarding flood vulnerability, which was often handled by investigators.

The regular participation of citizen scientists is a critical concern in citizen science programs. Consistent with the findings of Davids *et al.*, (2019), this research showed that citizen scientists recruited via social media and outreach methods were more actively involved in flooding surveys and measurements compared to those recruited through personal networks. Despite accounting for just over one-fifth of the total recruits, those engaged through social media and outreach provided nearly half of the total data (Appendix 8.7). This suggests that citizen scientists' perceptions significantly influence their level of participation (C. J. Davids et al., 2019; Weeser et al., 2018). Consequently, outreach and social media methods appear to be effective and sustainable strategies for engaging active participants. Although 45% of all citizen scientists participated only once, their contributions were valuable in closing information gaps (Lowry et al., 2019), encouraging others to participate (Weeser et al., 2018), and validating data from different areas (Walker et al., 2016). Furthermore, this research also observed a decline in the participation of citizen scientists over time, a common challenge in citizen science programs (C. J. Davids et al., 2019; Weeser et al., 2018).

5.1.2 Citizen science data quality

5.1.2.1 Flood hazard

In flood-affected areas, citizen scientists provided and collected useful flood information, thereby assisting scientists in gaining insight into the impacts of flooding. Local residents in flood-affected areas frequently report more flood events than are recorded in official records (de Bruijn et al., 2019). Furthermore, they identify larger flood extents than those indicated in focus group discussions (Canevari-Luzardo et al., 2017) or in remotely sensed image analysis (Sy et al., 2020). The agreement between citizen science data (i.e., flooded and nonflooded points) and a flooding map is over 80% for the 2018 flood, demonstrating the potential of citizen scientists to accurately collect and provide information on both flooded and non-flooded points (Sy et al., 2020). Some flooded points were not indicated on the flooding map, but they were identified in videos and photographs of floods as well as in detailed descriptions (ID 17, Figure 4.2). In terms of flood intensity, the flooding depths reported by citizen scientists were found to be higher than those obtained from flooding maps developed from 3m-DTM and flood marks, a pattern also observed in the findings of (Fohringer et al., 2015). This finding confirmed that community-based data is often overestimated in comparison to data measured by reference devices or sensors (Fehri, Khlifi, et al., 2020; Kipf et al., 2016).

5.1.2.2 Exposure data

The findings of this research indicate that citizen scientists are an effective mean of collecting and updating land-use data on the ground. The substantial overall agreement of 80% between citizen scientists and the author in land-use classification during the field experiment in April 2022 illustrates the potential of citizen science for land-use data collection (Olteanu-Raimond et al., 2018; See et al., 2015). Moreover, citizen scientists acted as "human sensors," monitoring and updating land-use changes in April and August 2022, as discussed in studies by Olteanu-Raimond et al., (2018) and See et al., (2015).

Two factors influenced the outcomes of land-use sampling and classification by citizen scientists. Firstly, participants were required to determine the typical land-use type for areas of about 400 m². Although they were instructed to survey sites where they could

identify a typical land-use class within a 20-meter radius and take photos of approximately 20 m x 20 m areas, some participants focused on specific objects such as buildings, gardens, and rivers. This led to misclassifications when they did not consider the overall typical land-use class. Secondly, participants faced difficulties in classifying land-use types in heterogeneous areas, such as those with non-paddy crops and shrublands. This challenge is common among citizen scientists, as noted by Sparks et al., (2015) and Visser (2015). However, the photos of land-use taken by participants may prove useful in validating and correcting inaccurate information.

5.1.2.3 Flood vulnerability

There was a decent agreement between the data gathered by the district authority and by citizen scientists regarding the flood damage to paddy crops for 2018. However, the damage rates gathered by citizen scientists in this study were found to be lower than those documented by the local government after the 2018 flood event. This discrepancy may have been influenced by the respondents' memories between the two surveys (Win et al., 2018). Respondents might have provided more accurate information when they were no longer affected by flood-related emotions (Glas et al., 2020). Additionally, the estimation of flood damage to paddy fields can be more precise when the affected paddy fields are harvested.

5.1.2.4 Rainfall data

The rainfall data of CS_48 demonstrated a high degree of consistency with the official data, with a correlation coefficient of 0.9 between the two datasets. The rainfall is a basic parameter that can be readily monitored by citizen scientists (Fehri, Khlifi, et al., 2020). In this research, the rainfall data correlation coefficient between the citizen scientists and official data was lower than that obtained in the analysis by Fehri et al. (2020). The lower accuracy observed in this research can be attributed to several factors. Firstly, the citizen scientist did not measure rainfall daily, which resulted in the stored rainfall in the gauges being evaporated (C. J. Davids et al., 2019). Furthermore, the low-cost rain gauges were made from curved plastic bottles, which resulted in the measured rainfall being higher than the actual rainfall. Third, the low-cost rain gauges were constructed from plastic bottles, which may become cracked at the bottom over time and in contact with concrete (Figure 5.1A). This may have resulted in rainwater leakage. In this

research, waterproof tape was employed to reduce the likelihood of cracked rain gauges or leakage of rainwater (Figure 5.1B).

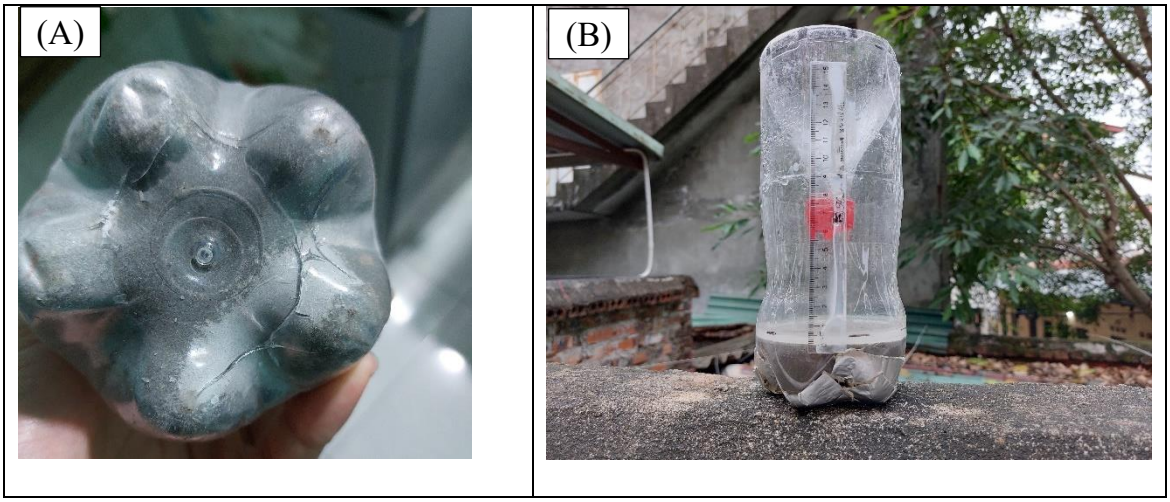

Figure 5.1. The foundation of the rain gauge cracked (A) and a -waterproof tape used (B)

5.2 Discussion of flood hazard assessment

5.2.1 Reliability of flood extent using S-1 images

In this research, Otsu's threshold method was used for detecting flood extent on bare land using S-1 images, which does not require any training samples. The optimal flood threshold value was determined at 14.97 dB for S-1 images with VV polarization for the Bui River Basin. This value is comparable to the results reported by Bekele et al. (2022) and Moharrami et al. (2021) for case study in Ethiopia and Iran, respectively. This research confirmed the efficacy of the Otsu method in detecting floods with minimal input data requirements.

The application of S-1 images for flood extent detection highly depends on the satellite overpass date. S-1 images are acquired at 6- or 12-day intervals depending on the location (Geographical Coverage, n.d.), with a 12-day interval for the Bui River Basin. Consequently, not all flood events can be captured by the satellite during the maximum flood level period, affecting the reliability of the flood extent documentation compared to the actual flood extent. According to the district authority, the flood extents of 2017 and 2018 in the Bui River Basin were similar. However, my results indicated that the flood extent in 2018 was approximately two times higher than that of the previous year.

The discrepancy in the flood extents observed between the two years can be attributed to the acquisition dates of the S-1 flood images. The S-1 flood image captured in 2018

was obtained during the maximum flood level period, whereas the S-1 flood image captured in 2017 was obtained 10 days after the maximum flood level period. This research has demonstrated that the image acquisition date has a significant impact on the detection of flood extents, as also highlighted in the research by Giordan et al. (2018).

While S-1 images are invaluable for identifying the extent of flooding, the flood maps produced from S-1 data have certain limitations. Firstly, the temporal resolution of S-1 may be inadequate for accurately monitoring the progression of flooding, given that flood extents can change rapidly (Singha et al., 2020). Some researchers have proposed the use of multisensory approaches (Giordan et al., 2018) or the combination of S-1 data with additional information from ground observations and crowdsourced data (Panteras & Cervone, 2018) as methods to enhance the temporal resolution of flood maps. Secondly, large, smooth surfaces such as roads, parking lots, stadiums, and shadow areas can be erroneously classified as flooded (Figure 5.2) due to the analogous backscatter characteristics of specular reflection, which results in lower backscatter (Tazmul Islam & Meng, 2022). To address this issue, this research employed flood level thresholds and slope data to reduce the overestimated flooded areas.

Figure 5.2. Misclassified flooding area at a soccer stadium in the pilot area in 2018 flood using Sentinel 1

Another uncertainty in retrieving flood extent from S-1 images is the challenge of defining flooded residence and vegetation (Figure 4.10). The documentation of flood extents within residential areas is complicated by the "double bounce" effect of radar signals from buildings, as described by Singha et al. (2020). Moreover, the C-band S-1 image is unable to penetrate the canopy to detect flooded vegetation (Tsyganskaya et al., 2018b). Consequently, it is frequently necessary to utilize supplementary data, such as flood photos and videos captured by locals acting as citizen scientists, ground observations, and digital elevation models (DEMs), to enhance the flood extent map derived from satellite images (Schnebele & Cervone, 2013).

5.2.2 Flooding map

The flood level surface in the subdomains of the pilot area were determined based on flood levels in the bare land and residential areas. This research found that flood levels on bare land were consistently lower than in residential areas within the same subdomain, aligning with the findings of Mason et al. (2021). Although the subdomain covers 1 km^2, the difference in flood levels between bare land and residential areas ranges from 0.95 to 3.92 m (2018 flood case) within the same subdomain. This reflects the complexity of the topographic conditions, as mentioned in Section 3.1.1.

The flooding area derived from the DTM-based approach and the flood-affected area reported by the district authority showed a difference of less than 10% for the two investigated floods (2017 and 2018). This result reflects the suitability of the flooding map derived from the DTM-based approach. It is noted that there is no official spatial flooding data gathered by the district authority. They used field surveys conducted post-flood to assess flood-affected agricultural areas and households for compensation purposes. Typically, data from field surveys, which require substantial effort and resources, are highly reliable (Parodi, 2019).

The flooding map derived from the modeling-based approach was used to validate the flooding area estimated by the DTM-based approach, showing reasonable agreement. However, some flooded areas were either underestimated or overestimated by each approach. Lowland areas connected to main rivers via sluice gates or small streams, which were not included in the flood modeling due to their complexity, were underestimated in the model-based approach compared to the DTM-based approach.

Conversely, some floodplain areas with dense vegetation along the upstream Bui River were identified as flooded in the model-based approach but not detected as such in the DTM-based approach. This discrepancy occurred, because the S1 image cannot detect flooded vegetation, or it lacked community-based flooding information. The flooding depth in the DTM-based approach was lower than in the modeling-based approach, which is consistent with the findings of (Peter et al., 2022).

DTM represents the most sensitive input data in the development of flood maps (Parodi, 2019). The reliability of flood levels is highly dependent on the accuracy of the DTM, which is closely linked to resolution and interpolation methods (Ribeiro et al., 2020). In this research, a 3-meter DTM was developed by interpolating the elevation point values of a topographic map using the B-spline interpolation method, considered the most suitable for developing flooding maps (Ribeiro et al., 2020). While the maximum flooding depths, characterized by the local pixel values, might not be consistent between investigated floods, the results for flooding extent and mean flooding depth are promising.

5.3 Discussion of flood damage estimation

5.3.1 Reliability in land-use map

The land-use map for the Bui River Basin is of high accuracy. Nevertheless, considerable uncertainty persists with regard to the classification of forest and shrubland areas. As demonstrated by Man et al. (2018), the spectral properties of these classes are quite similar. The accurate classification of forests and shrublands using remote sensing is a challenging endeavor (Dong et al., 2012) (Figure 5.3). This research focused on agricultural land, including paddy crops, non-paddy crops, and aquaculture, with the objective of estimating flood-affected agricultural areas and their damage. Consequently, the developed land-use map will be used for further analysis with minimal uncertainty. The majority of the land in the pilot area is paddy fields, which aligns with the map by Man et al. (2018).


A shrubland survey site

A forest survey site


A field photo of shrubland


A field photo of forest

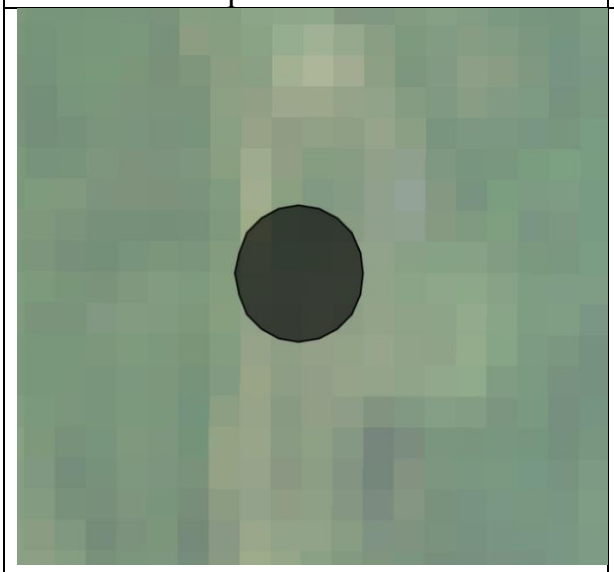
Spectral properties of shrubland in S2 composite image


Spectral properties of forest in S2 composite image

Figure 5.3. Field photos and spectral properties of shrubland and forest in the Bui River Basin

5.3.2 Factors influencing to stage damage curves

This research established the stage damage curves and formulas for subjects on agricultural land (i.e., paddy crops, nonpaddy crops, aquaculture) based on the relationship between the flooding depth and damage rate collected from field surveys, the citizen science program, and the previous literature. The damage rate to agricultural areas depends on several flood parameters, including the depth, duration, and velocity of the flooding. Of these factors, depth is the most significant in determining the degree of flood damage (Dang et al., 2011). This is reflected in the majority of studies on flood damage assessment (Ferri et al., 2020; Glas et al., 2018; B. B. Shrestha et al., 2016).

Figure 5.4. Embankment (A) and woven steel fence (B) heights in aquaculture area

The rate of damage to crops and aquaculture land depends on various factors, including the growth stage, type of crop or aquaculture, infrastructure, and farmers' adaptive measures (Dutta et al., 2003). For example, some families have adopted strategies to reduce flood impact, such as harvesting crops immediately before or during floods and replanting damaged crops afterward. Infrastructure adaptations have also been made, such as raising embankments in aquaculture areas to over 1 meter (Figure 5.4A). To further minimize damage, some households use 3-meter woven steel fences to contain fish within cultivated areas during the flood season (Figure 5.4B). These adaptations may alter the flooding threshold considered in stage-damage formulas. However, the main

objective of this research is to develop or select general stage-damage curves to assess flood damage broadly, so these complex factors are not included.

5.3.3 Flood risk analysis

The proportion of flood damage to aquaculture areas exceeds 50% of the total damage to agricultural production, indicating the role of this sector in developing agricultural economic activity and the impact of floods on it. Numerous studies have shown that aquaculture can be developed well in floodplain areas. This approach allows farmers to leverage the deposition of nutrients and the favorable conditions resulting from flooding to raise fish and shrimp (H. N. Pham et al., 2018; T. H. Tran et al., 2021; Vu et al., 2022).

The estimated total flood risk to agricultural production in the pilot area corresponds to 6% of the fiscal revenues for 2021 in the pilot area. In this research, flood damage maps for floods with lower probabilities (i.e., 1% and 0.5%) are unavailable, which may result in an underestimation of the annual flood damage (Ferri et al., 2020; Glas et al., 2020). Nevertheless, the 2% AEP flood, equivalent to the flood control standard in the study area (Hanoi, 2009), accurately reflects the real risk to the study area.

6 Conclusions, limitations, and recommendations

6.1 Conclusion

This research has sought to enhance flood risk assessments in data-scarce regions by integrating diverse data sources, including citizen science, remote sensing, field surveys, and literature. By leveraging diverse data sources, this research provides a robust framework for assessing flood risk components and estimating flood damage.

Citizen science, in particular, has emerged as a promising approach for collecting large volumes of data, driven by advances in ICT. The integration of citizen science data with remote sensing, field survey observations, and literature review helps bridge critical data gaps in flood risk assessment. Remote sensing data, with its extensive spatial, spectral, and temporal coverage, has been widely applied, enabled by open-access policies and modern cloud-computing platforms like GEE. Together, these data sources provide a comprehensive means of identifying and quantifying flood risk components.

It is necessary to gather flood-related data to assess flood risk. In this research, it was presented how the citizen science approach will help to collect and gather flood-related data, such as flooding in residential areas, land-use data, and flood damage to paddy fields. Local residents from flood-affected areas and nearby regions utilized data collection applications to gather and proactively share flood information. The citizen science data was found to be compatible with data gathered by the author or the district authority. Citizen involvement in rainfall monitoring not only sustained consistent participation but also fostered timely updates on flood conditions.

Flood maps are crucial for flood risk assessment and management. This research demonstrated how flood levels, integrated with DTM, can facilitate the rapid development of flood maps, especially in data-scarce areas. Combining remote sensing, citizen science, and field surveys improved the accuracy of flood maps by leveraging the unique strengths of each method. For instance, S-1 data proved highly effective in detecting flood extent in large open areas, such as paddy fields and aquacultural areas, where human presence is limited during flood events. Conversely, citizen science and field surveys excelled in documenting detailed flood situations in residential areas, often

supported by photo and video evidence. However, remote sensing data posed challenges in some cases due to resolution limitations and complex backscattering mechanisms.

The analysis of S-2 multi-spectral imagery offers essential insights into the land-use patterns of the Bui River Basin, serving as a critical foundation for creating a flood-exposure map of agricultural lands and an agricultural production value map for the pilot area. In this study, flooding depth is the primary factor considered in assessing agricultural damage levels. Logarithmic stage-damage curves and formulas for agricultural land assets were developed using data on flooding depth and damage rates gathered from field surveys, a citizen science initiative, and relevant literature. The estimated annual flood damage in the pilot area is approximately €65,386.

6.2 Research limitations

Although the current research has achieved its aims, there are some limitations due to time and budget constraints as well as data availability. It is therefore crucial to acknowledge these limitations to provide a comprehensive understanding of the research context and to identify areas for future improvement.

There are some limitations related to the citizen science approach to flood data collection. Firstly, due to the limitations of reference data, the proportion of citizen science data validated is relatively small. It is therefore necessary to evaluate all data provided by citizen scientists, categorizing them by age, educational background and collected data type, to determine the potential groups involved in flood-related data collection. Secondly, the accuracy of smartphone-generated coordinates of survey sites obtained from citizen scientists was not investigated, which affects the reliability of comparison results using spatial input data such as flooding or non-flooding and land-use sample sites. In this research, photos of survey sites were used to verify the reality of survey sites. Additionally, this research only evaluated the results of the citizen science program over two years. Maintaining the regular participation and continuity of the citizen science program is challenging, which requires substantial time and financial investments.

The incorporation of disparate sources of flood hazard data, including remote sensing, field surveys, and citizen science, along with digital terrain models (DTMs), can facilitate the development of flood maps using a DTM-based approach. Despite this,

some limitations of this approach must be considered. Firstly, the research did not consider the temporal coincidence between remote sensing and citizen science or field survey data. Attention to the temporal aspect is crucial for determining the maximum flooding extent, flood dynamics, and flood progress. Secondly, one drawback of the DTM-based approach is that it does not account for the hydraulic relationship of lowlands that lack a hydraulic connection with the flood level surface or flooding in areas such as behind flood-protected dike systems. Manual quality control is necessary to remove outliers, which is challenging when calculating large areas.

The flood risk assessment is based on certain assumptions, which might cause uncertainties in this research. Although the flood season typically occurs from June to October, the research used a land-use map retrieved from Sentinel-2 during the dry season (January to May) to increase the possibility of gathering cloud-free satellite images. The research assumed that the crop pattern change between the two seasons is minimal. Developed stage-damage curves should be validated (N. Y. Nguyen et al., 2017) by comparing the estimated flood damage results with actual flood damage data. However, actual flood damage data is not available in the study area or was not collected in this research. While flood damage to agricultural land depends on many factors, including flooding depth, flooding duration, flood velocity, and crop growth stages (Win et al., 2018), this research only focused on the flooding depth aspect. This flood parameter is also the unique parameter provided by the DTM-based approach.

6.3 Recommendations for future research

The sustainability of citizen science programs demands time and effort (Lowry et al., 2019). Therefore, these programs should be closely cooperated with local partners and relevant agencies relating to natural disaster management to determine collective targets and work together effectively. Regular training programs for citizens on how to collect and report data accurately should be established to enhance data quality. Floods have a direct and indirect impact on a wide range of objects, including buildings, infrastructure, life, and crops. However, this research was limited to direct flood damage to paddy fields. Therefore, it is worth investigating the capacity of locals to provide direct and indirect damage data for buildings, infrastructure, and incomes.

The combination of different remote sensing data can aid in determining flood extent (Notti et al., 2018; Rosser et al., 2017). In addition, the use of multi-temporal analysis can better understand the flood extent, flood dynamics (Bekele et al., 2022), and flood duration (N. Y. Nguyen et al., 2021). The accuracy of flood levels and flooding depth highly depends on the accuracy of the DTM. Future studies should investigate the effects of different resolutions (Cohen et al., 2018) and interpolation methods (Ribeiro et al., 2020) of DTM to choose the appropriate model and resolution for the study area.

The stage damage curves should be calibrated and validated for the Bui River Basin by comparing the estimated flood damage with actual flood damage. The stage damage curves considered only the aspect of flooding depth in this research. It is necessary to develop damage models with multiple variables, such as flooding duration, flood velocity, or the growth stages of crops, which can improve the accuracy of flood damage results (N. Y. Nguyen et al., 2021).

Flood damage encompasses many forms, including direct and indirect consequences for human life, the environment, and the economy. This study focused on the direct impact of floods on agricultural land. It would be beneficial in the future to investigate the indirect effects of floods on agricultural sectors, such as business interruption (H. N. Pham et al., 2018) and flood damage to farm infrastructures (Dutta et al., 2003). Moreover, it is crucial to assess the impact of flood damage on buildings, infrastructure, and waterworks, even in rural areas.

Overall, this research underscores the potential of integrating diverse data sources: citizen science, remote sensing, field surveys, and literature to address data gaps and enhance the accuracy of flood risk assessments in data-scarce areas. The methodologies and findings presented here provide a foundation for future research and practical applications in flood risk assessment and management.

7 References

Adam, A. M. (2020). Sample Size Determination in Survey Research. *Journal of Scientific Research and Reports*, 90–97. https://doi.org/10.9734/JSRR/2020/V26I530263

Agnihotri, A. K., Ohri, A., Gaur, S., Shivam, Das, N., & Mishra, S. (2019). Flood inundation mapping and monitoring using SAR data and its impact on Ramganga River in Ganga basin. *Environmental Monitoring and Assessment*, *191*(12). https://doi.org/10.1007/s10661-019-7903-4

Al-Areeq, A. M., Sharif, H. O., Abba, S. I., Chowdhury, S., Al-Suwaiyan, M., Benaafi, M., Yassin, M. A., & Aljundi, I. H. (2023). Digital elevation model for flood hazards analysis in complex terrain: Case study from Jeddah, Saudi Arabia. *International Journal of Applied Earth Observation and Geoinformation*, *119*, 103330. https://doi.org/10.1016/j.jag.2023.103330

Anjaneyulu, R., Swain, R., & Mukunda Behera, D. (2023). Future projections of worst floods and dam break analysis in Mahanadi River Basin under CMIP6 climate change scenarios. *Environmental Monitoring and Assessment*, *195*, 1173. https://doi.org/10.1007/s10661-023-11797-3

Apel, H., Aronica, G. T., Kreibich, H., & Thieken, A. H. (2009). Flood risk analyses - How detailed do we need to be? *Natural Hazards*, *49*(1), 79–98. https://doi.org/10.1007/s11069-008-9277-8

Assumpcao, T. H., Jonoski, A., Theona, I., Tsiakos, C., Krommyda, M., Tamascelli, S., Kallioras, A., Mierla, M., Georgiou, H. V., Miska, M., Pouliaris, C., Trifanov, C., Cimpan, K. T., Tsertou, A., Marin, E., Diakakis, M., Nichersu, I., Amditis, A. J., & Popescu, I. (2019). Citizens' campaigns for environmental water monitoring: Lessons from field experiments. *IEEE Access*, *7*, 134601–134620. https://doi.org/10.1109/ACCESS.2019.2939471

Azizi, K., Kofi Diko, S., & Meier, C. I. (2023). A Citizen Science Approach to the Characterisation and Modelling of Urban Pluvial Flooding. *Water Alternatives*, *1*(16), 265–294. www.water-alternatives.org

Basten, K. (2016). Classifying Landsat Terrain Images via Random Forests. *Bachelor*

Thesis Computer Science in Radboud University, Netherlands.

Bekele, T. W., Haile, A. T., Trigg, M. A., & Walsh, C. L. (2022). Evaluating a new method of remote sensing for flood mapping in the urban and peri-urban areas: Applied to Addis Ababa and the Akaki catchment in Ethiopia. *Natural Hazards Research*, *2*(2), 97–110. https://doi.org/10.1016/J.NHRES.2022.03.001

Beza, E. A. (2017). *Citizen science and remote sensing for crop yield gap analysis* [Wageningen University]. https://doi.org/10.18174/420049

Beza, E., Reidsma, P., Poortvliet, P. M., Belay, M. M., Bijen, B. S., & Kooistra, L. (2018). Exploring farmers' intentions to adopt mobile Short Message Service (SMS) for citizen science in agriculture. *Computers and Electronics in Agriculture*, *151*(February 2017), 295–310. https://doi.org/10.1016/j.compag.2018.06.015

Blaikie, P., Cannon, T., Davis, I., & Wisner, B. (1994). *At Risk : Natural Hazards, People's Vulnerability and Disasters* (1st Editio). Routledge. https://doi.org/10.4324/9780203974575

Blanco-Vogt, A., & Schanze, J. (2014). Assessment of the physical flood susceptibility of buildings on a large scale - Conceptual and methodological frameworks. *Natural Hazards and Earth System Sciences*, *14*(8), 2105–2117. https://doi.org/10.5194/nhess-14-2105-2014

Bonney, R., Cooper, C. B., Dickinson, J., Kelling, S., Phillips, T., Rosenberg, K. V, & Shirk, J. (2009). Citizen Science: A Developing Tool for Expanding Science Knowledge and Scientific Literacy. *BioScience*, *59*(11). https://doi.org/10.1525/bio.2009.59.11.9

Breiman, L. (2001). Random Forests. *Machine Learning*, *45*, 5–32.

Buytaert, W., Zulkafli, Z., Grainger, S., Acosta, L., Alemie, T. C., Bastiaensen, J., De Bièvre, B., Bhusal, J., Clark, J., Dewulf, A., Foggin, M., Hannah, D. M., Hergarten, C., Isaeva, A., Karpouzoglou, T., Pandeya, B., Paudel, D., Sharma, K., Steenhuis, T., … Zhumanova, M. (2014). Citizen science in hydrology and water resources: Opportunities for knowledge generation, ecosystem service management, and sustainable development. *Frontiers in Earth Science*,

2(October), 1–21. https://doi.org/10.3389/feart.2014.00026

Canevari-Luzardo, L., Bastide, J., Choutet, I., & Liverman, D. (2017). Using partial participatory GIS in vulnerability and disaster risk reduction in Grenada. *Climate and Development*, *9*(2), 95–109. https://doi.org/10.1080/17565529.2015.1067593

Casulli, V. (2009). A high-resolution wetting and drying algorithm for free-surface hydrodynamics. *International Journal for Numerical Methods in Fluids*, *60*(4), 391–408. https://doi.org/10.1002/FLD.1896

Chau, V. N. (2014). *Assessing the impacts of extreme floods on agriculture in Vietnam : Quang Nam case study* [Massey University]. https://mro.massey.ac.nz/handle/10179/6250

Chau, V. N., Holland, J., Cassells, S., & Tuohy, M. (2013). Using GIS to map impacts upon agriculture from extreme floods in Vietnam. *Applied Geography*, *41*, 65–74. https://doi.org/10.1016/J.APGEOG.2013.03.014

Cheung, W., & Feldman, D. (2019). Can citizen science promote flood risk communication? *Water*, *11*(10), 1–9. https://doi.org/10.3390/w11101961

Chuc, N., Singh, P., Komuravelly, S., Akkinapally, R., Chinh, N., Thang, N., Wani, S., & Long, T. (2006). Yield Gap Analysis of Major Rainfed Crops of Northern Vietnam Using Simulation Modeling. In *Global Theme on Agroecosystem*. https://www.researchgate.net/publication/277220863_Yield_Gap_Analysis_of_Major_Rainfed_Crops_of_Northern_Vietnam_Using_Simulation_Modeling_Global_Theme_on_Agroecosystems_Report_No_26#fullTextFileContent

Chuong My District People's Committee (2015). *The general construction planning of Chuong My district to 2030, the scale of 1/10.000 (Vietnamese)*.

Chuong My District People's Committee (2018). *Summary Report of flood damage and force, material, and vehicle mobilization in third strom in 2018 (unpublished)*.

Chuong My District People's Committee (2020). *Planning of social economic development for 5 years from 2021 - 2025 (unpublished)*.

Chuong My District People's Committee (2023). *Annual Natual disaster Report of Chuong My district in 2023*.

Clauss, K., Ottinger, M., Leinenkugel, P., & Kuenzer, C. (2018). Estimating rice production in the Mekong Delta, Vietnam, utilizing time series of Sentinel-1 SAR data. *International Journal of Applied Earth Observation and Geoinformation*, *73*, 574–585. https://doi.org/10.1016/J.JAG.2018.07.022

Cohen, S., Brakenridge, G. R., Kettner, A., Bates, B., Nelson, J., McDonald, R., Huang, Y. F., Munasinghe, D., & Zhang, J. (2018). Estimating Floodwater Depths from Flood Inundation Maps and Topography. *JAWRA Journal of the American Water Resources Association*, *54*(4), 847–858. https://doi.org/10.1111/1752-1688.12609

Cohen, S., Raney, A., Munasinghe, D., Derek Loftis, J., Molthan, A., Bell, J., Rogers, L., Galantowicz, J., Robert Brakenridge, G., Kettner, A., Huang, Y. F., & Tsang, Y. P. (2019). The Floodwater Depth Estimation Tool (FwDET v2.0) for improved remote sensing analysis of coastal flooding. *Natural Hazards and Earth System Sciences*, *19*(9), 2053–2065. https://doi.org/10.5194/NHESS-19-2053-2019

Cohn, J. P. (2008). Citizen Science: Can Volunteers Do Real Research? *BioScience*, *58*(3), 192–197. https://doi.org/10.1641/b580303

Congalton, R. G. (1991). A review of assessing the accuracy of classifications of remotely sensed data. *Remote Sensing of Environment*, *37*(1), 35–46. https://doi.org/10.1016/0034-4257(91)90048-B

Council, N. R. (2015). *Tying Flood Insurance to Flood Risk for Low-Lying Structures in the Floodplain*. The National Academies Press. https://doi.org/10.17226/21720

Coverage, G. (2018). *Geographical Coverage - Sentinel-1 - Sentinel Online*. https://sentiwiki.copernicus.eu/web/s1-mission

Dang, N. M., Babel, M. S., & Luong, H. T. (2011). Evaluation of food risk parameters in the Day River Flood Diversion Area, Red River Delta, Vietnam. *Natural Hazards*, *56*(1), 169–194. https://doi.org/10.1007/s11069-010-9558-x

Dasallas, L., Kim, Y., & An, H. (2019). Case Study of HEC-RAS 1D–2D Coupling Simulation: 2002 Baeksan Flood Event in Korea. *Water*, *11*(10), 2048. https://doi.org/10.3390/w11102048

David, A., & Schmalz, B. (2020). Flood hazard analysis in small catchments:

Comparison of hydrological and hydrodynamic approaches by the use of direct rainfall. *Jounral of Flood Risk Management*. https://doi.org/10.1111/jfr3.12639

Davids, C. J., Devkota, N., Pandey, A., Prajapati, R., Ertis, B. A., Rutten, M. M., Lyon, S. W., Bogaard, A. T., & van de Giesen, N. (2019). Soda Bottle Science—Citizen Science Monsoon Precipitation Monitoring in Nepal. *Frontiers in Earth Science*, *7*(March). https://doi.org/10.3389/feart.2019.00046

Davids, C. J., Rutten, M. M., Shah, T. R. D., Shah, N. D., Devkota, N., Izeboud, P., Pandey, A., & Van De Giesen, N. (2018). Quantifying the connections—linkages between land-use and water in the Kathmandu Valley, Nepal. *Environmental Monitoring and Assessment*, *190*(304). https://doi.org/10.1007/s10661-018-6687-2

Davids, J. C. (2019). Mobilizing Young Researchers, Citizen Scientists, and Mobile Technology o Close Water Data Gaps_ Methods Development and Initial Results in the Kahmandu Valley, Nepal. In *TU Delft University*. https://doi.org/10.4233/uuid

de Bruijn, J. A., de Moel, H., Jongman, B., de Ruiter, M. C., Wagemaker, J., & Aerts, J. C. J. H. (2019). A global database of historic and real-time flood events based on social media. *Scientific Data*, *6*(1), 311. https://doi.org/10.1038/s41597-019-0326-9

De Moel, H., Asselman, N. E. M., & H. Aerts, J. C. J. (2012). Uncertainty and sensitivity analysis of coastal flood damage estimates in the west of the Netherlands. *Natural Hazards and Earth System Science*, *12*(4), 1045–1058. https://doi.org/10.5194/nhess-12-1045-2012

de Moel, H., Jongman, B., Kreibich, H., Merz, B., Penning-Rowsell, E., & Ward, P. J. (2015). Flood risk assessments at different spatial scales. *Mitigation and Adaptation Strategies for Global Change*, *20*(6), 865–890. https://doi.org/10.1007/s11027-015-9654-z

DeVries, B., Huang, C., Armston, J., Huang, W., Jones, J. W., & Lang, M. W. (2020b). Rapid and robust monitoring of flood events using Sentinel-1 and Landsat data on the Google Earth Engine. *Remote Sensing of Environment*, *240*,

111664. https://doi.org/10.1016/J.RSE.2020.111664

Dibaba, W. T., Demissie, T. A., & Miegel, K. (2020). Drivers and Implications of Land Use/Land Cover Dynamics in Finchaa Catchment, Northwestern Ethiopia. *Land*, *9*(4), 113. https://doi.org/10.3390/land9040113

Do, T. K. A., & Le, M. C. (2013). Calibrating HEC-HMS Model with Limited Spatial Information: A Case Study in Nongson Watershed, Thubon River, Vietnam. *The University of Danang - Journal of Science and Technology*, *I*(1), 1–6.

Doan, T. M. T., & Bui, X. D. (2016). Floodplain development in Bui river due to land-use change from 2004 to 2015. *Journal of Forestry Science and Technology*, *5*, 90–101.

Dong, J., Xiao, X., Menarguez, M. A., Zhang, G., Qin, Y., Thau, D., Biradar, C., & Moore, B. (2016). Mapping paddy rice planting area in northeastern Asia with Landsat 8 images, phenology-based algorithm and Google Earth Engine. *Remote Sensing of Environment*, *185*, 142–154. https://doi.org/10.1016/J.RSE.2016.02.016

Dong, J., Xiao, X., Sheldon, S., Biradar, C., Duong, N. D., & Hazarika, M. (2012). A comparison of forest cover maps in Mainland Southeast Asia from multiple sources: PALSAR, MERIS, MODIS and FRA. *Remote Sensing of Environment*, *127*, 60–73. https://doi.org/10.1016/j.rse.2012.08.022

Duong, P. C., Nauditt, A., Nam, D. H., & Phong, N. T. (2016). Assessment of climate change impact on river flow regimes in The Red River Delta, Vietnam – A case study of the Nhue-Day River Basin. *Journal of Natural Resources and Development*, *6*, 81–91. https://doi.org/10.5027/jnrd.v6i0.09

Duong, V. H. T. (2018). *Land use based flood hazard analysis for the Mekong Delta (Doctoral thesis)*. Karsruhel Technology Institue.

Dutta, D., Herath, S., & Musiake, K. (2003). A mathematical model for flood loss estimation. *Journal of Hydrology*, *277*, 24–49. https://doi.org/10.1016/S0022-1694(03)00084-2

Efron, B. (1979). Bootstrap Methods: Another Look at the Jackknife. *The Annals of Statistics*, *7*(1), 1–26. https://doi.org/10.1214/aos/1176344552

Englhardt, J., De Moel, H., Huyck, C. K., De Ruiter, M. C., Aerts, J. C. J. H., & Ward, P. J. (2019). Enhancement of large-scale flood risk assessments using building-material-based vulnerability curves for an object-based approach in urban and rural areas. *Natural Hazards and Earth System Sciences*, *19*(8), 1703–1722. https://doi.org/10.5194/nhess-19-1703-2019

ESA. (n.d.). *SENTINEL-2 MISSION GUIDE*. Retrieved March 21, 2024, from https://sentinels.copernicus.eu/web/sentinel/missions/sentinel-2

Etter, S., Strobl, B., Seibert, J., & van Meerveld, H. J. I. (2020). Value of Crowd-Based Water Level Class Observations for Hydrological Model Calibration. *Water Resources Research*, *56*(2), 1–17. https://doi.org/10.1029/2019WR026108

Fehri, R., Bogaert, P., Khlifi, S., & Vanclooster, M. (2020). Data fusion of citizen-generated smartphone discharge measurements in Tunisia. *Journal of Hydrology*, *590*. https://doi.org/10.1016/j.jhydrol.2020.125518

Fehri, R., Khlifi, S., & Vanclooster, M. (2020). Testing a citizen science water monitoring approach in Tunisia. *Environmental Science and Policy*, *104*(November 2019), 67–72. https://doi.org/10.1016/j.envsci.2019.11.009

Ferri, M., Wehn, U., See, L., Monego, M., & Fritz, S. (2020). The value of citizen science for flood risk reduction: cost-benefit analysis of a citizen observatory in the Brenta-Bacchiglione catchment. *Hydrology and Earth System Sciences*, *24*, 5781–5798. https://doi.org/10.5194/hess-24-5781-2020

Fohringer, J., Dransch, D., Kreibich, H., & Schröter, K. (2015). Social media as an information source for rapid flood inundation mapping. *Natural Hazards and Earth System Sciences*, *15*(12), 2725–2738. https://doi.org/10.5194/nhess-15-2725-2015

Foody, G. M. (2002). Status of land cover classification accuracy assessment. *Remote Sensing of Environment*, *80*(1), 185–201. https://doi.org/10.1016/S0034-4257(01)00295-4

Forster, S., Kuhlmann, B., Lindenschmidt, K. E., & Bronstert, A. (2008). Assessing flood risk for a rural detention area. *Natural Hazards and Earth System Science*, *8*(2), 311–322. https://doi.org/10.5194/nhess-8-311-2008

Foudi, S., & Oses-Eraso, N. (2014). Flood risk management: Assessment for prevention with hydro-economic approaches. In *Handbook of the Economics of Climate Change Adaptation*.

Fuchs, S., Keiler, M., Ortlepp, R., Schinke, R., & Papathoma-Köhle, M. (2019). Recent advances in vulnerability assessment for the built environment exposed to torrential hazards: Challenges and the way forward. *Journal of Hydrology*, *575*(October 2018), 587–595. https://doi.org/10.1016/j.jhydrol.2019.05.067

Gain, A. K., & Hoque, M. M. (2013). Flood risk assessment and its application in the eastern part of Dhaka City, Bangladesh. *Journal of Flood Risk Management*, *6*(3), 219–228. https://doi.org/10.1111/jfr3.12003

Gain, Animesh K., Mojtahed, V., Biscaro, C., Balbi, S., & Giupponi, C. (2015). An integrated approach of flood risk assessment in the eastern part of Dhaka City (52). *Natural Hazards*, *79*(3), 1499–1530. https://doi.org/10.1007/s11069-015-1911-7

Gary W. Brunner. (2016). HEC-RAS River Analysis System. In *Hydrologic Engineering Center* (Issue February).

Gebremedhin, E. T., Basco-Carrera, L., Jonoski, A., Iliffe, M., & Winsemius, H. (2020). Crowdsourcing and interactive modelling for urban flood management. *Journal of Flood Risk Management*, *13*(2), 1–15. https://doi.org/10.1111/jfr3.12602

Gerl, T., Bochow, M., & Kreibich, H. (2014). Flood damage modeling on the basis of urban structure mapping using high-resolution remote sensing data. *Water (Switzerland)*, *6*(8), 2367–2393. https://doi.org/10.3390/w6082367

Giordan, D., Notti, D., Villa, A., Zucca, F., Calò, F., Pepe, A., Dutto, F., Pari, P., Baldo, M., & Allasia, P. (2018). Low cost, multiscale and multi-sensor application for flooded area mapping. *Natural Hazards and Earth System Sciences*, *18*(5), 1493–1516. https://doi.org/10.5194/NHESS-18-1493-2018

Glas, H., De Maeyer, P., Merisier, S., & Deruyter, G. (2020). Development of a low-cost methodology for data acquisition and flood risk assessment in the floodplain of the river Moustiques in Haiti. *Journal of Flood Risk Management*, *13*(2),

e12608. https://doi.org/10.1111/JFR3.12608

Glas, H., Deruyter, G., & De Maeyer, P. (2018). Flood risk assessment in data sparse regions: the use of questionnaires to collect historic flood data - A case study for the river moustiques in Haiti. *International Multidisciplinary Scientific GeoConference Surveying Geology and Mining Ecology Management, SGEM*, *18*(2.3), 377–384. https://doi.org/10.5593/sgem2018/2.3/S11.048

Glas, H., Deruyter, G., Maeyer, P. De, Mandal, A., & James-williamson, S. (2016). Analyzing the sensitivity of a flood risk assessment model towards its input data. *Natural Hazards and Earth System Science*, 2529–2542. https://doi.org/10.5194/nhess-16-2529-2016

Guth, P. L., Van Niekerk, A., Grohmann, C. H., Muller, J. P., Hawker, L., Florinsky, I. V., Gesch, D., Reuter, H. I., Herrera-Cruz, V., Riazanoff, S., López-Vázquez, C., Carabajal, C. C., Albinet, C., & Strobl, P. (2021). Digital elevation models: Terminology and definitions. *Remote Sensing*, *13*(18), 1–19. https://doi.org/10.3390/rs13183581

Hanoi City People's Committee (2009). *No 17/2009/NQ-HDND The decision of approving the plan of flood prevention for river dyke system in Hanoi to 2020*.

Hanoi City People's Committee (2018). *Hanoi Statistical Yearbook 2017* (D. Van Chien (ed.)). Statistics Publisher.

Hanoi City People's Committee (2019). *Kế hoạch ứng phó lũ lớn trên sông Tích, Bùi năm 2019 (Flood control planning on the Tich , Bui River in 2019)*.

Hartung, C., Anokwa, Y., Brunette, W., Lerer, A., Tseng, C., & Borriello, G. (2010). Open Data Kit: Tools to Build Information Services for Developing Regions. *4th ACM/IEEE International Conference on Information and Communication Technologies and Development, ICTD 2010;*, 12.

HEC. (2000). *Hydrologic modeling system HEC-HMS – Technical reference manual*. https://www.hec.usace.army.mil/software/hec-hms/documentation/HEC-HMS_Technical Reference Manual_(CPD-74B).pdf

HEC. (2016). *HEC-RAS river analysis system 2D modeling user's manual – Version 5.0*.

Herath, S., & Dushmanta, D. (2020). Flood Damage Estimation of an Urban Catchment Using Remote Sensing and Gis. *Conference*, *September*, 51–60.

Hess, T. M., & Morris, J. (1988). Estimating the value of flood alleviation on agricultural grassland. *Agricultural Water Management*, *15*(2), 141–153. https://doi.org/10.1016/0378-3774(88)90107-2

Ho, H. A., Martinsson, P., & Olsson, O. (2022). The origins of cultural divergence: evidence from Vietnam. *Journal of Economic Growth*, *27*(1), 45–89. https://doi.org/10.1007/S10887-021-09194-X/TABLES/8

Hoa Binh Provincial People's Committee. (2018). *Hoabinh Statistical Yearbook 2017*.

Hochrainer, S., Linnerooth-Bayer, J., & Mechler, R. (2010). The European Union Solidarity Fund Its legitimacy, viability and efficiency. *Mitig Adapt Strateg Glob Change*. https://doi.org/10.1007/s11027-009-9209-2

Horning, N. (2008). Remote Sensing. In S. E. Jørgensen & B. D. Fath (Eds.), *Encyclopedia of Ecology* (pp. 2986–2994). Academic Press. https://doi.org/https://doi.org/10.1016/B978-008045405-4.00237-8

Huang, X. (2020). Remote sensing and social sensing for improved flood awareness and exposure analysis in the big data era (Doctoral thesis). In *University of South Carolina* (Issue 1). University of South Carolina.

Huizinga, J., de Moel, H., & Szewczyk, W. (2017). Global flood depth-damage functions. Methodology and the database with guidelines. In *Joint Research Centre (JRC)*. https://doi.org/10.2760/16510

Irwin, A. (1995). *Citizen Science: A Study of People, Expertise and Sustainable Development*. https://philpapers.org/rec/IRWCSA

Iwao, K., Nishida, K., Kinoshita, T., & Yamagata, Y. (2006). Validating land cover maps with Degree Confluence Project information. *Geophysical Research Letters*, *33*(23). https://doi.org/10.1029/2006GL027768

JICA, S. (2014). *Climate Change Adaptation for Sustainable Development of Coastal Agriculture and Rural Areas in Vietnam's Mekong Delta (Thích ứng với BĐKH cho phát triển bền vững nông nghiệp và nông thôn vùng ven biển ĐBSCL*. https://openjicareport.jica.go.jp/pdf/12114641_02.pdf

Keough, H. L., & Blahna, D. J. (2006). Achieving Integrative, Collaborative Ecosystem Management. *Conservation Biology*, *20*(5), 1373–1382. https://doi.org/10.1111/J.1523-1739.2006.00445.X

Kipf, A., Brunette, W., Kellerstrass, J., Podolsky, M., Rosa, J., Sundt, M., Wilson, D., Borriello, G., Brewer, E., & Thomas, E. (2016). A proposed integrated data collection, analysis and sharing platform for impact evaluation. *Development Engineering*, *1*, 36–44. https://doi.org/10.1016/j.deveng.2015.12.002

Kittipongvises, S., Phetrak, A., Rattanapun, P., Brundiers, K., Buizer, J. L., & Melnick, R. (2020). AHP-GIS analysis for flood hazard assessment of the communities nearby the world heritage site on Ayutthaya Island, Thailand. *International Journal of Disaster Risk Reduction*, *48*, 101612. https://doi.org/10.1016/j.ijdrr.2020.101612

Klaus, S., Kreibich, H., Merz, B., Kuhlmann, B., & Schröter, K. (2016). Large-scale, seasonal flood risk analysis for agricultural crops in Germany. *Environmental Earth Sciences*, *75*(18), 1–13. https://doi.org/10.1007/S12665-016-6096-1/FIGURES/6

Klonner, C., Tomás, •, Usón, J., Aeschbach, N., & Höfle, • Bernhard. (2021). Participatory Mapping and Visualization of Local Knowledge: An Example from Eberbach, Germany. *International Journal of Disaster Risk Science*, *12*. https://doi.org/10.1007/s13753-020-00312-8

Kron, W. (2005). Flood risk = hazard • values • vulnerability. *Water International*, *30*(1), 58–68. https://doi.org/10.1080/02508060508691837

Kruger, L. E., & Shannon, M. A. (2000). Getting to Know Ourselves and Our Places Through Participation in Civic Social Assessment. *Society & Natural Resources: An International Journal*, *13*(5), 461–478. https://doi.org/10.1080/089419200403866

Kuhlmann, B. (2010). Schäden in der Landwirtschaft (Damages in Agricultulture). In A. H. Thieken, I. Seifert, & B. Merz (Eds.), *Hochwasserschäden : Erfassung, Abschätzung und Vermeidung*. oekom.

Le Coz, J., Patalano, A., Collins, D., Guillén, N. F., García, C. M., Smart, G. M., Bind,

J., Chiaverini, A., Le Boursicaud, R., Dramais, G., & Braud, I. (2016). Crowdsourced data for flood hydrology: Feedback from recent citizen science projects in Argentina, France and New Zealand. *Journal of Hydrology*, *541*, 766–777. https://doi.org/10.1016/j.jhydrol.2016.07.036

Le, V. S., Nguyen, V. T., Bui, T. H., Nguyen, D. Q., & Bui, T. Van. (2022). Studying into solutions for flood and inundation control in Bui River Basin and its vicinity. *Jounral of Water Resources Science and Technology*, *1*.

Liang, J., & Liu, D. (2020). A local thresholding approach to flood water delineation using Sentinel-1 SAR imagery. *ISPRS Journal of Photogrammetry and Remote Sensing*, *159*, 53–62. https://doi.org/10.1016/j.isprsjprs.2019.10.017

Liu, C. C., Shieh, M. C., Ke, M. S., & Wang, K. H. (2018). Flood prevention and emergency response system powered by Google Earth Engine. *Remote Sensing*, *10*(8). https://doi.org/10.3390/rs10081283

Lowry, C. S., Fienen, M. N., Hall, D. M., & Stepenuck, K. F. (2019). Growing pains of crowdsourced stream stage monitoring using mobile phones: The development of crowdhydrology. *Frontiers in Earth Science*, *7*(May), 1–10. https://doi.org/10.3389/feart.2019.00128

Luino, F. (2016). Floods. In P. T. Bobrowsky & B. Marker (Eds.), *Encyclopedia of Engineering Geology* (pp. 1–6). Springer International Publishing. https://doi.org/10.1007/978-3-319-12127-7_126-1

Luu, C., & von Meding, J. (2018). A Flood Risk Assessment of Quang Nam, Vietnam Using Spatial Multicriteria Decision Analysis. *Water*, *10*(4), 461. https://doi.org/10.3390/w10040461

Luu, C., Von Meding, J., & Kanjanabootra, S. (2017). Assessing flood hazard using flood marks and analytic hierarchy process approach: a case study for the 2013 flood event in Quang Nam, Vietnam. *Natural Hazards*, *90*(3), 1031–1050. https://doi.org/10.1007/s11069-017-3083-0

Luu, C., von Meding, J., & Mojtahedi, M. (2019). Analyzing Vietnam's national disaster loss database for flood risk assessment using multiple linear regression-TOPSIS. *International Journal of Disaster Risk Reduction*, *40*, 101153.

https://doi.org/10.1016/J.IJDRR.2019.101153

Maleska, D. V. (2021). *A Methodology for Investigating the Dynamics and Uncertainties of Flood Risks* (T. Dresden (ed.); Issue May). TU Dresden.

Man, C. D., Nguyen, T. T., Bui, H. Q., Lasko, K., & Nguyen, T. N. T. (2018). Improvement of land-cover classification over frequently cloud-covered areas using Landsat 8 time-series composites and an ensemble of supervised classifiers. *International Journal of Remote Sensing*, *39*(4), 1243–1255. https://doi.org/10.1080/01431161.2017.1399477

Mancusi, L., Albano, R., & Sole, A. (2015). *FloodRisk: a QGIS plugin for flood consequences estimation*. https://www.researchgate.net/publication/295626726_FloodRisk_a_QGIS_plugin_for_flood_consequences_estimation?channel=doi&linkId=56cc1be308ae5488f0dc50f4&showFulltext=true

Mason, D. C., Dance, S. L., & Cloke, H. L. (2021). Floodwater detection in urban areas using Sentinel-1 and WorldDEM data. *Journal of Applied Remote Sensing*, *3*, 15. https://doi.org/10.1117/1.JRS.15.032003

Merz, B., Kreibich, H., Schwarze, R., & Thieken, A. (2010). Review article " Assessment of economic flood damage ." *Natural Hazards and Earth System Sciences Review*, *10*, 1697–1724. https://doi.org/10.5194/nhess-10-1697-2010

Merz, B., & Thieken, A. H. (2009). Flood risk curves and uncertainty bounds. *Natural Hazards*, *51*(3), 437–458. https://doi.org/10.1007/s11069-009-9452-6

Messner, F., & Meyer, V. (2005). Flood damage, vulnerability and risk perception – challenges for flood damage research. In J. M. Jochen Schanze, Evzen Zeman (Ed.), *Flood Risk Management - Hazards, Vulnerability and Mitigation Measures* (Issue 13). Springer Publisher.

Messner, F., Penning-rowsell, E., Green, C., Tunstall, S., Veen, A. Van Der, Tapsell, S., Wilson, T., Krywkow, J., Logtmeijer, C., Fernández-bilbao, A., Geurts, P., & Haase, D. (2007). Evaluating flood damages: guidance and recommendations on principles and methods. In *Flood Risk Management: Hazards, Vulnerability and Mitigation Measures*.

Meyer, V., Hasse, D., & Scheuer, S. (2007). *GIS-based Multicriteria Analysis as Decision Support in Flood Risk Management* (Issue August). https://www.ufz.de/export/data/2/26194_DP_2007_06_Meyer.pdf

Miegel, K. (2006). *Flood protection (Hochwasserschutz)(Lecture notes)*. Rostock University

Minkman, E., Van Der Sanden, M., & Rutten, M. (2017). Practitioners' viewpoints on citizen science in water management: A case study in Dutch regional water resource management. *Hydrology and Earth System Sciences*, *21*(1), 153–167. https://doi.org/10.5194/hess-21-153-2017

Moharrami, M., Javanbakht, M., & Attarchi, S. (2021). Automatic flood detection using sentinel-1 images on the google earth engine. *Environmental Monitoring and Assessment*, *193*(5), 1–17. https://doi.org/10.1007/S10661-021-09037-7/FIGURES/14

Mohr, S., Ehret, U., Kunz, M., Ludwig, P., Caldas-Alvarez, A., Daniell, J. E., Ehmele, F., Feldmann, H., Franca, M. J., Gattke, C., Hundhausen, M., Knippertz, P., Küpfer, K., Mühr, B., Pinto, J. G., Quinting, J., Schäfer, A. M., Scheibel, M., Seidel, F., & Wisotzky, C. (2022). A multi-disciplinary analysis of the exceptional flood event of July 2021 in central Europe. Part 1: Event description and analysis. *Natural Hazards and Earth System Science*. https://doi.org/10.5194/nhess-2022-137

MONRE. (2019). *Ban hành Thông tư quy định kỹ thuật về nội dung và ký hiệu bản đồ địa hình quốc gia tỉ lệ 1:2.000, 1:5.000*. http://stnmt.kontum.gov.vn/vi/laws/detail/Ban-hanh-Thong-tu-quy-dinh-ky-thuat-ve-noi-dung-va-ky-hieu-ban-do-dia-hinh-quoc-gia-ti-le-1-2-000-1-5-000-1592/

Moriasi, D. N., Arnold, J. G., Liew, M. W. Van, Bingner, R. L., Harmel, R. D., & Veith, T. L. (2007). Model Evaluation Guidelines for Systematic Quantification of Accuracy in Watershed Simulations. *American Society of Agricultural and Biological Engineers*, *50*(3), 885–900.

Mouazen, A. M., Alexandridis, T., Buddenbaum, H., Cohen, Y., Moshou, D., Mulla, D., Nawar, S., & Sudduth, K. A. (2020). Chapter 2 - Monitoring. In A.

Castrignanò, G. Buttafuoco, R. Khosla, A. M. Mouazen, D. Moshou, & O. Naud (Eds.), *Agricultural Internet of Things and Decision Support for Precision Smart Farming* (pp. 35–138). Academic Press. https://doi.org/https://doi.org/10.1016/B978-0-12-818373-1.00002-0

Munasinghe, D., Cohen, S., Huang, Y. F., Tsang, Y. P., Zhang, J., & Fang, Z. (2018). Intercomparison of Satellite Remote Sensing-Based Flood Inundation Mapping Techniques. *Journal of the American Water Resources Association*, *54*(4), 834–846. https://doi.org/10.1111/1752-1688.12626

Munich RE. (2013). *Floods dominate Natural Catastrophe Statistics in First Half of 2013* (Issue July). https://www.munichre.com/en/media-relations/publications/press-releases/2013/2013-07-09-press-release/index.html (accessed

NAWAPI. (2009). *Water usage and water environment protection planning and management in Nhue - Day river basin to 2015, vision to 2020*.

Nguyen, C. T., Nguyen, K. C., & Phan, P. T. T. (2018). Hydrological-Quasi 2D Hydraulic Linked Model for Flood Forecasting. *American Journal of Engineering Research (AJER*, *7*(8), 237–241. www.ajer.org

Nguyen, H. L., Nguyen, T. H., Vo, N. D., Pham, T. H., & Nguyen, C. C. (2017). Construction of daily maximum rainfals atlat for Vietnam (XÂY DỰNG ATLAS MƯA NGÀY CỰC ĐẠI CHO VIỆT NAM). *Vietnam Journal of Hydro Meteology*.

Nguyen, H. T. T., Doan, T. M., Tomppo, E., & McRoberts, R. E. (2020). Land Use/Land Cover Mapping Using Multitemporal Sentinel-2 Imagery and Four Classification Methods—A Case Study from Dak Nong, Vietnam. *Remote Sensing*, *12*(9), 1367. https://doi.org/10.3390/RS12091367

Nguyen, M. T., Sebesvari, Z., Souvignet, M., Bachofer, F., Braun, A., Garschagen, M., Schinkel, U., Yang, L. E., Nguyen, L. H. K., Hochschild, V., Assmann, A., & Hagenlocher, M. (2021). Understanding and assessing flood risk in Vietnam: Current status, persisting gaps, and future directions. *Journal of Flood Risk Management*, *14*(2), e12689. https://doi.org/10.1111/JFR3.12689

Nguyen, N. Y., Ichikawa, Y., & Ishidaira, H. (2017). Establishing flood damage

functions for agricultural crops using estimated inundation depth and flood disaster statistics in data-scarce regions. *Hydrological Research Letters*, *11*(1), 12–18. https://doi.org/10.3178/hrl.11.12

Nguyen, N. Y., Kha, D. D., & Ichikawa, Y. (2021). Developing a multivariable lookup table function for estimating flood damages of rice crop in Vietnam using a secondary research approach. *International Journal of Disaster Risk Reduction*, *58*, 102208. https://doi.org/10.1016/J.IJDRR.2021.102208

Nguyen, T. C. (2018). *Application of Information Technology on numerical modelling specializing in flood forcasting on the Bui River (Ứng dụng CNTT xây dựng mô hình hỗ trợ công tác dự báo lũ và ngập lụt sông Tích Bùi)*.

Nguyen, T. T. H., & Doan, M. T. (2018). Application of Random Forest Algorithm for land use mapping in Daklak from Landsat 8. *Agricultture and Rural Development Journal*, 122–131.

Nguyen, T. T., & Le, T. T. H. (2019). Water Level Prediction at Tich-Bui river in Vietnam Using Support Vector Regression. *International Conference on Machine Learning and Cybernetics (ICMLC)*. https://doi.org/10.1109/ICMLC48188.2019.8949273.

Notti, D., Giordan, D., Caló, F., Pepe, A., Zucca, F., & Galve, J. P. (2018). Potential and limitations of open satellite data for flood mapping. *Remote Sensing*, *10*(11). https://doi.org/10.3390/rs10111673

Olesen, L., Löwe, R., & Arnbjerg-Nielsen, K. (2016). *Flood Damage Assessment - Literature Review and Application to the Elster Creek Catchment*. TU Denmark.

Olteanu-Raimond, A. M., Jolivet, L., Van Damme, M. D., Royer, T., Fraval, L., See, L., Sturn, T., Karner, M., Moorthy, I., & Fritz, S. (2018). An Experimental Framework for Integrating Citizen and Community Science into Land Cover, Land Use, and Land Change Detection Processes in a National Mapping Agency. *Land*, *7*(3), 103. https://doi.org/10.3390/LAND7030103

Opendevelopmendevelopment. (n.d.). *Soil types of Vietnam*. Retrieved April 5, 2024, from https://vietnam.opendevelopmentmekong.net/

Otsu, N. (1979). A Threshold Selection Method from Gray-Level Histograms. *IEEE*

Transactions on Systems, Man, and Cybernetics, *C*(1), 62–66.

Overdevest, C., Orr, C. H., & Stepenuck, K. (2004). Volunteer Stream Monitoring and Local Participation in Natural Resource Issues. *Human Ecology Review 0.5*, *11*(2).

Pandeya, B., Uprety, M., Paul, J. D., Sharma, R. R., Dugar, S., & Buytaert, W. (2021). Mitigating flood risk using low-cost sensors and citizen science: A proof-of-concept study from western Nepal. *Journal of Flood Risk Management*, *14*(1), e12675. https://doi.org/10.1111/JFR3.12675

Panteras, G., & Cervone, G. (2018). Enhancing the temporal resolution of satellite-based flood extent generation using crowdsourced data for disaster monitoring. *International Journal of Remote Sensing*, *39*(5), 1459–1474. https://doi.org/10.1080/01431161.2017.1400193

Parodi, M. U. (2019). *Investigating Uncertainty in Coastal Flood Risk Assessment in Small Island Developing States A Case Study in São Tomé and Príncipe* [TU Delft]. repository.tudelft.nl

Patel, D. P., Ramirez, J. A., Srivastava, P. K., Bray, M., & Han, D. (2017). Assessment of flood inundation mapping of Surat city by coupled 1D/2D hydrodynamic modeling: a case application of the new HEC-RAS 5. *Natural Hazards*, *89*(1), 93–130. https://doi.org/10.1007/s11069-017-2956-6

Penning-Rowsell, E., Johnson, C., Sylvia, T., Sue, T., Joe, M., John, C., Annabel, C., & Colin, G. (2003). *The Benefits of Flood and Coastal Defence: Techniques and Data for 2003*. Flood Hazard Research Centre.

Perera, E. D. P., Hiroe, A., Shrestha, D., Fukami, K., Basnyat, D. B., Gautam, S., Hasegawa, A., Uenoyama, T., & Tanaka, S. (2015). Community-based flood damage assessment approach for lower West Rapti River basin in Nepal under the impact of climate change. *Natural Hazards*, *75*(1), 669–699. https://doi.org/10.1007/S11069-014-1339-5/FIGURES/20

Pérez-Cutillas, P., Pérez-Navarro, A., Conesa-García, C., Zema, D. A., & Amado-Álvarez, J. P. (2023). What is going on within google earth engine? A systematic review and meta-analysis. *Remote Sensing Applications: Society and*

Environment, *29*, 100907. https://doi.org/10.1016/J.RSASE.2022.100907

Pernat, N., Kampen, H., Jeschke, J. M., & Werner, D. (2021). Citizen science versus professional data collection: Comparison of approaches to mosquito monitoring in Germany. *Journal of Applied Ecology*, *58*(2), 214–223. https://doi.org/10.1111/1365-2664.13767

Peter, B. G., Cohen, S., Lucey, R., Munasinghe, D., Raney, A., & Robert Brakenridge, G. (2022). Google Earth Engine Implementation of the Floodwater Depth Estimation Tool (FwDET-GEE) for Rapid and Large Scale Flood Analysis. *IEEE Geoscience and Remote Sensing Letters*, *19*, 2022. https://doi.org/10.1109/LGRS.2020.3031190

Peters-Guarin, G. (2008). *Integrating local knowledge into GIS-based flood risk assessment: The case of Traingulo and Mabolo communities in Naga City, The Philippines* [International Institute for Geo-Information Science and Earth observation (ITC)]. http://www.itc.nl/library/papers_2008/phd/peters.pdf

Pham, H. N., Takara, K., & Nguyen, C. Van. (2018). Integrated approach to analyze the total flood risk for agriculture: The significance of intangible damages – A case study in Central Vietnam. *International Journal of Disaster Risk Reduction*, *31*, 862–872. https://doi.org/10.1016/j.ijdrr.2018.08.001

Pham, T. K. O., Le, D. K., Trinh, H. N., Hang, T. V., & Nguyen, T. L. C. (2019). *Impacts of land use changes to flood on the Tich River Basin (Đánh giá ảnh hưởng của sự biến đổi sử dụng đất đến dòng chảy lũ trên lưu vực sông Tích)*.

Phan, A., Ha, D. N., Man, C. D., Nguyen, T. T., Bui, H. Q., & Nguyen, T. T. N. (2019). Rapid assessment of flood inundation and damaged rice area in Red River Delta from Sentinel 1A imagery. *Remote Sensing*, *11*(17), 1–24. https://doi.org/10.3390/rs11172034

Phillips, T. B., Ballard, H. L., Lewenstein, B. V., & Bonney, R. (2019). Engagement in science through citizen science: Moving beyond data collection. *Science Education*, *103*(3), 665–690. https://doi.org/10.1002/sce.21501

Portengen, L. (2017). *Classifying Mangroves in Vietnam using Radar and Optical Satellite Remote Sensing Processing Sentinel-1 and Sentinel-2 Imagery in Google*

Earth Engine. Delft University ofTechnology.

Prajapati, R., Talchabhadel, R., Thapa, B. R., Upadhyay, S., Thapa, A. B., Ertis, B., & Davids, J. C. (2021). Measuring the unseen: mobilizing citizen scientists to monitor groundwater in Nepal. *Environmental Monitoring and Assessment*, *193*, 1–21. https://doi.org/10.1007/s10661-021-09265-x

Rahman, M. S., & Di, L. (2020). A Systematic Review on Case Studies of Remote-Sensing-Based Flood Crop Loss Assessment. *Agriculture*, *10*(4), 131. https://doi.org/10.3390/AGRICULTURE10040131

Ribeiro, A. A. da S., Oliveira, G. A. de, Cirilo, J. A., Alves, F. H. B., Batista, L. F. D. R., & Melo, V. B. (2020). Floodplain reconstitution based on data collected via smartphones: a methodological approach to hydrological risk mapping. *RBRH*, *25*, 1–13. https://doi.org/10.1590/2318-0331.252020190179

Rosser, J. F., Leibovici, D. G., & Jackson, M. J. (2017). Rapid flood inundation mapping using social media, remote sensing and topographic data. *Natural Hazards*, *87*(1), 103–120. https://doi.org/10.1007/s11069-017-2755-0

Rwanga, S. S., & Ndambuki, J. M. (2017). Accuracy Assessment of Land Use/Land Cover Classification Using Remote Sensing and GIS. *International Journal of Geosciences*, *08*(04), 611–622. https://doi.org/10.4236/ijg.2017.84033

Sairam, N., Brill, F., Sieg, T., Farrag, M., Kellermann, P., Nguyen, V. D., Lüdtke, S., Merz, B., Schröter, K., Vorogushyn, S., & Kreibich, H. (2021). Process-Based Flood Risk Assessment for Germany. *Earth's Future*, *9*(10), 12. https://doi.org/10.1029/2021EF002259

Scaini, A., Stritih, A., Brouillet, C., & Scaini, C. (2021). Flood Risk and River Conservation: Mapping Citizen Perception to Support Sustainable River Management. *Frontiers in Earth Science*, *9*, 510. https://doi.org/10.3389/FEART.2021.675131/BIBTEX

Schmitz, A., Tonn, B., Schöppner, A. K., & Isselstein, J. (2020). Using a citizen science approach with German horse owners to study the locomotion behaviour of horses on pasture. *Sustainability (Switzerland)*, *12*(5), 1–12. https://doi.org/10.3390/su12051835

Schnebele, E., & Cervone, G. (2013). Improving remote sensing flood assessment using volunteered geographical data. *Natural Hazards and Earth System Science*, *13*(3), 669–677. https://doi.org/10.5194/nhess-13-669-2013

Schnebele, E., Cervone, G., & Waters, N. (2014). Road assessment after flood events using non-authoritative data. *Hazards Earth Syst. Sci*, *14*, 1007–1015. https://doi.org/10.5194/nhess-14-1007-2014

Schröter, K., Kreibich, H., Vogel, K., Riggelsen, C., Scherbaum, F., & Merz, B. (2014). How useful are complex flood damage models? *Water Resources Research*, *50*(4), 3378–3395. https://doi.org/10.1002/2013WR014396

Schultz, M. T., Gouldby, B. P., Simm, J., & Wibowo, J. L. (2010). *Beyond the Factor of Safety: Developing Fragility Curves to Characterize System Reliability*. https://api.semanticscholar.org/CorpusID:5772346

See, L., Fritz, S., Perger, C., Schill, C., McCallum, I., Schepaschenko, D., Duerauer, M., Sturn, T., Karner, M., Kraxner, F., & Obersteiner, M. (2015). Harnessing the power of volunteers, the internet and Google Earth to collect and validate global spatial information using Geo-Wiki. *Technological Forecasting and Social Change*, *98*, 324–335. https://doi.org/10.1016/j.techfore.2015.03.002

Seibert, J., Strobl, B., Etter, S., Hummer, P., & van Meerveld, H. J. I. (2019). Virtual staff gauges for crowd-based stream level observations. *Frontiers in Earth Science*, *7*, 70. https://doi.org/10.3389/FEART.2019.00070/BIBTEX

Seibert, J., & van Meerveld, H. J. (Ilja). (2022). Bridge over changing waters–Citizen science for detecting the impacts of climate change on water. *PLOS Climate*, *1*(11), 1–3. https://doi.org/10.1371/journal.pclm.0000088

Shamshiri, R., Eide, E., & Høyland, K. V. (2022). Spatio-temporal distribution of sea-ice thickness using a machine learning approach with Google Earth Engine and Sentinel-1 GRD data. *Remote Sensing of Environment*, *270*, 112851. https://doi.org/10.1016/J.RSE.2021.112851

Shelestov, A., Lavreniuk, M., Kussul, N., Novikov, A., & Skakun, S. (2017). Exploring Google earth engine platform for big data processing: Classification of multi-temporal satellite imagery for crop mapping. *Frontiers in Earth Science*,

5(February), 1–10. https://doi.org/10.3389/feart.2017.00017

Shen, X., Anagnostou, E. N., Allen, G. H., Robert Brakenridge, G., & Kettner, A. J. (2019). Near-real-time non-obstructed flood inundation mapping using synthetic aperture radar. *Remote Sensing of Environment*, *221*(August 2018), 302–315. https://doi.org/10.1016/j.rse.2018.11.008

Shirk, J. L., Ballard, H. L., Wilderman, C. C., Phillips, T., Wiggins, A., Jordan, R., McCallie, E., Minarchek, M., Lewenstein, B. V., Krasny, M. E., & Bonney, R. (2012). Public Participation in Scientific Research: a Framework for Deliberate Design. *Ecology and Society*, *17*(2). https://doi.org/10.5751/ES-04705-170229

Shrestha, B. B., Okazumi, T., Miyamoto, M., & Sawano, H. (2016). Flood damage assessment in the Pampanga river basin of the Philippines. *Journal of Flood Risk Management*, *9*(4), 355–369. https://doi.org/10.1111/JFR3.12174

Shrestha, Badri Bhakta, Kawasaki, A., & Zin, W. W. (2021). Development of flood damage functions for agricultural crops and their applicability in regions of Asia. *Journal of Hydrology: Regional Studies*, *36*, 100872. https://doi.org/10.1016/J.EJRH.2021.100872

Shrestha, R., Di, L., Yu, G., Shao, Y., Kang, L., & Zhang, B. (2013). Detection of flood and its impact on crops using NDVI - Corn case. *2013 Second International Conference on Agro-Geoinformatics (Agro-Geoinformatics)*, 200–204. https://doi.org/10.1109/Argo-Geoinformatics.2013.6621907

Silleos, N., Perakis, K., & Petsanis, G. (2002). Assessment of crop damage using space remote sensing and GIS. *International Journal of Remote Sensing*, *23*(3), 417–427. https://doi.org/10.1080/01431160110040026

Silvertown, J. (2009). A new dawn for citizen science. *Trends in Ecology and Evolution*, *24*(9), 467–471. https://doi.org/doi:10.1016/j.tree.2009.03.017, 2009.

Singha, M., Dong, J., Sarmah, S., You, N., Zhou, Y., Zhang, G., Doughty, R., & Xiao, X. (2020). Identifying floods and flood-affected paddy rice fields in Bangladesh based on Sentinel-1 imagery and Google Earth Engine. *ISPRS Journal of Photogrammetry and Remote Sensing*, *166*, 278–293. https://doi.org/10.1016/J.ISPRSJPRS.2020.06.011

Sparks, K., Klippel, A., Wallgrün, J. O., & Mark, D. (2015). Citizen science land cover classification based on ground and aerial imagery. In *Lecture Notes in Computer Science (including subseries Lecture Notes in Artificial Intelligence and Lecture Notes in Bioinformatics)* (Vol. 9368). Springer Verlag. https://doi.org/10.1007/978-3-319-23374-1_14/FIGURES/7

Starkey, E., Parkin, G., Birkinshaw, S., Large, A., Quinn, P., & Gibson, C. (2017). Demonstrating the value of community-based ('citizen science') observations for catchment modelling and characterisation. *Journal of Hydrology*, *548*, 801–817. https://doi.org/10.1016/j.jhydrol.2017.03.019

Steinhausen, M. J., Wagner, P. D., Narasimhan, B., & Waske, B. (2018). Combining Sentinel-1 and Sentinel-2 data for improved land use and land cover mapping of monsoon regions. *International Journal of Applied Earth Observation and Geoinformation*, *73*(August), 595–604. https://doi.org/10.1016/j.jag.2018.08.011

Survey, U. S. G. (n.d.). *30-Meter SRTM Elevation Data Downloader*. Retrieved April 22, 2024, from https://dwtkns.com/srtm30m/

Sy, B. (2019). *Approche multidisciplinaire de l'évaluation de l'aléa d'inondation à Yeumbeul Nord, Dakar, Sénégal : la contribution de la science citoyenne (In Spanish)* [Université de Genève]. https://doi.org/10.13097/ARCHIVE-OUVERTE/UNIGE:126388

Sy, B., Frischknecht, C., Dao, H., Consuegra, D., & Giuliani, G. (2019). Flood hazard assessment and the role of citizen science. *Journal of Flood Risk Management*, *12*(October 2018), 1–14. https://doi.org/10.1111/jfr3.12519

Sy, B., Frischknecht, C., Dao, H., Consuegra, D., & Giuliani, G. (2020). Reconstituting past flood events: The contribution of citizen science. *Hydrology and Earth System Sciences*, *24*(1), 61–74. https://doi.org/10.5194/hess-24-61-2020

Sy, B., Frischknecht, C., Dao, H., Giuliani, G., Consuegra, D., Wade, S., & Kedowide, C. (2016). Participatory approach for flood risk assessment : the case of Yeumbeul Nord (YN), Dakar , Senegal. *The Proceedings of the 5 International Conference on Flood Risk Management and Response (FRIAR 2016)*.

https://doi.org/10.2495/UW160291

Szel, M. (2020). Evaluation of Cracking Patterns in Cement Composites-From Basics to Advances: A Review. *Materialsaterials*, *13*(2490), 27. https://doi.org/10.3390/ma13112490

Tamiminia, H., Salehi, B., Mahdianpari, M., Quackenbush, L., Adeli, S., & Brisco, B. (2020). Google Earth Engine for geo-big data applications: A meta-analysis and systematic review. *ISPRS Journal of Photogrammetry and Remote Sensing*, *164*, 152–170. https://doi.org/10.1016/J.ISPRSJPRS.2020.04.001

Tazmul Islam, M., & Meng, Q. (2022). An exploratory study of Sentinel-1 SAR for rapid urban flood mapping on Google Earth Engine. *International Journal of Applied Earth Observation and Geoinformation*, *113*. https://doi.org/10.1016/J.JAG.2022.103002

Ţîncu, R., Zêzere, J. L., Crăciun, I., Lazăr, G., & Lazăr, I. (2020). Quantitative micro-scale flood risk assessment in a section of the Trotuș River, Romania. *Land Use Policy*, *95*(July 2018), 103881. https://doi.org/10.1016/j.landusepol.2019.02.040

Tiwari, V., Kumar, V., Matin, M. A., Thapa, A., Ellenburg, W. L., Gupta, N., & Thapa, S. (2020). Flood inundation mapping- Kerala 2018; Harnessing the power of SAR, automatic threshold detection method and Google Earth Engine. *PLOS ONE*, *15*(8), e0237324. https://doi.org/10.1371/JOURNAL.PONE.0237324

Thuy Xuan Tien Commune People's Committee (2021). *Annual report on social economic development in Thuy Xuan Tien in 2021*.

Tran, H. N., Rutten, M., Prajapati, R., Tran, H. T., Duwal, S., Nguyen, D. T., Davids, J. C., & Miegel, K. (2024). *Citizen science for monitoring rainfall in Vietnam*. *13*(1), 104–116. https://easychair.org/publications/preprint/MQkd

Tran, N. H., Häusler-Nguyen, T., Tran, T. H., Nguyen, T. D., & Miegel, K. (2022). Application of Google Earth Engine in Flood Extent Detection in the Bui River Basin. *Conference Proceeding of International Conference "Technology in Natural Disaster Prevention and Risk Reduction,"* 154–163. https://hoithao.hunre.edu.vn/attachment/hoithao/news/2022/08/30/212809_Proceedings of International Conference 1st, 2022.pdf

Tran, N. H., Nguyen, T. H., Luu, T. H., Rutten, M. M., & Pham, Q. N. (2021). Citizen Science on Water Resources Monitoring in the Nhue River, Vietnam. In M. Babel, A. Haarstrick, L. Ribbe, V. R. Shinde, & N. Dichtl (Eds.), *Water Security in Asia: Opportunities and Challenges in the Context of Climate Change* (pp. 749–762). Springer Nature. https://doi.org/10.1007/978-3-319-54612-4_55/FIGURES/9

Tran, N. H., Rutten, M., Prajapati, R., Tran, H. T., Duwal, S., Nguyen, D. T., Davids, J. C., & Miegel, K. (2024). Citizen scientists' engagement in flood risk-related data collection: a case study in Bui River Basin, Vietnam. *Environ Monit Assess*, *196*, 280. https://doi.org/10.1007/s10661-024-12419-2

Tran, P., Shaw, R., Chantry, G., & Norton, J. (2009). GIS and local knowledge in disaster management: A case study of flood risk mapping in Viet Nam. *Disasters*, *33*(1), 152–169. https://doi.org/10.1111/j.1467-7717.2008.01067.x

Tran, T. H., Do, T. H., Pham, T. Q., Ho, V. H., & Phung, M. T. (2021). Factors affecting consensus of local people for new rural development planning program : A case study of Hoang Van Thu commune , Chuong My district , Hanoi . *Journal of Forestry Science and Technology*, *10*, 1–11.

Trinh, M. X. (2023). *A methodological framework for future flood risk assessment in ungauged and data-scarce coastal river catchments in Southeast Asia (Doctoral thesis)*. https://doi.org/10.26127/BTUOpen-6441

Trinh, M. X., & Molkenthin, F. (2021). Flood hazard mapping for data-scarce and ungauged coastal river basins using advanced hydrodynamic models, high temporal-spatial resolution remote sensing precipitation data, and satellite imageries. *Natural Hazards*, *109*(1), 441–469. https://doi.org/10.1007/S11069-021-04843-1/FIGURES/10

Tsiakos, C., Krommyda, M., Kopsinis, Y., Tsertou, A., Amditis, A., Jonoski, A., Popescu, I., & Assumpcao T. (2019). Improved LC/LU maps and flood models through crowdsourced information. *16 Th International Conference on Environmental Science and Technology*, CEST2019_00330.

Tsyganskaya, V., Martinis, S., Marzahn, P., & Ludwig, R. (2018a). Detection of

temporary flooded vegetation using Sentinel-1 time series data. *Remote Sensing*, *10*(8). https://doi.org/10.3390/rs10081286

Tsyganskaya, V., Martinis, S., Marzahn, P., & Ludwig, R. (2018b). SAR-based detection of flooded vegetation–a review of characteristics and approaches. *International Journal of Remote Sensing*, *39*(8), 2255–2293. https://doi.org/10.1080/01431161.2017.1420938

UNISDR. (2015a). *Sendai Framework for Disaster Risk Reduction 2015 - 2030*.

UNISDR. (2015b). *The human cost of weather related disasters*.

UNISDR. (2017). *National Disaster Risk Assessment*. https://www.unisdr.org/files/globalplatform/591f213cf2fbe52828_wordsintoactionguideline.nationaldi.pdf

Visser, T. (2015). *Socialising the pixel . The use of citizen science in land use classification and its potential uncertainties* . http://resolver.tudelft.nl/uuid:013c82dd-0a70-4a0a-84a4-e70a462f0c0f

von Gönner, J., Bowler, D. E., Gröning, J., Klauer, A. K., Liess, M., Neuer, L., & Bonn, A. (2023). Citizen science for assessing pesticide impacts in agricultural streams. *Science of the Total Environment*, *857*. https://doi.org/10.1016/J.SCITOTENV.2022.159607

Vu, H. T. D., Tran, D. D., Schenk, A., Nguyen, C. P., Vu, H. L., Oberle, P., Trinh, V. C., & Nestmann, F. (2022). Land use change in the Vietnamese Mekong Delta: New evidence from remote sensing. *Science of The Total Environment*, *813*, 151918. https://doi.org/10.1016/J.SCITOTENV.2021.151918

Walker, D., Forsythe, N., Parkin, G., & Gowing, J. (2016). Filling the observational void: Scientific value and quantitative validation of hydrometeorological data from a community-based monitoring programme. *Journal of Hydrology*, *538*, 713–725. https://doi.org/10.1016/j.jhydrol.2016.04.062

Waseem, M., Mani, N., Andiego, G., & Usman, M. (2017). *A REVIEW OF CRITERIA OF FIT FOR HYDROLOGICAL MODELS*. https://api.semanticscholar.org/CorpusID:229787149

Weeser, B., Stenfert Kroese, J., Jacobs, S. R., Njue, N., Kemboi, Z., Ran, A., Rufino,

M. C., & Breuer, L. (2018). Citizen science pioneers in Kenya – A crowdsourced approach for hydrological monitoring. *Science of The Total Environment*, *631–632*, 1590–1599. https://doi.org/10.1016/J.SCITOTENV.2018.03.130

Whitelaw, G., Vaughan, H., Craig, B., & Atkinson, D. (2003). Establishing the Canadian Community Monitoring Network. *Environmental Monitoring and Assessment*, *88*(1), 409–418. https://doi.org/10.1023/A:1025545813057

Wiggins, A., & Crowston, K. (2011). *From Conservation to Crowdsourcing: A Typology of Citizen Science*.

Win, S., Zin, W. W., Kawasaki, A., & San, Z. M. L. T. (2018). Establishment of flood damage function models: A case study in the Bago River Basin, Myanmar. *International Journal of Disaster Risk Reduction*, *28*(November 2017), 688–700. https://doi.org/10.1016/j.ijdrr.2018.01.030

Wolff, C. (2020). *Addressing data limitations and uncertainties in broad-scale coastal flood-risk assessments*. https://macau.uni-kiel.de/servlets/MCRFileNodeServlet/macau_derivate_00002317/PhD_thesis_ClaudiaWolff_final_bib_v2.pdf

Wunnava, A., Naik, M. K., Panda, R., Jena, B., & Abraham, A. (2020). An adaptive Harris hawks optimization technique for two dimensional grey gradient based multilevel image thresholding. *Applied Soft Computing*, *95*, 106526. https://doi.org/10.1016/J.ASOC.2020.106526

Xuan Mai Commune People's Committee (2021). *Annual report on social economic development in Xuan Mai in 2021*.

Yang, M. (2017). *Urban Flood Simulation and Integrated Flood Risk Management* [Technical University of Dortmund]. https://eldorado.tu-dortmund.de/bitstream/2003/36992/1/Dissertation_Mu Yang.pdf

Zeng, Z., Lan, J., Hamidi, A. R., & Zou, S. (2020). Integrating Internet media into urban flooding susceptibility assessment: A case study in China. *Cities*, *101*(1037), 102697. https://doi.org/10.1016/j.cities.2020.102697

8 Appendixes

8.1 Data collection for the Bui River Basin

Table 8.1. A summary of S-2 images and other data collected for this research

Data	**Years**	**Resolution or scale**	**Provided**	**Purpose of this study**
Remote sensing				
Sentinel-2 images	2022 (Jan-May)	10 m	European Space Agency (ESA)	Developing land-use map
Other data				
Soil map	2016	-	Open Data Development (https://data.opendevelopmentcambodia.net/dataset/)	Estimating Curve Number for hydrological modeling
Topographic maps	- 2009 - 2014 & 2016	1: 2000	- Hanoi Municipal People's Committee - Center of Survey and Mapping Data, Vietnam Mapping and Surveying Agency	Setting-up hydraulic modeling
SRTM	2000	30 m	NASA Jet Propulsion Laboratory	Delineating Bui River Basin and sub-catchments Setting up hydraulic modeling

Data	**Years**	**Resolution or scale**	**Provided**	**Purpose of this study**
River cross sections	2021	-	Hanoi University of Natural Resources and Environment under project number TNMT.2023.06.14.	Setting-up hydraulic modeling
Statistical yearbook, annual district flood reports, and annual district socioeconomic development reports.	2017-2022	-	- Hanoi Municipal and Hoa Binh People's Committee - Chuong My District People's Committee	Validating flooding areas Estimating flood damage results.

8.2 Investigating flood marks

Figure 8.1. Flood mark of 2018 at Xuan Linh hamlet, Thuy Xuan Tien commune, Chuong My district (Flooding depth: 2.5 m, Lat/Long: 20.880, 105.562)

8.3 Construction of a low-cost rain gauge

The low-cost rain gauge was made of 1.2 to 2-liter clear plastic bottles, concrete, rulers, and glue, as proposed by C. J. Davids et al. (2019). A tutorial video on the construction of a low-cost rain gauge is available on the YouTube (https://bit.ly/3sciMeg, in Vietnamese). The plastic bottles with a uniform diameter are not common in Vietnam. Consequently, plastic bottles with uniform or relatively uniform diameters extending at least 150mm in height from the base upwards to the top were utilized in this research (Figure 8.2). In the same area, the rainfall level collected from bottles with non-uniform diameters was found to be 5% to 20% higher than that collected from bottles with uniform diameters (Figure 8.2). This discrepancy can be attributed to the fact that the diameter size of the non-uniform bottle is curved inwards to a certain degree.

Concrete was poured into the bottom of the bottle until the point where the uniform or relatively uniform cross-section begins, creating a flat surface for low-cost rain gauges and providing additional weight to stabilize the gauge in windy conditions (C. J. Davids et al., 2019). The bottle lid was cut off where the inward taper starts, then inverted and placed on top of the gauge to reduce evaporation losses. Waterproof tape can be used to cover the bottom of the bottle to create a funnel and reduce the leakage of rainwater caused by a cracked rain gauge. A millimeter-marked plastic ruler was vertically glued to the side of the bottle, with the zero mark aligned precisely with the concrete flat (C. J. Davids et al., 2019).

Figure 8.2. The low-cost rain gauge made of plastic bottles with relatively uniform (A) and uniform (B) diameters

8.4 The flood level at bare land and residential areas of the 2017 and 2022 floods

Table 8.2. The flood level in subdomains on bare land of the 2017 flood

	1	2	3	4	5	6	7	8
A	NA	NA	-	5.32	5.34	5.33	PA	PA
B	NA	NA	-	5.18	6.18	5.96	-	PA
C	NA	NA	-	4.94	6.71	5.48	4.99	4.58
D	6.55	4.16	6.83	7.01	5.86	5.87	4.90	NA
E	5.68	5.96	-	-	9.48	-	NA	NA
F	NA	NA	-	-	10.27	-	NA	NA
G	NA	NA	NA	NA	NA	NA	NA	NA

Note: NA, -, and PA represent non-accounting, non-value, and flood-protected areas, respectively.

Table 8.3. The flood level in subdomains in residential areas of the 2017 flood

	1	2	3	4	5	6	7	8
A	NA	NA	-			8.09	PA	PA
B	NA	NA	-			7.78	-	PA
C	NA	NA	-			7.87	7.60	
D			7.96					NA
E			-	-		-	NA	NA
F	NA	NA	-	-		-	NA	NA
G	NA	NA	NA	NA	NA	NA	NA	NA

Note: NA, -, and PA represent non-accounting, non-value, and flood-protected areas, respectively.

Table 8.4. The flood level in subdomains on bare land of the 2022 flood

	1	2	3	4	5	6	7	8
A	NA	NA	-	5.18	5.51	5.7	NA	NA
B	NA	NA	-	4.73	6.21	6.02	-	NA
C	NA	NA	-	4.94	6.8	5.47	4.99	4.59
D	4.59	-	7.19	6.79	5.9	5.74	5.13	NA
E	5.59	-	-	-	9.21	-	NA	NA
F	NA	NA	-	-	10.7	-	NA	NA
G	NA	NA	NA	NA	NA	NA	NA	NA

Note: NA, -, and PA represent non-accounting, non-value, and flood-protected areas, respectively.

Table 8.5. The flood level in subdomains in residential areas of the 2022 flood

	1	2	3	4	5	6	7	8
A	NA	NA	-	-	-		PA	PA
B	NA	NA	-	-	-	7.04	PA	PA
C	NA	NA	-	-	-	-	6.29	-
D	-	-	10.74	-	6.29	-	-	NA
E	-	-	-	-	-	-	NA	NA
F	NA	NA	-	-	-	-	NA	NA
G	NA	NA	NA	NA	NA	NA	NA	NA

Note: NA, -, and PA represent non-accounting, non-value, and flood-protected areas, respectively.

8.5 Flood modeling in Bui River Basin

8.5.1 Used input data

The Bui River Basin consists of two main rivers: the Tich River and the Bui River. In addition to these, several tributaries transport runoff from the high mountain areas to the floodplain and flow into the Bui River, especially in floodplain and storage areas. The floodplain of the Xuan Mai urban area includes tributaries such as Da Giang, Vai Bo, and Cau Tay (Figure 8.3). Numerous rainfall stations are located within and surrounding the Bui River Basin, including those at Hoa Binh, Son Tay, Viet Tri, Ba Vi, Ha Dong, and Xuan Mai (Figure 3.1). Most of these stations record rainfall hourly, except for the

Xuan Mai station, which is situated centrally in the upstream Bui River Basin and the floodplain area. The daily data from this station was allocated into hourly rainfall data using hourly rainfall data from the Hoa Binh station as a reference.

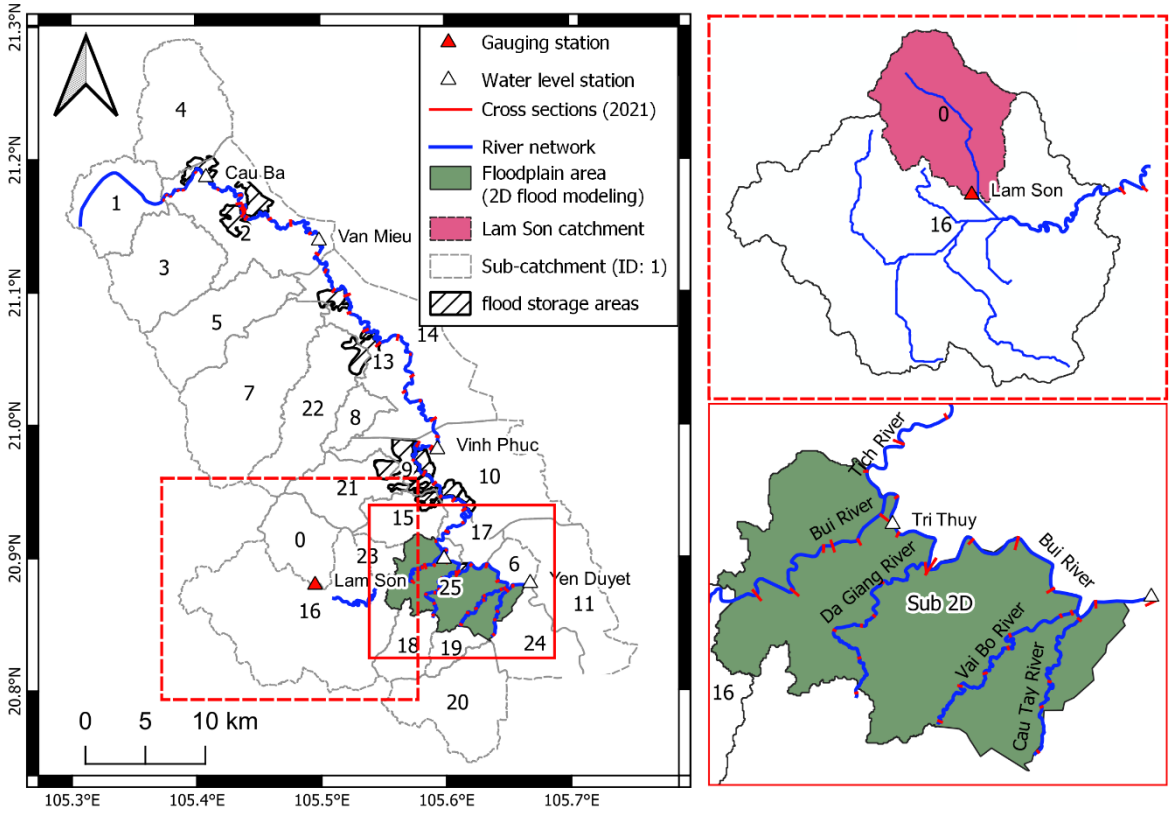

Figure 8.3. The river network and hydro-meteorological stations on the Bui River Basin

A single stream gauge station is situated within the Bui River Basin, specifically at Lam Son. During the flood season, this station is responsible for measuring discharge every six hours. Water level stations, including those at Cau Ba, Van Mieu, Tri Thuy, and Yen Duyet, have been installed along the Tich and Bui Rivers with the objective of measuring the water level on a daily basis in order to operate irrigation and drainage systems. Over the past decade, the two most significant floods in the Bui River Basin at Tri Thuy occurred in 2017, 2018. The characteristics of these events are summarized in Table 8.6. The meteorological and hydrological data collected during these flood periods were utilized to calibrate and validate flood models, as well as to simulate flood events in the pilot area.

Table 8.6. Flood information for model calibration and validation

No	Start time	End time	$Q_{Max\ Lam\ Son}$ (m^3/s)	$H_{Max\ Tri\ Thuy}$ (m)
1	08/10/2017	13/10/2017	267.0	7.53
2	19/07/2018	24/07/2018	319.0	7.78

The Bui River Basin was divided into 25 sub-basins, each of which is directly connected to the Tich and Bui Rivers. The Lam Son catchment (ID: 0) is a part of Con sub-catchment (ID:16), which was used as a donor catchment to determine rainfall-runoff modeling parameters for ungauged sub-catchments. The 2022 land-use map and the 2016 soil map (Opendevelopmendevelopment, n.d.) were used to estimate the land use and soil characteristics for each sub-catchment (Figure 3.2). The areal rainfall for each sub-catchment was determined using the Thiessen polygon method.

The 52 river cross-sections on the Tich and Bui Rivers, measured in 2021 and provided by Hanoi University of Natural Resources and Environment, were utilized to represent the geometry of the Tich-Bui River system. The 30-meter SRTM data was employed to determine the boundaries of the catchment and sub-catchments within the Bui River Basin, as well as to assess physical catchment characteristics, including basin slope and river length. Furthermore, a topographic map of the Tich-Bui River area at a scale of 1:2000, in conjunction with the 30-meter SRTM data, was used to develop a digital terrain model (DTM) with a resolution of 3 meters and to ascertain the elevation-volume curves for 13 floodplain storage areas. In the case of some smaller rivers for which cross-sections were unavailable, typical cross-sections provided by irrigation companies, in conjunction with the 3-meter digital terrain model (DTM), were employed to estimate the missing data. It should be noted that the waterworks, including reservoirs, pumping stations, culverts and bridges, were not considered in the flood modeling.

Table 8.7. The list of sub-catchments in the Bui River Basin

No	ID	Catchment	A_km^2	No	ID	Catchment	A_km^2
1	Sub_0	Lam Son	33.7	14	Sub 20	B_R_DSuong_lake	59.7
2	Sub 1	Dlong	45.6	15	Sub 21	T_R_LuongSon	37.4
3	Sub 10	B_L_DongPhuong_YDuyet	72.3	16	Sub 22	T_R_HanoiUni	60.1
4	Sub 11	Ha Duc _ CM	64.8	17	Sub 23	T_L_XuanMai1	9.6

No	ID	Catchment	A_km^2	No	ID	Catchment	A_km^2
5	Sub 12	T_L_Bavi2_Cauba_Van mieu	33.1	18	Sub 24	B_H_TranPhu_Hong Phong	37.6
6	Sub 13	T_R_DStream_Dmolake	47.2	19	Sub_2D	Xuan Mai urban area	56.4
7	Sub 14	T_L_VanMieu_VPhuc	70.6	20	Sub 3	T_R SHai_Right	63.3
8	Sub 15	T_R_ForestUni	24.8	21	Sub 4	T_L_Bavi	67.8
9	Sub 16	Con River	178.7	22	Sub 5	T_R_HangRiver	59.3
10	Sub 17	Tu Ne _ Trung Hoang	10.8	23	Sub 6	YDuyet	11.4
11	Sub 18	B_R_Mieu_Lake	22.1	24	Sub 7	T_R_DongMoLake	104.7
12	Sub 19	B_R_VanSon1_Lake	11.3	25	Sub 8	T_R_HoaLac	14.8
13	Sub 2	T_R_XKhanh	54.1	26	Sub 9	T_R_Thachthat	23.6

8.5.2 Rainfall-runoff modeling

The hydrologic processes in this research were modeled by using the HEC-HMS software developed by USACE. HEC-HMS is designed to simulate various hydrologic processes, including losses, runoff transformation, baseflow, and open channel routing. Detailed documentation of all model elements and their mathematical descriptions can be found in the HEC-HMS technical reference manual (HEC, 2000). The methods selected in this research are briefly outlined below.

Table 8.8. The description of the mathematical model in HEC-HMS hydrologic model

Hydrologic process: Simulation method	**Mathematical model (HEC, 2000)**		
Runoff generation SCS-Curve Number	Rainfall excess P_e	$P_e = \frac{(P - I_a)}{(P - I_a + S)}$	Eq 8.1
	Initial abstraction I_a	$I_a = 0.2 * S$	Eq 8.2
	Maximum retention S	$S = \frac{(25400 - 254 * CN)}{CN}$	Eq 8.3
	Composite Curve number for drainage area A_i of subdivision i ($CN_{composite}$)	$CN_{composite} = \frac{\sum A_i * CN}{\sum A_i}$	Eq 8.4

Hydrologic process: Simulation method	**Mathematical model (HEC, 2000)**	
Runoff transformation: Snyder Unit Hydrograph	Peak coefficient C_p	Calibrated parameter
	Basin lag t_p	$t_p = CC_t * (LL_c)^{0.3}$ Eq 8.5 C - conversion constant (0.75 for SI unit) L – length of main stream from outlet to divide L_c – length of the main stream from outlet to center C_t – basin coefficient (calibrated parameter)
Baseflow: Regression method	Baseflow at time t, Q_t	$Q_t = Q_0 * k^t$ Eq 8.6 Q_0 – initial baseflow k – recession constant

The runoff generation for each catchment was determined using the Soil Conservation Service Curve Number (SCS-CN) method. The fundamental equations (Eq *8.1*) for calculating excess rainfall P_e are provided in Table 8.8. The direct runoff for each sub-catchment was calculated using the Snyder Unit Hydrograph method, which is suitable for estimating peak flow and flood volume for catchments in Vietnam (Do & Le, 2013). The fundamental equation (Eq 8.5) for determining the catchment-specific unit hydrograph is also listed in Table 8.8. The baseflow during the event was estimated by using a recession curve model (Eq 8.6). The channel routing process was not considered in this research, because the flows from sub-catchments were calculated to provide input data for the hydraulic model.

8.5.3 Hydrodynamic modeling

The hydrodynamic modeling was carried out by utilizing the HEC-RAS model, which was developed by USACE. The model is designed to simulate one- and two-

dimensional flows (1D and 2D) in the river system as well as to model sediment transport and water quality (Dasallas et al., 2019). Detailed documentation of the theoretical basis and their mathematical description of 1D and 2D unsteady flow can be found in the manual of technical reference (Gary W. Brunner, 2016). The model employs a representation of geometric data and the routines of geometric and hydraulic calculation for natural and artificial channel networks (Dasallas et al., 2019).

This research utilized HEC-RAS model to simulate flood flows in the Tich-Bui river system and model flooding in the floodplain area of Xuan Mai's urban region, employing 1D flow, 2D flood inundation, and a combined 1D-2D approach. The simulation incorporated flood flows from sub-catchments, which were linked to the model as boundary conditions - either as upstream inflows or as lateral flows along both sides of the river system. The hydrodynamic model was developed in a simplified manner, serving as a reference framework for comparative analysis.

8.5.3.1 One-dimensional flow modeling

In the 1D flow model, water flows are assumed to move exclusively in the longitudinal direction. The model represents the terrain as a series of cross-sections and employs a set of equations to determine flow parameters, including flow velocity and water depth. To simplify calculations, HEC-RAS model assumes a horizontal water surface at each cross-section, perpendicular to the flow direction, thereby neglecting momentum exchange between the channel and the floodplain (Gary W. Brunner, 2016). The one-dimensional equations of motion primarily consist of the continuity equation (Eq 8.7) and the momentum equation (Eq 8.8). The unsteady flow equations in the 1D model are solved using a four-point implicit scheme.

Table 8.9. Mathematical models for one-dimensional and two-dimensional hydrodynamic modeling

Hydrodynamic process: Calculation routine	**Mathematical model (HEC, 2016)**		
1D modeling	Continuity equation	$\frac{\partial A}{\partial t} + \frac{\partial (Q)}{\partial x} + q = 0$ Q - total flow; A – flow area, q − lateral inflow per unit length	Eq 8.7
	Momentum equation	$\frac{\partial Q}{\partial t} + \frac{\partial (QV)}{\partial x} + gA \left[\frac{\partial Z}{\partial x} + S_f\right] = 0$ V – flow velocity; Z - elevation of water surface; S_f - friction slope	Eq 8.8
	Friction slope	$S_f = \frac{Q\|Q\|n^2}{2.208 R^{4/3} A^2}$ n – Roughness coefficient (calibrated parameter) R – Hydraulic radius	Eq 8.9
2D modeling	Continuity equation	$\frac{\partial H}{\partial t} + \frac{\partial (hu)}{\partial x} + \frac{\partial (hv)}{\partial y} + q = 0$ H – water surface level; h – water depth; u, v – velocity in x, y direction	Eq 8.10
	Momentum equation	$\frac{\partial u}{\partial t} + u\frac{\partial (u)}{\partial x} + v\frac{\partial (v)}{\partial y} = -g\frac{\partial H}{\partial x} + v_t\left(\frac{\partial^2 u}{\partial x^2} + \frac{\partial^2 u}{\partial y^2}\right) - c_f u + fv$ $\frac{\partial v}{\partial t} + u\frac{\partial (v)}{\partial x} + v\frac{\partial (v)}{\partial y} = -g\frac{\partial H}{\partial y} + v_t\left(\frac{\partial^2 v}{\partial x^2} + \frac{\partial^2 v}{\partial y^2}\right) - c_f v + fu$ v_t – eddy viscosity coefficient; c_f – bottom friction coefficient; g – gravitational acceleration; f – Coriolis parameter	Eq 8.11
	Bottom friction	$c_f = \frac{n^2 g\|V\|}{R^{4/3}}$	Eq 8.12

Hydrodynamic process: Calculation routine	**Mathematical model (HEC, 2016)**	
		|V| - magnitude of velocity; n – Roughness coefficient (calibrated parameter); R – Hydraulic radius
1D-2D combined method: lateral connection	Standard weir equation	$dQ = C(y_{ws} - y_w)^{2/3}dx$ Eq 8.13 dQ – structural flow over length element dx; y_{ws} – water surface elevation; y_w – structure elevation; C – weir coefficient

8.5.3.2 Two-dimensional flow modeling

A two-dimensional flow model allows for the simulation of water flow in both the longitudinal and lateral directions, with the velocity in the vertical (z) direction assumed to be negligible (Dasallas et al., 2019). The model represents the terrain as a continuous surface using a mesh or grid (Dasallas et al., 2019). The HEC-RAS 2D model employs a sub-grid bathymetry approach (Casulli, 2009), which incorporates detailed topographical data for each cell through a characteristic cell volume property table. This method allows for the use of a coarser mesh resolution than that of the digital elevation model (DEM). The mathematical model primarily comprises the 2D equations for mass continuity (Eq 8.10) and momentum (Eq 8.11). HEC-RAS resolves these equations using a hybrid discretization scheme that combines finite differences and finite volumes.

8.5.3.3 Combined 1D-2D model

The HEC-RAS 1D–2D combined approach entails the establishment of a lateral connection, whereby the 2D flow areas are linked to the 1D cross-sections through a lateral structure. In HEC-RAS, the lateral structure can be configured as a lateral weir. The flow over this structure is calculated utilizing either the weir equation or the 2D flow equations (Eq 8.13).

8.5.4 Model calibration and validation

8.5.4.1 Model performance evaluation criteria

Model performance evaluation is crucial to ensure the accuracy of the simulation results. A comparison between measured and modeled values is employed primarily for the purpose of evaluating the efficiency of the model, with the goodness-of-fit measures outlined in Table 8.10. Waseem et al. (2017) advised that the use of a single measure is insufficient for assessing the suitability of a model due to the advantages and disadvantages of each measure. In this research, five measures were analyzed: Nash-Sutcliffe Efficiency (NSE) (Eq 8.14), Correlation Coefficient (R), relative peak error ($\Delta Q/H_{Max}$) (Eq 8.15), peak time error (ΔT_{Max}) (Eq 8.16), and relative volume error (ΔW) (Eq 8.17) (Trinh, 2023) to evaluate the suitability of hydrological and hydrodynamic models. The last measure was only applied to the HEC-HMS hydrological modelling in this research due to the absence of measured discharge in the Bui River system.

Table 8.10. The selection of measures for hydrologic and hydrodynamic model calibration and validation

Measures/ Target	**Formular**	**Applied for HEC-HMS**	**Applied for HEC - RAS**
Nash–Sutcliffe Efficient (NSE)/ ≥0.5	$NAE = 1 - \frac{\sum_{t=1}^{T}(X_o^t - X_m^t)^2}{\sum_{t=1}^{T}(X_o^t - \overline{X_o})^2}$ Eq 8.14 X_o^t – Observed value at time t $\overline{X_o}$ – Mean of observed values X_m^t– Modeled value at time t	✓	✓
Pearson's correlation coefficient (R)/ ≥ 0.8	As mentioned in Section 3.3.3.	✓	✓

Measures/ Target	Formular		Applied for HEC-HMS	Applied for HEC - RAS
Relative peak error (ΔQ/H Max) / Non-defined	$\Delta Q/H_{Max} = \frac{\left(Q^{m}_{Max} - Q^{o}_{Max}\right)}{Q^{o}_{Max}} \times 100\%$ Q/H^{m}_{Max} – Modeled peak flow or water level (m^3/s) Q/H^{o}_{Max} – Observed peak flow or water level (m^3/s)	Eq 8.15	✓	✓
Peak time error (ΔT_{Max})/ Non-defined	$\Delta T_{Max} = T^{m}_{Max} - T^{o}_{Max}$ T^{m}_{Max}- Time of modeled peak flow (hour) T^{o}_{Max}- Time of observed peak flow (hour)	Eq 8.16	✓	✓
Relative volume error (ΔW)/ ≤ ±30%	$\Delta W = \frac{\sum_{t=1}^{T}\left(Q_{m,t}\Delta t - Q_{o,t}\Delta t\right)}{\sum_{t=1}^{T} Q_{o,t}\Delta t}$ $Q_{o,t,}$ – Observed discharge at time t (m^3/s) Δt – Time interval (second) $Q_{m,t}$ – Modeled discharge at time t (m^3/s)	Eq 8.17	✓	

The values of measures reflect the goodness-of-fit between the modeled and measured data. The Nash-Sutcliffe Efficiency (NSE) ranges from $-\infty$ to 1, where an NSE value of 1 denotes perfect fit between the modeled and measured data (Moriasi et al., 2007). NSE values greater than 0.5 are generally considered acceptable (Moriasi et al., 2007). Pearson's Correlation Coefficient (R) ranges from -1 to 1, with an R=0 indicating no

linear relationship, and R=−1 or R=1 indicating a perfect negative or positive linear relationship, respectively (Moriasi et al., 2007). The relative errors (i.e., $\Delta Q/H_{Max}$ or ΔW) range from -∞ to +∞, with a value of 0 indicating a perfect fit (Moriasi et al., 2007).

The mentioned criteria are primarily used to evaluate the performance of hydrological and 1D hydraulic models at specific control points (Trinh, 2023). Typically, 2D hydrodynamic models are calibrated by comparing the modeled flood extent with flood extents derived from remotely sensed images (Trinh, 2023). The objective of this research is to develop a flooding map by integrating remote sensing data and field data, which will then be compared with the results of the 2D model. As a result, the flood extent obtained from 2D model was not calibrated in this study.

8.5.4.2 Rainfall-runoff modeling calibration

For rainfall-runoff modeling, this research used several performance measures, including NAE, R, ΔQ_{Max}, ΔT_{Max}, ΔW indexes, to calibrate the model parameters for the Bui River Basin at Lam Son station (Sub_LS). The calibration focused on key hydrologic processes: runoff generation (CN value, initial abstraction I_a), runoff transformation (time lag, basin coefficient), and base flow (initial baseflow, recession constant). Table 8.11 provides the calibrated parameters used for hydrological modeling. These values were then transferred to ungauged catchments using the physical similarity approach (Trinh & Molkenthin, 2021). While many parameters were initially derived from topographic, geomorphological, vegetation cover, and soil property maps through spatial analysis, they were further adjusted to fit specific flood events and local conditions.

Table 8.11. Calibration parameters and their calibrated values for hydrological modeling in the Bui River Basin at Lam Son station

Calculation routine	Calibrated parameter	Calibrated average value
Loss Method: SCS Curve Number Method	CN values	65
	Initial abstraction (mm)	10
	Impervious (%)	4

Calculation routine	Calibrated parameter	Calibrated average value
Transform Method: Snyder Unit Hydrograph	Standard Lag (hr) Peaking coefficient	2.9 0.7
Baseflow method: Recession	Initial baseflow (m^3/s) Recession Constant Ration flow	4.5 0.48 0.15

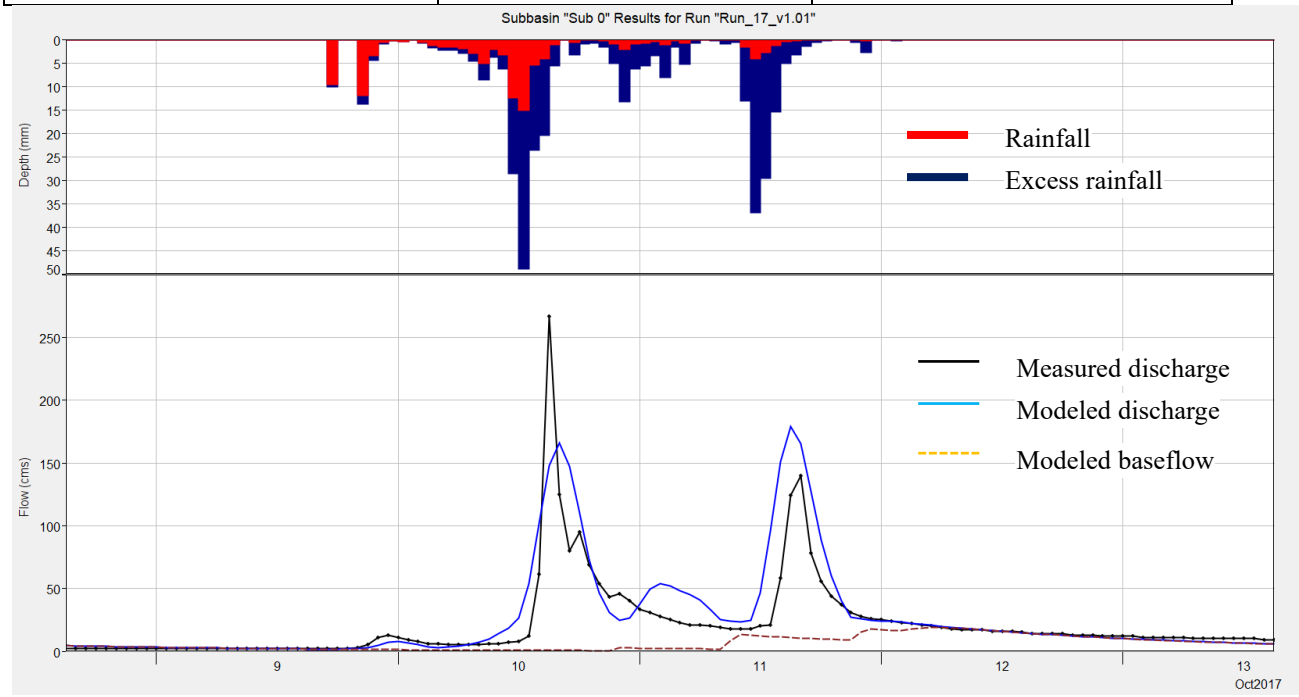

Figure 8.4. Observed and modeled discharge hydrographs for the 2017 flood on the Bui River at Lam Son station (Calibration case)

The calibrated and validated hydrographs for the 2017 and 2018 floods, modeled in HEC-HMS model, are presented in Figure 8.4 and Figure 8.5. The evaluation of rainfall-runoff model parameters is summarized in Table 8.5. Overall, the measured and simulated hydrographs exhibit similar trends in both the rising and falling limbs. The Nash-Sutcliffe efficiency index, which reflects the overall agreement of the hydrograph, exceeds 0.5, indicating satisfactory model performance. The correlation coefficients between the measured and simulated discharge are above 0.8, demonstrating a close agreement between the two datasets. Due to the lack of hourly measured rainfall data in the Lam Son catchment, calibrating the peak values proved challenging. Consequently,

the research focused on validating the flood volume, with a margin of error up to 30% considered acceptable.

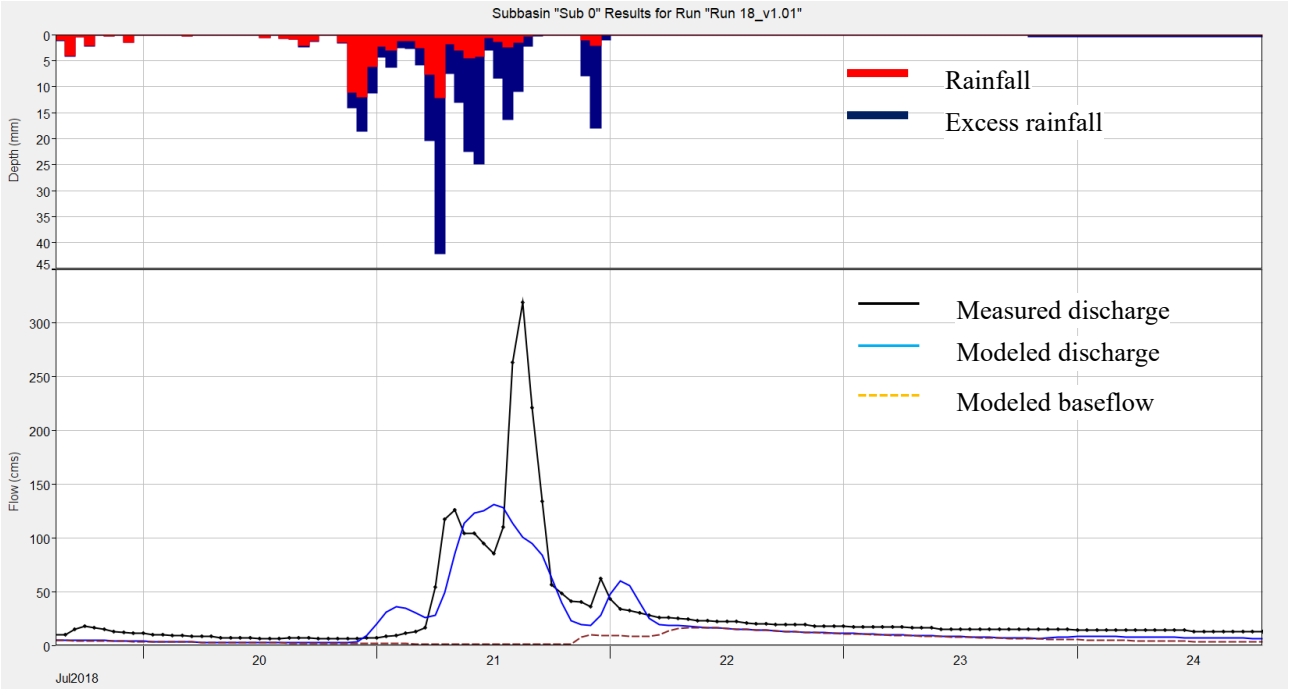

Figure 8.5. Observed and modeled discharge hydrographs for the 2018 flood on the Bui River at Lam Son station (Validation case)

Table 8.12. Hydrological model performance statistics for calibration and validation cases

Flood event	NSE	R	Q mod Max (m^3/s)	Q obs Max (m^3/s)	Δ Q Max (%)	Δ Vol (%)	Δ T Max (hrs.)
10/2017	0.62	0.85	179.0	267.0	-33%	22.3	24
07/2018	0.58	0.80	132.0	319.0	-59%	-30	-3

8.5.4.3 Hydrodynamic modeling calibration

For hydrodynamic modeling, this research employed performance measures such as NSE, R, ΔH_{Max}, *and* ΔT_{Max} to calibrate hydraulic model parameters for the Bui River network. The roughness coefficient (Manning's n) is a crucial parameter in the hydraulic model. The HEC-RAS flood model was calibrated and validated by adjusting Manning's n for each river section. Due to data limitations and the relatively small two-dimensional calculation area in comparison to the entire Bui River Basin, the roughness coefficient in this area was not validated. Instead, this research used standard roughness coefficients

from David & Schmalz (2020), based on the 2022 land-use map. The roughness values for the river networks and floodplain areas ranged from 0.035 to 0.056.

Figure 8.6 and Figure 8.7 show the modeled and observed stage hydrographs at three stations (Cau Ba, Van Mieu, and Tri Thuy) on the Bui River for the calibration and validation cases, respectively. Overall, the results indicate a good fit in terms of both shape and magnitude between the modeled and observed values. Table 8.13 presents the hydraulic model performance evaluation measures. Most of the correlation coefficient (R) values exceed 0.80, demonstrating a strong agreement between the modeled and observed data. NSE ranges from -4.40 to 0.99 for the calibration case, and from -3.45 to 0.94 for the validation case. Model performance improves from upstream to downstream. Performance at the Tri Thuy station, which is located in a floodplain area simulated using a 2D model, is particularly well. The NSE and R values exceed 0.90, and the relative peak flow error is less than 3%.

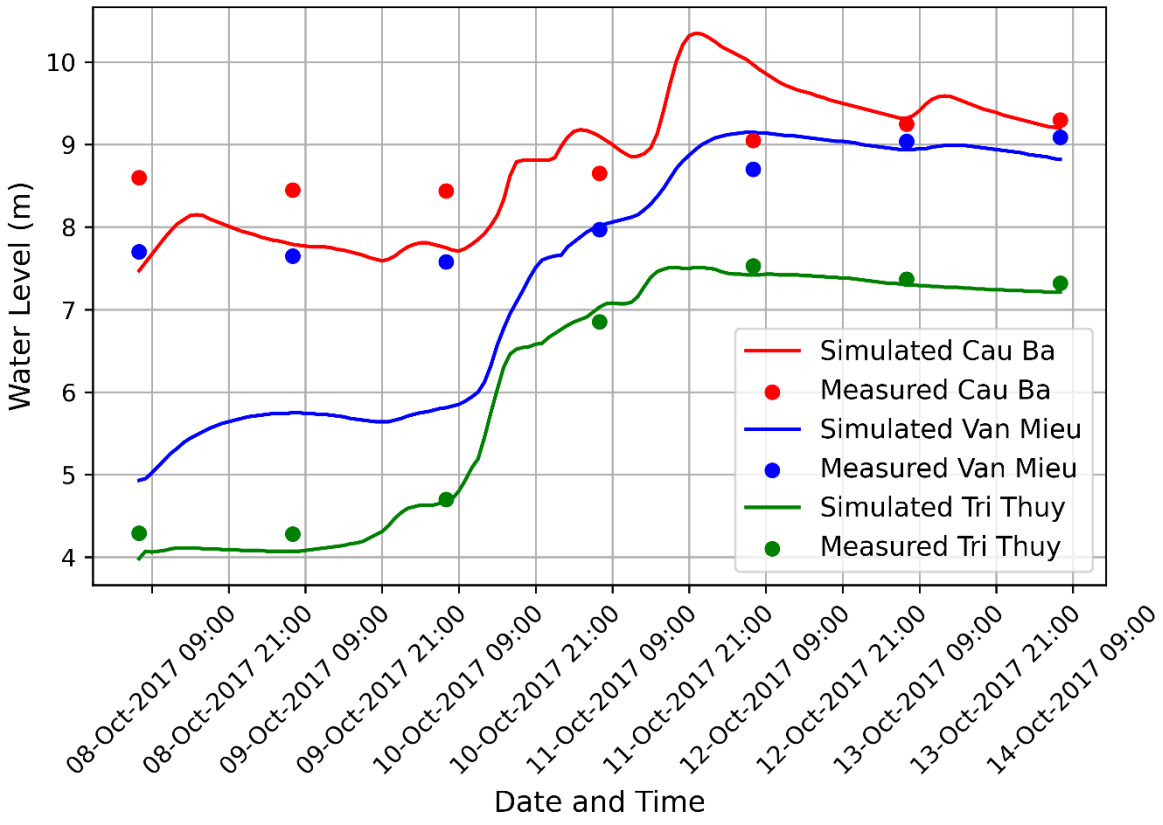

Figure 8.6. Observed and simulated stage hydrographs for the 2017 flood at three stations on the Bui River – Calibration case.

The model performance at Cau Ba and Van Mieu stations located upstream in the Bui River network, is unsatisfactory for some indexes. This poor performance may be due to the complexity of overflows in upstream floodplain areas and the uncertainty in estimating flood flows from sub-catchments in the hydrological modeling. Additionally, the lack of hourly water level data in the Bui River Basin makes it challenging to accurately calibrate and validate the model for peak values and timing.

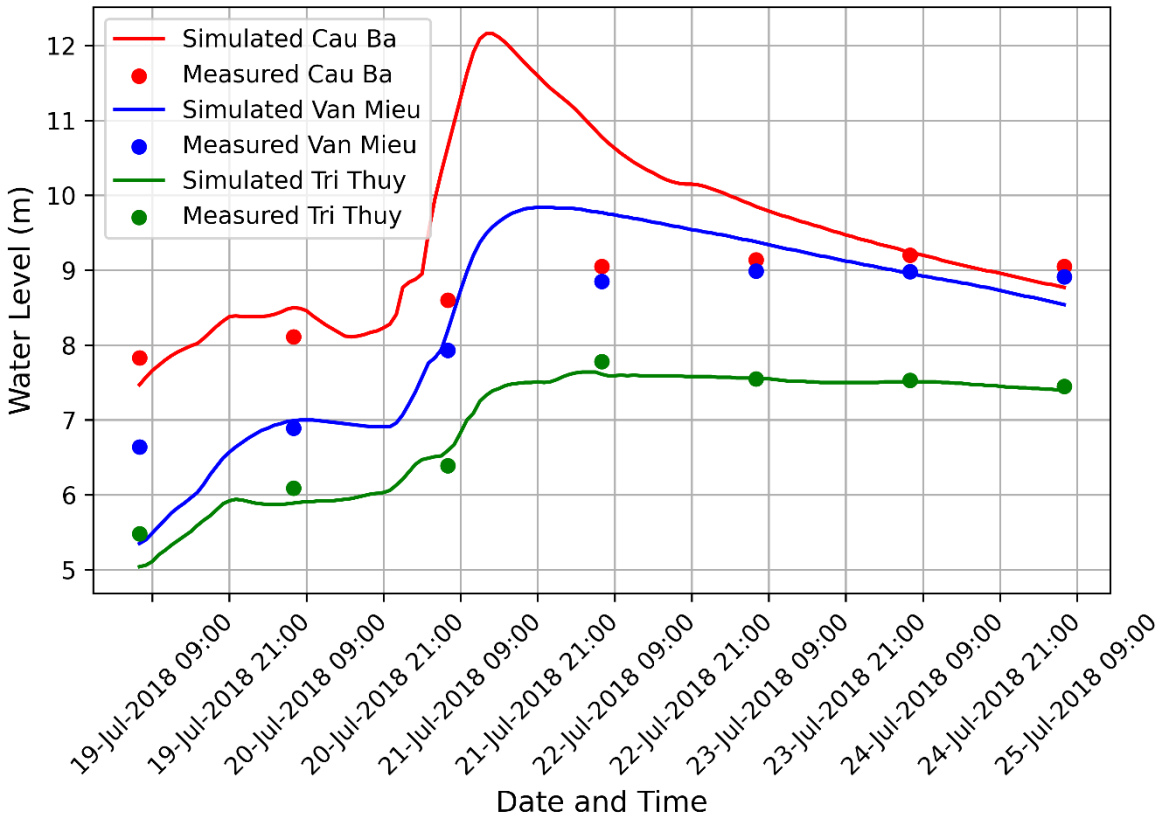

Figure 8.7. Observed and simulated stage hydrographs for the 2018 flood at three stations on the Bui River – Validation case

Table 8.13. Hydrodynamic model performance statistics for calibration and validation cases

Flood case	**Station**	**NSE**	**R**	**$H_{sim\ Max}$ (m)**	**$H_{obs\ Max}$ (m)**	**ΔH_{Max} (%)**	**ΔT_{Max} (hrs)**
10/2017	Cau Ba	-2.93	0.79	10.35	9.30	-11.3	-48
	Van Mieu	-4.40	0.89	9.15	9.09	-0.7	-48
	Tri Thuy	0.99	1.00	7.51	7.53	0.3	0

Flood case	Station	NSE	R	$H_{sim\ Max}$ (m)	$H_{obs\ Max}$ (m)	ΔH_{Max} (%)	ΔT_{Max} (hrs)
07/2018	Cau Ba	-3.45	0.63	12.16	9.20	-32.2	-48
	Van Mieu	0.55	0.93	9.84	8.99	-9.5	-12
	Tri Thuy	0.94	0.98	7.64	7.78	1.8	0

This research primarily focused on assessing flooding in the downstream area near Tri Thuy station. Therefore, the performance of the hydrological and hydraulic models is acceptable for simulating actual flood events (e.g., in 2017, 2018).

8.6 The location of land-use samples

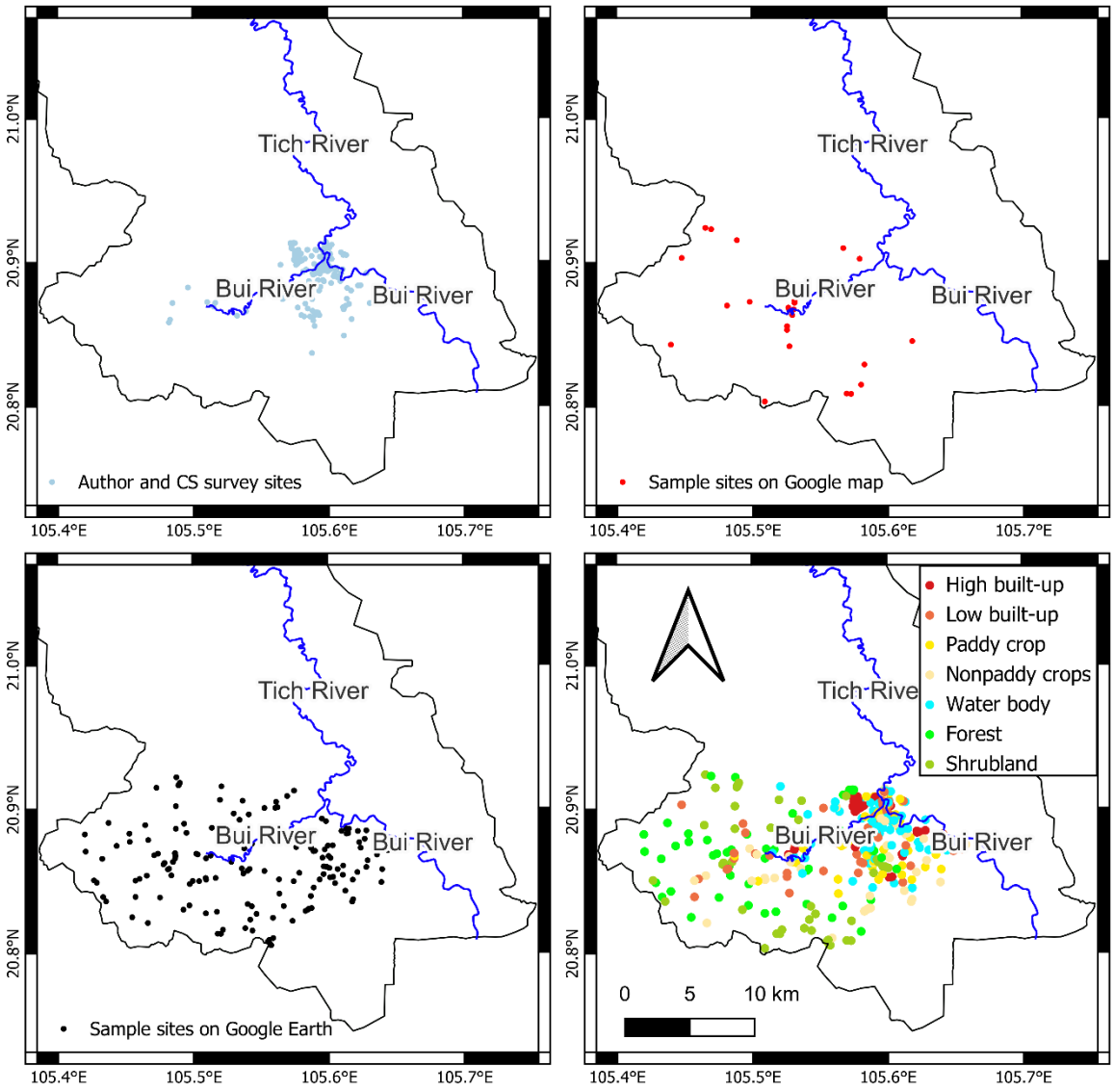

Figure 8.8. Map of land-use sample sites

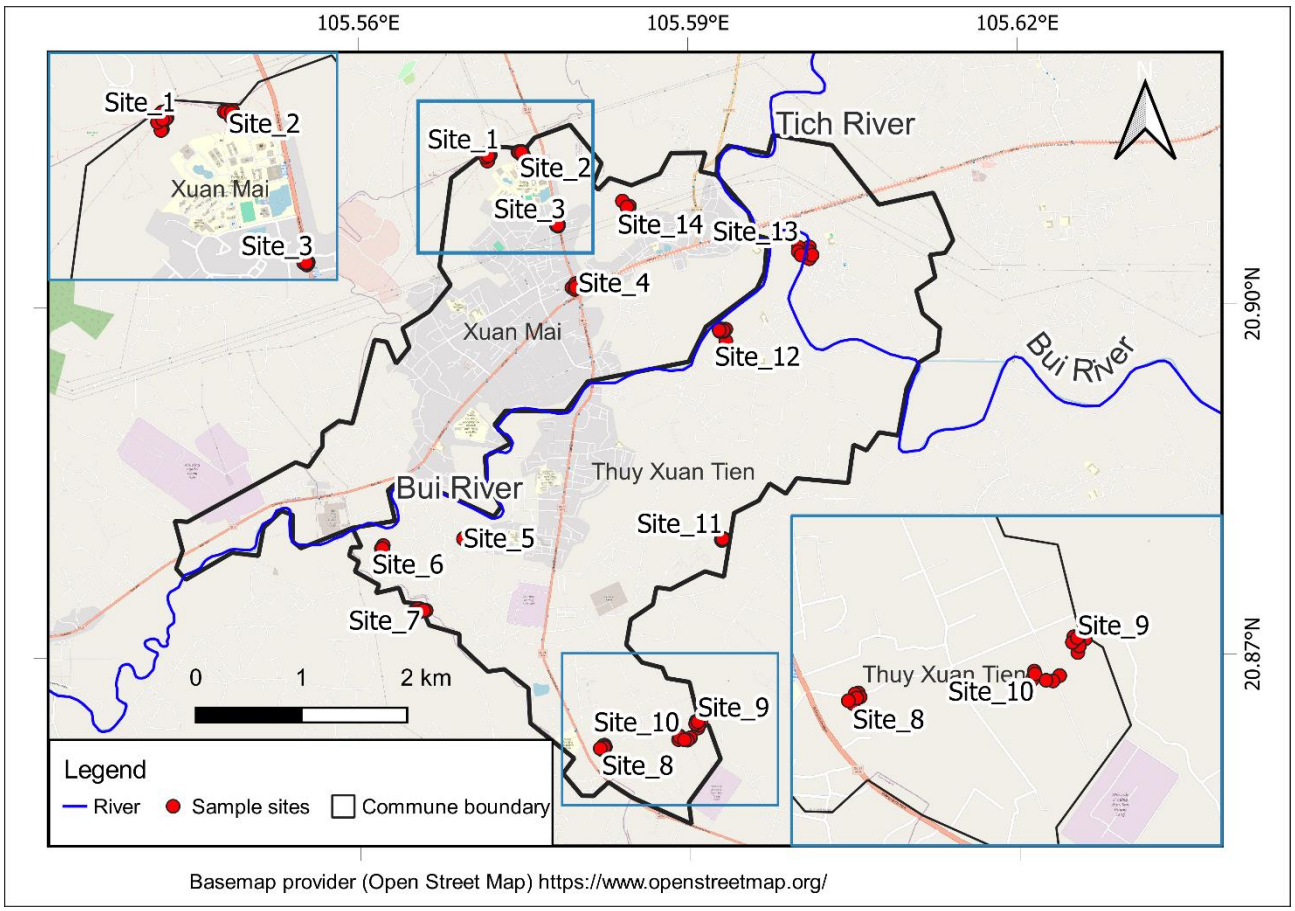

Figure 8.9. Location of land-use sample site during the field experiment

8.7 List of citizen scientists

Table 8.14. Detailed information on citizen scientists

CS_ID	Gender	Birth year	Educational level	Recruitment method	Type of participant	No. of data contributions
CS_1	Female	1982	Under Bachelor	Personal connection	Self-investigator	1
CS_2	Female	2007	Under Bachelor	Random visit	Self-investigator	4
CS_3	Female	1989	Post-graduate	Personal connection	Self-investigator	1
CS_4	Female	1992	Post-graduate	Personal connection	Self-investigator	2
CS_5	Male	1999	Bachelor	Personal connection	Self-investigator	1
CS_6	Female	1989	Bachelor	Personal connection	Self-investigator	1
CS_7	Female	1998	Under Bachelor	Random visit	Self-investigator	1
CS_8	Male	1998	Bachelor	Personal connection	Self-investigator	1
CS_9	Female	1980	Under Bachelor	Personal connection	Self-investigator	1
CS_10	Female	2007	Under Bachelor	Personal connection	Self-investigator	1
CS_11	Male	2002	Bachelor	Personal connection	Self-investigator	1
CS_12	Female	2006	Under Bachelor	Personal connection	Self-investigator	1

CS_ID	Gender	Birth year	Educational level	Recruitment method	Type of participant	No. of data contributions
CS_13	Male	2007	Under Bachelor	Personal connection	Self-investigator	1
CS_14	Female	2004	Under Bachelor	Personal connection	Self-investigator	1
CS_15	Male	2002	Bachelor	Personal connection	Self-investigator	1
CS_16	Male	2007	Under Bachelor	Personal connection	Self-investigator	1
CS_17	Male	2003	Under Bachelor	Personal connection	Self-investigator	1
CS_18	Female	2003	Under Bachelor	Personal connection	Self-investigator	1
CS_19	Female	2009	Under Bachelor	Personal connection	Self-investigator	1
CS_20	Female	1981		Personal connection	Self-investigator	1
CS_21	Female	2000	Bachelor	Personal connection	Self-investigator	1
CS_22	Female	2009	Under Bachelor	Personal connection	Self-investigator	1
CS_23	Male	2004	Under Bachelor	Personal connection	Self-investigator	1
CS_24	Female	2001	Bachelor	Outreach	Self-investigator	1
CS_25	Female	2008	Under Bachelor	Investigators	Investigator	1
CS_26	Female	2000	Bachelor	Outreach	Investigator	25
CS_27	Male	1962	Under Bachelor	Random visit	Self-investigator	5
CS_28	Female	2004	Under Bachelor	Random visit	Self-investigator	1
CS_29	Male	2008	Under Bachelor	Outreach	Self-investigator	54
CS_30	Female	2010	Under Bachelor	Random visit	Self-investigator	1
CS_31	Male	1984	Post-graduate	Social_media	Self-investigator	17
CS_32	Male		Under Bachelor	Random visit	Self-investigator	2
CS_33	Male	2006	Bachelor	Random visit	Self-investigator	2
CS_34	Female	2003	Bachelor	Random visit	Self-investigator	54
CS_35	Male	2000	Bachelor	Personal connection	Investigator	60
CS_36	Male	2000	Bachelor	Random visit	Self-investigator	1
CS_37	Male	2011	Under Bachelor	Personal connection	Self-investigator	42
CS_38	Male	2001	Under Bachelor	Random visit	Self-investigator	2
CS_39	Female	1984	Post-graduate	Personal connection	Investigator	25
CS_40	Male	2000	Under Bachelor	Personal connection	Investigator	9
CS_41	Male	2000	Under Bachelor	Personal connection	Investigator	2
CS_42	Female	2000	Bachelor	Outreach	Investigator	13
CS_43	Female	2000	Bachelor	Outreach	Investigator	4
CS_44	Female	2000	Bachelor	Outreach	Investigator	6
CS_45	Female	2000	Bachelor	Outreach	Investigator	14
CS_46	Male	2000	Bachelor	Outreach	Investigator	14
CS_47	Male	2000	Bachelor	Outreach	Investigator	13
CS_48	Male		Under Bachelor	Random visit	Self-investigator	72

CS_ID	Gender	Birth year	Educational level	Recruitment method	Type of participant	No. of data contributions
CS_49	Male	1981	Under Bachelor	Random visit	Self-investigator	1
CS_50	Female	2008	Under Bachelor	Outreach	Self-investigator	56
CS_51	Male	2008	Under Bachelor	Outreach	Self-investigator	64
CS_52	Male	2000	Bachelor	Outreach	Investigator	8
CS_53	Male		Under Bachelor	Random visit	Self-investigator	2
CS_54	Male	2010	Under Bachelor	Random visit	Self-investigator	5
CS_55	Male	2005	Bachelor	Random visit	Self-investigator	10
CS_56	Female	2008	Under Bachelor	Random visit	Self-investigator	11
CS_57	Female	2001	Bachelor	Personal connection	Investigator	14
CS_58	Male	2007	Under Bachelor	Random visit	Self-investigator	2
CS_59	Female	2005	Under Bachelor	Random visit	Self-investigator	2
CS_60	Female	1991	Post-graduate	Personal connection	Self-investigator	7

8.8 Flood hazard data collection by citizen scientists

Table 8.15. Detailed information on flood hazard collected by citizen scientists

Haz_ID	Surveyor	Lat	Long	Flood frequency	Flooded years	2018 FD (m)	2018 FD_DTM (m)
1	CS_30	20.91	105.60	3 - 5 times	2013, 2017, 2018, 2021	NA	
2	CS_35	20.91	105.60	No		0	
3	CS_35	20.91	105.60	No		0	
4	CS_35	20.91	105.60	No		0	
5	CS_35	20.91	105.60	≥ 5 times	2013, 2017, 2018	0.8	0.49
6	CS_35	20.91	105.60	No		0	
7	CS_35	20.91	105.60	≥ 5 times	2013, 2017, 2018	0.6	0.27
8	CS_35	20.91	105.60	No		0	
9	CS_35	20.91	105.60	3 - 5 times	2017, 2018, 2019	0.6	0.44
10	CS_35	20.88	105.56	3 - 5 times	2018	0.6	Non flooded
11	CS_35	20.88	105.57	No		0	
12	CS_35	20.88	105.57	No		0	

Haz_ID	Surveyor	Lat	Long	Flood frequency	Flooded years	2018 FD (m)	2018 FD_DTM (m)
13	CS_35	20.88	105.57	No		0	
14	CS_35	20.88	105.57	No		0	
15	CS_35	20.86	105.59	No		0	
16	CS_35	20.87	105.59	No		0	
17	CS_35	20.87	105.58	every year		0.8	Non flooded
18	CS_35	20.86	105.58	No		0	
19	CS_35	20.87	105.58	No		0	
20	CS_35	20.86	105.58	No		0	
21	CS_35	20.90	105.59	No		0	
22	CS_35	20.89	105.59	No		0	
23	CS_35	20.91	105.60	1 time	2017, 2018	NA	
24	CS_2	20.90	105.60	every year		NA	
25	CS_39	20.90	105.60	2 times	2018	0.2	0.35
26	CS_39	20.90	105.60	2 times	2018	NA	
27	CS_39	20.90	105.60	2 times	2018	NA	
28	CS_39	20.90	105.60	3 - 5 times	2013, 2017, 2018	1	0.27
29	CS_39	20.90	105.60	2 times	2018	NA	
30	CS_39	20.90	105.60	2 times	2008	NA	
31	CS_39	20.90	105.60	2 times	2017	NA	
32	CS_39	20.90	105.60	2 times	2019	NA	
33	CS_39	20.90	105.60	2 times	2019	NA	
34	CS_39	20.89	105.58	1 time	2013	NA	
35	CS_39	20.90	105.59	2 times	2017	NA	
36	CS_39	20.90	105.59	2 times	2018	1	0.57
37	CS_39	20.87	105.63	2 times	2018	1.3	0.87
38	CS_33	20.87	105.58	3 - 5 times	(Outside pilot area)		
39	CS_29	20.88	105.57	1 time	2017	NA	
40	CS_50	20.92	105.58	2 times	2018	0.4	Non flooded
41	CS_3	20.90	105.57	No		0	
42	CS_4	20.90	105.58	No		0	
43	CS_5	20.48	105.80	No		0	
44	CS_6	20.90	105.60	No	(Outside pilot area)		
45	CS_7	20.90	105.60	every year	2018	1.3	0.80

Haz_ID	Surveyor	Lat	Long	Flood frequency	Flooded years	2018 FD (m)	2018 FD_DTM (m)
46	CS_8	20.89	105.62	every year		NA	
47	CS_10	20.89	105.59	2 times	(Outside pilot area)		
48	CS_13	20.89	105.59	No		0	
49	CS_14	20.89	105.59	No		0	
50	CS_15	20.89	105.59	1 time	2003	NA	
51	CS_34	20.91	105.59	No		0	
52	CS_16	20.90	105.63	No		0	
53	CS_17	20.87	105.58	every year	(Outside pilot area)		
54	CS_20	20.87	105.58	every year		NA	
55	CS_21	20.87	105.58	every year		NA	
56	CS_22	20.87	105.58	every year		NA	
57	CS_23	20.91	105.57	every year		NA	
58	CS_24	20.87	105.58	No		0	
59	CS_29	20.88	105.62	1 time	2018	0.4	Non flooded
60	CS_25	20.91	105.58	1 time	(Outside pilot area)		
61	CS_1	20.87	105.63	No		0	
62	CS_55	20.90	105.60	≥ 5 times	(Outside pilot area)		
63	CS_60	20.90	105.60	ND	2022	ND	
64	CS_60	20.91	105.60	ND	2022	ND	
65	CS_60	20.91	105.60	ND	2022	ND	
66	CS_60	20.88	105.57	ND	2022	ND	
67	CS_50	20.88	105.59	ND	2022	ND	
68	CS_60	20.89	105.61	ND	2022	ND	
69	CS_60	20.89	105.61	ND	2022	ND	
70	CS_60	20.91	105.60	ND	2022	ND	

Note: *FD*, *FD_DTM*, and *ND* represent flooding depth, flooding depth obtained from the DTM-based flooding map, and nondefined information, respectively.

8.9 Flood damage to paddy fields collected by citizen scientists and the district authority

Table 8.16. Flood damage to paddy field collected by citizen scientists and district authority for 2018 flood

Vul_ID	Surveyor	Household ID	Flood frequency	Damage rate_CS (%)	Damage rate_DA (%)
1	CS_28	Household 1	Every year	90	≥ 70
2	CS_35		No		
3	CS_35	Household 2	1 time	0	30- 70
4	CS_35	Household 3	5 times	90	30 - 70
5	CS_35	Household 4	≥ 5 times	90	≥ 70
6	CS_35	Household 5	1 time	50	30 - 70
7	CS_35	Household 6	≥ 5 times	50	30 - 70
8	CS_35	Household 7	3 - 5 times	90	≥ 70
9	CS_35		2 times		
10	CS_35		Every year		
11	CS_39	Household 8	2 times	70	30 - 70
12	CS_39	Household 9	3 - 5 times	30	30 - 70
13	CS_36		2 times		
14	CS_2	Household 10	2 times	90	≥ 70
15	CS_2		No		
16	CS_55		Every year		
17	CS_34	Household 11	≥ 5 times	70	≥ 70
18	CS_4		No		
19	CS_9	Household 12	Every year	70	≥ 70
20	CS_11		Every year		
21	CS_12		Every year		
22	CS_18		3 - 5 times		
23	CS_19		Every year		
24	CS_26	Household 13	≥ 5 times	10	30 - 70
25	CS_40	Household 14	Every year	70	≥ 70
26	CS_40	Household 15	Every year	90	≥ 70
27	CS_41	Household 16	Every year	50	30 - 70
28	CS_40		No		
29	CS_40	Household 17	2 times	90	≥ 70
30	CS_26	Household 18	Every year	90	≥ 70
31	CS_40	Household 19	Every year	90	≥ 70

Vul_ID	Surveyor	Household ID	Flood frequency	Damage rate_CS (%)	Damage rate_DA (%)
32	CS_40	Household 20	Every year	30	30 - 70
33	CS_26		No		
34	CS_26	Household 21	3 - 5 times	70	≥ 70
35	CS_26		No		
36	CS_26	Household 22	Every year	70	≥ 70
37	CS_26	Household 23	3 - 5 times	50	30 - 70
38	CS_26	Household 24	1 time	0	30- 70
39	CS_40	Household 25	2 times	90	≥ 70
40	CS_40	Household 26	2 times	70	≥ 70
41	CS_41		3 - 5 times		
42	CS_26	Household 27	3 - 5 times	30	30 - 70
43	CS_26		No		
44	CS_40	Household 28	2 times	10	≥ 70
45	CS_49	Household 29	3 - 5 times	50	≥ 70
46	CS_27	Household 30	3 - 5 times	90	≥ 70

Note: Damage rate_CS and Damage rate_DA represent the flood damage rate to paddy fields collected by citizen scientists and the district authority, respectively.

8.10 List of flooding depth points in residential area

Table 8.17. List of flooding depth points in residential area

Unit: meters

ID	Surveyor	Lat	Long	Grid_ID	FD_2017	FD_ 2018	FD_2022
1	Author & CS60	20.90	105.60	B6	0.2	1.2	0.1
2	Author & CS60	20.90	105.60	B6	0.6	0.8	0.1
3	Author & CS60	20.90	105.60	B6		1.2	
4	Author	20.90	105.60	B6		1.3	
5	Author	20.90	105.60	B6		1.3	
6	Author	20.90	105.59	C5		0.2	
7	Author	20.90	105.60	B6		1	
8	Author	20.90	105.59	C6		1.1	
9	Author	20.91	105.60	B6		0.4	
10	Author	20.91	105.60	B6	0.7	0.7	
11	Author	20.90	105.60	C7	0.6	0.6	

ID	Surveyor	Lat	Long	Grid_ID	FD_2017	FD_ 2018	FD_2022
12	Author	20.90	105.60	C6	0.2	0.4	
13	Author	20.90	105.60	C6	0.6	0.4	
14	Author	20.91	105.60	A6		0.2	
15	Author	20.91	105.58	B4		0.9	
16	Author	20.89	105.59	C5		0.5	
17	Author	20.89	105.59	C5		1.6	
18	Author	20.89	105.59	C5		0.6	
19	Author	20.88	105.56	D2		2.5	
20	Author	20.88	105.56	E3		0.7	
21	Author	20.88	105.56	D3		1.6	
22	Author	20.88	105.56	D3		0.5	
23	Author	20.88	105.56	D3		2	
24	Author	20.88	105.56	D3	0.4	0.4	
25	Author	20.88	105.57	D3		1.3	
26	Author	20.88	105.56	D3		1.5	
27	Author	20.90	105.60	C7		1.3	
28	Author	20.89	105.61	C7		0.9	
29	Author	20.90	105.60	B6		0.95	
30	Author	20.90	105.60	C6		0.3	
31	Author	20.91	105.60	B6		0.7	
32	Author	20.91	105.60	B6		0.6	
33	Author	20.91	105.60	B6		1	
34	Author	20.91	105.60	B7		0.4	
35	Author & CS60	20.91	105.60	B6		1	0.1
36	Author	20.91	105.60	B6		1	
37	Author	20.91	105.60	B6		1	
38	Author & CS60	20.91	105.60	B6		1.3	0.2
39	Author	20.90	105.60	C6		0.5	
40	Author	20.89	105.58	C5		0.4	
41	Author	20.90	105.60	C6		0.5	
42	Author	20.90	105.60	B6		1.2	
43	Author	20.90	105.60	B6		1.3	
44	Author	20.90	105.60	B6		1.2	
45	Author	20.90	105.60	B6		1.3	
46	Author	20.90	105.60	B6		1.3	

ID	Surveyor	Lat	Long	Grid_ID	FD_2017	FD_ 2018	FD_2022
47	Author	20.91	105.59	A5		0.9	
48	Author	20.88	105.57	D3		1.7	
49	Author	20.91	105.60	A6		1.6	
50	Author	20.90	105.60	C7		2	
51	Author	20.90	105.61	C7		2	
52	Author	20.88	105.59	D5		1.3	
53	Author	20.89	105.60	C7		2.5	
54	Author	20.89	105.59	D6		1.8	
55	Author	20.90	105.60	B6		2	
56	Author	20.90	105.59	B6		2.25	
57	Author	20.90	105.59	B6		1.2	
58	Author	20.89	105.61	C7		2.5	
59	Author	20.89	105.61	C7		2.5	
60	Author	20.90	105.60	C7		1.8	
61	Author	20.89	105.60	D7		0.2	
62	Author	20.89	105.60	D7		2.5	
63	Author	20.89	105.59	D6		1.8	
64	Author	20.89	105.60	D6		1.8	
65	Author	20.88	105.59	D5		1.2	
66	Author	20.88	105.59	D5		1.4	
67	Author	20.89	105.61	C7		2.5	
68	Author	20.88	105.58	D5		1.4	
69	Author	20.90	105.60	B6	2	2.25	
70	Author	20.90	105.60	B6		2	
71	Author	20.89	105.60	D7		2.5	
72	Author	20.91	105.58	A4		1.2	
73	Author	20.91	105.58	A4		2.5	
74	Author	20.89	105.61	C7		2.5	
75	Author	20.90	105.60	B6		1.6	
76	Author	20.89	105.61	C7		2.5	
77	Author	20.90	105.59	B5		0.6	
78	Author	20.91	105.60	B6		1.6	
79	Author	20.90	105.59	B6		1.8	
80	Author	20.88	105.58	E4		0.75	
81	Author	20.90	105.60	B6		1	
82	Author	20.90	105.60	B6		1	
83	Author	20.90	105.59	B6		1	

ID	Surveyor	Lat	Long	Grid_ID	FD_2017	FD_ 2018	FD_2022
84	Author	20.90	105.60	B6		1.3	
85	Author	20.90	105.60	B6		1.3	
86	Author	20.90	105.60	B6		0.8	
87	Author	20.90	105.60	B6		1.3	
88	Author	20.90	105.60	B6		1.3	
89	Author	20.90	105.60	B6		1	
90	CS_35	20.91	105.60	A6	0.8	0.8	
91	CS_35	20.91	105.60	A6	0.6	0.6	
92	CS_35	20.91	105.60	A6	0.6	0.6	
93	CS_35	20.91	105.60	A6		0.6	
94	CS_35	20.87	105.59	F5		0.8	
95	CS_39	20.90	105.60	C6		0.2	
96	CS_39	20.90	105.60	B7		1	
97	CS_39	20.90	105.59	C6		1	
98	CS_39	20.90	105.59	C6		1.3	
99	CS_50	20.88	105.57	D3		0.4	1.3
100	CS_7	20.90	105.59	B6		1.3	
101	CS_29	20.87	105.58	F4		0.4	
102	CS_60	20.88	105.59	D5			0.2
103	CS_60	20.89	105.61	C7			0.1
104	CS_60	20.89	105.61	C7			0.2
105	Author	20.90	105.60	B6		0.2	
106	CS_35	20.87	105.59	F5		0.6	

Note: FD represents flooding depth.

8.11 Selected field photos

Pre-surveying

Recruiting citizen scientists

Training citizen scientists

Measuring rainfall data

Figure 8.10. Field photos from the implementation of the citizen science program

In dieser Reihe bisher erschienen

Band I
10. DIALOG Abfallwirtschaft MV
– Von der Abfallwirtschaft zur Energiewirtschaft.
Tagungsband, erschienen im Juni 2007, ISBN 987-3-86009-004-6

Band II
Ellen-Rose Trübger
Entwicklung eines Ansatzes zur Berücksichtigung der ungesättigten Zone bei der Grundwassersimulation von Feuchtgebieten.
Dissertation, erschienen im August 2007, ISBN 978-3-86009-006-0

Band III
René Dechow
Untersuchungen verschiedener Ansätze der Wasserhaushalts- und Stofftransportmodellierung hinsichtlich ihrer Anwendbarkeit in Stickstoffhaushaltsmodellen.
Dissertation, erschienen im September 2007, ISBN 978-3-86009-016-9

Band IV
Carolin Wloczyk
Entwicklung und Validierung einer Methodik zur Ermittlung der realen Evapotranspiration anhand von Fernerkundungsdaten in Mecklenburg-Vorpommern.
Dissertation, erschienen im September 2007, ISBN 978-3-86009-009-1

Band 5
1. Rostocker Bioenergieforum.
Bioenergieland Mecklenburg-Vorpommern.
Tagungsband, erschienen im Oktober 2007, ISBN 978-3-86009-013-8

Band 6
Kulturtechniktagung 2007.
Ostseeverschmutzung und Flächenentwässerung.
Tagungsband, erschienen im Januar 2008, ISBN 978-3-86009-018-3

Band 7
Enrico Frahm
Bestimmung der realen Evapotranspiration für Weide (Salix spp.) und Schilf (Phragmites australis) in einem nordostdeutschen Flusstalmoor.
Dissertation, erschienen im Mai 2008, ISBN 978-3-86009-023-7

Band 8
Jenny Haide
Methode zur Quantifizierung der Einflüsse auf Vorgangsdauern lohnintensiver Arbeiten am Beispiel von Pflasterarbeiten.
Dissertation, erschienen im Juni 2008, ISBN 978-3-86009-024-4

Band 9
11. DIALOG Abfallwirtschaft MV
Chancen und Risiken für die deutsche Abfallwirtschaft im Ausland.
Tagungsband, erschienen im Juni 2008, ISBN 978-3-86009-029-9

Band 10
Stefan Cantré
Ein Beitrag zur Bemessung geotextiler Schläuche für die Entwässerung von Baggergut.
Dissertation, erschienen im Juni 2008, ISBN 978-3-86009-032-9

Band 11
Birgit Wüstenberg
Praxis der Standortwahl von Sportboothäfen im Küstenbereich Mecklenburg-Vorpommerns und Entwicklung einer Bewertungsmethode als Planungshilfe.
Dissertation, erschienen im Juli 2008, ISBN 978-3-86009-033-6

Band 12
André Clauß
Erhöhung der Trinkwasserversorgungssicherheit in Havarie- und Krisensituationen durch neue Handlungsalgorithmen sowie Einbeziehung bisher ungenutzter Ressourcen am Beispiel von Bergbaugrubenwasser.
Dissertation, erschienen im September 2008, ISBN 978-3-86009-037-4

Band 13
Peter Degener
Sickerwasserkreislauf zur Behandlung von Sickerwässern der aerob-biologischen Restabfallbehandlung (Restabfallrotte).
Dissertation, erschienen im Oktober 2008, ISBN 978-3-86009-043-5

Band 14
2. Rostocker Bioenergieforum
Innovationen für Klimaschutz und wirtschaftliche Entwicklung.
Tagungsband, erschienen im Oktober 2008, ISBN 978-3-86009-044-2

Band 15
7. Rostocker Abwassertagung
Fortschritte auf dem Gebiet der Abwasserentsorgung.
Tagungsband, erschienen im November 2008, ISBN 978-3-86009-045-9

Band 16
Christian Noß
Strömungsstrukturen kleiner naturnaher Fließgewässer unter Berücksichtigung von Turbulenztheorie und Dispersionsmodellen.
Dissertation, erschienen im Januar 2009, ISBN 978-3-86009-054-1

Band 17
Ralf Schröder
Entwicklung von Möglichkeiten zur Messung der N2-Übersättigung sowie Methoden zur Reduzierung der Schwimmschlammbildung.
Dissertation, erschienen im Februar 2009, ISBN 978-3-86009-055-8

Band 18
Elmar Wisotzki
Bodenverfestigungen mit Kalk-Hüttensand-Gemischen.
Dissertation, erschienen im April 2009, ISBN 978-3-86009-059-6

Band 19
Ramez Mashkouk
Untersuchungen zur Adsorption und biologischen Aktivität an Aktivkohlefilter unter den Bedingungen der Wasseraufbereitung im Wasserwerk Rostock.
Dissertation, erschienen im April 2009, ISBN 978-3-86009-060-2

Band 20
Torsten Birkholz
Handlungserfordernisse und Optimierungsansätze für kommunale Ver- und Entsorgungsunternehmen im Zusammenhang mit demografischen Veränderungen im ländlichen Raum aufgezeigt an einem Beispiel in Mecklenburg-Vorpommern.
Dissertation, erschienen im Mai 2009, ISBN 978-3-86009-061-9

Band 21
12. DIALOG Abfallwirtschaft MV
Aktuelle Entwicklungen in der Abfallwirtschaft.
Tagungsband, erschienen im Juni 2009, ISBN 978-3-86009-062-6

Band 22
Thomas Fritz
Entwicklung, Implementierung und Validierung eines praxisnahen Verfahrens zur Bestimmung von Biogas- bzw. Methanerträgen.
Dissertation, erschienen im Oktober 2009, ISBN 978-3-86009-065-7

Band 23
3. Rostocker Bioenergieforum
Bioenergie – Chance und Herausforderung für die regionale und globale Wirtschaft.
Tagungsband, erschienen im Oktober 2009, ISBN 978-3-86009-065-8

Band 24
Muhammad Mariam
Analyse von Gefahrenpotenzialen für die Trinkwasserversorgung der Stadt Rostock unter besonderer Berücksichtigung von Schadstoffausbreitungsvorgängen in der Warnow.
Dissertation, erschienen im Februar 2010, ISBN 978-3-86009-078-7

Band 25
Manja Steinke
Untersuchungen zur Behandlung von Abwässern der Fischverarbeitungsindustrie.
Dissertation, erschienen im Juni 2010, ISBN 978-3-86009-085-5

Band 26
13. DIALOG Abfallwirtschaft MV
Die Kreislauf- und Abfallwirtschaft im Wandel. Wohin gehen die rechtlichen und technischen Entwicklungen?
Tagungsband, erschienen im Juni 2010, ISBN 978-3-86009-087-9

Band 27
4. Rostocker Bioenergieforum
Zukunftstechnologien für Bioenergie
Tagungsband, erschienen im Oktober 2010, ISBN 978-3-940364-12-8

Band 28
Dirk Banemann
Einfluss der Silierung und des Verfahrensablaufs der Biomassebereitstellung auf den Methanertrag unter Berücksichtigung eines Milchsäurebakteriensiliermittel
Dissertation, erschienen im Januar 2011, ISBN 978-3-86009-087-9

Band 29
14. DIALOG Abfallwirtschaft MV
Abfall als Wertstoff- und Energiereserve
Tagungsband, erschienen im Juni 2011, ISBN 978-3-940364-18-0

Band 30
5. Rostocker Bioenergieforum
Tagungsband, erschienen im November 2011, ISBN 978-3-940364-20-3

Band 31
8. Rostocker Abwassertagung
Erhöhung der Effektivität von Abwasserentsorgungsanlagen
Tagungsband, erschienen im November 2011, ISBN 978-3-86009-120-3

Band 32
6. Rostocker Bioenergieforum
Tagungsband, erschienen im Juni 2012, ISBN 978-3-940364-27-2

Band 33
Ishan Machlouf
Untersuchungen zur Nitratelimination bei der Trinkwasseraufbereitung unter Berücksichtigung syrischer Verhältnisse
Dissertation, erschienen im März 2013, ISBN 978-3-86009-204-0

Band 34
Ralph Sutter
Analyse und Bewertung der Einflussgrößen auf die Optimierung der Rohbiogasproduktion hinsichtlich der Konstanz von Biogasqualität und -menge
Dissertation, erschienen im März 2013, ISBN 978-3-86009-202-6

Band 35
Wolfgang Pfaff-Simoneit
Entwicklung eines sektoralen Ansatzes zum Aufbau von nachhaltigen Abfallwirtschaftssystemen in Entwicklungsländern vor dem Hintergrund von Klimawandel und Ressourcenverknappung
Dissertation, erschienen im Mai 2013, ISBN 978-3-86009-203-3

Band 36
7. Rostocker Bioenergieforum
Tagungsband, erschienen im Juni 2013, ISBN 978-3-86009-207-1

Band 37
Markus Helftewes
Modellierung und Simulation der Gewerbeabfallaufbereitung vor dem Hintergrund der Outputqualität, der Kosteneffizienz und der Klimabilanz
Dissertation, erschienen im Oktober 2013, ISBN 978-3-86009-402-0

Band 38
Jan Stefan Riha
Detektion und Quantifizierung von Cyanobakterien in der Ostsee mittels Satellitenfernerkundung
Dissertation, erschienen im Oktober 2013, ISBN 978-3-86009-403-7

Band 39
Peter Helmke
Optimierung der Verarbeitungs-, Gebrauchs- und Entsorgungseigenschaften eines naturfaserverstärkten Kunststoffes unter Berücksichtigung automobiler Anforderungen
Dissertation, erschienen im November 2013, ISBN 978-3-86009-404-4

Band 40
Andrea Siebert-Raths
Modifizierung von Polylactid (PLA)für technische Anwendungen
Verfahrenstechnische Optimierung der Verarbeitungs- und Gebrauchseigenschaften
Dissertation, erschienen im Januar 2014 ISBN 978-3-86009-405-1

Band 41
Fisiha Getachew Argaw
Agricultural Machinery Traffic Influence on Clay Soil Compaction as Measured by the Dry Bulk Density
Dissertation, erschienen im Januar 2014 ISBN 978-3-86009-406-8

Band 42
Tamene Adugna Demissie
Climate change impact on stream flow and simulated sediment yield to Gilgel Gibe 1 hydropower reservoir and the effectiveness of Best Management Practices
Dissertation, erschienen im Februar 2014 ISBN 978-3-86009-407-5

Band 43
Paul Engelke
Untersuchungen zur Modellierung des Feststofftransports in Abwasserkanälen: Validierung in SIMBA®
Dissertation, erschienen im Februar 2014 ISBN 978-3-86009-408-2

Band 44
16. DIALOG Abfallwirtschaft MV
Aktuelle Entwicklungen in der Abfall- und Ressourcenwirtschaft
Tagungsband, erschienen im April 2014, ISBN 978-3-86009-410-5

Band 45
8. Rostocker Bioenergieforum, 19.-20. Juni 2014 an der Universität Rostock
Tagungsband, erschienen im Juni 2014, ISBN 978-3-86009-412-9

Band 46
Abschlussbericht Projekt CEMUWA − Climate protection, natural resources management and soil improvement by combined Energetic and Material Utilization of lignocellulosic agricultural WAstes and residues
Projektbericht, erschienen im September 2014, ISBN 978-3-86009-413-6

Band 47
8. Rostocker Baggergutseminar, 24.-25. September 2014 in Rostock
Tagungsband, erschienen im September 2014, ISBN 978-3-86009-414-3

Band 48
Michael Kuhn
Mengen und Trockenrückstand von Rechengut kommunaler Kläranlagen
Dissertation, erschienen im Oktober 2014 ISBN 978-3-86009-415-0

Band 49
8. Rostocker Abwassertagung, 10.-11. November 2014 in Rostock
Tagungsband, erschienen im November 2014, ISBN 978-3-86009-416-7

Band 50
Mulugeta Azeze Belete
Modeling and Analysis of Lake Tana Sub Basin Water Resources Systems, Ethiopia
Dissertation, erschienen im Dezember 2014 ISBN 978-3-86009-422-8

Band 51
Daniela Dressler
Einfluss regionaler und standortspezifischer Faktoren auf die Allgemeingültigkeit ökologischer und primärenergetischer Bewertungen von Biogas
Dissertation, erschienen im Mai 2015 ISBN 978-3-86009-424-2

Band 52
9. Rostocker Bioenergieforum, 18.-19. Juni 2015 in Rostock
Tagungsband, erschienen im November 2014, ISBN 978-3-86009-425-9

Band 53
Nils Engler
Spurenelementkonzentrationen und biologische Aktivität in NaWaRo-Biogas-fermentern
Dissertation, erschienen im September 2015 ISBN 978-3-86009-427-3

Band 54
Thomas Schmidt
Möglichkeiten der Effizienzsteigerung bei der anaeroben Vergärung von Weizenschlempe
Dissertation, erschienen im Oktober 2015 ISBN 978-3-86009-428-0

Band 55
Thomas Dorn
Principles, Opportunities and Risks associated with the transfer of environmental technology between Germany and China using the example of thermal waste disposal
Dissertation, erschienen im Dezember 2015 ISBN 978-3-86009-429-7

Band 56
Uwe Holzhammer
Biogas in einer zukünftigen Energieversorgungsstruktur mit hohen Anteilen fluktuierender Erneuerbarer Energien
Dissertation, erschienen im Dezember 2015 ISBN 978-3-86009-430-3

Band 57
17. DIALOG Abfallwirtschaft MV
Aktuelle Entwicklungen in der Abfall- und Ressourcenwirtschaft,
15. Juni 2016 in Rostock,
Tagungsband, erschienen im Juni 2016, ISBN 978-3-86009-432-7

Band 58
10. Rostocker Bioenergieforum, 16.-17. Juni 2016 in Rostock
Tagungsband, erschienen im Juni 2016, ISBN 978-3-86009-433-4

Band 59
Michael Friedrich
Adaptation of growth kinetics and degradation potential of organic material in activated sludge
Dissertation, erschienen im Juli 2016 ISBN 978-3-86009-434-1

Band 60
Nico Schulte
Entwicklung von Qualitätsprüfungen für die haushaltsnahe Abfallsammlung im Holsystem
Dissertation, erschienen im Juli 2016 ISBN 978-3-86009-435-8

Band 61
Ullrich Dettmann
Improving the determination of soil hydraulic properties of peat soils at different scales
Dissertation, erschienen im September 2016 ISBN 978-3-86009-436-5

Band 62
Anja Schreiber
Membranbasiertes Verfahren zur weitergehenden Vergärung
von feststoffreichen Substraten in landwirtschaftlichen Biogasanlagen
Dissertation, erschienen im Oktober 2016 ISBN 978-3-86009-446-4

Band 63
André Körtel
Entwicklung eines selbstgängigen statischen Verfahrens zur biologischen Stabilisierung und Verwertung organikreicher Abfälle unter extrem ariden Bedingungen für Entwicklungs- und Schwellenländer, am Beispiel der Stadt Teheran
Dissertation, erschienen im Oktober 2016 ISBN 978-3-86009-447-1

Band 64
Ayman Elnaas
Actual situation and approach for municipal solid waste treatment in the Arab region
Dissertation, erschienen im Oktober 2016 ISBN 978-3-86009-448-8

Band 65
10. Rostocker Abwassertagung, Wege und Werkzeuge für eine zukunftsfähige Wasserwirtschaft im norddeutschen Tiefland, 8. November 2016 in Rostock
Tagungsband, erschienen im November 2016, ISBN 978-3-86009-449-5

Band 66
Gunter Weißbach
Mikrowellen-assistierte Vorbehandlung lignocellulosehaltiger Reststoffe
Dissertation, erschienen im November 2016 ISBN 978-3-86009-450-1

Band 67
Leandro Janke
Optimization of anaerobic digestion of sugarcane waste for biogas production in Brazil
Dissertation, erschienen im Mai 2017 ISBN 978-3-86009-454-9

Band 68
11. Rostocker Bioenergieforum, 22.-23. Juni 2017 in Rostock
Tagungsband, erschienen im Juni 2017, ISBN 978-3-86009-455-6

Band 69
Claudia Demmig
Einfluss des Erntezeitpunktes auf die anaerobe Abbaukinetik der Gerüstsubstanzen im Biogasprozess
Dissertation, erschienen im Juli 2017, ISBN 9978-3-86009-456-3

Band 70
Christian Koepke
Die Ermittlung charakteristischer Bodenkennwerte der Torfe und Mudden Mecklenburg-Vorpommerns als Eingangsparameter für erdstatische Berechnungen nach Eurocode 7 / DIN 1054
Dissertation, erschienen im Juni 2017, ISBN 978-3-86009-457-0

Band 71
Sven-Henning Schlömp
Geotechnische Untersuchung und Bewertung bautechnischer Eignung von Müllverbrennungsschlacken und deren Gemischen mit Böden
Dissertation, erschienen im Juni 2017, ISBN 978-3-86009-458-7

Band 72
Anne-Katrin Große
Baggergut im Deichbau – Ein Beitrag zur geotechnischen Charakterisierung und Erosionsbeschreibung feinkörniger, organischer Sedimente aus dem Ostseeraum zur Einschätzung der Anwendbarkeit
Dissertation, erschienen im Juni 2017, ISBN 978-3-86009-459-4

Band 73
Thomas Knauer
Steigerung der Gesamteffizienz von Biogasanlagen durch thermische Optimierung
Dissertation, erschienen im Juli 2017, ISBN 978-3-86009-460-0

Band 74
Mathhar Bdour
Electrical power generation from residual biomass by combustion in externally fired gas turbines (EFGT)
Dissertation, erschienen im August 2017, ISBN 978-3-86009-468-6

Band 75
Johannes Dahlin
Vermarktungsstrategien und Konsumentenpräferenzen für Dünger und Erden aus organischen Reststoffen der Biogasproduktion
Dissertation, erschienen im September 2017, ISBN 978-3-86009-469-3

Band 76
Sören Weinrich
Praxisnahe Modellierung von Biogasanlagen
Systematische Vereinfachung des Anaerobic Digestion Model No. 1 (ADM1)
Dissertation, erschienen im März 2018, ISBN 978-3-86009-471-6

Band 77
18. DIALOG Abfallwirtschaft MV
Aktuelle Entwicklungen in der Abfall- und Ressourcenwirtschaft
Tagungsband, erschienen im Juni 2018, ISBN 978-3-86009-472-3

Band 78
12. Rostocker Bioenergieforum
Tagungsband, erschienen im Juni 2018, ISBN 978-3-86009-473-0

Band 79
Tatyana Koegst
Screening approaches for decision support in drinking water supply
Dissertation, erschienen im Juni 2018, ISBN 978-3-86009-474-7

Band 80
Liane Müller
Optimierung des anaeroben Abbaus stickstoffhaltiger Verbindungen durch den Einsatz von Proteasen
Dissertation, erschienen im September 2018, ISBN 978-3-86009-475-4

Band 81
Projektbericht Wasserwirtschaft
KOGGE – **Ko**mmunale **G**ewässer **G**emeinschaftlich **E**ntwickeln
Ein Handlungskonzept für kleine urbane Gewässer am Beispiel der Hanse- und Universitätsstadt Rostock
Projektbericht, erschienen im September 2018, ISBN 978-3-86009-476-1

Band 82
Adam Feher
Untersuchungen zur Bioverfügbarkeit von Mikronährstoffen für den Biogasprozess
Dissertation, erschienen im Oktober 2018, ISBN 978-3-86009-477-8

Band 83
Constanze Uthoff
Pyrolyse von naturfaserverstärkten Kunststoffen zur Herstellung eines kohlenstoffhaltigen Füllstoffs für Thermoplasten
Dissertation, erschienen im November 2018, ISBN 978-3-86009-478-5

Band 84
Ingo Kaundinya
Prüfverfahren zur Abschätzung der Langzeitbeständigkeit von Kunststoff-dichtungsbahnen aus PVC-P für den Einsatz in Dichtungssystemen von Straßentunneln
Dissertation, erschienen im Dezember 2018, ISBN 978-3-86009-484-6

Band 85
Eric Mauky
A model-based control concept for a demand-driven biogas production
Dissertation, erschienen im Januar 2019, ISBN 978-3-86009-485-3

Band 86
Michael Kröger
Thermochemical Utilization of Algae with Focus on hydrothermal Processes
Dissertation, erschienen im Februar 2019, ISBN 978-3-86009-486-0

Band 87
13. Rostocker Bioenergieforum
Tagungsband, erschienen im Juni 2019, ISBN 978-3-86009-487-7

Band 88
12. Rostocker Abwassertagung
Tagungsband, erschienen im September 2019, ISBN 978-3-86009-488-4

Band 89
Philipp Stahn
Wasser- und Nährstoffhaushalt von Böden unter Mischkulturen und Trockenstress
Dissertation, erschienen im Juli 2019, ISBN 978-3-86009-489-1

Band 90
BioBind: Luftgestützte Beseitigung von Verunreinigungen durch Öl mit biogenen Bindern
Projektbericht, erschienen im September 2019, ISBN 978-3-86009-490-7

Band 91
Jürgen Müller
Die forsthydrologische Forschung im Nordostdeutschen Tiefland: Veranlassung, Methoden, Ergebnisse und Perspektiven
Habilitation, erschienen im Oktober 2019, ISBN 978-3-86009-491-4

Band 92
Marcus Siewert
Bewertung der Ölhavarievorsorge im deutschen Seegebiet auf Grundlage limitierender Randbedingungen – Ein Beitrag zur Verbesserung des Vorsorgestatus
Dissertation, erschienen im November 2019, ISBN 978-3-86009-492-1

Band 93
Camilo Andrés Wilches Tamayo
Technical optimization of biogas plants to deliver demand oriented power
Dissertation, erschienen im Februar 2020, ISBN 978-3-86009-493-8

Band 94
Robert Kopf
Technisches Benchmarking mit Standortqualifikationsstudie biochemischer Energieanlagenprojekte (Beispiel Biogas)
Dissertation, erschienen im Februar 2020, ISBN 978-3-86009-494-5

Band 95
14. Rostocker Bioenergieforum und 19. DIALOG Abfallwirtschaft MV
Tagungsband, erschienen im Juni 2020, ISBN 978-3-86009-507-2
DOI: https://doi.org/10.18453/rosdok_id00002650

Band 96
Safwat Hemidat
Feasibility Assessment of Waste Management and Treatment in Jordan
Dissertation, erschienen im Juli 2020, ISBN 978-3-86009-509-6

Band 97
Andreas Heiko Metzing
Verdichtung von ungebundenen Pflasterdecken und Plattenbelägen - Untersuchungen zur Lagerungsdichte des Fugenmaterials
Dissertation, erschienen im Juli 2020, ISBN 978-3-86009-510-2
DOI: https://doi.org/10.18453/rosdok_id00002742

Band 98
Ying Zhou
Research on Utilization of Hydrochars Obtained by the Organic Components of Municipal Solid Waste
Dissertation, erschienen im November 2020, ISBN 978-3-86009-515-7

Band 99
Mathias Gießler
Ein prozessbasiertes Modell zur wirtschaftlich-technischen Abbildung von Abwasserunternehmen **–** Beispielhafte Anwendung für eine ländliche Region mit Bevölkerungsrückgang
Dissertation, erschienen im November 2020, ISBN 978-3-86009-516-4
DOI: https://doi.org/10.18453/rosdok_id00002790

Band 100
Dodiek Ika Candra
Development of a Virtual Power Plant based on a flexible Biogas Plant and a Photovoltaic-System
Dissertation, erschienen im Dezember 2020, ISBN 978-3-86009-518-8
DOI: https://doi.org/10.18453/rosdok_id00002814

Band 101
Thomas Zeng
Prediction and reduction of bottom ash slagging during small-scale combustion of biogenic residues
Dissertation, erschienen im Dezember 2020, ISBN 978-3-86009-519-5

Band 102
Edward Antwi
Pathways to sustainable bioenergy production from cocoa and cashew residues from Ghana
Dissertation, erschienen im Dezember 2020, ISBN 978-3-86009-520-1
DOI: https://doi.org/10.18453/rosdok_id00002818

Band 103
Muhammad Waseem
Integrated Hydrological and Mass Balance Assessment in a German Lowland Catchment with a Coupled Hydrologic and Hydraulic Modelling
Dissertation, erschienen im Januar 2021, ISBN 978-3-86009-521-8
DOI: https://doi.org/10.18453/rosdok_id00002884

Band 104
Martin Rinas
Sediment Transport in Pressure Pipes
Dissertation, erschienen im März 2021, ISBN 978-3-86009-538-6
DOI https://doi.org/10.18453/rosdok_id00003915

Band 105
15. Rostocker Bioenergieforum
Tagungsband, erschienen im Juni 2021, ISBN 978-3-86009-524-9
DOI https://doi.org/10.18453/rosdok_id00003024

Band 106
Jan Sprafke
Potenziale der biologischen Behandlung von organischen Abfällen zur Sektorenkopplung
Dissertation, erschienen im Oktober 2021, ISBN 978-3-86009-527-0
DOI https://doi.org/10.18453/rosdok_id00003118

Band 107
Mingyu Qian
The Demonstration and Adaption of the Garage - Type Dry Fermentation Technology for Municipal Solid Waste to Biogas in China
Dissertation, erschienen im Oktober 2021, ISBN 978-3-86009-528-7

Band 108
Haniyeh Jalalipour
Sustainable municipal organic waste management in Shiraz, Iran
Dissertation, erschienen im November 2021, ISBN 978-3-86009-526-3
https://doi.org/10.18453/rosdok_id00003116

Band 109
Michael Cramer
Umgang mit stark verschmutzem Niederschlagswasser aus Siloanlagen
Dissertation, erschienen im Dezember 2021, ISBN 978-3-86009-530-0
https://doi.org/10.18453/rosdok_id00003358

Band 110
16. Rostocker Bioenergieforum und 20. DIALOG Abfallwirtschaft MV
Tagungsband, erschienen im Juni 2022, ISBN 978-3-86009-535-5
DOI: https://doi.org/10.18453/rosdok_id00003615

Band 111
Fachtagung Wasserwirtschaft – Gute Stadt-Land-Beziehungen für eine nachhaltige Entwicklung in MV
Tagungsband, erschienen im Juni 2022, ISBN 978-3-86009-538-6
DOI: https://doi.org/10.18453/rosdok_id00003915

Band 112
Zelalem Abera Angello
Selection of Optimal Pollution Management Strategy for the Little Akaki River, Ethiopia, Based on Determination of Spatio-temporal Pollutant Dynamics and Water Quality Modeling
Dissertation, erschienen im Oktober 2022, ISBN 978-3-86009-542-3
https://doi.org/10.18453/rosdok_id00003948

Band 113
Qahtan Thabit
Hybrid waste Incineration – Solar Parabolic System with Thermal Energy Recovery in Sea wate Disalination in MENA Region
Dissertation, im Druck, ISBN 978-3-86009-545-4
https://doi.org/10.18453/rosdok_id00004181

Band 114
17. Rostocker Bioenergieforum
Tagungsband, erschienen im Juni 2023, ISBN 978-3-86009-547-8
https://doi.org/10.18453/rosdok_id00004269

Band 115
Megersa Kebede Leta
Modeling Optimal Operation of Nashe
Hydropower Reservoir under LandUse Land Cover Changes in blue Nile River Basin, Ethopia
Dissertation, ISBN 978-3-86009-548-5
https://doi.org/10.18453/rosdok_id00004427

Band 116
13. Rostocker Abwassertagung. Bewirtschaftung und Behandlung von Niedeschlagswasser.
Tagungsband, erschienen im November 2023, ISBN 978-3-86009-549-2
https://doi.org/10.18453/rosdok_id00004432

Band 117
Semaria Moga Lencha
Estimating pollutant fluxes and their impact on Lake Hawassa in Ethiopia's Rift Valley basin based on combined monitoring and modelling
Dissertation, ISBN 978-3-86009-550-8
https://doi.org/10.18453/rosdok_id00004446

Band 118
Fabian Gievers
Vergleichende Untersuchungen und Bilanzierungen von Prozessketten zur Herstellung und Nutzung von Biokohlen aus Klärschlämmen
Dissertation, ISBN 978-3-86009-551-5
https://doi.org/10.18453/rosdok_id00004455

Band 119
Tim Jurisch
Untersuchungen hydraulischer Eigenschaften von Baggergut im Deichbau am Beispiel des Rostocker Forschungsdeiches
Dissertation, ISBN 978-3-86009-552-2
https://doi.org/10.18453/rosdok_id00004489

Band 120
Projekt PROSPER-RO
Prospektive Synergistische Planung von Entwicklungsoptionen in Regiopolen am Beispiel des Stadt-Umland-Raums Rostock.
Abschlussbericht, erschienen im Februar 2024, ISBN 978-3-86009-553-9
https://doi.org/10.18453/rosdok_id00004532

Band 121
Roberto Eloy Hernández Regalado
Optimization of the efficiency and flexibility of agricultural biogas plants by integrating an expanded granular sludge bed reactor
Dissertation, ISBN 978-3-86009-554-6
https://doi.org/10.18453/rosdok_id00004560

Band 122
Clement Owusu Prempeh
Generation of biogenic silica from biomass residues for sutainable industrial material applications
Dissertation, ISBN 978-3-86009-555-3
https://doi.org/10.18453/rosdok_id00004559

Band 123
Frauke Kachholz
Model-based Generation of High-Resolution Flood Flow Characteristics for Small Ungauged Streams in the Northeast German Lowlands
Dissertation, ISBN 978-3-86009-556-0
https://doi.org/10.18453/rosdok_id00004530

Band 124
18. Rostocker Biomasseforum
Tagungsband, erschienen im Juni 2024, ISBN 978-3-86009-559-1
https://doi.org/10.18453/rosdok_id00004587

Band 125
Vicky Shettigondahalli Ekanthalu
Hydrothermal Carbonization of Sewage Sludge and the Influence of pH Phosphorus Transformation and Hydrochar Properties
Dissertation, ISBN 978-3-86009-562-1
https://doi.org/10.18453/rosdok_id00004601

Band 126
Nguyen Van Than
Development of an anaerobic pre-treatment of high strength organic wastewater from the cleaning of tanks of food and fodder road transports
Dissertation, ISBN 978-3-86009-560-7
https://doi.org/10.18453/rosdok_id00004600

Band 127
Christian Ochsmann
Untersuchung der Adsorption von CO_2 an Ionenaustauschern anhand eines Modellbiogases
Dissertation, ISBN 978-3-86009-561-4

Band 128
Jan Olschewski
Ein Beitrag zur Bestimmung der Erosionsstabilität von Deichbinnenböschungen
Dissertation, ISBN 978-3-86009-563-8
https://doi.org/10.18453/rosdok_id00004629

Band 129
Christian Kaehler
Ein Beitrag zur Bemessung von Küstenschutzbauwerken auf Basis der bivariaten Wahrscheinlichkeitsanalyse mit Copula-Modellen
Dissertation, ISBN 978-3-86009-566-9
https://doi.org/10.18453/rosdok_id00004689

Band 130
Felix Heumer
Risikoanalyse von Trinkwasserversorgungssystemen in kleinen bis mittleren Wasserversorgungsunternehmen und Ableitung von Maßnahmen der Risikominimierung
Dissertation, ISBN 978-3-86009-567-6
https://doi.org/10.18453/rosdok_id00004734

Band 131
19. Rostocker Biomasseforum
Tagungsband, erschienen im Juni 2025, ISBN 978-3-86009-570-6
https://doi.org/10.18453/rosdok_id00004784